Novel Approaches For Investigating Marine Planktonic Mixotrophy

MIXOTROPH.ORG
MIXITIN

MixITiN Project Report D3.8

H2020-MSCA-ITN
Bringing marine ecology into 21st century

Training next generation marine ecologists in the mixotroph paradigm

MixITiN

Project no. 766327

Work Package 3

Deliverable 3.8

Novel Approaches For Investigating Marine Planktonic Mixotrophy

Edited by: Aditee Mitra, Kevin J Flynn, Konstantinos Anestis, Joost S Mansour, Guilherme D Ferreira, Albert Calbet

Contributors: Konstantinos Anestis, Anna-Adriana Anschütz, Albert Calbet, Guilherme D Ferreira, Per Juel Hansen, Kevin J Flynn, Uwe John, Joost Samir Mansour, Maira Maselli, Nikola Medić, Aditee Mitra, Fabrice Not, Paraskevi Pitta, Filomena Romano

Acknowledgements

*Project **MixITiN** has received funding from the European Union's Horizon 2020 research and innovation programme under the Marie Skłodowska-Curie grant agreement No 766327. This document reflects only the author's view; the REA and the European Commission are not responsible for any use that may be made of the information it contains.*

How to cite this work

Manual Reporting Novel Approaches For Investigating Marine Planktonic Mixotrophy

Aditee Mitra, Kevin J Flynn, Konstantinos Anestis, Joost S Mansour, Guilherme D Ferreira, Albert Calbet (Editors) 2021

Published by Zenodo, http://doi.org/10.5281/Zenodo.5148500

How to cite each section:

Section 2:

Mansour J, Anestis K, Maselli M, Hansen PJH, Not F, John U (2021) Genomic sampling protocols for application to mixoplankton. In: *Novel Approaches For Investigating Marine Planktonic Mixotrophy*. Aditee Mitra, Kevin J Flynn, Konstantinos Anestis, Joost S Mansour, Guilherme D Ferreira, Albert Calbet (Editors) Published by Zenodo, http://doi.org/10.5281/Zenodo.5148500

Contact: Fabrice Not, not@sb-roscoff.fr

Section 3:

Ferreira GD, Calbet A, Not F, Mansour JS, Hansen PJ, Medić N, Pitta P, Romano F, Flynn KJ, Mitra A (2021) Development and validation of new methods for measuring predation rates in mixoplanktonic protists. In: *Novel Approaches For Investigating Marine Planktonic Mixotrophy*. Aditee Mitra, Kevin J Flynn, Konstantinos Anestis, Joost S Mansour, Guilherme D Ferreira, Albert Calbet (Editors) Published by Zenodo, http://doi.org/10.5281/Zenodo.5148500

Contact: Albert Calbet, acalbet@icm.csic.es

Section 4:

Anestis K, Mansour JS, Maselli M, Hansen PJ, Not F, John U* (2021) Reporting interpretative toolkit to enable the use of genomic data aligned with physiological status for representative mixoplankton. In: *Novel Approaches For Investigating Marine Planktonic Mixotrophy*. Aditee Mitra, Kevin J Flynn, Konstantinos Anestis, Joost S Mansour, Guilherme D Ferreira, Albert Calbet (Editors) Published by Zenodo, http://doi.org/10.5281/Zenodo.5148500

Contact: Uwe John, uwe.john@awi.de

Section 5:

Mitra A, Flynn KJ, Anschütz AA (2021) Novel systems dynamics modelling approaches for investigating marine planktonic mixotrophy. In: *Novel Approaches For Investigating Marine Planktonic Mixotrophy*. Aditee Mitra, Kevin J Flynn, Konstantinos Anestis, Joost S Mansour, Guilherme D Ferreira, Albert Calbet (Editors) Published by Zenodo, http://doi.org/10.5281/Zenodo.5148500

Contact: Aditee Mitra, MitraA2@Cardiff.ac.uk

MixITiN Deliverable 3.8 Report

Section 1

Introduction

Aditee Mitra
MixITiN Project Coordinator
Cardiff University UK

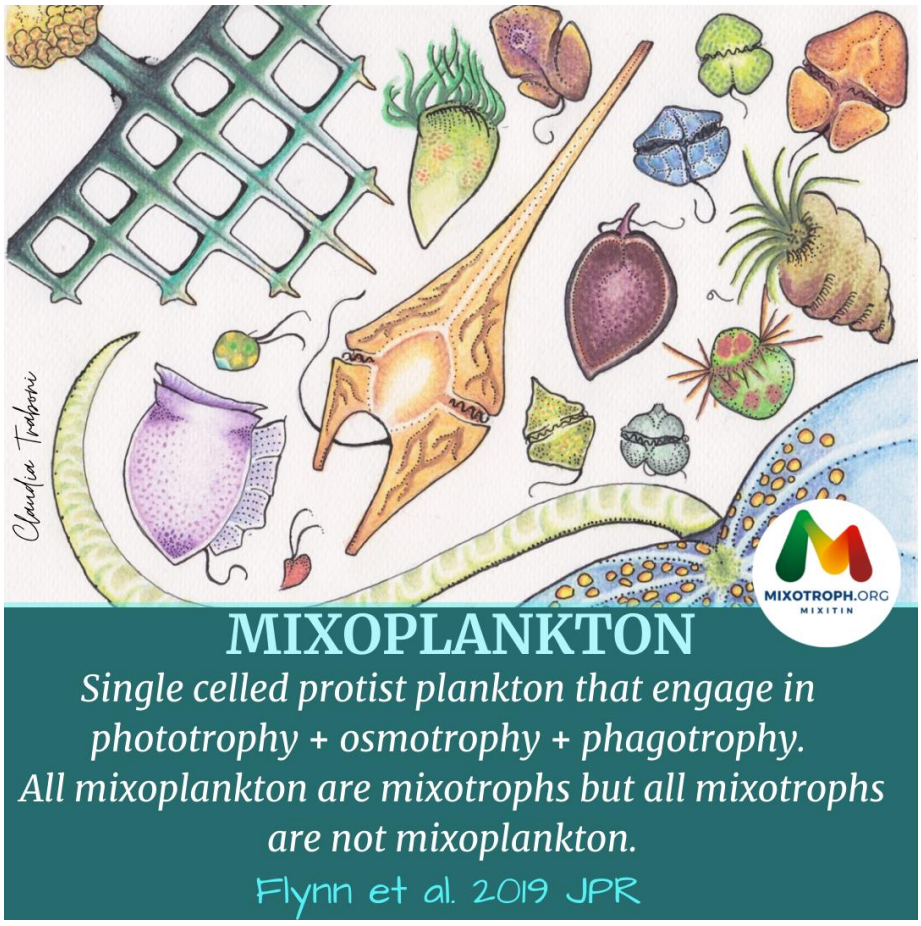

Artwork: Claudia Traboni, Institut de Ciències del Mar Spain

MixITiN comprises seven work packages (WPs). WP3 is a research work package focusing upon development and deployment of molecular and physiological methods to collectively establish new approaches for measuring and monitoring mixotrophic activity in laboratory and field -based setting, and for their description within *in silico* activities.

Marine planktonic mixotrophy, in the context of MixITiN, describes the coupling of phototrophy and phagotrophy within individual plankton protist cells. Early in the project we argued[1] to term these organisms, 'mixoplankton', and we use this descriptor throughout this report.

The accepted view in the marine research community, over decades, has been that the single-celled plankton can be divided between phytoplankton (primary producers) and protozooplankton (primary consumers) akin to the plant-animal dichotomy in terrestrial ecosystems. In between these "plant-like" phytoplankton and "animal-like" protozooplankton, in physiological terms, are the mixoplankton.

The mixoplankton are so named because they use a mixture of photo-auto- and phago-hetero- trophic strategies for growth[1,2]. While mixoplankton *per se* are not new to science, they have typically not been provided the same status as other marine plankton such as phytoplankton, bacterioplankton, zooplankton etc. For decades mixoplankton have been considered to be curiosities of nature with the assumption that they prosper only when the strict primary producers (phototrophic phytoplankton) and the strict primary consumers (phagotrophic protozooplankton) are disadvantaged. Alternatively, they have been labelled as phytoplankton that eat, or perhaps as protozooplankton that photosynthesise.

Over the last decade there has seen a radical reshaping of how scientists view the functioning of the marine food-web in the sunlit upper layer. It has been shown that in nature mixoplankton are often common components of the plankton community, and thus are closer to the norm rather than the exception. In short, the traditional dichotomy between "plant-like" phytoplankton and the "animal-like" protozooplankton used to describe the oceanic food-web is no longer tenable[2] (**Fig.1**) and that the protist plankton can now be broadly divided into six functional groups[1,2] (**Fig.2**).

At opposite ends of the spectrum are the non-phagotrophic phytoplankton (comprised primarily of diatoms) and the non-phototrophic protozooplankton; these two groups define the archetypical components of the traditional "plant-animal"-like paradigm (upper panel, **Fig.1**). The new mixoplankton paradigm shows a continuum between these extremes, with many combining some degree of both trophic routes (lower panel, **Fig.1**).

[1] Flynn *et al.* (2019) *J Plankton Res* **41**:375-391
[2] Flynn *et al.* (2013) *J Plankton Res* **35**:3-11; Mitra *et al.* (2016) *Protist* **167**:106-120

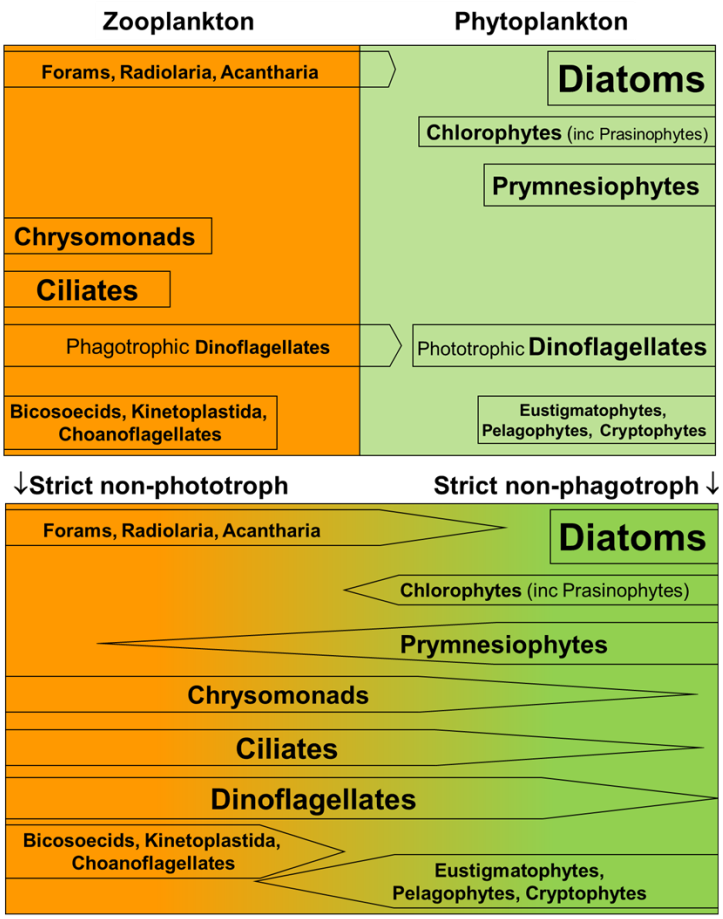

Fig. 1 | The traditional dichotomy of protist plankton (top panel) is now replaced by a gradation (lower panel) from non- phototroph to strict non- phagotrophy. In contrast to the classic misrepresentation shown in the upper panel, the potential for individual organisms to contribute both to primary and secondary production is now acknowledged. Figure modified from Flynn et al. (2013).

The mixoplankton themselves are divided into two major functional groups, with one of those being split into three sub-groups (**Fig.2**). Constitutive Mixoplankton (CM) have inherent capability to photosynthesize; these would have traditionally been labelled "phytoplankton". Other mixoplankton do not have a constitutive capability to photosynthesize but acquire phototrophic capabilities through retention of "body" parts from their prey or entire prey cells as symbionts. These non-constitutive mixoplankton (NCM) would have traditionally been labelled as "microzooplankton".

NCM comprise:

- Generalist Non-Constitutive Mixoplankton (GNCM) which acquire phototrophy from a range of different prey types;
- Specialist Non-Constitutive Mixoplankton (SNCM) which are "fussy" and acquire their phototrophic capabilities from very specific prey types through retention of i) parts of prey (plastidic SNCM; pSNCM) or, ii) entire prey cells as symbionts (endosymbiotic SNCM; eSNCM).

This new marine paradigm thus sees a radical shift from the traditional view of a food-web dominated by phytoplankton and microzooplankton to one that contains as a major component the mixoplankton in global oceans[3]. However, routine field sampling and monitoring techniques are very much based on, rooted in, the phototrophy-phagotrophy

[3] Leles *et al*. (2017) *Proc Roy Soc B* **284**:20170664; Leles *et al.* (2019) *Global Ecol Biogeog* **28**:418-428

dichotomy. Within this guide we look at the different methods required for mixoplankton field sampling.

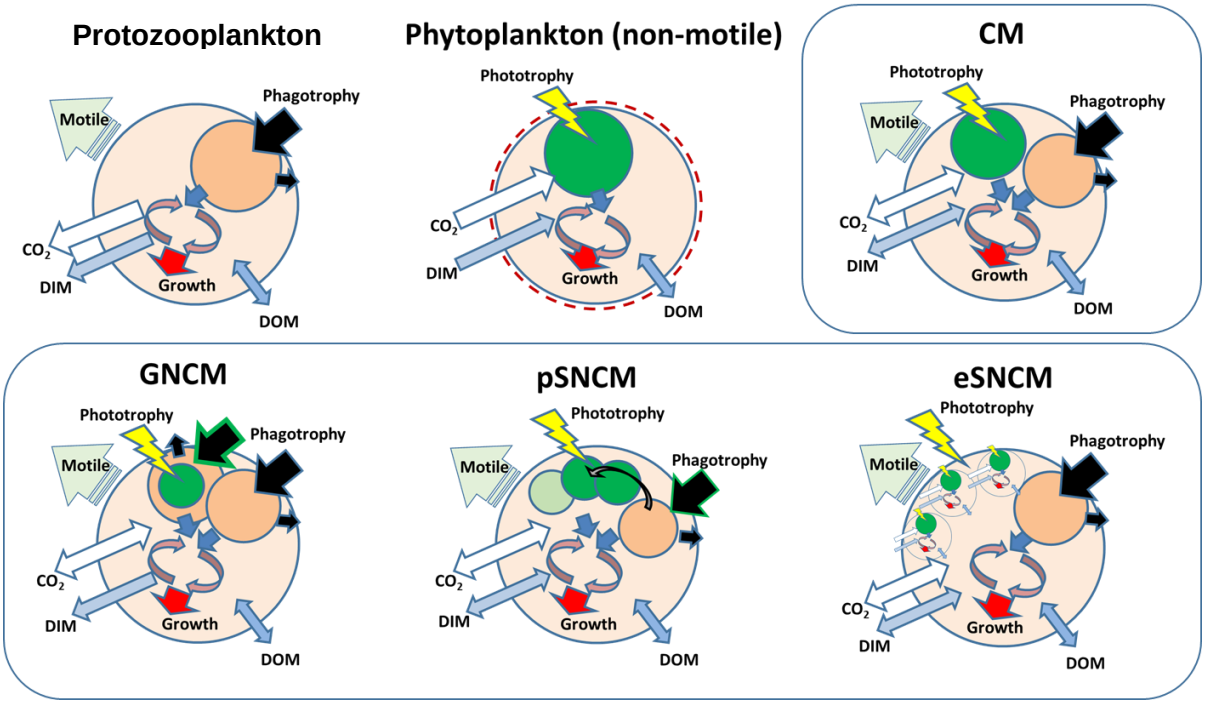

Fig. 2 | Schematics showing differences between protist plankton physiologies. Protozooplankton are osmo–phagotrophic; they are incapable of phototrophy. Phytoplankton are photo-osmo-mixotrophic; they are incapable of phagotrophy. The constitutive mixoplankton (CM) and non-constitutive mixoplankton (NCM) are all photo-, osmo- and phago-mixotrophic. The generalist NCM (i.e., GNCM) may acquire phototrophy from many types of phototroph prey; pSNCM are plastidic specialists acquiring phototrophy from specific prey only. eSNCM are endosymbiotic NCM, acquiring phototrophy by harbouring specific phototrophic prey cells. See Mitra *et al.* (2016) and Flynn *et al.* (2019) for further information.

This manual, Deliverable 3.8 of the project, brings together the different novel approaches developed within MixITiN for investigating marine mixoplankton activity. It comprises four sections, *de facto* chapters, as follows:

- **Section 2** *Genomic sampling protocols for application to mixoplankton*
- **Section 3** *Development and validation of new methods for measuring predation rates in mixoplanktonic protists*
- **Section 4** *Reporting interpretative toolkit to enable the use of genomic data aligned with physiological status for representative mixoplankton*
- **Section 5** *Novel systems dynamics modelling approaches for investigating marine planktonic mixotrophy*

MixITiN Deliverable 3.8 Report

Section 2

Genomic Sampling Protocols For Application To Mixoplankton

Joost S Mansour, Université Pierre et Marie Curie France
Konstantinos Anestis, Alfred Wegener Institute Germany
Maira Maselli**,** Kobenhavns Universitet Denmark
Per J Hansen, Kobenhavns Universitet Denmark
Fabrice Not, Université Pierre et Marie Curie France
Uwe John**,** Alfred Wegener Institute Germany

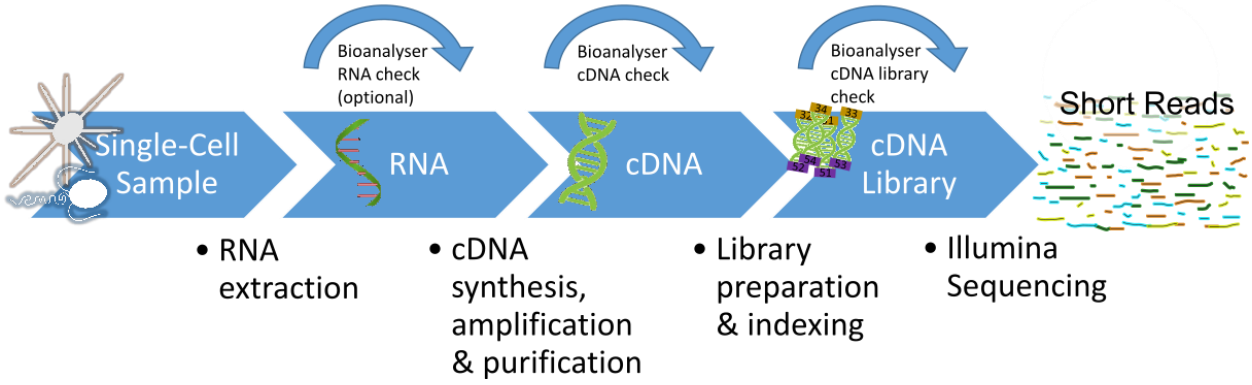

Table of Contents

2.1. Introduction

Application of ‘omics approaches to constitutive and non-constitutive mixoplankton functional groups offers us the opportunity to better understand major processes in plankton evolution, such as phagotrophy, endosymbiosis and acquired phototrophy. The increasing interest of the scientific community towards studying kleptoplastidic and endosymbiotic mixoplankton indicates the importance of such model organisms in understanding the transition from heterotrophy to phototrophy with permanently established chloroplasts (reviewed in Mansour and Anestis, 2021). In addition to the evolutionary aspect, ‘omics approaches provide substantial input for understanding physiology of mixoplankton. Genomic approaches can help identify and disentangle heterotrophic processes such as phagotrophy from osmo-heterotrophy and photo-autotrophy (Burns et al., 2018). This information could then support cellular and metabolic modelling by better elucidating the physiological mechanisms and quantifying their importance in different scenarios.

Physiological studies and responses to environmental parameters are predominantly based on the use of monocultures. This is a major obstacle to gaining deeper understanding of metabolic process in mixoplankton, as they are characterised by their interactions with other organisms (the presence of prey is often required to sustain the grazer). As a result, the use of conventional culture-based genomic approaches results in issues or ambiguity in downstream bioinformatics. To tackle this, novel cultivation-independent approaches like single-cell sampling and transcriptomics can be an outcome to study NCMs (Liu et al., 2017). Such approaches, though, have been little applied for studying protists. Single-cell transcriptomics allows us to study organisms in single-cell level and thence accurately link gene expression to the physiological state of the cell at the point of isolation. For example, when grazing rates are low this approach offers the potential for a detailed investigation of cellular and metabolic processes.

In this section, we present the sampling and transcriptomic methods that we have successfully performed on single cells of the endosymbiotic specialist non-constitutive (eSNCM) Acantharia, the generalist non-constitutive (GNCM) *Strombidium basimorphum*, the constitutive (CM) *Prymnesium parvum,* and putatively mixotrophic uncultured nanociliates. Commercially available low input RNA kits for transcriptomics are made for and tested with mammalian cells (Song et al., 2018), as such the feasibility

and efficiency of single-cell transcriptomics on highly diverse mixotrophic protists is not always known. Often single-cell transcriptomics of microbial eukaryotes show low transcript recovery rates and large variability (Liu et al., 2017). We have adopted and adapted such protocols for use with mixoplankton. Our description provides a guide of these methodologies from sampling to bench transcriptomics methods.

2.2. Sampling Methods

Various recent studies (Leles et al., 2017, 2019; Faure et al., 2019) have highlighted the importance of establishing effective protocols for field sampling of mixoplankton. The protist plankton community shows different degree of sensitivity to sampling procedures, with some organisms being more robust than others. As a result, data (qualitative and quantitative) on the more fragile species is jeopardised. Special care should therefore be taken when sampling.

First, we focus on methods for the sampling of protists from cultures (in bulk and single-cell) and then discuss methods for sampling of single-cells from the field. These sampling methods account for the fragility of these organisms, and allow follow-up analysis with sensitive molecular techniques; here are described transcriptomics, qPCR, and Fluorescence *in situ* hybridisation.

2.2.1 Single-cell samples from culture

We used culture samples of the NCM ciliate *Strombidium* cf *basimorphum* (isolated and cultured as in Maselli et al. (2020)) to study the dynamics of kleptoplasty. The CM *Prymnesium parvum* was used in order to study the dynamics of phagotrophy under different conditions (e.g., different salinity and phosphorous availability).

Materials

Ensure clean equipment and work area where possible (i.e., cleaned with ethanol and a RNase Decontamination Solution (e.g., RNaseZAP, Invitrogen #AM9780))

- Filter-sterilised (0.2 µm) seawater
- Lysis buffer (RNAqueous micro kit, ThermoFisher #AM1931)
- Micropipette or Pasteur pipette (and a flame to modify it by heating and extension)
- 0.2 mL RNAse-free PCR tubes

- -80 °C freezer
- Inverted Microscope

Safety

Exercise care when using laboratory equipment and chemicals for both extraction and library preparation protocols. Follow all health and safety protocols as required under local regulations.

Cell isolation and sample preparation procedure for RNA extraction of culture samples

- Isolate, under a light microscope, cells from cultures using a micropipette or modified Pasteur pipette.
- Meticulously clean the cells in filter-sterilised seawater in order to eliminate the presence of prey and avoid contamination. Perform at least three steps of cleaning.
- Inspect carefully by eye under a microscope for potential contaminating organisms.
- Prepare on ice 100 µL lysis buffer (RNAqueous kit) in 0.2 mL PCR tubes.
- Transfer one cell in lysis buffer filled tube using a micropipette or modified Pasteur pipette and immediately freeze at -80 °C.

2.2.2 Bulk culture or natural population samples

Processing of the entire planktonic population (either in the field or in mixed cultures) on which molecular markers will be used for prey nuclei detection and improve the understanding of role and function of kleptoplasty in planktonic protists. Described here is the methodology for bulk sample preparation for qPCR or Fluorescence in situ hybridisation (FISH).

Materials

- Nylon (e.g., Millipore by Merck, Darmstadt, Germany) and polycarbonate (e.g., Whatman Nucleopore) filters with pore size > 5 µm
- Paraformaldehyde solution: 10% in Phosphate Buffered Saline (PBS): i.e., 10 g in 100 mL PBS

- NucleoSpin Soil DNA isolation kit (e.g., Macherey-Nagel, Düren, Germany)
- 4 °C fridge
- -80 °C freezer

Safety

Paraformaldehyde should be handled under a fume hood, as dictated under local Health & Safety regulations.

Sample preparation procedure for qPCR or Fluorescence in situ hybridisation of bulk samples

Special precaution has to be taken if cell-integrity needs to be preserved. Ciliates are extremely fragile, and cell breakage during filtration will result in low yield of nucleic acid extraction.

1. If it is required to preserve cell integrity and morphology (i.e., for FISH,) fixative (paraformaldehyde) has to be added to the cell-suspension (in an appropriate volume to obtain a 4% paraformaldehyde final concentration), and, incubated at 4 °C for 1 h prior to filtration (step 2) for hardening of the organisms. This step can be skipped if the follow-up analysis is qPCR.
2. Collect cells on polycarbonate membrane filter.

- The volume of cell-suspension to be filtered is dependent on the culture density (NCM cells mL^{-1}). Ideally, at least 3000 NCM cells would have to be collected on each filter. The pore size would depend on the size of the organism of interest. NCM ciliates are generally retained on filters with pore size > 5 µm which would allow separation from smaller protist, including potential prey.
- FISH: cells have to be collected on polycarbonate filters. Filters can be stored at 4 °C until further processing.
- qPCR: cells can be collected either on nylon or polycarbonate filters. Filters with cells samples for qPCR are added to a 2 mL tube containing NucleoSpin Soil DNA isolation kit (Macherey-Nagel, Düren, Germany) lysis buffer and stored at -80 °C until further processing.

2.2.3 Single-cell field samples

To date no method exists which allows for various eSNCM species to be maintained in culture; these include Radiolaria. For these endosymbiotic uncultivatable mixoplankton, sampling using slow horizontal plankton net tows are proven to be the best compromise between ease of sampling while maintaining cell integrity and thus quality (Graham et al., 1976; Mansour et al., 2021c).

The method to acquire clean isolated cells for transcriptomic analysis is described in this section. This work is conducted under field conditions, where facilities are often not as good as in terrestrial-bound laboratories. Thus, sample preparations are typically not conducted working in a controlled air-stream, under a hood, nor has the work area necessarily been treated with RNAse inhibitors (or similar). Aseptic techniques and gloves, to minimise further contamination, should still be used. Detailed protocol is also available on dx.doi.org/10.17504/protocols.io.bqvrmw56 (Mansour and Not, 2021).

Materials

If possible, ensure clean equipment and work area where possible (i.e., cleaned with ethanol and a RNase Decontamination Solution such as RNaseZAP, Invitrogen #AM9780)

- Filtered seawater (FSW, 0.2 µm-pore-size)
- Ice
- Lysis buffer (RNAqueous micro kit, ThermoFisher #AM1931)
- RNAse Away (or similar product, optional)
- 0.2 mL RNAse-free PCR tubes
- Liquid Nitrogen
- -80 °C freezer
- Micropipette or Pasteur pipette (and flame to elongate it)
- Inverted Microscope/Stereoscope
- Petri dishes

Safety

Exercise care when handling liquid nitrogen and using laboratory equipment, as dictated under local Health & Safety regulations.

Cell isolation and sample preparation procedure for RNA extraction of field samples

- Prepare filter-sterilised seawater (FSW, 0.2 µm-pore-size)
- Isolate cells from plankton net samples into a Petri dish with FSW using a micropipette or modified Pasteur pipette.
- Incubate cells in FSW (1 h) and repeat the isolating procedure with a transfer to fresh FSW three times. (This procedure allows for self-cleaning of particles attached to the cells and dilution to achieve effective extinction of any contaminating organisms accidentally taken with during isolation).
- Clean cells can be used for physiological experiments before proceeding to next step.
- Prepare 100 µL lysis buffer (from RNAqueous kit) in 0.2 mL PCR tubes in a frozen Alurack.
- Where possible continue to work on ice.
- Transfer one cell per lysis buffer filled tube and immediately freeze in liquid nitrogen.
- Immediate storing at -80 °C, disregarding freezing in liquid nitrogen, has proven to suffice, though flash freezing is still preferred when possible (**see section 2.6.3**).
- Store at -80 °C

2.3. Molecular techniques: Transcriptomics

We report on transcriptomic methods that we have successfully performed on single cells of Acantharia, *Strombidium basimorphum,* and *Prymnesium parvum*. Commercially available low input RNA kits for transcriptomics are made for and tested with mammalian cells (Song et al., 2018), as such the feasibility and efficiency of single-cell transcriptomics on highly diverse mixotrophic protists is not always known. Often single-cell transcriptomics of microbial eukaryotes show low transcript recovery rates and large variability (Liu et al., 2017). Despite this, genomics gives us the possibility to get deep

enough into the cellular and metabolic networks involved in mixotrophy and is a powerful tool for studying microbial eukaryotes.

This section describes the methodology to extract RNA and prepare cDNA libraries for Illumina sequencing and transcriptomic study **of single cells**. The process steps, starting from a single-cell sample, up to transcriptome sequencing, are shown in **Figure 2-1**. The methods and protocols below indicate methods adopted and modified from commercially available kits. Details of these protocols are also available at dx.doi.org/10.17504/protocols.io.bp6xmrfn and dx.doi.org/10.17504/protocols.io.bp7vmrn6 (Mansour et al., 2021b, 2021a)

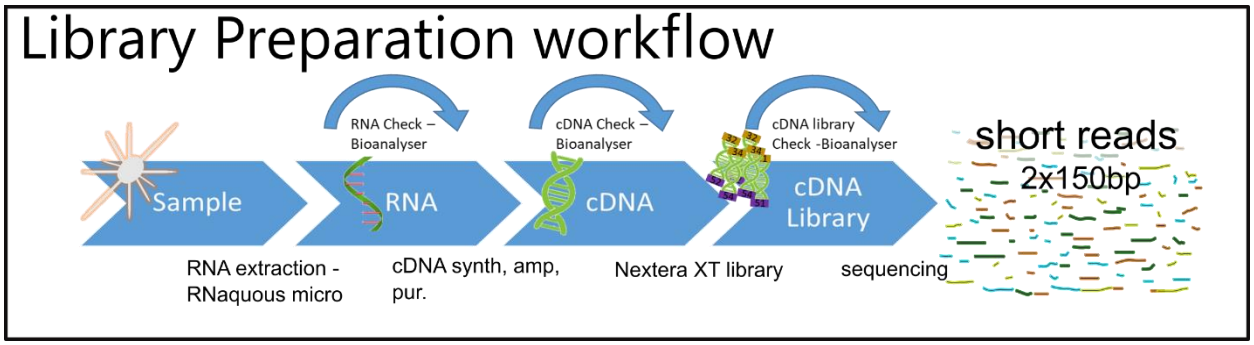

Figure 2-1. cDNA library preparation workflow from sample to transcriptome sequencing. All major steps are indicated including quality checks by Bioanalyzer. Specific workflow is illustrated in **Figure 2-5**.

2.3.1 RNA extraction of single cells

Materials

- 0.2 mL RNAse free tubes (2x #samples) / or strips
- 2 mL nuclease-free reaction tube (Eppendorf) (for Elution Buffer)
- Ice box + rack for PCR tubes
- Heatblock (75 °C) (any heatblock for 1.5 mL tubes will suffice)
- Microcentrifuge for 1.5 mL tubes (any benchtop centrifuge will suffice)
- Mini-centrifuge for 0.2 mL tubes or strips (any will suffice)
- Bench vortex mixer (any will suffice)
- EtOH (100% - molecular grade)
- RNAqueous – Micro kit (ThermoFisher #AM1931) including:
    - Elution Solution (12.5 µL x #sample)
    - Wash Solution 1

- Wash Solution 2/3
- Micro filter cartridges and Elution tubes

Safety

PPE, as dictated under local Health & Safety regulations.

Procedure

Guidelines

- All our protocols are performed at 18 – 22 °C room temperature (RT).
- To avoid possible RNA degradation, try to work quickly in all steps and work on ice. To help achieve this, do not extract RNA from too many samples simultaneously.
- Always wear clean RNase-free gloves.
- Clean workspace with ethanol and an RNase Decontamination Solution (e.g. RNaseZAP, Invitrogen #AM9780).
- If possible, use a dedicated set of pipettes for RNA and use filter tips.

Preparations

- Be sure to have prepared the Wash Solutions by adding ethanol according to the manual
- Prepare 12.5 µL of Elution Solution per sample and put in 75 °C heatblock.
- Thaw and Vortex twice 10 sec all samples (be sure to secure the lids)
- Spin down gently
- RT for 5 min

RNA extraction protocol

1. Add 50 µL ethanol (100% molecular grade) to samples
    - Brief vortex and gentle / short spin down
2. Load the (150 µL) sample onto a column / Microfilter cartridge (use 100 µL pipet twice)
    - Centrifuge 10 sec at maximum (e.g. 10000xg)
3. Add 180 µL of Wash Solution 1 unto the column (Microfilter cartridge)
    - Centrifuge 30 sec at maximum (e.g. 10000xg)
4. Add 180 µL of Wash Solution 2/3 unto the column (Microfilter cartridge)

- Centrifuge 30 sec at maximum (e.g. 10000xg)

5. Repeat addition of 180 µL of Wash Solution 2/3 unto the column (Microfilter cartridge)
    - Centrifuge 30 sec at maximum (e.g. 10000xg)
6. Remove and discard all flow-through (pour out)
7. Centrifuge 1 min at max (removing any liquid still on the filter)
8. Replace the collection/elution tube with a new one
9. Add 6.5 µL Elution Solution (pre-heated at 75 °C)
    - Do this directly to the centre of the filter
    - Incubate 1 min at RT (more time is still ok)
    - Centrifuge 30 sec at maximum (e.g. 10000xg)
10. Add 6.0 µL (heated at 75 °C) Elution Solution
    - Do this directly to the centre of the filter
    - Incubate 1 min at RT (more time is still ok)
    - Centrifuge 30 sec at maximum (e.g. 10000xg)
11. Transfer your 12.5 µL RNA to 0.2 mL tubes on ice (use 100 µL pipet)
    - For Bioanalyser take an aliquot of 1.5 µL in a separate tube, also on ice.
12. Store RNA at -80 °C
13. Check quality and purity of RNA by Agilent 2100 C. Example electrographs in **Figures 2-2, 2-3, and 2-4**

Total RNA extracted from single cells are often low in concentration and yield which challenge the quality control over Agilent Bioanalyser, even when the most sensitive kits are used. In this case, RNA was used directly for cDNA synthesis. For Acantharia RNA was measurable but could still be < 20 pg/µL (e.g. **Figure 2-2 and 2-3**), hence quantification of RNA (e.g. by Bioanalyzer) was difficult. For our purposes, we assessed a subset of each biological replicates and if the subset was consistent, we assumed the other replicates were similar. With these single-cell low RNA concentrations, the total RNA extract would anyway be used in subsequent protocols without dilution making accurate quantification of concentrations incidental, in addition to minimising cost and workload.

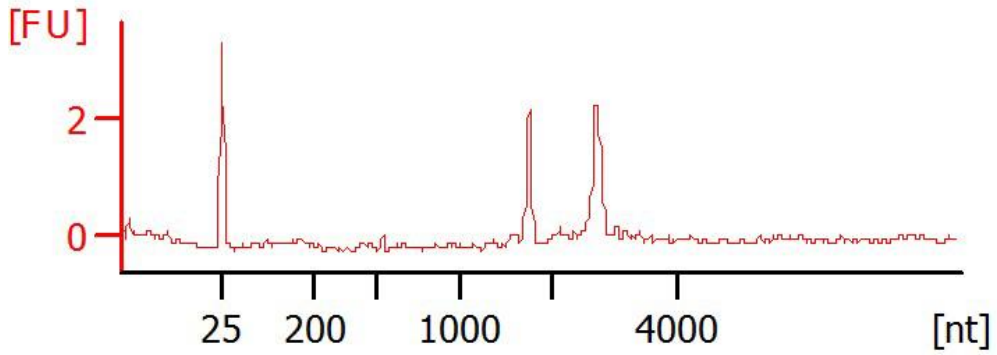

Figure 2-2. Example of a desirable electrograph showing clear 18S and 28S ribosomal RNA peaks indicating good RNA quality (acantharian sample). The first peak indicates a size and concentration marker of the Bioanalyser chip.

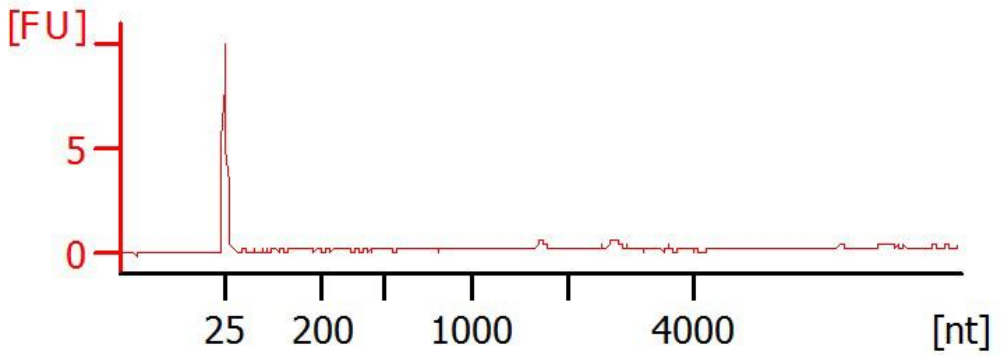

Figure 2-3. Example of an electrograph showing minimal ribosomal RNA peaks. Due to the single-cell approach RNA quantity is generally low (or not measurable) and even in this case subsequent steps provided quality cDNA product (acantharian sample). The first peak indicates a size and concentration marker of the Bioanalyser chip.

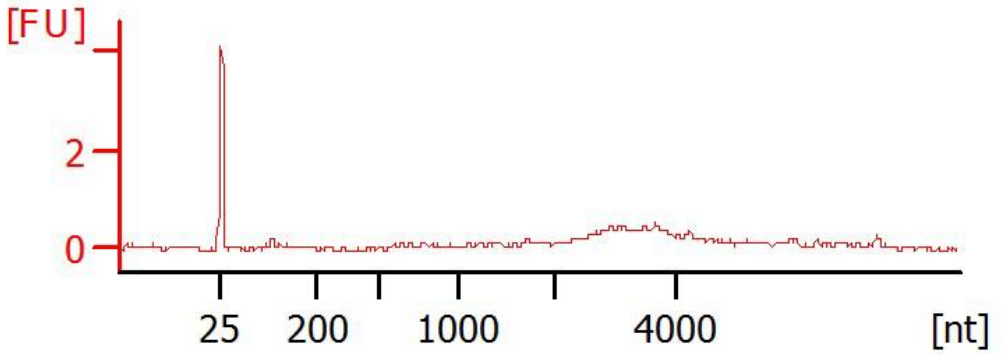

Figure 2-4. Example of an electrograph showing degradation, 18S and 28S ribosomal RNA peaks are not clearly seen instead it is more a smear (acantharian sample). The first peak indicates a marker.

2.3.2 cDNA synthesis – amplification – purification

We have performed cDNA synthesis, amplification and purification with methods adapting the SMART-Seq4 kit (Takara #634891, **section 2.3.3, 2.6.4, 2.6.5**), as well as the NEBNext kit (NEB #E6421, **section 2.6.6, 2.3.7, 2.3.8**). Both kits seemed similar in cDNA library quality production (**see section 5.31**). Though the NEBNext kit is the more cost-efficient method. Workflow is illustrated in **Figure 2-5**.

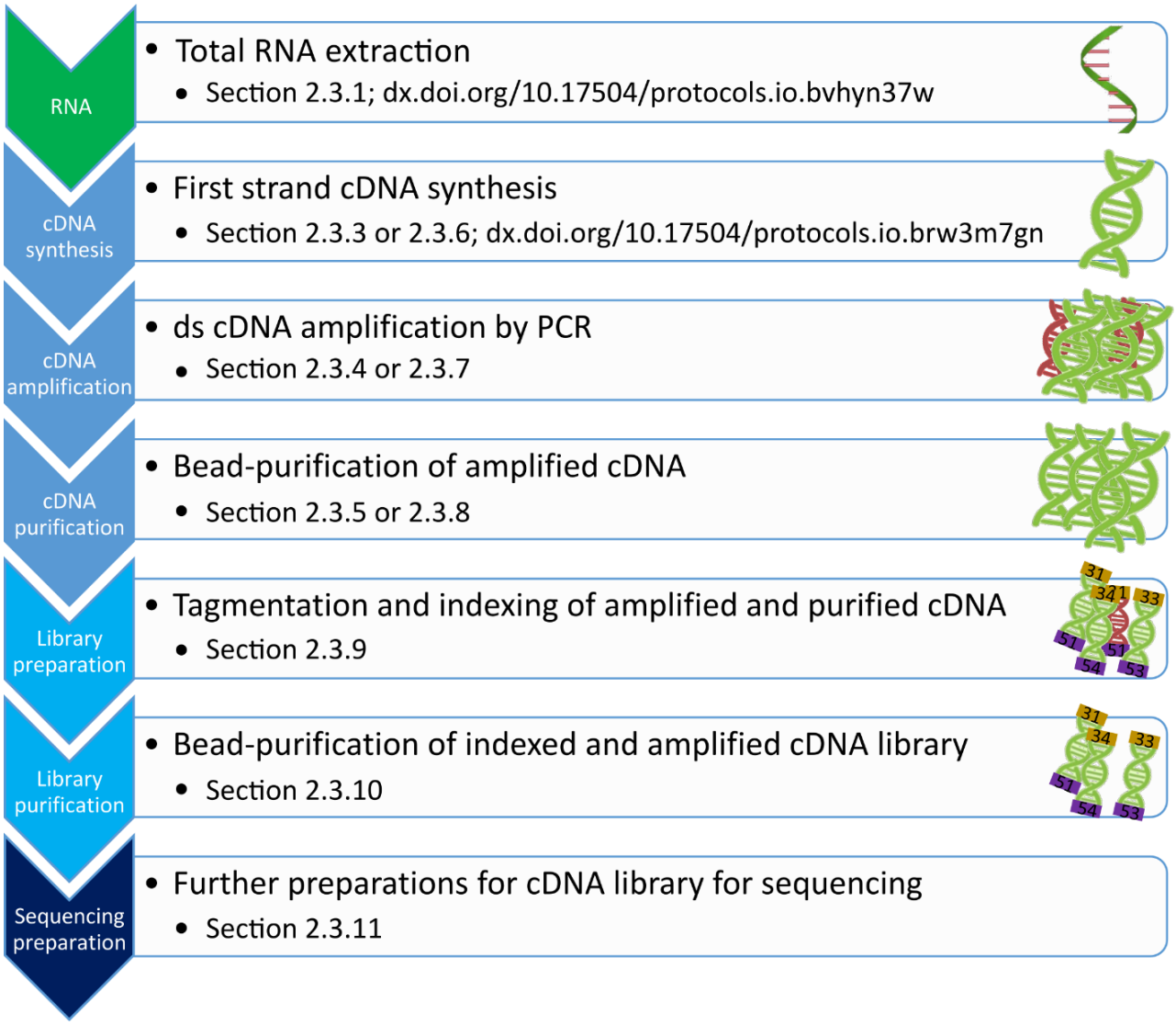

Figure 2-5. Specific workflow of protocols to follow in order to produce a cDNA library ready to sequence. Each colour change of the arrows indicates distinct blocks in which the workflow can be interrupted.

2.3.3 cDNA synthesis – SMART-Seq 4

Materials

- 0.2 mL RNAse free tubes (x samples)
- 2 mL nuclease-free reaction tube (Eppendorf) (x2 for Master Mix & Reaction Buffer)
- Ice box + rack for pcr tubes
- Thermocycler
- Mini-centrifuge for 0.2 mL tubes or strips (any will suffice)
- Bench vortex (any will suffice)

SMART-Seq4 kit (Takara #634891) reagents on ice:

- 3'SMART-Seq CDS primer II A (blue) (1 µL per sample)
- Smart Seq 4 Oligo (48 uM) (pink) (1 µL per sample)
- 10X Lysis Buffer
- RNAse inhibitor (40 U/µL) (white)

SMART-Seq4 kit (Takara #634891) reagents at room temperature:

- (5X) Ultra low FS buffer (red) (4 µL per sample)
- RNase/Nuclease Free water

SMART-Seq4 kit (Takara #634891) reagents taken at the last minute from freezer:

- SmartScribe Reverse Transcriptase (purple) (2 µL per sample)

Safety

PPE, as dictated under local Health & Safety regulations.

Procedure

With low total RNA samples (20-200 pg/µL) 5 µL total RNA sample in combination with 18 amplification cycles (**section 2.6.2**) proved sufficient. This additionally would allow leftover RNA to be used for a retry. Nonetheless it is advisable to test for each specimen type. For higher total RNA concentrations, the total RNA used for cDNA synthesis and the number of amplification cycles should be adjusted negatively.

Refer also to pages 7-10 of the SMART-Seq4 manual (https://www.takarabio.com/a/114896).

All our protocols are performed at 18 – 22 °C room temperature (RT).

- Prepare a 72 °C incubator (for 0.2 mL tubes, e.g., a thermocycler)

14. Thaw at RT the 5X Ultra low FS buffer. (Vortex and spin down reagents except enzyme)
15. Other reagents thaw on ice – except SmartScribe Reverse Transcriptase, take that from freezer once needed
16. Prepare 10X Reaction Buffer (RB), on ice – 1 µL is used per sample (adjust as needed, & write down exact volumes)
    - 19 µL 10X Lysis Buffer (from SMART-Seq4 kit)
    - 1 µL RNase Inhibitor (white)
    - Mix/vortex and spin down (avoid bubbles)
17. Take into a clean Nuclease free 0.2 mL tube 1 to 9.5 µL of RNA sample & 1 µL of RB (total 10.5 µL volume, adjust with nuclease free water depending on RNA sample)
    - 5 µL total RNA. (in essence either all total RNA sample can be used, or safer to use <50% to allow redo when needed and [RNA] permitting.
18. Place on samples on **Ice** and add 1 µL of 3'SMART-Seq CDS primer II A (blue) to samples (when performing 17+ PCR cycles)
    - And add 1 µL Nuclease free water (keep total volume 12.5 µL)
    - Mix gently (vortex) & spin down
19. Incubate samples at 72 °C for 3 minutes
20. Prepare Master Mix (MM) as below for each sample (+10%; write down exact volumes) on ice:
    - 4 µL (5X) Ultra low FS buffer (red) (make sure precipitates are dissolved)
    - 1 µL Smart Seq 4 Oligo (48 µM) (pink)
    - 0.5 µL RNase inhibitor
21. Immediately after the 3 min 72 °C incubation put samples on ice for 2 min
22. Preheat the thermocycler to 42 °C
23. Take the Reverse Transcriptase, gently mix it without vortexing and add to MM

- 2 µL Reverse Transcriptase per sample (x samples +10%)
- Mix MM by gentle vortex and spin down

24. Add 7.5 µL of MM to the samples (total volume now 20 µL)
    - Mix by pipetting
    - Spin down
25. Incubate with thermocyler program: 42 °C 90 min; 70 °C 10 min; 4 °C "forever" –
26. Potential stopping 4 °C overnight

2.3.4 cDNA Amplification by LD PCR – single cell – SMART-Seq4

Materials

- 2 mL nuclease-free reaction tube (Eppendorf) (for PCR MasterMix)
- Thermocycler
- Mini-centrifuge for 0.2 mL tubes or strips (any will suffice)
- Bench vortex (any will suffice)
- Ice box
- SMART-Seq4 kit (Takara #634891)

Safety

PPE, as dictated under local Health & Safety regulations.

Procedure

Refer also to page 11 of the SMART-Seq4 manual (https://www.takarabio.com/a/114896)

- Thaw all the reagents on ice except enzyme
    - (Vortex and spin down reagents except enzyme)
- Preheat thermocycler at 95 °C
- Prepare Mastermix (+10%), one sample is as below:
    - 25 µL 2X SeqAMP PCR Buffer
    - 1 µL PCR Primer II A (green)
    - 3 µL Nuclease free water

- 1 µL SeqAMP DNA Polymerase (take out last minute and mix without vortexing, spin down)
    - Mix Master Mix well and gently (finger flick) and spin down
- Add 30 µL of Mastermix to each sample from cDNA synthesis
    - Mix well (pipetting) and spin down
- PCR protocol (preheated):

95 °C	1 min	
98 °C	10 sec	18 – 25
65 °C	30 sec	cycles*
68 °C	3 min	
72 °C	10 min	
4 °C	forever	

*The number of cycles needs to be adjusted upon preliminary work

STOPPING POINT 4 °C overnight

2.3.5 cDNA purification – SMART-Seq4

Materials

- GC nucleic acids purification beads – CleanNGS (GC Biotech, CNGS-0050)
- 5 mL reaction tube (Eppendorf) (for bead aliquot)
- 80% EtOH (prepare fresh, 400 µL x samples)
- Nuclease free 0.2 mL tube (x samples x 2)
- SMART-Seq4 (Takara #634891) Elution buffer (10 mM Tris-Cl, pH 8.5) (15 µL x samples)
- Magnetic separation device (Life technologies #AM10027)
- Bench centrifuge for 0.2 mL tubes or strips
- Bench vortex

Safety

PPE, as dictated under local Health & Safety regulations.

Procedure

Refer also to pages 12-13 of the SMART-Seq4 manual (https://www.takarabio.com/a/114896).

All our protocols are performed at 18 – 22 °C room temperature (RT).

- Vortex the bead stock well, this needs to be very well and evenly mixed
- Aliquot beads, 22.5 µL x samples (plus extra)
- Bring the bead aliquot to RT for at least 30 min
- Vortex the bead aliquot until evenly mixed
- **Add 22.5 µL** of beads to each sample (amplified cDNA from 2.3.4)
    - Mix by pipetting up and down at least 10 times, and vortex
- Incubate at **RT for 8 minutes** to let cDNA bind to the beads
- Briefly spin down and place the samples **on a magnetic separation device for 5 minutes** or longer. Until the liquid appears completely clear and there are no beads in the supernatant.
- Pipet and discard the supernatant (72.5 µL), keeping the samples in the magnetic device
- Keep samples in the magnetic device, **add 200 µL fresh 80% EtOH** to each sample
    - Do not disturb the beads
    - Wait 30 seconds
    - Pipet and discard (use 100 µL pipet) supernatant containing contaminants
- Repeat EtOH wash: **add 200 µL 80% EtOH** to each sample, without disturbing the beads
    - Wait 30 seconds
    - Pipet and discard supernatant (use 100 µL pipet)
- Briefly spin the samples to collect liquid off the sides
- Place samples back in the **magnetic device for 30 seconds**, beads will again be collected on the side
    - Remove all remaining ethanol / supernatant with a pipet (use 10 µL pipet)

- Place samples at **RT for 2 - 2.5 minutes** until the pellet is no longer shiny, but before a crack appears. It needs to be 'just' dry, matte with no shine.
- Once the beads are dry add **15 µL of Elution buffer to all samples** to cover the bead pellet
    - Remove samples from the magnetic device
    - Mix to re-suspend the beads by (multi)pipetting (can scrap of beads from the side)
- Incubate at **RT for 2 min (longer)** to rehydrate
- Briefly spin the samples to collect liquid off the sides
- Place samples back in the **magnetic device for 1 minute**, until the solution is completely clear
- **Transfer the clear supernatant** containing purified cDNA to a nuclease free 0.2 mL tube (use 10 µL pipet)
    - Beads that do not pellet can be pipetted for resuspension and then towards the magnet, and incubation continued until there are no more beads in the supernatant
    - Make immediately an aliquot for Bioanalyser analysis to prevent unnecessary freeze-thawing cycles.
- Label and store at -20 °C

Check the quality of cDNA by Bioanalyser High Sensitivity DNA Kit (Agilent #5067-4626). Example electrographs in **Figures 2-6 and 2-7**.

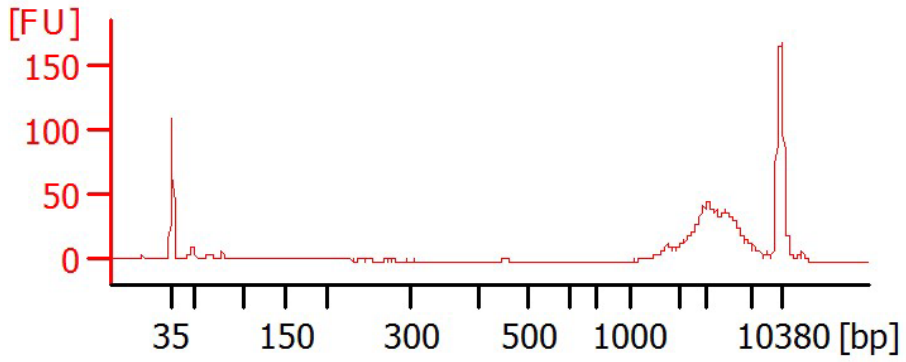

Figure 2-6. Example of a desirable electrograph. Showing cDNA with few primer dimers (acantharian sample). Example of an acantharian sample. The peaks on the outsides markers for size and concentration of the Bioanalyser chip.

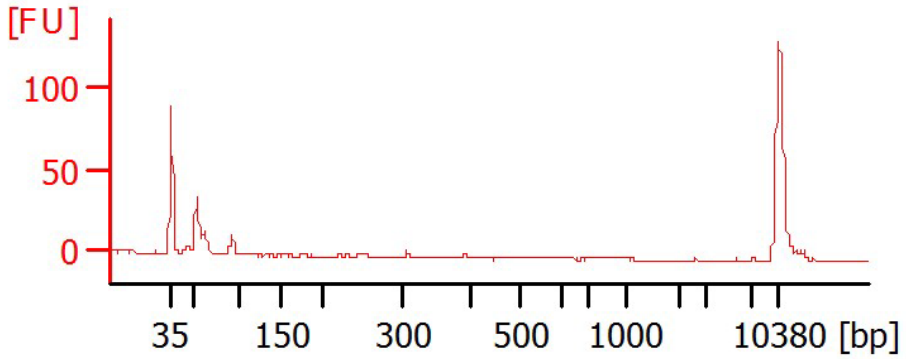

Figure 2-7. Example of failed amplification showing only primer dimers. The peaks on the outsides are markers.

2.3.6 cDNA synthesis – NEBNext

Materials

- 0.2 mL RNAse free tubes (x samples)
- 2 mL nuclease-free reaction tube (Eppendorf) (for Master Mix)
- Ice box + rack for PCR tubes
- Thermocycler
- Mini-centrifuge for 0.2 mL tubes or strips (any will suffice)
- Bench vortex (any will suffice)

NEBNext kit Single Cell cDNA Synthesis and amplification module (NEB #E6421), reagents on ice

- NEBNext Single Cell RT Primer Mix
- NEBNext Single Cell RT Buffer
- NEBNext Template Switching Oligo
- Nuclease-free water
- NEBNext Single Cell RT Enzyme Mix

At room temperature

- NEBNext Cell lysis buffer

Safety

PPE, as dictated under local Health & Safety regulations.

Procedure

Refer also to pages 8-9 of the NEBNext manual (https://international.neb.com/-/media/nebus/files/manuals/manuale6421.pdf?rev=b0de9c86eb1a44918e1f74f12381ae0d&hash=29EB8D330BBC131937FC8A64D26ADF86).

All our protocols are performed at 18 – 22 °C room temperature (RT).

- Work on ice, prepare mix and spin reagents
- Prepare annealing reaction for low (<5 ng) RNA, total volume 9 µL with up to 8 µL total RNA + 1ul RT primer mix + Nuclease-free water (variable)
    - Mix by pipetting 10 times
- Incubate for 5 minutes in thermocycler at 70°C with heated lid at 105°C, then hold at 4°C or place samples on ice
    - Prepare the following Reverse transcription mix during this step
- Reverse transcription Master Mix (MM) as below for each sample (+10%; write down exact volumes) on ice:
    - 5 µL NEBNext Single Cell RT Buffer
    - 1 µL NEBNext Template Switching Oligo,
    - 3 µL Nuclease-free water,
    - 2 µL NEBNext Single Cell RT Enzyme Mix (add last)
    - Mix by pipetting
- Add 11 µL MM to each 9 µL annealed sample
    - Mix well by pipetting
    - Quick spin down
- Incubate with Thermocyler program (heated lid 105 °C): 42 °C 90 min, 70 °C 10 min; 4° C forever

STOPPING POINT 4 °C overnight

2.3.7 cDNA amplification – NEBNext

Materials

- 2 mL nuclease-free reaction tube (Eppendorf) (for PCR MasterMix)

- Thermocycler
- Mini-centrifuge for 0.2 mL tubes or strips (any will suffice)
- Bench vortex (any will suffice)
- Ice box

NEBNext kit (NEB #E6421) reagents on ice:

- NEBNext Cell Lysis Buffer (10X)
- NEBNext Single Cell cDNA PCR Master Mix
- NEBNext Single Cell cDNA PCR Primer
- Nuclease-free water

Safety

PPE, as dictated under local Health & Safety regulations.

Procedure

Refer also to pages 9-10 of the NEBNext manual (https://international.neb.com/-/media/nebus/files/manuals/manuale6421.pdf?rev=b0de9c86eb1a44918e1f74f12381ae0d&hash=29EB8D330BBC131937FC8A64D26ADF86).

All our protocols are performed at 18 – 22 °C room temperature (RT).

- Vortex and spin down reagents
- Prepare cDNA amplification Mastermix (+10%), one sample is as below:
  - 0.5 µL NEBNext Cell Lysis Buffer (10X)
  - 50 µL NEBNext Single Cell cDNA PCR Master Mix
  - 2 µL NEBNext Single Cell cDNA PCR Primer
  - 27.5 µL Nuclease-free water
    - Mix MM well and gently (finger flick) and spin down
- Add 80 µL of Mastermix to each 20 µL sample of cDNA (from cDNA synthesis protocol 4.3.4)
  - Mix well (pipetting 10 times) and spin down
- Incubate in PCR thermocycler with heated lid at 105 °C and the following program:

98 °C	45 sec	
98 °C	10 sec	16 cycles *
62 °C	15 sec	
72 °C	3 min	
65 °C	5 min	
4 °C	forever	

*The number of cycles is to be adjusted upon preliminary work

STOPPING POINT 4 °C overnight

2.3.8 cDNA cleanup/bead purification – NEBNext

Materials

- GC nucleic acid purification beads – CleanNGS (GC Biotech, CNGS-0050)
- 5 ml reaction tube (Eppendorf) (for bead aliquot)
- Nuclease-free 0.2 mL tubes (2x #samples)
- Elution buffer (15 µL x #samples)
- Magnetic separation device (Life technologies #AM10027)
- Mini-centrifuge for 0.2 mL tubes or strips (any will suffice)
- Bench vortex (any will suffice)
- 80% EtOH (prepare fresh, 800 µL x #samples)
- 0.1x TE buffer (50 µL x sample, 1x TE buffer diluted 1:10 in nuclease-free water)
- 10 mM Tris (pH 8.0) (33 µL x #samples)
- NEBNext Bead Reconstitution Buffer (from NEB #E6421)

Procedure

Refer also to pages 10-11 of the NEBNext manual (https://international.neb.com/-/media/nebus/files/manuals/manuale6421.pdf?rev=b0de9c86eb1a44918e1f74f12381ae0d&hash=29EB8D330BBC131937FC8A64D26ADF86).

All our protocols are performed at 18 – 22 °C room temperature (RT).

- Vortex the bead stock well, this needs to be very well and evenly mixed
- Aliquot beads, 60 µL x samples (plus extra)
- Bring the bead aliquot to RT for at least 30 min
- Vortex the bead aliquot until evenly mixed
- Spin down the sample (amplified cDNA from 2.3.7)
- **Add 60 µL** of beads to each sample
    - Mix by pipetting up and down
    - Shake / vortex for 30 sec
- Incubate at **RT for 6 minutes** to let cDNA bind to the beads

- Very briefly spin down and place the samples **on a magnetic separation device for 5 minutes**. Until the liquid appears completely clear and there are no beads in the supernatant.
- Pipet and discard the supernatant, keeping the samples in the magnetic device and not disturbing the beads.
- Keep samples in the magnetic device, **add 200 µL fresh 80% EtOH** to each sample
    - Do not disturb the beads
    - Wait 30 seconds
    - Pipet and discard (use 100 µL pipet) supernatant containing contaminants
- Repeat EtOH wash: **add 200 µL 80% EtOH** to each sample, without disturbing the beads
    - Wait 30 seconds
    - Pipet and discard supernatant (use 100 µL pipet)
- Briefly spin the samples to collect liquid off the sides
- Place samples back in the **magnetic device for 30 seconds**, beads will again be collected on the side
    - Remove all remaining ethanol / supernatant with a pipet (use 10 µL pipet)
- Place samples at **RT for 5 minutes** until the pellet is no longer shiny, but before a crack appears. It needs to be 'just' dry, matte with no shine.
- Once the beads are dry add **50 µL of 0.1x TE buffer to all samples** to cover the bead pellet
    - Remove samples from the magnetic device
    - Mix to re-suspend the beads by (multi)pipetting 10 times
    - Shake/vortex for 30 sec
    - Very quick spin down
- Incubate at **RT for (at least) 2 min** to rehydrate
- Add 45 µL NEBNext Bead Reconstitution Buffer to each sample
    - Mix by pipetting up and down
    - Shake / vortex for 30 sec
    - Quick spin down

Second clean-up step

- Incubate at **RT for 5 minutes** to let cDNA bind to the beads
- Very briefly spin down and place the samples **on a magnetic separation device for 5 minutes**. Until the liquid appears completely clear and there are no beads in the supernatant.
- Pipet and discard the supernatant, keeping the samples in the magnetic device and not disturbing the beads.
- Keep samples in the magnetic device, **add 200 µL fresh 80% EtOH** to each sample
    - Do not disturb the beads
    - Wait 30 seconds
    - Pipet and discard (use 100 µL pipet) supernatant containing contaminants
- Repeat EtOH wash: **add 200 µL 80% EtOH** to each sample, without disturbing the beads
    - Wait 30 seconds
    - Pipet and discard supernatant (use 100 µL pipet)
- Briefly spin the samples to collect liquid off the sides
- Place samples back in the **magnetic device for 30 seconds**, beads will again be collected on the side
    - Remove all remaining ethanol / supernatant with a pipet (use 10 µL pipet)
- Place samples at **RT for 5 minutes** until the pellet is no longer shiny, but before a crack appears. It needs to be 'just' dry, matte with no shine.
- Elute the cDNA in 33 µL 10 mM Tris (pH 8.0)
    - Remove samples from the magnetic device
    - Incubate at **RT for 2 min** to rehydrate
    - Mix to re-suspend the beads by (multi)pipetting 10 times
    - Shake/vortex for 30 sec
    - Very quick spin down
- Place the samples **on a magnetic separation device for 4 minutes**.
- **Transfer the clear supernatant (30 µL**) containing purified cDNA to a nuclease-free 0.2 mL tube

- Make immediately an aliquot for Bioanalyser analysis to prevent unnecessary freeze-thawing cycles.
- Label and store at -20 °C

Check quality of cDNA using a Bioanalyser High Sensitivity DNA Kit (Agilent #5067-4626). Example electrographs in **Figures 2-6 and 2-7**.

2.3.9 cDNA library preparation and indexing – Nextera XT

Materials

- 0.2 mL RNAse free tubes (2 x #samples) or strips or 96-well PCR plate
- 0.2 mL RNAse free tube strip of 8 (2 for reagent aliquots)
- Ice box + rack
- Thermocycler
- Mini-centrifuge for 0.2 mL tubes or strips (any will suffice)
- Bench vortex (any will suffice)
- *Plate adhesive seal (optional, only for when working with plates)*
- Nextera XT Index Kit v2 Set A (96 indexes, 384 samples) (Illumina FC-131-2001)

Nextera XT (Illumina #FC-131-1096) Reagents:

- Amplicon Tagment Mix (ATM) (5 µL x sample)
- Tagment DNA buffer (TD) (10 µL x sample)
- Neutralize Tagment Buffer (NT) (5 µL x sample)
- Nextera PCR master Mix (NPM) (15 µL x sample)

Safety

PPE, as dictated under local Health & Safety regulations.

Procedure

Refer also to pages 7-9 of the Nextera XT manual (https://tinyurl.com/nextera-xt-ref-guide-15031942)

All our protocols are performed at 18 – 22 °C room temperature (RT).

Part 1 - Tagmentation of cDNA samples

- Dilute each sample of amplified and purified cDNA to 30 pg/µL in either Elution buffer or as per the final step of the used protocol for cDNA purification. Work with a minimum of 1 µL amplified cDNA and a total volume of 5 µL.
- Prepare to work very timely for this protocol
    - Preheat a PCR thermocycler to 55 °C, with preheat lid at 100 °C
    - Prepare ATM and NT in sufficient quantity separated over multiple tubes to facilitate multi-pipetting
- Add to each tube/well in order:
    - 10 µL TD
    - 5 µL sample (30 pg/µL = 150 pg DNA)
    - Mix by pipetting
- Add to each tube/well 5 µL ATM
    - Mix 10 times by pipetting, close/seal tubes/plate
    - Quick spin down
- Place in thermocycler and run the program:

  55°C 5 min

  10°C forever
- **As soon as** the 10 °C step starts add 5 µL NT
    - Mix by pipetting 10 times (close tubes/ seal plate) and spin down
- Incubate at room temperature for 5 min

Part 2 - Indexing and amplification of tagmented DNA

- Thaw index adapters, mix by vortex and spin down
- Prepare NPM in sufficient quantity separated over multiple tubes to facilitate multi-pipetting
- Prepare a table delineating the indexing setup scheme

- Add to each 25 µL sample (from part 1) 5 µL of both i7 and i5 indexes according to the scheme
- Add 15 µL NPM to each sample
    - Mix by pipetting 10 times
    - Spin down
- Run samples with the following PCR thermocycler program

72 °C	3 min	
95 °C	30 sec	
95 °C	10 sec	12 cycles
55 °C	30 sec	
72 °C	30 sec	
72 °C	5 min	
10 °C	forever	

STOPPING POINT 4 °C, up to 2 days

2.3.10 cDNA library cleanup/bead purification

Materials

- GC beads – CleanNGS (GC Biotech, CNGS-0050)
- 5 mL reaction tube (Eppendorf) (for bead aliquot)
- 80% EtOH (prepare fresh, 400 µL x samples)
- Nuclease-free 0.2 mL reaction vial (x samples x 2)
- Resuspension buffer (RSB) (52.5 µL x samples) (Nextera XT Kit)
- Magnetic separation device (Life technologies #AM10027)
- Mini-centrifuge for 0.2 mL tubes or strips (any will suffice)
- Bench vortex (any will suffice)

Safety

PPE, as dictated under local Health & Safety regulations.

Procedure

Refer also to pages 9-10 of the Nextera XT manual (https://tinyurl.com/nextera-xt-ref-guide-15031942).

All our protocols are performed at 18 – 22 °C room temperature (RT).

- Vortex the bead stock well, this needs to be very well and evenly mixed
- Aliquot beads, 30 µL x samples (plus extra)
- Bring the bead aliquot to RT for at least 30 min
- Vortex the bead aliquot until evenly mixed
- Spin down the sample (indexed and amplified from 2.3.9, total 50 µL)
- **Add 30 µL** of beads to each sample
    - Mix by pipetting up and down
    - Shake / vortex for 2 min
- Incubate at **RT for 5 minutes** to let cDNA bind to the beads
- Very briefly spin down and place the samples **on a magnetic separation device for 5 minutes**. Until the liquid appears completely clear and there are no beads in the supernatant.
- Pipet and discard the supernatant (80 µL), keeping the samples in the magnetic device and not disturbing the beads.
- Keep samples in the magnetic device, **add 200 µL fresh 80% EtOH** to each sample
    - Do not disturb the beads
    - Wait 30 seconds
    - Pipet and discard (use 100 µL pipet) supernatant containing contaminants
- Repeat EtOH wash: **add 200 µL 80% EtOH** to each sample, without disturbing the beads
    - Wait 30 seconds
    - Pipet and discard supernatant (use 100 µL pipet)
- Briefly spin the samples to collect liquid off the sides
- Place samples back in the **magnetic device for 30 seconds**, beads will again be collected on the side
    - Remove all remaining ethanol / supernatant with a pipet (10 µL pipet)
- Place samples at **RT for 5 minutes** until the pellet is no longer shiny, but before a crack appears. It needs to be ‘just’ dry, matte with no shine.

- Once the beads are dry add **52.5 µL of RSB to all samples** to cover the bead pellet
    - Remove samples from the magnetic device
    - Mix to re-suspend the beads by (multi)pipetting (can scrap of beads from the side)
    - Shake/vortex for 2 minutes
    - Very quick spin down
- Incubate at **RT for 2 min** to rehydrate
- Briefly spin the samples to collect liquid off the sides
- Place samples back in the **magnetic device for 2 minutes**, until the solution is completely clear
- **Transfer the clear supernatant (50 µL**) containing purified cDNA to a nuclease-free 0.2 mL tube
    - Make immediately an aliquot for Bioanalyser analysis to prevent unnecessary freeze-thawing cycles.
- Label and store at -20 °C for sequencing

Check quality of cDNA by Bioanalyser High Sensitivity DNA Kit (Agilent #5067-4626). Example electrographs in **Figures 2-8, 2-9 and 2-10**.

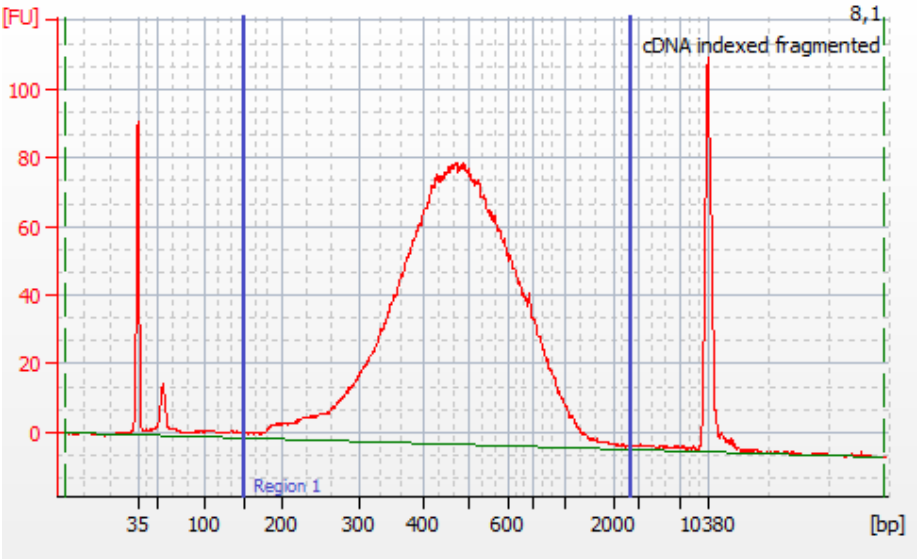

Figure 2-8 Example electrograph for a good cDNA library run with a Bioanalyser High Sensitivity DNA Kit (Agilent #5067-4626). Though primer dimers are here still present and follow up cleaning is recommended. The region for smear analysis is indicated between vertical blue lines. Example of an acantharian sample. The peaks on the outsides are markers.

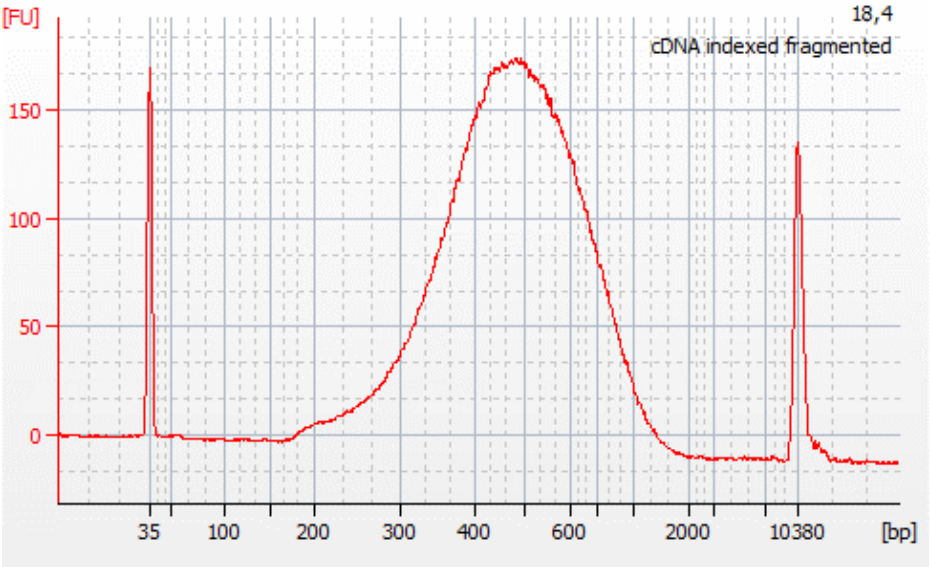

Figure 2-9. Example electrograph for a desirable cDNA library run with a Bioanalyser High Sensitivity DNA Kit (Agilent #5067-4626). Example of an acantharian sample. The peaks on the outsides are markers.

Figure 2-10. Example electrograph for a desirable cDNA library run with a Bioanalyser DNA 7500 Kit (Agilent # 5067-1506) instead of a Bioanalyser High Sensitivity DNA Kit (Agilent #5067-4626). This still allows for smear analysis (area indicated by vertical blue lines), though the concave parabola is less clear. This is more cost-effective than using the high sensitivity kit. Example of an acantharian sample. The peaks on the outsides are markers.

2.3.11 Follow up steps: library quality control; sample normalisation/dilution and pooling for sequencing

The quality and quantity control of the generated cDNA libraries is performed using the Agilent High Sensitivity DNA kit (Agilent #5067-4626). In case primer dimers or adapters are still present, an additional step of cleaning with magnetic beads is to be performed. A bead to sample ratio of 0.7:1 was found to be efficient in eliminating both primer dimers and remaining adapters. The cDNA libraries are normalised to equal molarity, as well as fragment size before the final pooling and subsequent sequencing. Calculate nM cDNA of each sample as: nM DNA = [ng/µL] x 10^6 / (660 x fragment length bp). Where the concentration in ng/µL and the average fragment length in base pairs are obtained from Bioanalyzer smear analysis (**Figure 2-8**). The molarity upon which the cDNA libraries are normalised is determined based on the yield of cDNA, as well as the requirements for the subsequent sequencing (e.g. > 0.5 nM). The final pool of all the samples should again be checked using the Bioanalyzer in order to verify that the normalisation process was successful. The pools are now ready for sequencing.

2.4. Quantitative PCR

qPCR assays are used to detect the presence of prey genetic material in DNA extracted from NCM organisms, and provide a semi-quantitative estimation of its concentration. If performed on cultures of NCM organisms with a known feeding history, provide information about the potential for retention of prey genetic material and eventually the duration of retention. Cultures of NCM organisms need to be subjected to this technique when actively feeding on the target prey, following prey depletion and during starvation.

Materials

- NucleoSpin Soil DNA isolation kit (Macherey-Nagel, Düren, Germany)
- Primers specific for the target prey species
- FAST SYBR Green Master Mix (Applied biosystem, Thermo-Fisher Scientific, Waltham, USA)
- Molecular biology grade H_20
- StepOnePlus Real Time PCR system (Applied Biosystems, Foster City, CA)

Procedure

- Extract DNA with NucleoSpin Soil DNA isolation kit following the manufacturer's instructions. Refer to pages 16-20 of the manual : https://www.mn-net.com/media/pdf/f5/e4/7a/Instruction-NucleoSpin-Soil.pdf
- Elute DNA in 35 µL of the elution buffer (provided in the kit)
- Add 1 ng of DNA to 5 µL FAST SYBR Green Master Mix
- Add reverse and forward primes in a final concentration of 125 nM
- Bring to a final volume of 10 µL adding nuclease free water
- Run samples with the following qPCR program
- Run control reaction with purified water in place of DNA (as a general control for extraneous nucleic acid contamination.)

The following program is run:

95 °C	20 sec	
95 °C	3 sec	40 cycles
60 °C	30 sec	

Melting curve analysis

95 °C	15 sec	
60 °C	1 min	
+0.3 °C	15 sec	Repeat up to 95 °C

2.5. Fluorescence in situ hybridisation (FISH)

Fluorescence in situ hybridisation can be used to detect the presence of prey genetic material in NCM organisms and visualize its location inside the cell. Different from qPCR, this technique does not allow the quantification of prey DNA in the sample but is useful to discriminate for presence/absence of prey DNA within individual cells of the same population.

Materials

- Fluorescent DNA probe specific for the target prey species (target sequence with fluorophore at the 5´) suggested fluorophore: Alexa 488 (Invitrogen)

- Incubator/ oven (37 °C)
- Glass microscope slides and coverslips
- Epifluorescence microscope (e.g. Axio Vert.A1 equipped with a 117 Colibri 7 (Zeiss) light source)
- Deltapix camera HDMIDPX16 119 (Denmark, Smorum)
- V2.1.2806 USB Capture HDMI4+ (Nanjing Magewell Electronics, 120 Nanjing, China)
- Magewell Capture Express software

Solutions :

- 50% dimethylformamide (DMF) in molecular grade water
- 25 x SET buffer stock solution prepared in water as follows :
  - 3.75 M NaCl
  - 25 mM EDTA 0.5 M Tris/HCl
  - adjust pH to 7.8
  - filter-sterilise
- hybridization buffer prepared as follow:
  - 5 x SET solution diluted in water (1:5 from the 25X stock)
  - 0.1 % (v/v) Nonidet-P40 (Sigma N-6507)
  - 30% (v/v) Formamide
- Wash buffer: 1 x SET diluted in water (1:25 from the 25X stock)
- DAPI stock solution: 1 µg/µL. (DAPI: 4´,6-diamidino-2-116 phenylindole, Invitrogen)
- DAPI working solution prepared as follow:
  - 1 mL Citifluor
  - 0.5 mL H_20
  - 1,5 µL DAPI stock solution

Procedure

- Bleach chlorophyll by incubating the filters with cell sample (prepared as in section 3.2) for 1 h in 1 mL of 50% DMF (optional, only required if the chlorophyll signal is expected to cover the fluorescent signal of the fluorophores)
- Add 1 µL of the probe stock solution to 10 µL of the hybridization buffer
- Cover the filters with hybridization buffer
- Incubate for 3 h at 37 °C
- Remove filters from the hybridization buffer
- Cover the filters with the washing buffer
- Incubate for 10 minutes at 37 °C

- Remove the filters from the washing buffer and dry them on paper for 5 sec
- Place filters on microscopy glass slides
- Cover the filters with 30 µL of DAPI working solution
- Cover with glass coverslip
- Proceed with microscopy inspection or store at 4 °C (for up to 1 week)

- Detect the NCM organism on the filter using firstly a lower magnification (e.g., 100x) and UV light (excitation wavelength 350 nm). The DAPI stain of the NCM nucleus returns a blue fluorescent signal (emission 450 nm).
- Switch to a higher magnification (400x), and to the excitation wavelength of the fluorophore probe (480 nm if fluorophore is Alexa 488). The fluorescent signal of the probe (green emission, 530 nm if fluorophore is Alexa 488) would only be observable if hybridization took place, i.e. if the NCM organism contained prey nuclei material.

- Acquire images

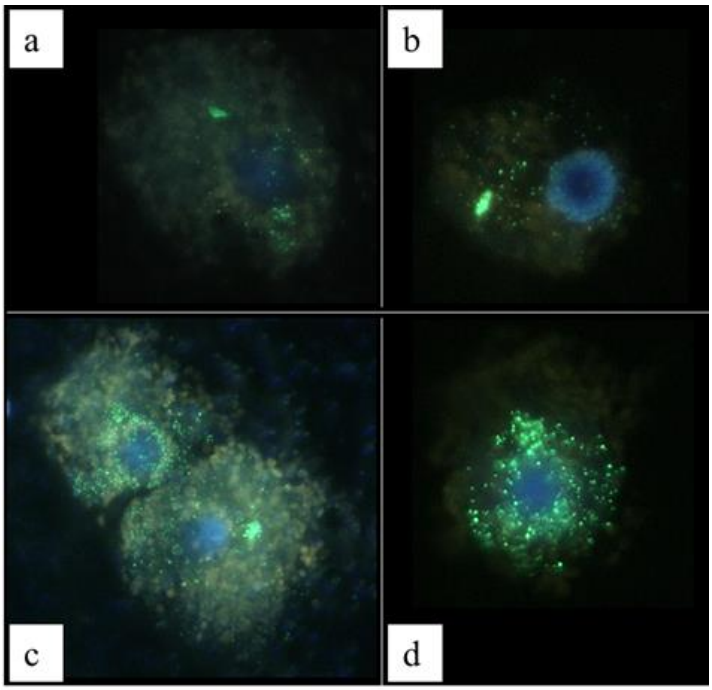

Figure 2-11. Example Micrographs of *Strombidium*. cf. *basimorphum* cells hybridised with the probe for the prey TxD2 DNA region (Alexa Fluor 488 dye labelled) and counterstained with DAPI. Blue: ciliates nuclei, green: prey DNA, light orange: chloroplasts.

2.6. Procedure verifications

2.6.1 SMART-Seq v4 or NEBNext protocol

Methods were first established using the SMART-Seq v4 (Takara #634891) methodology. The NEBNext kit (NEB #E6421) is newer on the market and provides more customised buying options and thereby significantly reducing the cost. Several samples have been tested to assess the NEBNext kit methodology as an alternative to the cDNA synthesis, amplification and purification by SMART-Seq v4. The NEBNext protocol as we used is outlined above in **sections 2.3.6, 2.3.7, and 2.3.8**. This is not a full methodological comparison, but provides us with sufficient insights into the results obtained from both protocols as to assess whether the NEBNext protocol could substitute SMART-Seq v4 as a more cost-effective alternative.

The NEBNext protocol is quite similar to the protocol utilised for SMART-Seq v4. Major differences being that the NEBNext uses less separate reagents and a preassembled mastermix. This increases the ease of the protocol. The purification step by NEBNext protocol is more elaborate, possibly allowing better clean-up of primer dimers. Overall, we find similar results for both protocols (**Figure 2-12**).

In conclusion, the NEBNext protocol can be used alternatively to the Smart-Seq v4 kit, providing a more economic workflow.

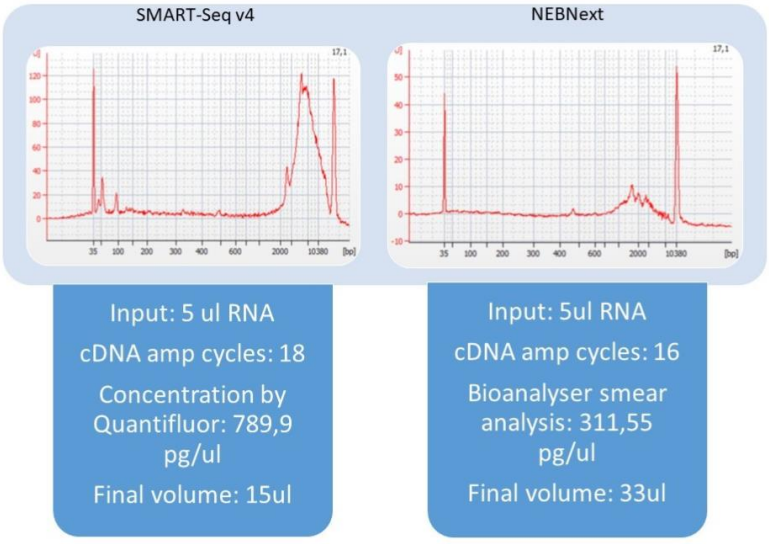

Figure 2-12. Example comparison of Bioanalyser electropherograms of an Acantharia single cell sample amplified cDNA. The right graph shows amplified cDNA by the NEBNext kit the left on by the Takara SMART-Seq v4 kit. Note that the final elution volume for the NEBNext sample is larger and that the number of cycles has been lowered as well.

2.6.2 Number of amplification cycles optimisation

Even though the RNA extraction kit provides information on the required amount of RNA to further process into library preparation, the yield was low as only one protist cell was used. As a result, even the most sensitive kit for RNA quantification (Agilent RNA 6000 Pico Kit, qualitative range of > 50 pg/μL) was often not able to allow us to quantify the total RNA content. The initial amount of RNA that is used for the preparation of cDNA, is critical as it is the criterion for selecting the number of cycles to be applied to the PCR for the amplification of the cDNA. Accordingly, the number of cycles applied after the cDNA synthesis is critical for the quality of the final transcriptome. Over-amplification can result in higher yield of cDNA, however it introduces a bias towards more abundant transcripts. For this purpose, different number of amplification cycles were applied as part of the preliminary work to test the optimal amplification strategy (data not shown). As a result, the protocol and number of amplifications were adjusted for each species given their variable content of RNA (**Table 2-1**).

Table 2-1. Number of amplification cycles applied for cDNA amplification for each species and cDNA kit combination tested.

Species	cDNA kit	Number of cycles
Strombidium basimorphum	SMARTseq-v4	18
Prymnesium parvum	NEBNext	25
Acantharia	SMARTseq-v4	18
Acantharia	NEBNext	16

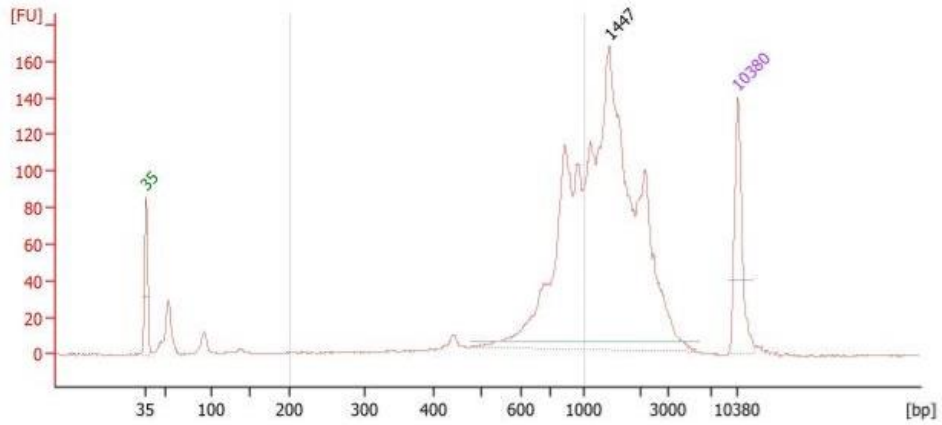

Figure 2-13. Example of Bioanalyser electropherogram of *Strombidium basimorphum* cDNA after 18 amplification cycles (NEBNext kit).

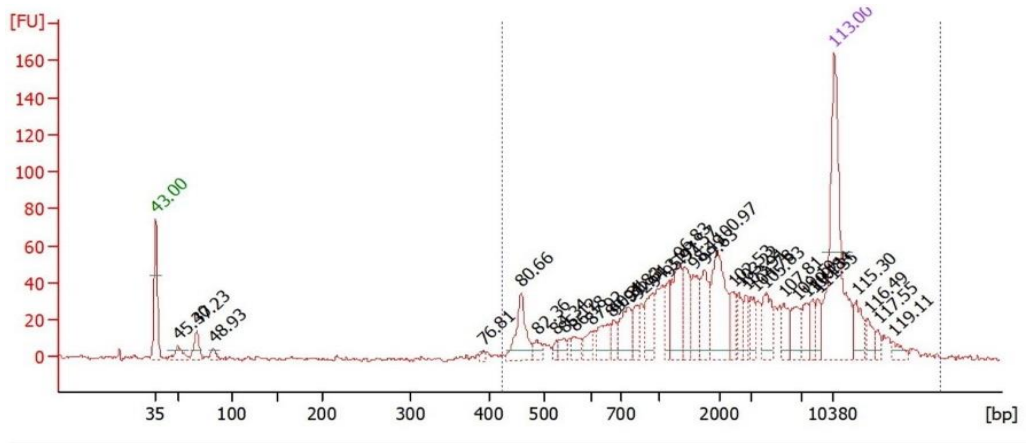

Figure 2-14. Example of Bioanalyser electropherogram of *Prymnesium parvum* cDNA after 25 amplification cycles (NEBNext kit).

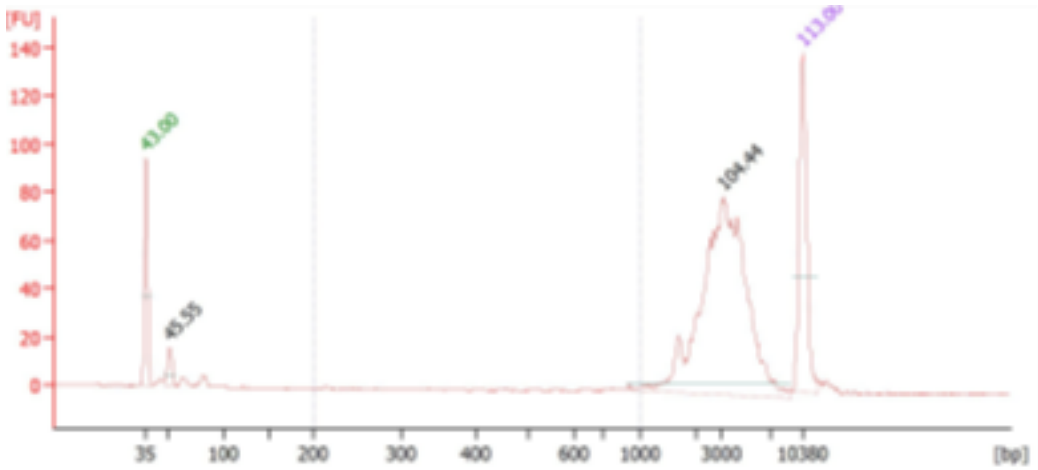

Figure 2-15. Example of Bioanalyser electropherogram of Acantharia cDNA after 18 amplification cycles (NEBNext kit).

2.6.3 Testing single-cell sampling for transcriptomics of uncultivatable protists

Studies of eSNCMs are extremely challenging to perform, largely depending on chance encounters with suitable experimental material at sea. Preliminary tests for RNA sampling have been performed in order to determine the best sampling and preservation procedure for samples from which RNA needs to be extracted for transcriptomics. From these we have established methods for sampling and subsequent extraction of RNA from single cells of eSNCMs, such as Radiolaria. This work is conducted under field conditions, where facilities are not often as good as in terrestrial-bound laboratories. Thus, sample preparations are typically not conducted working in a controlled air-stream, under a hood, nor has the work area been treated with RNAse inhibitors (or similar). Aseptic techniques and gloves, to minimise further contamination, have been used though.

Samples have been collected by horizontal plankton net tows and specimens of interest were isolated using a pulled-glass Pasteur pipette and deposited in a petri-dish with filter-sterilised seawater (FSW, 0.2-µm-pore-size). Specimen were left in FSW for at least several hours. This allows for self-cleaning of particles attached to the cells and dilution to extinction of any organisms accidentally taken with. The treatments and samples obtained are given in **Table 2-2.**

Table 2-2. Experimental treatments and the number of samples per treatment. β- = RA1 buffer without β-mercaptoethanol; β+ = RA1 buffer with β-mercaptoethanol; FF = flash frozen (liquid N_2) and stored at -80 °C; -80 = stored at -80 °C; RT = room temperature. The numbers indicate the total number of samples taken, the number of which contain Acantharia are indicated in brackets. The remainder of the samples contain 'unknowns', foraminifera, Taxopodia, Collodaria, and/or *Ornithocercus* sp.

Total	β-	β+
FF	12 (8)	12 (8)
-80	4 (3)	7 (5)
RT	5 (3)	6 (4)

Samples were sent to Genoscope for analysis. For selected samples cDNA profiles have made. These cDNA profiles show that RNA extraction and subsequent processes work for Acantharia which have been flash frozen or directly put in -80 °C, whereas the addition of β-mercaptoethanol did not matter (**figure 2-18**). The RNA extraction and cDNA synthesis did not seem to work for Collodarian samples (**figure 2-19**). Additional analyses are yet to be performed, but in general we already find that freezing will give that best results. Different methods will be compared, seeking approaches that could facilitate field sampling where liquid nitrogen might not be available.

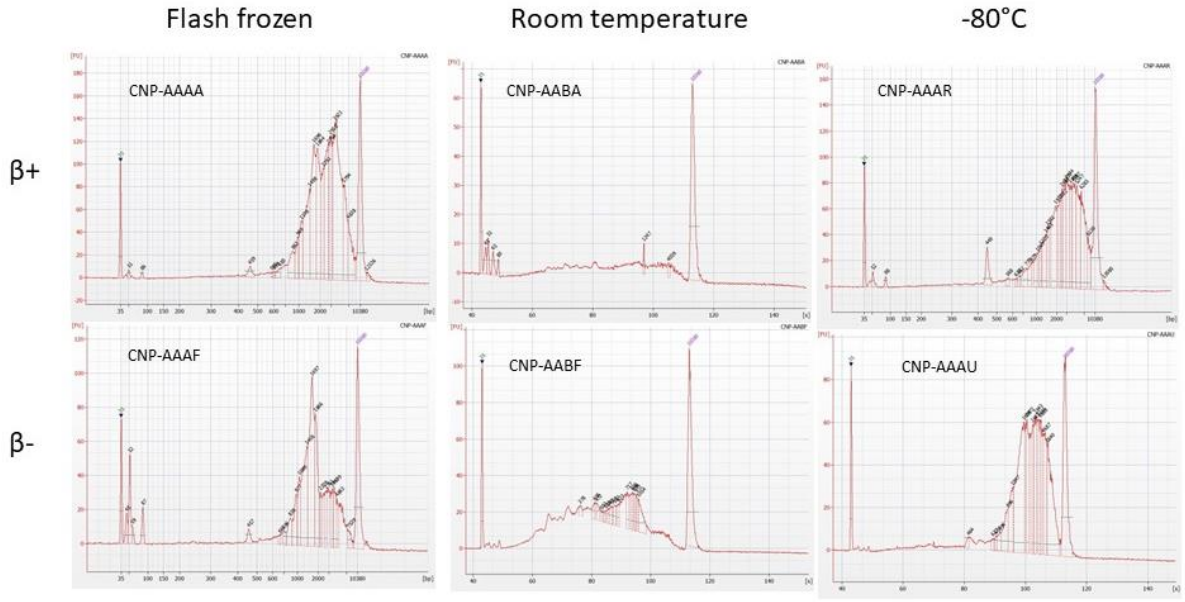

CNP_AAAA	20_B_FF	42ng	valid
CNP_AAAF	25_-B_FF	6,51ng	valid
CNP_AAAR	38_B_-80	32,1ng	valid
CNP_AAAU	41_-B_-80	25,56ng	valid
CNP_AABA	47_B_RT	2,828ng	Not valid
CNP_AABF	52_-B_RT	34,5ng	Not valid

Figure 2-18. cDNA profiles for selected samples of Acantharia. β+ is with β-mercaptoethanol whereas β- is without it added to the RNA extraction buffer. Total cDNA yield per sample is given in the table below the plots, as well as the validity of the cDNA profile.

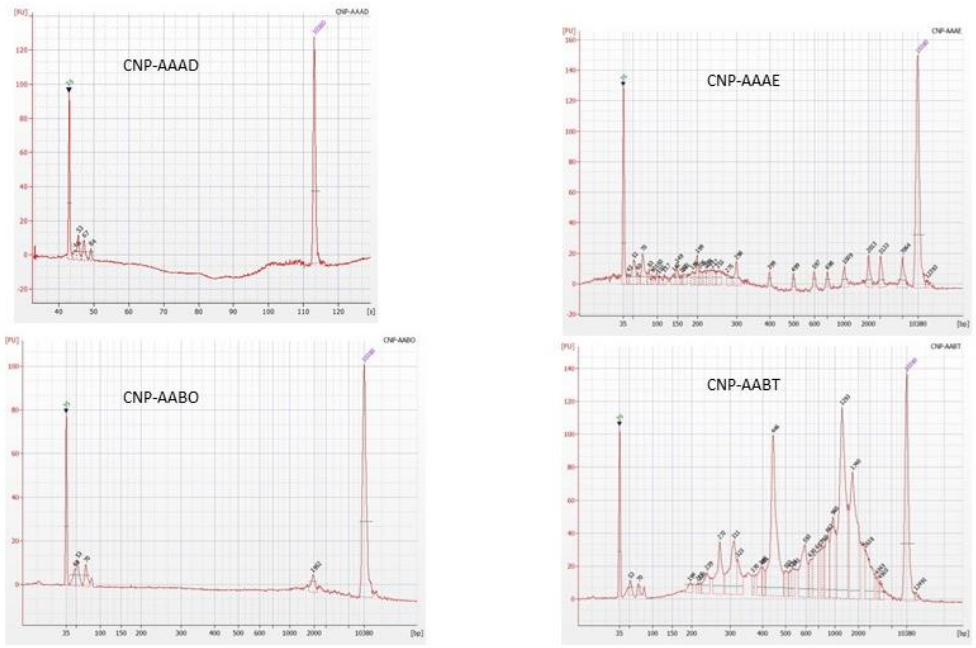

CNP_AAAD	23_B_FF	17,76ng	Non validé
CNP_AAAE	24_-B_FF	10,86ng	Non validé
CNP_AABO	61_B_FF	2,24ng	Non validé
CNP_AABT	66_-B_FF	11,63ng	validé

Figure 2-19. cDNA profiles for selected samples of Collodaria (AAAD & AAAE), dinoflagellate (AABO) and foraminifera (AABT). All samples are of the flash frozen treatment, AABT and AAAE were without β-mercaptoethanol added to the RNA extraction buffer, the other two with. Total cDNA yield per sample is given in the table below the plots, as well as the validity of the cDNA profile.

Concluding remarks for sampling of Radiolaria for Transcriptomic analysis

Work on the eSNCM Radiolaria present challenges, such as little available material and that is from the field only. Typically these organisms are sampled in “rough-and-ready” conditions. The tests of RNA extraction with Radiolaria show that the sampling methodology for transcriptomic purposes works under these suboptimal conditions. A rapid freezing step is still needed, but liquid nitrogen for freezing is not an obligatory requirement, nor is the use of β-mercaptoethanol. This is convenient as both of these present health-and-safety risks. However, the quality of the cDNA profiles can vary, sometimes with large fragments within the cDNA smear, which is not ideal. In consequence, for the final protocols different buffer and extraction kits have been used (finalised as in section 2.3). Unfortunately, our tests failed for Collodaria colonies, likely because the gelatinous colonial form interferes with the preservatives or inhibits the RNA extraction. This forces us to explore different protocols. Transcriptomes of solitary Collodaria have been successful in a study by Liu et al. (2019) and libraries of colonial species have been made under the context different projects, these protocols could be explored if needed.

2.7. References

Burns, J. A., Pittis, A. A., and Kim, E. (2018). Gene-based predictive models of trophic modes suggest Asgard archaea are not phagocytotic. *Nat. Ecol. Evol.* 2, 697–704. doi:10.1038/s41559-018-0477-7.

Faure, E., Not, F., Benoiston, A.-S., Labadie, K., Bittner, L., and Ayata, S.-D. (2019). Mixotrophic protists display contrasted biogeographies in the global ocean. *ISME J.* 13, 1072–1083. doi:10.1038/s41396-018-0340-5.

Graham, L. B., Colburn, A. D., and Burke, J. C. (1976). A new, simple method for gently collecting planktonic protozoa. *Limnol. Oceanogr.* 21, 336–341. doi:10.4319/lo.1976.21.2.0336.

Leles, S. G., Mitra, A., Flynn, K. J., Stoecker, D. K., Hansen, P. J., Calbet, A., et al. (2017). Oceanic protists with different forms of acquired phototrophy display contrasting biogeographies and abundance. *Proc. R. Soc. B Biol. Sci.* 284, 20170664. doi:10.1098/rspb.2017.0664.

Leles, S. G., Mitra, A., Flynn, K. J., Tillmann, U., Stoecker, D., Jeong, H. J., et al. (2019). Sampling bias misrepresents the biogeographical significance of constitutive mixotrophs across global oceans. *Glob. Ecol. Biogeogr.* 28, 418–428. doi:10.1111/geb.12853.

Liu, Z., Hu, S. K., Campbell, V., Tatters, A. O., Heidelberg, K. B., and Caron, D. A. (2017). Single-cell transcriptomics of small microbial eukaryotes: Limitations and potential. *ISME J.* 11, 1282–1285. doi:10.1038/ismej.2016.190.

Liu, Z., Mesrop, L. Y., Hu, S. K., and Caron, D. A. (2019). Transcriptome of *Thalassicolla nucleata* holobiont reveals details of a radiolarian symbiotic relationship. *Front. Mar. Sci.* 6, 284. doi:10.3389/fmars.2019.00284.

Mansour, J., Anestis, K., Not, F., and John, U. (2021a). cDNA library preparation from total RNA extracts of Single-cell marine protists (e.g. Acantharia, Strombidium basimorphum, and Prymnesium parvum) for transcriptome sequencing V.2. *protocols.io*. doi:10.17504/protocols.io.brw3m7gn.

Mansour, J., Anestis, K., Not, F., and John, U. (2021b). Single-cell total RNA extraction from marine protists (e.g. Acantharia, Strombidium cf basimorphum, and Prymnesium parvum) V.2. *protocols.io*. doi:10.17504/protocols.io.bp6xmrfn.

Mansour, J., and Not, F. (2021). Isolation of clean single-cell samples for physiological or molecular experiments (Radiolaria, Acantharia) V.2. *protocols.io*. doi:10.17504/protocols.io.bqvrmw56.

Mansour, J. S., and Anestis, K. (2021). Eco-Evolutionary Perspectives on Mixoplankton. *Front. Mar. Sci.* 8, 666160. doi:10.3389/fmars.2021.666160.

Mansour, J. S., Norlin, A., Llopis Monferrer, N., L'Helguen, S., and Not, F. (2021c). Carbon and nitrogen content to biovolume relationships for marine protist of the Rhizaria lineage (Radiolaria and Phaeodaria). *Limnol. Oceanogr.* 66, 1703–1717. doi:10.1002/lno.11714.

Maselli, M., Altenburger, A., Stoecker, D. K., and Hansen, P. J. (2020). Ecophysiological traits of mixotrophic *Strombidium spp*. *J. Plankton Res.* 42, 485–496. doi:10.1093/plankt/fbaa041.

Song, Y., Milon, B., Ott, S., Zhao, X., Sadzewicz, L., Shetty, A., et al. (2018). A comparative analysis of library prep approaches for sequencing low input translatome samples. *BMC Genomics* 19, 1–16. doi:10.1186/s12864-018-5066-2.

MixITiN Deliverable 3.8 Report

Section 3

Development And Validation Of New Methods For Measuring Predation Rates In Mixoplanktonic Protists

Edited by:

Guilherme D Ferreira & Albert Calbet

Contributing authors:

Guilherme D Ferreira & Albert Calbet, Institut de Ciències del Mar Spain

Joost S Mansour & Fabrice Not, Université Pierre et Marie Curie France

Nikola Medić & Per J Hansen, University of Copenhagen Denmark

Filomena Romano & Paraskevi Pitta, Hellenic Centre for Marine Research Greece

Kevin J Flynn, Plymouth Marine Laboratory UK

Aditee Mitra, Cardiff University UK

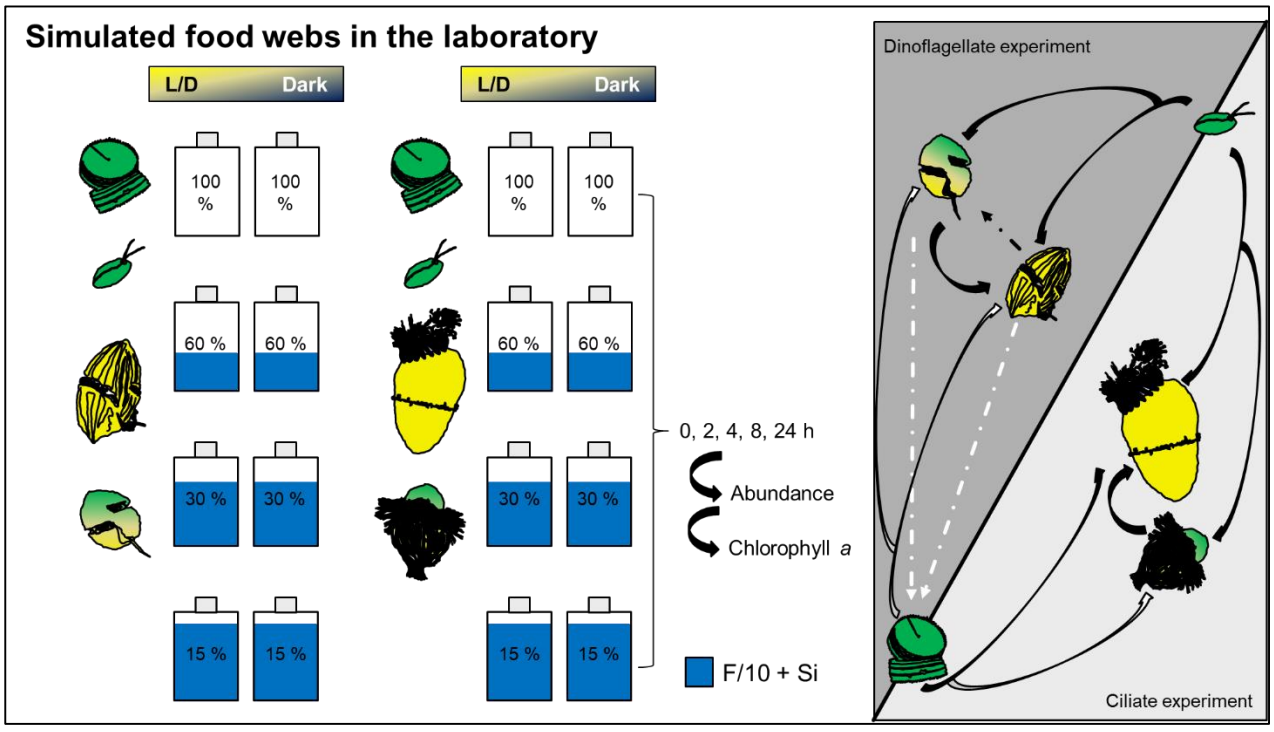

Table of Contents

3.1 Introduction

Despite the supposed relevance of mixoplankton (Stoecker *et al.* 2017, Flynn *et al.* 2019) we still lack standardized techniques to measure their grazing impact in the field. This is mostly because of the difficulty in separating grazers and prey (similar sizes and/or pigments). To date, most approaches to estimate mixoplankton grazing are based on extrapolating to the field the rates obtained in the laboratory (e.g. Yih *et al.* 2004). For instance, to estimate grazing on protists it is common to measure the disappearance of prey during 24h incubations under strictly controlled conditions. Given the impossibility to obtain data for all the species present at sea on a given time, and to predict the particular interactions between groups, the approach is, if not completely erroneous, at least very limited and inaccurate. Moreover, the fact that some species, like *Prymnesium parvum* or *Karlodinium armiger*, release allelopathic compounds (e.g. Shilo & Aschner 1953, Rasmussen *et al.* 2017) that may cause immobilization and lysis of potential prey may introduce further complications to the interpretation of the results.

To overcome this problem, we investigated several existing methods and adapted them to measure herbivory in mixoplankton. For instance, in mixotrophic organisms, stable isotopes have been used to track contributions of symbiotic partners to the growth of their holobiont (reviewed in Ferrier-Pagès & Leal 2019). While the stable isotope approach has been predominantly used in plankton research to assess non-phagotrophic uptake, it has also been used to show feeding, examples include: feeding of invertebrate larvae on both bacteria and diatoms (Leroy *et al.* 2012); phytodetritus uptake by benthic foraminifera (Enge *et al.* 2016) and heterotrophy in corals (Seemann *et al.* 2013). A use of stable isotope probing to quantify contribution of photosynthesis and bacterivory to the metabolic needs of a mixotrophic protist has been reported by Terrado *et al.* (2017). The methodology used here uses a similar approach but attempts to assess phagotrophy on live algal cells.

We also evaluated the pros and cons of using the addition of rotenone (Ferreira & Calbet 2020), a mitochondrial inhibitor, as a means to partition the contribution of protozooplankton and mixoplankton within a standard dilution technique. This chemical has been previously used to get rid of contaminations by heterotrophs in large algal culture facilities. In theory, by inhibiting protozooplanktonic grazing, in a natural ecosystem the remaining one should be result of mixoplankton activity (provide these

organisms are not affected by rotenone). Here, we present our results on the effects of different concentrations of rotenone on survival, growth and grazing rates of several species of mixoplankton and protozooplankton.

Conversely, other traditional methods to estimate protozoan bacterivory or herbivory rely on the addition of fluorescently labelled tracers (usually bacteria, FLB, or algae, FLA) to the population. These fluorochromes enable the estimation of incorporation rates of the tracer and obtain an approximation to grazing (Sherr *et al.* 1987). Yet, this widely used technique to account for bacterivory has been seldom used to estimate feeding activity of mixoplankton (but see for example Unrein *et al.*, 2014 for mixotrophic bacterivory). Even less studies target algae instead of bacteria as prey, mostly because of a discrimination against inert particles (Verity 1991) by protistan grazers, which lead to the replacement of dead FLA (Rublee & Gallegos 1989) for live ones (e.g., Putt 1991, Li *et al.* 1996), with all the due advantages and disadvantages. As such, we used this approach to assess and compare mixoplankton and protozooplankton grazing impacts. Therefore, our experiments included several species of different taxonomic groups, nutritional strategies, and feeding mechanisms. This approach is not novel in itself, however, the implementation of this for understanding mixoplanktonic activity is novel. Therefore, our experiments included several species of different taxonomic groups, nutritional strategies, and feeding mechanisms (Ferreira *et al.* in prep.).

Finally, given the caveats associated to all the previously described methods, we proposed to decipher mixoplanktonic predation in the most widely used technique to estimate protistan grazing rates, the dilution technique (Landry & Hassett 1982). This technique is based on the diminution of encounter rates between grazers and prey, by sequentially diluting the natural planktonic community with particle-free water. The technique relies on two precepts: a constant proportionality between microplankton grazing rates and prey concentration, and a constant rate of instantaneous phytoplankton growth through the dilution series. In the original wording of this technique, the growth of the “phytoplankton” prey is assessed by using chlorophyll a (Chl a) as a proxy for its biomass, and the grazing is assumed to be exclusively due to “microzooplankton” (i.e., de facto protozooplankton). Thus, it becomes clear that the activity of mixoplankton is simultaneously “phytoplankton” and “microzooplankton”, effectively rendering the dilution grazing technique blind to this form of mixotrophy (Paterson *et al.* 2008, Calbet *et al.* 2012) and, therefore, they are usually omitted from the interpretation of the results.

Keeping this in mind, we designed a set of laboratory experiments to feed a mathematical model (to be built) in order to extract the contribution of mixoplankton to the total predation measured in these experiments (Ferreira *et al.* submitted).

3.2 Stable Isotopes for the assessment of prey uptake by eSNCM Acantharia

3.2.1 Methods

The stable isotope methodology was tested with the endosymbiotic Specialist NCM (eSNCM) Acantharia (Radiolaria) and prey *Isochrysis galbana*. Symbiotic Acantharia (clade F3b) were collected, as in Mansour *et al.* (2021), by gentle plankton net tows along the sub-surface in the bay of Villefranche (Mediterranean Sea, Villefranche-sur-Mer, 43°41′10″ N, 7°18′50″ E, France). Acantharia from the genus *Amphistaurus sp.*, *Acanthostaurus sp.* and *Acanthometra sp.* were left to self-clean in Filtered Sea Water (FSW, 0.2-µm-pore-size), and transferred twice to clean FSW. The specimens used for experiments all harboured photosynthetic symbionts which provide the hosts with photosynthates (Anderson 1978, Anderson *et al.* 1983, Decelle *et al.* 2012, Probert *et al.* 2014).

I. galbana (strain RCC 178) was grown in 50 mL K/2 medium without extra nitrogen addition, and subsequently incubated for a minimum of 24 h with 95 µM ^{13}C; 0.12 µM $^{15}NO_3$ and 0.02 µM $^{15}NH_4$. Prior to experimental incubations, *I. galbana* was filtered onto a 0.2 µm filter, rinsed with FSW to remove the remnants of enriched nutrients, and subsequently submerged and re-suspended in FSW. The vitality of the culture was ascertained by the observation of motile cells. A sample of the new (^{13}C/^{15}N labelled) suspension of *I. galbana* was fixed in a final concentration of 0.25 % glutaraldehyde (1 mL total volume) for subsequent flow cytometry cell counts (T0 sample). For the assessment of the enrichment of the prey, a remainder of 30 mL of the culture to be used with Acantharia incubations was filtered on pre-combusted GF/F for isotopic analysis.

Of the originally isolated and acclimated Acantharia cells, a total of 40-60 were transferred to a 6-well culture plate prefilled with 1 mL FSW. The *I. galbana* prey were then added to the well in a volume of 10 mL to start the incubation. After five hours of dark incubation, a sample of *I. galbana* was again fixed in a final concentration of 0.25 % glutaraldehyde (1 mL total volume, T5 sample). The Acantharia were pipetted through three instances of clean FSW to remove attached prey and dilute out any residual prey. Finally, the Acantharia were picked and put on pre-combusted GF/F, and a separate filter with FSW equal in volume to the picked Acantharia. This last sample was taken to assess the contribution of any remaining prey to the Acantharia sample. The experimental

incubations were done in triplicate, and in duplicate with unlabelled prey. All experimental incubations were in an incubator with a 14:10 Light/Dark (L/D) cycle at 24 °C with 100-120 µmol photons m^{-2} s^{-1}. This temperature was the same as in the field at the time of the experiment. All GF/F Filters were directly stored at -20 °C until isotopic analysis. The complete analysis is still pending at the time of writing.

3.2.2 Results

Uptake of prey was investigated by isotopic ratio change in the host after incubations with isotopically labelled prey. Acantharia can clearly uptake ^{15}N and ^{13}C (**Figure 3-1**), which is very likely due to uptake of the algal prey. However, from this analysis alone, prey adherence to the Acantharia cell cannot be excluded. Nevertheless, we expect that adhered prey are rapidly digested. Therefore, as differences between non-enriched and enriched treatments are quite large, it is unlikely that these results are a consequence of coincidental adherence and not ingestion. To confirm whether there is actual ingestion of prey, we will conduct an experiment with LFLA (*I. galbana*) and analyse it with confocal microscopy, to ensure that prey are inside the predator and not just attached. This experiment is yet to be completed at the time of writing.

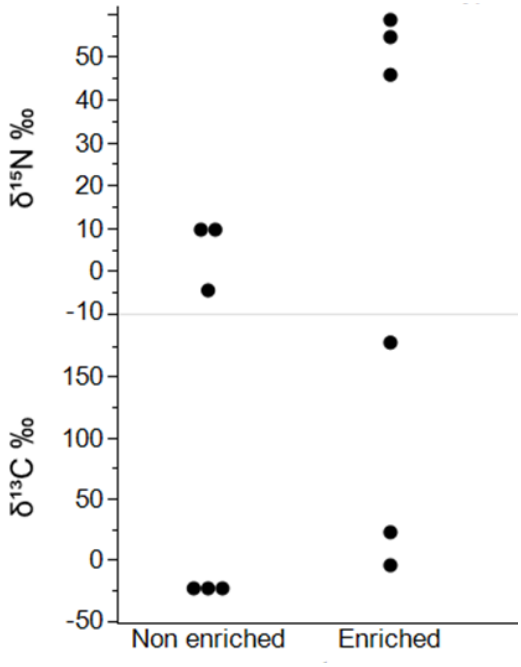

Figure 3-1 $\delta^{15}N$ (top) and $\delta^{13}C$ (bottom) in control samples containing unlabelled prey (non-enriched) and after dark incubation with labelled prey (enriched).

Calculating the algal prey C and N uptake in Acantharia from isotopic data gives the data as per **Table 3-1** for the three samples. By these measurements we calculated prey C

and N uptake as between 468 and 3510 pg C $Cell^{-1}$ h^{-1}, and between 6 and 124 pg N $Cell^{-1}$ h^{-1}. **Table 3-2** shows the carbon and nitrogen mass of samples used during these experiments. Acantharian C and N content averages 122.6 ± 65.6 ng C per cell and 26.5 ± 18.2 ng N per cell, this is coherent with results in Mansour *et al.* 2021.

Table 3-1 Algal carbon and nitrogen uptake of each Acantharia sample as measured by isotopic analysis. The average prey density during the 5 h incubation is also given (sample 1 was incubated 4 h, no prey density was measured at the end of incubation so no average density could be calculated, initial prey density was ca. $3.9x10^4$ Cells mL^{-1}).

Sample#	Average prey density (Cells mL^{-1})	Algal N uptake (pg N $Cell^{-1}$ h^{-1})	Algal C uptake (pg C $Cell^{-1}$ h^{-1})
#1	NA	125	3510
#2	$321x10^2$	4.75	136
#4	$337x10^2$	6.31	468

Table 3-2 Carbon and nitrogen content per cell and C:N ratio of each sample (Radiolaria and *I. galbana* prey).

Identifier	ng N $Cell^{-1}$	ng C $Cell^{-1}$	C:N
0 radiolaria	66.88	255.69	4.67
1 radiolaria	16.17	99.42	5.26
2 radiolaria	18.61	69.43	5.30
3 radiolaria	17.13	135.37	6.58
4 radiolaria	22.48	54.99	6.08
5 radiolaria	17.57	120.71	5.58
1 prey	0.0064	0.081	12.63
3 prey	0.0082	0.055	6.69
4 prey	0.0054	0.058	10.89
5 prey	0.0022	0.027	12.06

3.2.3 Discussion

Work on the eSNCM Radiolaria presents challenges, such as small amount of available material, and only from the field. Typically, these organisms are sampled in “rough-and-ready” conditions. As such, improvements in sustaining the cells would greatly help physiological studies. Especially for bulk isotopic approaches where quantity requirements are too high to effectively do multiple experiments. Prey uptake experiments employing stable isotopes have thus been foregone for traditional prey disappearance techniques (Frost 1972, Heinbokel 1978).

3.3 Can rotenone be used to measure mixoplankton grazing?

3.3.1 Methods

i. Cultures

The experiments were conducted with two protozooplankton, the dinoflagellate *Gyrodinium dominans* (strain ICM-ZOO-GD001) and the ciliate *Strombidium arenicola* (strain ICM-ZOO-SA001); two mixoplankton, the CM dinoflagellate *Karlodinium armiger* (strain ICM-ZOO-KA001) and the pSNCM ciliate *Mesodinium rubrum* (strain DK-2009); two phytoplanktonic flagellates, *Rhodomonas salina* (strain K-0294) and *Tetraselmis chuii*, and one phytoplanktonic diatom, *Conticribra weissflogii* (previously known as *Thalassiosira weissflogii*). All cultures were kept in a controlled-temperature room at 19°C with a 10:14 L/D cycle. Additionally, all cultures were maintained at a salinity of 38.

R. salina, *T. amphioxeia*, and *T. chuii* were kept in f/2 medium (Guillard 1975) under exponential growth conditions. These organisms were irradiated at 100-200 µmol photons m^{-2} s^{-1} provided by cool white fluorescent lights. *C. weissflogii* was grown under the same conditions with the exception that silicate was added to the medium and bubbling was applied to maintain cells in suspension. *G. dominans*, *S. arenicola*, and *K. armiger* were kept at a PFD of 35-55 µmol photons m^{-2} s^{-1} in autoclaved 0.1 µm-filtered seawater that contained EDTA and trace metals in accordance with f/2 medium. *R. salina* was offered as prey to all three species *ad libitum*. *M. rubrum* was grown under the same light conditions though kept in autoclaved 0.1 µm filtered seawater without the addition of metals and supplied with *T. amphioxeia* as prey at a proportion of ca. 5 prey per predator (Smith & Hansen 2007).

ii. Rotenone effects on growth and grazing rates

Rotenone solutions were prepared according to the guidelines provided by El-Sayed (2018). Briefly, a stock solution of 1 g L^{-1} (2.535 mM) was prepared by dissolving 0.05 g of rotenone (≥ 95 %, Sigma-Aldrich) in 50 mL of dimethylsulfoxide (DMSO) (≥ 99.5 %, PanReac AppliChem) and stored at -20°C while not in use. Standard solutions of 50 mg L^{-1} were prepared on the days of the experiments by diluting the stock solution 20 times with deionized water.

The experiments were conducted in 132 mL Pyrex bottles and consisted of three concentrations of rotenone (0.5, 1.0 and 2.0 mg L^{-1}, i.e., 1.27 to 5.08 µM), and two

controls, one containing only water (0 mg L^{-1}) and another with DMSO (solvent control). DMSO controls comprised only the highest concentration of DMSO (ca. 0.2 %) used with the rotenone solutions of 2.0 mg L^{-1}. Additionally, experimental and control suspensions were prepared in f/40 to guarantee that the incubated prey was not nutrient limited during the experimental period.

Each treatment with rotenone was conducted in triplicate experimental (predator and prey) and control bottles (only prey) and mounted on a plankton wheel (0.2 rpm). The incubations begun shortly after the onset of the light period to maximise the odds of survival for chloroplast-bearing organisms by enabling a longer period for ATP synthesis using the light phase of photosynthesis (Dawson *et al.* 1991, El-Sayed *et al.* 2018). The bottles were incubated for ca. 24 h at 19°C with a 10:14 L/D cycle. At the same time, as the preparation of the triplicate experimental and control bottles, a fourth bottle of each treatment was also prepared for sacrifice as an initial bottle. All bottles were filled gradually, in three to four steps, before being capped. The suspension was gently stirred between fillings. The formation of air bubbles during the filling and capping processes was avoided because shear may damage the organisms (Broglio *et al.* 2004) and thus bias the measured rates. Rotenone was added to the bottles with an automatic pipette just before capping them to avoid exposing the organisms to very high concentrations of the compound, though only temporarily.

For mixoplankton and protozooplankton, prey was added at saturating concentrations (**Table 3-3**) to minimise the effect of different food concentrations on the measured ingestion rate. Predator concentrations were adjusted to allow for ca. 30 % prey depletion after the incubation time (Calbet *et al.* 2013). All organisms were counted, and their volumes were assessed using a Beckman Coulter Multisizer III particle counter, with the exception of *M. rubrum*, which can escape the current flow generated by the particle counter due to their shear sensitivity (Fenchel & Hansen 2006). Aliquots of the experiments with *M. rubrum* were therefore fixed in acidic Lugol's (final concentration 5 %) and enumerated manually using a Sedgwick-Rafter counting chamber. A minimum of 300 cells (of both predator and prey) were counted using a 10× objective on an inverted microscope.

Table 3-3 Summary of the prey and predator concentrations used for the acute toxicity assays with rotenone for the mixoplankton *M. rubrum* and *K. armiger*, and protozooplankton *S. arenicola* and *G. dominans*.

Species	Target concentration, Cells mL^{-1}		Reference
	Prey	Predator	
Gyrodinium dominans	100 000	1 500	Calbet *et al.* 2013
Mesodinium rubrum	15 000	1 500	Smith & Hansen 2007
Karlodinium armiger	100 000	3 750	Arias, unpublished
Strombidium arenicola	100 000	400	Arias, unpublished

Grazing rates and average prey concentrations were calculated using Frost (1972) equations; the average concentration of grazers in each replicate was used to assess the grazing per predator (Heinbokel 1978). The magnitude of the effects of the different concentrations of rotenone on the grazing impact reduction (GIR, %) on the prey populations was assessed separately for each grazer species by **Equation 3.1**

$$GIR_{species\ A} = 100 - \left(\frac{< C >_i \times I_i}{< C >_0 \times I_0} \times 100\right) \qquad \mathbf{3.1}$$

where <*C*> and *I* are the mean predator concentration (Cells mL^{-1}) during the incubation period and the average ingestion rate (Cells Ind^{-1} d^{-1}) measured for each treatment *i* (<*C*>$_0$ and I_0 refer to the control treatment of 0 mg L^{-1}). The control suspensions with only DMSO added (no rotenone) were considered a treatment. Non-significant ingestion rates (see section *iv.* Statistical analysis) were considered 0 for the calculation of the GIR.

iii. Physiological condition effects on the response to rotenone

Additionally, whether the physiological condition of an organism affected its response to rotenone was assessed. The experiments were conducted with *R. salina,* which was exposed to rotenone both during the exponential and stationary growth phases, with all target concentrations tested at once. The experimental protocol was the same as described above.

iv. Statistical analysis

Species-specific effects of rotenone on growth were analysed using One-Way ANOVAs followed by Tukey's HSD post hoc tests (n = 15 for each treatment; Zar 2010). In the case

of *S. arenicola*, in which the assumptions of homoscedasticity were not met, the non-parametric Kruskal-Wallis test was applied, followed by the Games-Howell post hoc test (n =15; Zar 2010).

Ingestion rates were deemed significant only when the prey growth rates in the control and experimental bottles were significantly different (two-tailed Student's t-test, n = 6 for each treatment) (Saiz *et al.* 2014). Subsequently, the results for this parameter were analysed with the same procedure as described for growth rates, with the normality and homoscedasticity assumptions met and Tukey's HSD post hoc tests applied (Zar 2010). Finally, the effects of rotenone on the exponential and stationary *R. salina* were analysed separately for each growth phase using One-Way ANOVAs followed by Tukey's HSD post hoc tests. The interaction between growth phases and treatment was assessed using a two-way ANOVA followed by Bonferroni post hoc tests due to the unequal sample size between factors (Zar 2010). Calculations were conducted using IBM SPSS Statistics 25, and all the results were considered significant at $p < 0.05$.

3.3.2 Results

i. Rotenone effects on growth rates

The increase in rotenone concentration progressively reduced the growth rates of the two autotrophic flagellates tested (**Figure 3-2a,b**). The response was more drastic in *T. chuii*, which even displayed mortality at the lowest concentration (**Figure 3-2b**). Conversely, at the same concentration, *R. salina* was not significantly affected (**Figure 3-2**a; Tukey HSD, $p = 0.261$). On the other hand, the diatom *C. weissflogii* was unaffected by all concentrations of rotenone (One-Way ANOVA, $p = 0.792$; **Figure 3-2c**). DMSO at ca. 0.2 % had no visible effect in any of the target autotrophic species when compared to the treatment with 0 mg L^{-1} (Tukey HSD tests, $p > 0.05$ in all cases). The mixoplankton *M. rubrum* and *K. armiger* were not significantly affected by the presence of DMSO or by the lowest concentration of rotenone, although a negative tendency was observed for *K. armiger* in this last instance (**Figure 3-3**; Tukey HSD, $p = 0.098$). However, higher concentrations of the chemical compound severely reduced the growth rates of both protists, even resulting in mortality (**Figure 3-3**).

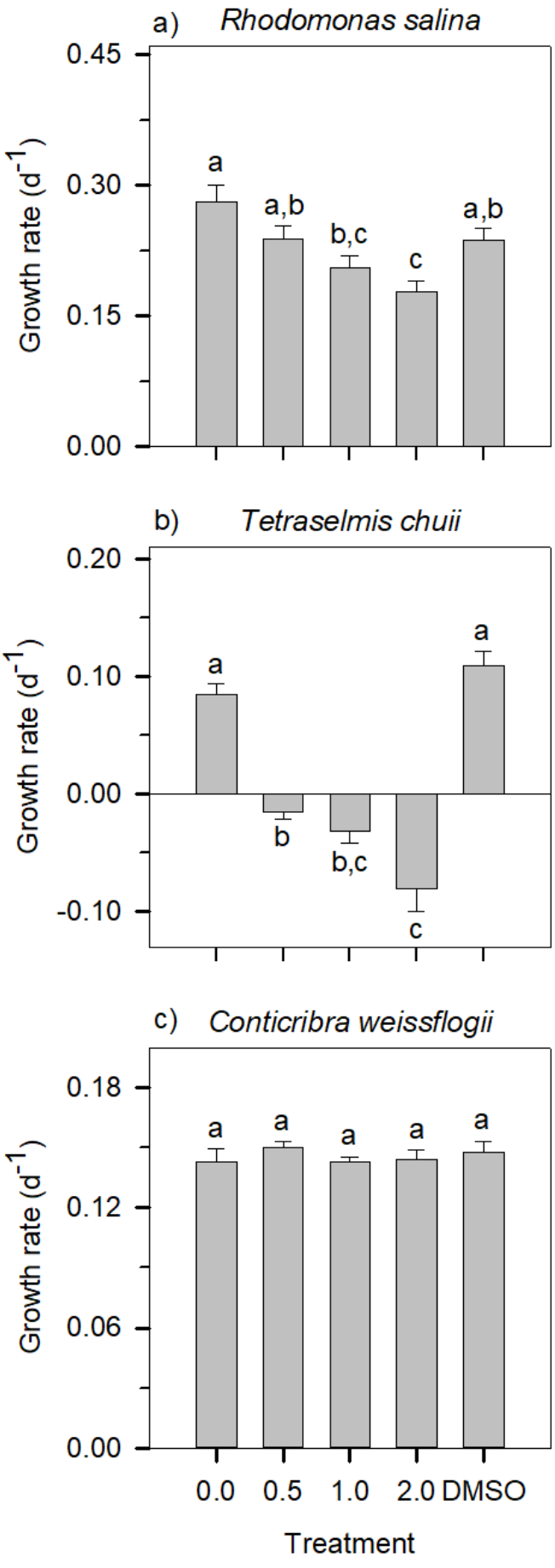

Figure 3-2 Growth rate (d^{-1}) of the phytoplankton species (a) *R. salina*, (b) *T. chuii*, and (c) *C. weissflogii* upon exposure to increasing concentrations of rotenone. The data plotted for *R. salina* include all the results for the experiments with the different grazers. Different letters within the same organism indicate statistically significant differences (Tukey HSD, $p < 0.05$). Error bars ± se.

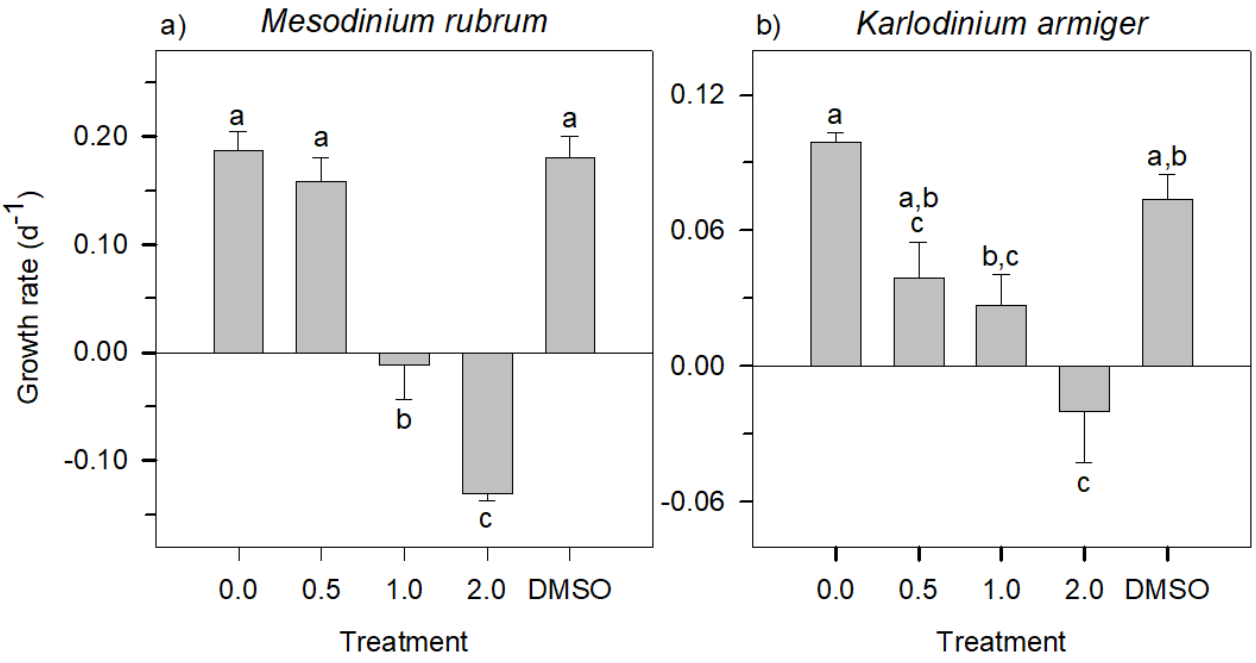

Figure 3-3 Growth rate (d^{-1}) of the mixoplankton species (a) *M. rubrum* and (b) *K. armiger* upon exposure to increasing concentrations of rotenone. Different letters within the same organism indicate statistically significant differences (Tukey HSD, $p < 0.05$). Error bars ± se.

The growth of the heterotrophic species was, on average, the most affected by rotenone (**Figure 3-4**). For the protozooplanktonic dinoflagellate *G. dominans*, the maximum growth inhibition was achieved immediately at the lowest concentration tested (0.5 mg L^{-1}); at this concentration, however, the ciliate *S. arenicola* still exhibited positive growth, although it was almost 80% lower than that under the control condition of 0 mg L^{-1}. This ciliate species appeared to be particularly sensitive, being the only species significantly affected by the sole presence of DMSO in the water (Games-Howell, $p = 0.017$). Further supporting a high sensitivity of *S. arenicola*, the ciliates that remained alive after the 24 h were nearly immotile, suggesting severe deleterious effects. Independent of the trophic mode, all motile species exhibited a reduction in the speed of displacement in the presence of the highest concentrations of rotenone, although the magnitude of the reduction was not quantified.

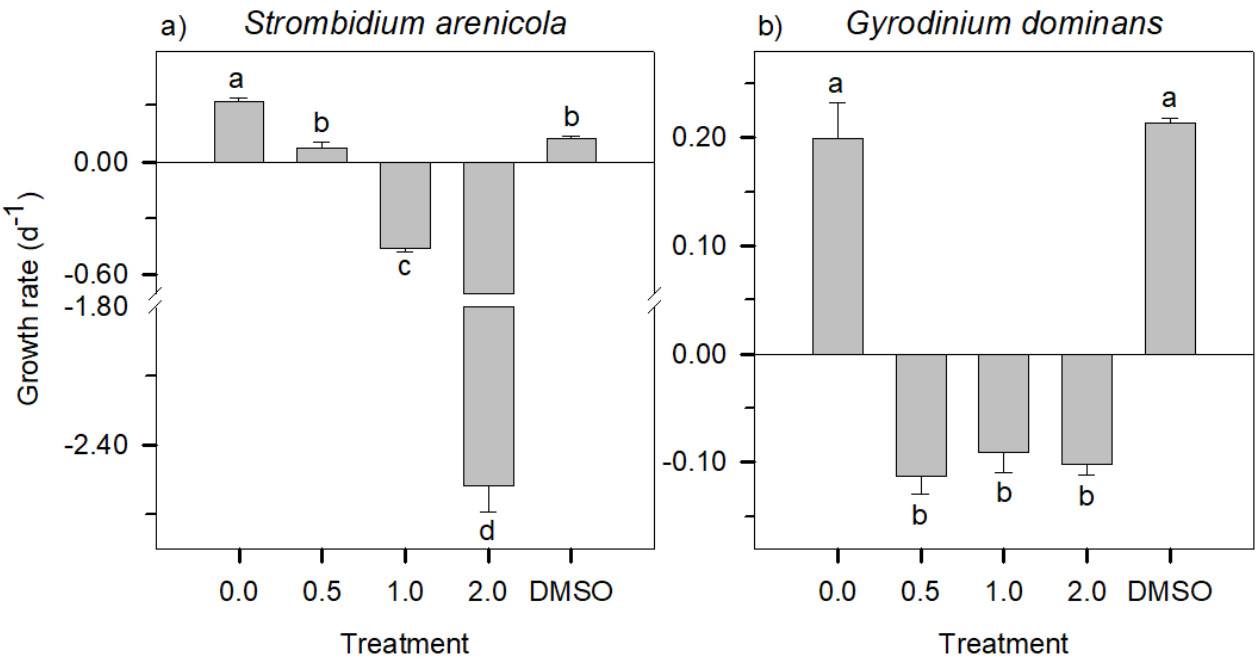

Figure 3-4 Growth rate (d^{-1}) of the protozooplankton species (a) *S. arenicola* and (b) *G. dominans* upon exposure to increasing concentrations of rotenone. Different letters within the same organism indicate statistically significant differences (Tukey HSD, $p < 0.05$). Error bars ± se.

ii. Rotenone effects on ingestion rates

The presence of rotenone impaired feeding in both ciliates, *M. rubrum* (**Figure 3-5a**) and *S. arenicola* (**Figure 3-5c**), regardless of the trophic mode of nutrition. The responses varied between no significant grazing (two-tailed Student's t-tests, $p > 0.05$ in all cases) and significantly negative ingestion rates (Tukey HSD tests, $p < 0.05$ in all cases). A significantly negative ingestion rate (1.0 and 2.0 mg L^{-1} for *M. rubrum*, and 0.5 and 1.0 mg L^{-1} for *S. arenicola*) implies a positive growth of the prey in the experimental with respect to the control bottles, and likely results from an increase in the nutrient pool originating from the dead grazers. The presence of DMSO also deterred the feeding of these two species, with *M. rubrum* being the most affected (**Figure 3-5a,c**). On the other hand, neither the mixoplanktonic *K. armiger* (**Figure 3-5b**) nor the protozooplanktonic *G. dominans* (**Figure 3-5d**) were significantly affected by the DMSO treatment (Tukey HSD tests, $p > 0.05$ in all cases). Rotenone, however, did affect the feeding rates of these dinoflagellates. *K. armiger* displayed no evidence of feeding whenever rotenone was present, and *G. dominans* showed null ingestion rates at 2.0 mg L^{-1} of rotenone (two-tailed Student's t-tests, $p > 0.05$ in all cases).

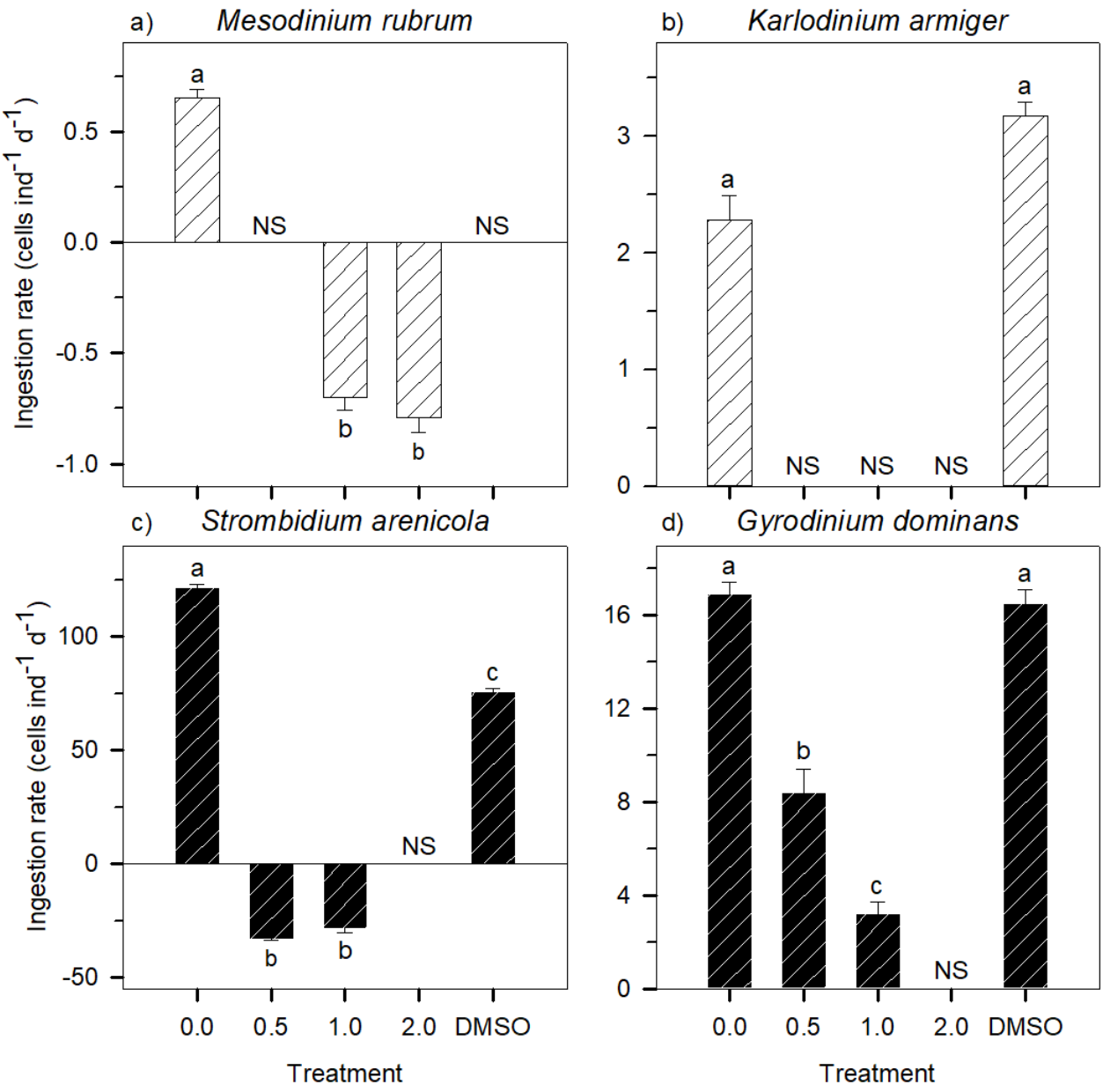

Figure 3-5 Ingestion rate (Cells Ind^{-1} d^{-1}) of the mixoplankton (▨) (a) *M. rubrum* and (b) *K. armiger*, and protozooplankton (■) (c) *S. arenicola* and (d) *G. dominans* upon exposure to increasing concentrations of rotenone. All organisms were fed *R. salina* during the exposure period. Different letters within the same organism indicate significant differences (Tukey HSD, $p < 0.05$). NS represents the non-significant ingestion rates (two-tailed Student's t-test, $p > 0.05$). Error bars ± se.

iii. Rotenone effects on the overall grazing impact

The reduction in the impact of the chosen predators on the standing stock of *R. salina*, defined using **Equation 3.1** as the combined effect of feeding rates and grazer abundances during the incubations, is summarised in **Table 3-4**. Regardless of the

trophic mode of nutrition, the grazing pressure by dinoflagellates was overall less inhibited by rotenone than that exhibited by ciliates.

Table 3-4 Combined effects of rotenone on grazer survival and on their feeding rates on *R. salina* (GIR, %) throughout the incubation. The values were calculated using **Equation 3.1**. Non-significant ingestion rates were considered 0, and GIR was thus capped at 100% in these situations, with the values highlighted with an *. No effect of the treatment on the overall grazing impact is indicated by a zero in the table.

Species	Grazing Impact Reduction (GIR), %				
	0.0 mg L^{-1}	0.5 mg L^{-1}	1.0 mg L^{-1}	2.0 mg L^{-1}	DMSO
Gyrodinium dominans	0.00	56.83	83.62	100.00*	0.15
Strombidium arenicola	0.00	123.07	114.80	100.00*	45.59
Karlodinium armiger	0.00	100.00*	100.00*	100.00*	0.00
Mesodinium rubrum	0.00	100.00*	197.07	202.77	100.00

iv. Effects of physiological conditions on the resistance to rotenone

Rotenone affected *R. salina* in different ways depending on its physiological condition (**Figure 3-6**). During the deceleration phase, the flagellate was roughly unaffected by the presence of rotenone, independent of the concentration (One-Way ANOVA, $p = 0.071$). On the other hand, during exponential growth, progressively higher concentrations of rotenone diminished the growth of this cryptophyte up to a maximum of ca. 40% lower than that under the control treatment with 0 mg L^{-1} (Tukey HSD test, $p = 0.000$).

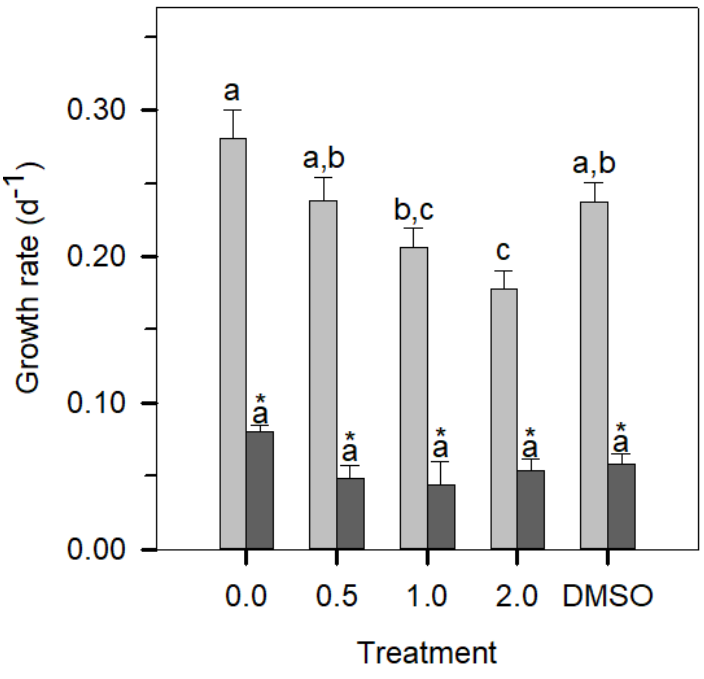

Figure 3-6 Growth rate (d^{-1}) of the phytoplanktonic *R. salina* upon exposure to increasing concentrations of rotenone on the exponential (▒) and deceleration (■) growth phases. The data regarding the exponential phase are the same as those displayed in **Figure 3-2a**. Different letters within the same growth phase indicate significant differences (Tukey HSD, $p < 0.05$). *Indicates statistically significant differences between exponential and deceleration phases for each individual treatment (Bonferroni, $p < 0.05$). Error bars ± se.

3.3.3 Discussion

As expected, phytoplankton species were more resistant to rotenone, with the exception of *T. chuii*. Other species of the genus *Tetraselmis* are also reported to be more vulnerable to rotenone than other algae species, such as the marine *Nannochloropsis oculata* (Van Ginkel *et al.* 2016) and the freshwater *Chlorella kessleri* (Van Ginkel *et al.* 2015). This observation suggests that there may be a factor that is common to the genus *Tetraselmis* that enhances cellular susceptibility to this compound, although it is currently unknown. Conversely, the diatom and *R. salina* were quite resistant to rotenone effects. In the particular case of the cryptophyte, the effects of this compound were only evident during the exponential growth phase.

Cells undergo drastic metabolic changes when switching from exponential to stationary phases. For example, photosynthesis and respiration rates are, on average, higher during the exponential growth phase for phyto- and mixoplanktonic species (López-Sandoval *et al.* 2014). Similarly, protozooplanktonic ciliates and flagellates displayed higher respiration rates when actively growing than when stationary (Fenchel & Finlay 1983). Therefore, it seems that the increased respiratory chain activity during the exponential phase enhances an organism's susceptibility to rotenone. This conclusion aligns with the mechanism of action of rotenone, which, among other effects, is known to inhibit the synthesis of ATP (Palmer *et al.* 1968). A consequence of the reduced pool of available ATP can be seen in the assembly of microtubules, which becomes impaired and ultimately results in mitotic arrest and inhibition of cell proliferation (Srivastava & Panda 2007). Without these processes, the cell cannot divide, which would have a much higher impact on actively growing cells than on those progressing towards stationary phase.

The observed differences between growth phases under exposure to rotenone may have important consequences for the interpretation of laboratory and field experiments on single-celled organisms, not only with rotenone but with other toxic compounds as well. Despite having data exclusively from *R. salina* (which forces caution in the extrapolation of conclusions to other species), the results indicate that the effect of pollutants should always be tested using the same physiological conditions to minimise intra-specific differences. In the laboratory, this can be easily accomplished by controlling sampling times and/or by using a single batch of cultured organisms (as used in the experiments with mixo- and protozooplankton). On the other hand, for field work this may represent a

challenge. Nonetheless, organisms in the field are likely living on an almost constant exponential growth phase (e.g. Dortch *et al*. 1983), diminishing the risk of comparisons.

A major result of the study is the high sensitivity of the ciliate *S. arenicola* to rotenone, in particular compared to the other protozooplanktonic predator tested, the dinoflagellate *G. dominans*. In fact, *G. dominans*, displayed a peculiar response to rotenone, showing negative growth rates and high ingestion rates at the lowest concentration, and similar growth rates and non-significant ingestion rates (two-tailed Student's t-test, $p = 0.114$) at the highest. These results suggest that this dinoflagellate may be able to tolerate the presence of rotenone up to a concentration of 1.0 mg L^{-1} by maintaining key cellular processes (like phagocytosis) active while avoiding expensive ones such as cellular division. This could be a mechanism of survival that enables the endurance of harsh conditions for short time periods. Nonetheless, more data is needed to validate this hypothesis. On the other hand, planktonic ciliates are known to be highly susceptible to several chemical compounds, such as hydrocarbons and chemical dispersants (Almeda *et al.* 2014, Schmoker *et al.* 2016), but also to DMSO, although the toxicity of the latter is usually evidenced at higher concentrations than the ones used in this study (Fok & Valin 1983 Rajini *et al.* 1989). Indeed, the ciliate *S. arenicola* was the only species whose growth was reduced by ca. 60% solely by the presence of DMSO.

Analogous to the results observed for protozooplankton, with the ciliate being more sensitive than the dinoflagellate, the pSNCM *M. rubrum* was more sensitive than *K. armiger*. In fact, the ingestion rate of *M. rubrum* was already negligible even with DMSO as the only added compound (**Figure 3-5a**). Indeed, DMSO hindered the ingestion of prey for both ciliates (**Figure 3-5a,c**). In this regard, a precursor of DMSO, β-dimethylsulfoniopropionate (DMSP), reduced the feeding of protozooplanktonic marine ciliates by 50-75%, whereas for dinoflagellates of the same trophic mode, this reduction was 28-40% (Fredrickson & Strom 2009).

Overall, chloroplast-bearing predators displayed better resilience than protozooplankton at a concentration of 0.5 mg of rotenone L^{-1}. However, their feeding rates were more affected, rendering the overall mixoplankton grazing impact on prey populations considerably lower than that of protozooplanktonic species. In particular, *K. armiger* did not exhibit any evidence of feeding in the presence of rotenone (irrespective of concentration), while displaying only a slight negative growth rate in the highest concentration. These results are in agreement with those of previous studies on this species, in which it has been observed that *K. armiger* can survive long starvation periods

using only chloroplasts for C acquisition, although barely dividing in the absence of food (Berge & Hansen 2016), comparable to the non-significant ingestion rates observed in this study in the presence of rotenone.

One of the main motivations of this study was to test the effectiveness of the use of rotenone combined with the dilution technique to determine mixotrophic grazing. For the method to be useful, protozooplanktonic grazing should be impaired while leaving mixoplankton grazing unaffected. Despite the promising results for the effects of rotenone in terms of growth rates (with perhaps the caveat of the high sensitivity of *T. chuii*), the analysis of the effects of this compound on grazing highlighted severe limitations that were not predicted by the theoretical mechanism of action for rotenone (see **Table 3-4**). For instance, one of the assumptions of the study was that chloroplast-bearing organisms would be less affected by rotenone despite likely displaying a reduced ATP pool. A question that remains unanswered by this assumption is how large is the dependence of mixoplankton grazing processes on the ATP produced by the oxidative phosphorylation. In other words, can the photo phosphorylation supply enough ATP to maintain basal functions while enabling phagocytosis? The answer, at least from the present experiments, seems to be no, as explained next.

At 30 µmol photons m^{-2} s^{-1} (the experimental conditions used in the present study), a well fed *K. armiger* fixes C at a higher rate than the maximum observed for unfed cells, and the chlorophyll *a* content is close to the maximum registered (Berge & Hansen 2016). These observations suggest that this dinoflagellate maximises the use of the chloroplasts in situations akin to those used on the present study. Therefore, it seems plausible to assume that these conditions are less prone to magnify potential negative effects of rotenone on the behaviour of the CM.

For *M. rubrum*, it is known that the photosynthetic capacities depend on the quality of the chloroplasts acquired through the ingestion of cryptophytes from the genera *Teleaulax*, *Plagioselmis* or *Geminigera* (Hansen *et al.* 2012), and peak around 30 µmol photons m^{-2} s^{-1} (Moeller *et al.* 2011). Ultimately, the sequestered chloroplasts require the presence of active cryptophyte nuclei, and start to lose photosynthetic efficiency after 3 days without the adequate food source (Kim *et al.* 2017). Accordingly, during the exposure to rotenone, the chloroplasts of the NCM were also likely close to their full potential despite being fed with *R. salina*.

Contrary to all other tested predators, *G. dominans* was still able to ingest *R. salina* under concentrations of rotenone up to 1.0 mg L^{-1} (although with ca. 9% mortality and a grazing

impact reduction, GIR, of ca. 83%). Indeed, it is important to note that with a concentration of 0.5 mg L^{-1}, the absolute number of *R. salina* cells ingested per *G. dominans* was approximately 3.8× higher than that of *K. armiger* and 13.2× higher than that of *M. rubrum* in their respective control situations.

Thus, despite the fact that the chloroplasts of both mixoplankton tested here should have been in good conditions and that the available ATP pool for *G. dominans* was (likely) severely reduced during the exposure to rotenone, field grazing estimates using rotenone would be, at best, conservative. Indeed, the analysis of the GIR suggests that in a hypothetical dilution setting with rotenone (0.5 mg L^{-1}) and all 3 predators, *G. dominans* would still be the major grazer. Hence, mixoplanktonic grazing is clearly affected by the reduced ATP concentration, although future physiological studies are required to elucidate the actual contribution of the oxidative phosphorylation for mixoplankton and its role on phagotrophy.

An example that further corroborates that protozooplanktonic dinoflagellates can display a substantial grazing impact on natural populations (thus further complicating the use of a protozooplanktonic grazing deterrent such as rotenone) is the fact that some areas of the Mediterranean Sea possess a biomass of protozooplanktonic dinoflagellates approximately 4× higher than that of phytoplanktonic (with high potential for phagotrophy, Jeong *et al.* 2010) and mixoplanktonic species combined when not blooming (Ignatiades 2012). Additionally, the average C-specific ingestion rate of protozooplanktonic dinoflagellates is ca. 4.5× higher than that of their mixoplankton counterparts (see Figure 10 in Calbet *et al*. 2011a and references therein), meaning that one can assume that protozooplankton would impact prey nearly 20× more than mixoplankton. Assuming that *G. dominans* is a good representative of protozooplanktonic dinoflagellates (Kim & Jeong 2004), the presence of 0.5 mg L^{-1} would still render their impact (see **Table 3-4**) on prey populations ca. 11× higher than that of mixoplankton, which would be virtually zero (as per *K. armiger* results). Thus, rotenone cannot be used as an addition to the standard dilution technique for the purpose of deterring heterotrophic predation.

On an ecological note, rotenone has been used for decades to kill undesirable fish species *in situ*, and typical concentrations varied between 0.5 and 5.0 mg L^{-1}, depending on the sensitivity of the target species (Hinson 2000) . However, as evidenced by the results of this study, considerably lower concentrations cause nefarious or even lethal effects on several planktonic species of distinct taxonomic groups. Additionally, the half-life of rotenone in aquatic environments ranges from hours to weeks (Dawson *et al.* 1991)

and depends on several factors, namely temperature and pH, increases in which quicken degradation (El-Sayed *et al.* 2018). Hence, this information, together with the data gathered in this study for protists, and previous studies on zooplankton (Naess 1991, Beal & Anderson 1993) and rotifers (Van Ginkel *et al.* 2015, 2016) suggest that the indiscriminate use of this compound in the past may have had disastrous consequences for aquatic food webs, whose extent is largely unknown.

3.4 Pros and cons of using Live FLA to account for protist grazing

3.4.1 Methods

We wanted to assess the occasions on which Live Fluorescently Labelled Algae (LFLA) could be successfully used to measure protist grazing in situ and, therefore, prepared three independent sets of laboratory-controlled experiments to answer distinct questions.

i. Preparation of LFLA

I. galbana, *T. chuii*, *Heterocapsa sp.* and *M. rubrum* were fluorescently labelled following the guidelines by Martínez *et al.* (2014) with slight modifications. Briefly, cells were stained overnight with the fluorochrome CellTracker™ Blue CMAC (7-amino-4-chloromethylcoumarin), a vital cytoplasmic stain, at a final concentration of 10 µM. After the staining period, excess stain was removed from the medium by centrifugation (1000 g) for 10 min for all species except for *M. rubrum*. The supernatant was discarded and the cells were re-suspended in filtered sea water (0.1 µm). This clean-up process was repeated two times, to reduce the carryover of stain which can enter predator cells and mask the actual ingestion of LFLA. *M. rubrum* was hand-picked and moved through five wells of FSW for the same reason.

ii. Experiment 1 – The effects of prey concentration and incubation time

For the first experiment, we decided to use common protozooplankton and mixoplankton species (encompassing several taxonomic groups and feeding strategies to increase variability and thus, provide a better overview of natural populations) to determine optimal incubation times to measure grazing on tracer concentrations of LFLA. Additionally, we assessed how different prey concentrations affected the estimation of grazing using this technique.

For this experiment, we selected three protozooplankton species which conduct phagocytosis through direct engulfment: the dinoflagellates *Oxyrrhis marina* (strain ICM-ZOO-OM001) and *G. dominans* (strain ICM-ZOO-GD001), and the ciliate *S. arenicola* (strain ICM-ZOO-SA001). Additionally, we selected three mixoplankton species, the CM dinoflagellates *K. armiger* (peduncle feeder, strain ICM-ZOO-KA001) and *K. veneficum* (engulfment feeder, strain ICMB-274), and the pSNCM ciliate *M. rubrum* (strain DK-2009).

R. salina (cryptophyte, strain K-0294) was offered as prey to *G. dominans*, *O. marina*, *S. arenicola* and *K. armiger*. *K. veneficum* and *M. rubrum* were offered *Teleaulax amphioxeia* (cryptophyte, strain K-1837) prey instead. During the experiments, all predators were offered a mixture of the LFLA *I. galbana* (ca. 30 % of the total prey concentration) and the cryptophyte prey. The final predator concentrations were adjusted to avoid the depletion of prey at the target concentration. Additionally, we prepared a second incubation for *M. rubrum* where we gave it only the LFLA (i.e., 100 % of the offered prey were labelled *I. galbana*). All three prey species were kept in f/2 medium (Guillard 1975) at 100-200 µmol photons m^{-2} s^{-1} (provided by cool white fluorescent lights) under exponential growth conditions. All predators were kept in autoclaved 0.1 µm-filtered seawater at 35-55 µmol photons m^{-2} s^{-1}. All cultures were kept in a temperature-controlled room at 19°C with a 10:14 L/D cycle, at a salinity of 38.

Experiments were done in Pyrex bottles and consisted of two concentrations of prey, one saturating ([Prey] = High) and one non-saturating ([Prey] = Low). The experimental bottles were prepared in duplicates, which were filled in two to three steps using a common master suspension containing both predator and prey at the target concentrations. The master suspension was gently stirred between fillings and the formation of air bubbles was avoided (Broglio *et al.* 2004). The bottles were incubated on a plankton wheel (0.2 rpm) at 19°C at 35-55 µmol photons m^{-2} s^{-1}. Each experimental bottle was sampled (9-45 mL depending on final predator concentration) every 20 min during the first 2 h of incubation, and then after 3 and 5 h. The samples were fixed with cold Glutaraldehyde (4°C, final concentration of 1%) for ca. 2 h and then filtered with a vacuum pump onto 2 µm pore-size black polycarbonate filters, which were mounted on microscope slides. The first 100 predators encountered on each slide were examined for the presence or absence of ingested prey, determined as blue-fluorescent inclusions (BFI).

In the incubations where the mixture of prey was within different size ranges (i.e., when the cryptophyte prey was *R. salina*), an initial and a final sample were also collected from each experimental bottle and quantified using a Beckman Coulter Multisizer III particle counter, to calculate clearance rates using Frost (1972) equations as modified by Heinbokel (1978) to account for the growth of protist predators. From the calculated clearance rates we estimated the selection coefficient (Wi) and the electivity index (Ei*) according to Vanderploeg & Scavia (1979). The former is calculated according to the

Equation 3.2

$$Wi = \frac{Fi}{\sum Fi} \qquad \mathbf{3.2}$$

where *Fi* is the clearance rate for a given food type *i* and *ΣF*i is the sum of clearance rates on all food types. The latter is calculated using the **Equation 3.3**

$$Ei^* = \frac{\left[Wi - \frac{1}{n}\right]}{\left[Wi + \frac{1}{n}\right]} \qquad \mathbf{3.3}$$

where *n* is the total number of food types. This index can vary between -1 and 1. Negative values imply active avoidance of prey whereas the opposite implies selection for a given species.

iii. Experiment 2 – The diel effects on prey incorporation and digestion

For the second experiment we decided to focus only on one grazer, the NCM *Strombidium basimorphum*, due to the laborious and time-consuming analysis of the samples. This species was maintained on *T. amphioxeia* before the experiment (Maselli *et al.* 2020) but was allowed to graze down its prey to negligible levels before the onset of the incubations. We conducted two independent incubations with the LFLA *T. chuii* in a proportion of ca. 5 prey per predator under non-saturating concentrations, one incubation during the day and one during the night. *S. basimorphum* were kept in a temperature-controlled room at 15 °C with a 14:10 L/D cycle, at a salinity of 15 in FSW. Both *T. amphioxeia* and *T. chuii* were kept in the same conditions although f/2 media (Guillard 1975) was used instead of FSW. The experiments were always conducted in FSW.

We prepared triplicate experimental bottles containing the mixture of the NCM and the LFLA, which were filled as described above. We coordinated the experiment so that the initial samples for both the day and night periods would be as close as possible to the lights-on/lights-off event in the temperature-controlled chamber. Both incubations lasted 5 hours and were sampled hourly with the exception of the second sampling point, which occurred within 30 minutes of incubation. The fixation and processing of the samples was as mentioned above. The ingested volume of LFLA (μm^3 BFI^{-1}) was obtained from linear dimensions measured on photographs using the Fiji software (Schindelin *et al.* 2012). Carbon (C) contents for *T. chuii* were estimated using the chlorophyte equation of Menden-Deuer & Lessard (2000).

iv. Experiment 3 – The effects of peduncle feeding

The results obtained with *K. armiger* in the first experiment suggested that there could be issues concerning the feeding mechanism of the predator, as suggested before by Archer et al. (1996). Accordingly, we prepared an experiment to ascertain whether or not the feeding mechanism could be an issue when using LFLAs as tracer particles, by selecting known peduncle feeders and offering them labelled prey. This experiment was designed to be qualitative instead of quantitative as the previous two experiments and, thus, prey was always offered in a proportion of ca. 1 prey per predator.

The species that were chosen for this experiment were the protozoan *Lessardia elongata* (strain ICM-ZOO-LSP001), and three mixoplanktonic species, *K. armiger* (CM, strain ICM-ZOO-KA001), *Dinophysis acuminata* (pSNCM, strain FR101009), and the previously thought-to-be phytoplankton *Gymnodinium litoralis* (CM, strain CGA). *L. elongata* and *K. armiger* were maintained with *R. salina* as prey in conditions akin to those described for the first experiment and fed the LFLA *I. galbana* during the experiment. *D. acuminata* was maintained as described by Nielsen *et al.* (2012) and Rusterholz *et al.* (2017). The co-existent unlabelled prey were removed before the incubation with labelled *M. rubrum* using a similar approach as used for the cleaning of extra stain in *M. rubrum*, as described above. Lastly, *G. litoralis* was maintained under exclusive autotrophic conditions before the experiment (see prey maintenance conditions in the experiment 1), and was given the LFLA *Heterocapsa sp.* Yet, phagotrophy in this species was confirmed first on *T. amphioxeia.*

v. Calculations of clearance and grazing rates using LFLA

The average number of blue fluorescent inclusions (BFI) per protist was determined using UV light by epifluorescence microscopy on samples collected at several time points. Plotting this information versus time (h) typically yields a linear relationship for the initial time points, levelling off as the experiment progresses due to digestion of ingested algae (Rublee & Gallegos 1989, Caron 2001). The slope of the linear portion of this regression yields the ingestion of LFLA per predator per hour. This value can be converted to total algae ingested per predator per hour by multiplying it by the unlabelled algae:LFLA ratio assuming that there is no discrimination for or against fluorescently labelled tracers (e.g., Kamiyama 2000, Johnson *et al.* 2003, Martínez *et al.* 2014). Clearance rates (both LFLA-specific and total) are determined by dividing the ingestion rates by the concentration of

LFLA or by the total concentration of prey (Frost 1972, Heinbokel 1978). In the field, estimates of community-level herbivory are obtained by multiplying group-specific clearance rates by the abundance of each group, determining the latter with standard microscopic methods (Caron 2001).

3.4.2 Results

i. Advantages of LFLA

a. Incorporation of LFLA over time

All dinoflagellates exhibited a significantly ($p < 0.01$ for all species) higher Imax (maximum number of Cells per predator) at saturating food conditions than when the concentration of prey was low (**Figure 3-7**). *G. dominans* was the predator with the largest difference between saturating and non-saturating conditions, being followed by *O. marina* (ca. 6.05 and 2.05x more LFLA ingestion at the highest prey concentration, respectively; **Figure 3-7a,b**). Conversely, mixoplanktonic species displayed lower Imax differences between concentrations, being *K. armiger* the species exhibiting the lowest fold-increase (ca. 1.57x). *K. veneficum* increased its Imax by ca. 1.76x.

The differences obtained in the half-saturation constants between saturating and non-saturating conditions were never statistically significant. However, for mixoplankton, the trend was to require more time to achieve food-satiation as the concentration of prey increased (i.e., [High] Km > [Low] Km), whereas the opposite trend was noted in protozooplankton. Overall, all species reached the plateau phase of the tracer incorporation curve within 45 min irrespective of the prey concentration.

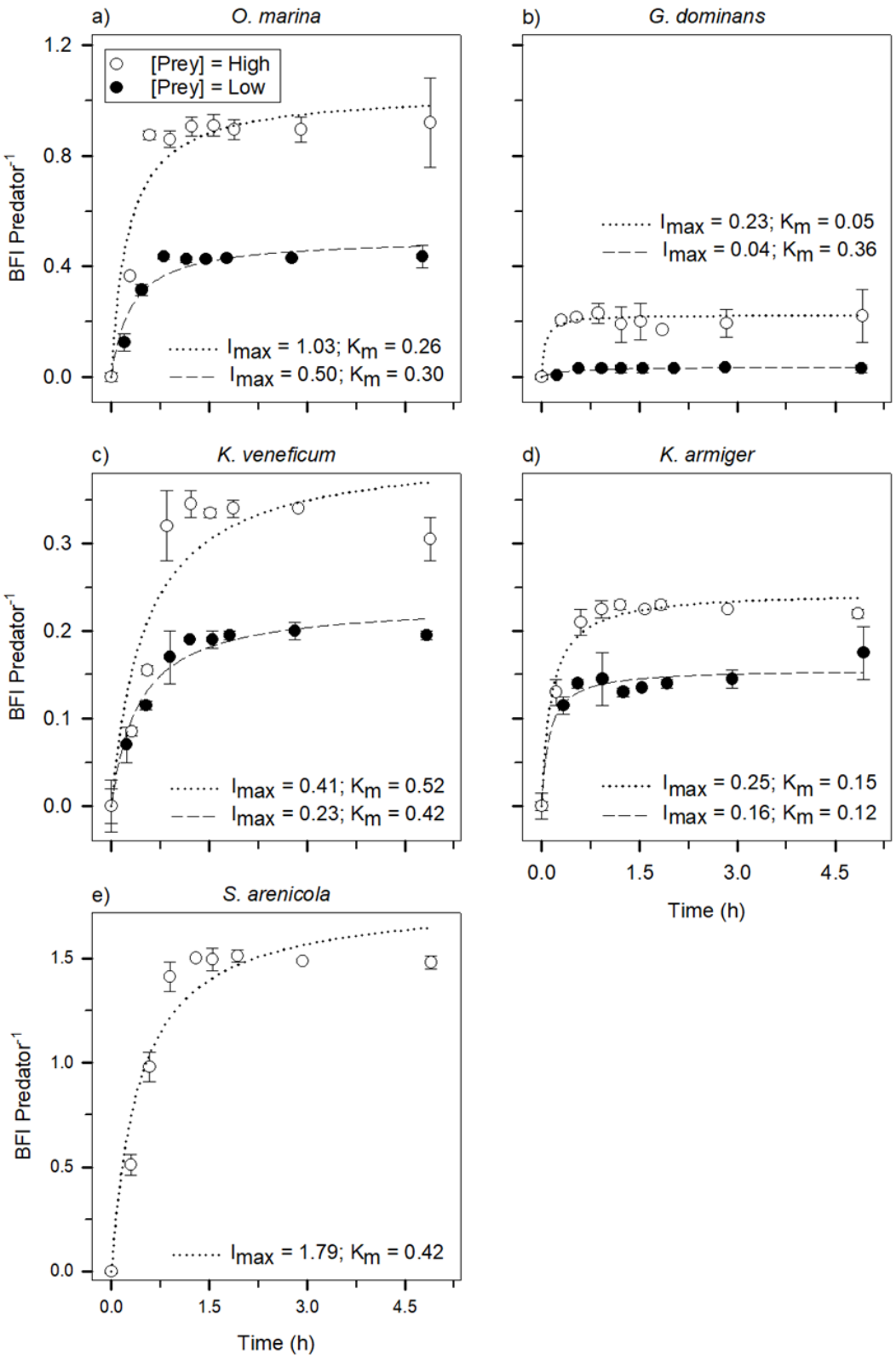

Figure 3-7 Incorporation of prey (BFI predator^{-1}) over time: a, b and e) protozooplankton - *O. marina*, *G. dominans* and *S. arenicola* respectively; c and d) mixoplankton - *K. veneficum* and *K. armiger* respectively. All predators were incubated using two concentrations of prey, one saturating (open circles) and one non-saturating (black circles) with the exception of the ciliate *S. arenicola* which was only followed under saturating conditions. Imax (maximum ingestion rate) and Km (half-saturation constant) were calculated by applying Michaelis-Menten kinetics to the data.

b. Diel ingestion and digestion rates

A very similar procedure was applied to follow the diel incorporation of the LFLA *T. chuii* by the NCM *S. basimorphum* (**Figure 3-8**). The Imax obtained during the day incubation was ca. 1.93x higher than the one obtained during the night ($p < 0.01$) but the half-saturation constants were similar ($p = 0.97$).

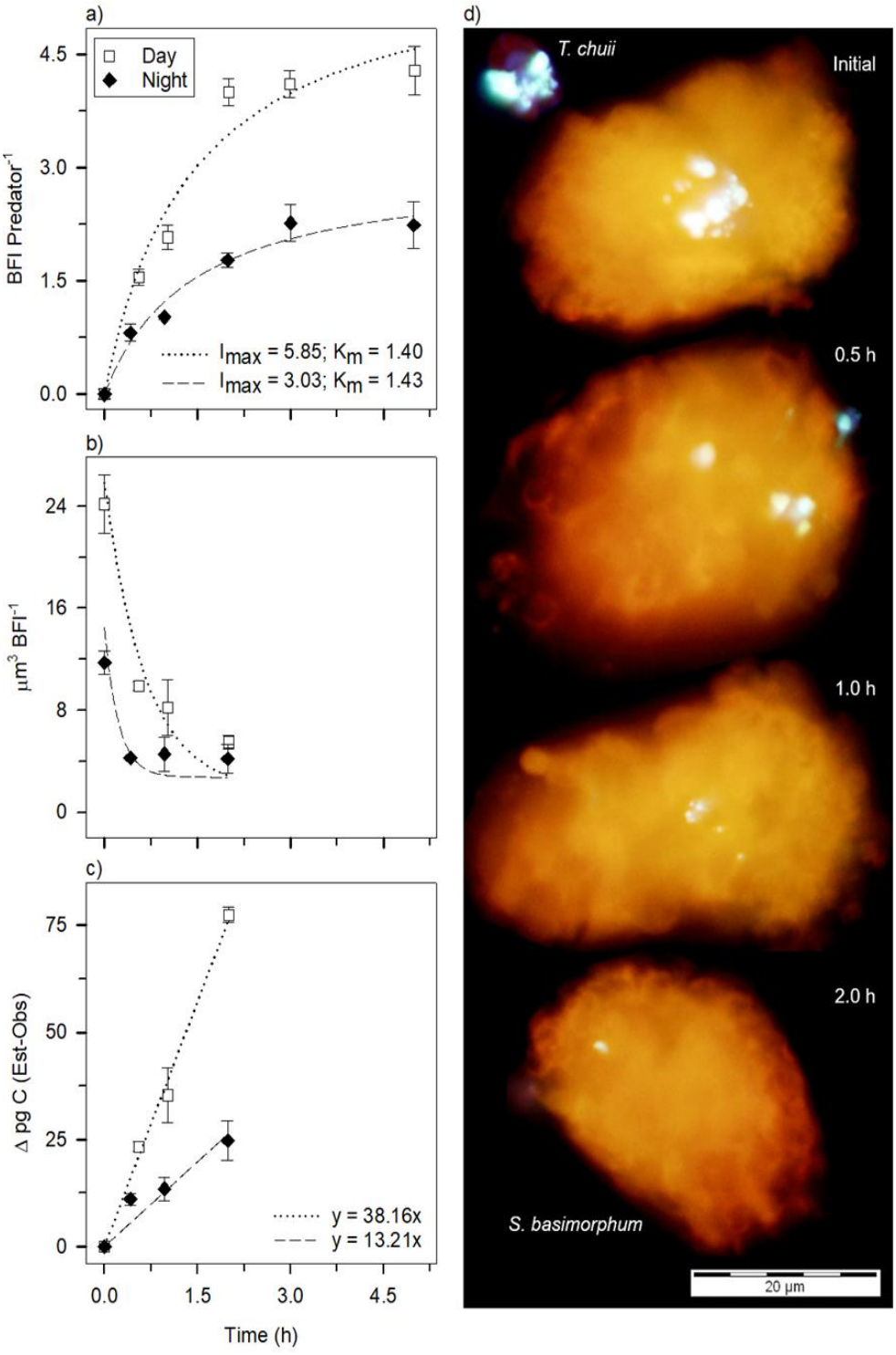

Figure 3-8 Incubation of the CM *S. basimorphum* with the LFLA *T. chuii*. White square points correspond to day samples whereas black diamond points correspond to night ones. a) incorporation of prey over time (BFI predator^{-1}); b) changes in the average fluorescent volume inside a ciliate (µm^3 BFI^{-1}); c) differences between estimated and observed C content in the ingested prey (i.e., digestion rate); d) epifluorescence pictures obtained under UV light excitation where the fluorescent volume inside a given ciliate is decreasing over time.

Regarding volume changes in the ingested BFIs over time (**Figure 3-8b,d**), there was a faster disappearance of fluorescence during the day (18.68 μm^3 over two hours) than during the night (7.55 μm^3 over the same period). Nevertheless, the parameters in both decay curves are not statistically different with the exception of the one controlling the initial volume of the BFI, likely due to the variability of the data. Altogether, from the combined information (and normalized to C units) of the **Figure 3-8a** and **Figure 3-8b**, one can estimate digestion rates by calculating the differences between the estimated and observed pg C per BFI. Despite having statistically insignificant decay parameters, the fact that diurnal ingestion rates were higher than the nocturnal resulted in significantly higher (ca. 2.88x) digestion rates between the day and the night (**Figure 3-8c**, $p < 0.01$).

c. Detection of new mixoplankton species

Another advantage of the use of LFLA is that it enables the direct visualisation of an individual prey inside an individual predator. In particular, it enabled the detection of the phycoerythrin-containing *T. amphioxeia* inside the dinoflagellate *G. litoralis* (**Figure 3-9**), due to the different photosynthetic pigment that each organism possesses. This dinoflagellate can, consequently, be moved from the phyto- into the mixoplankton group.

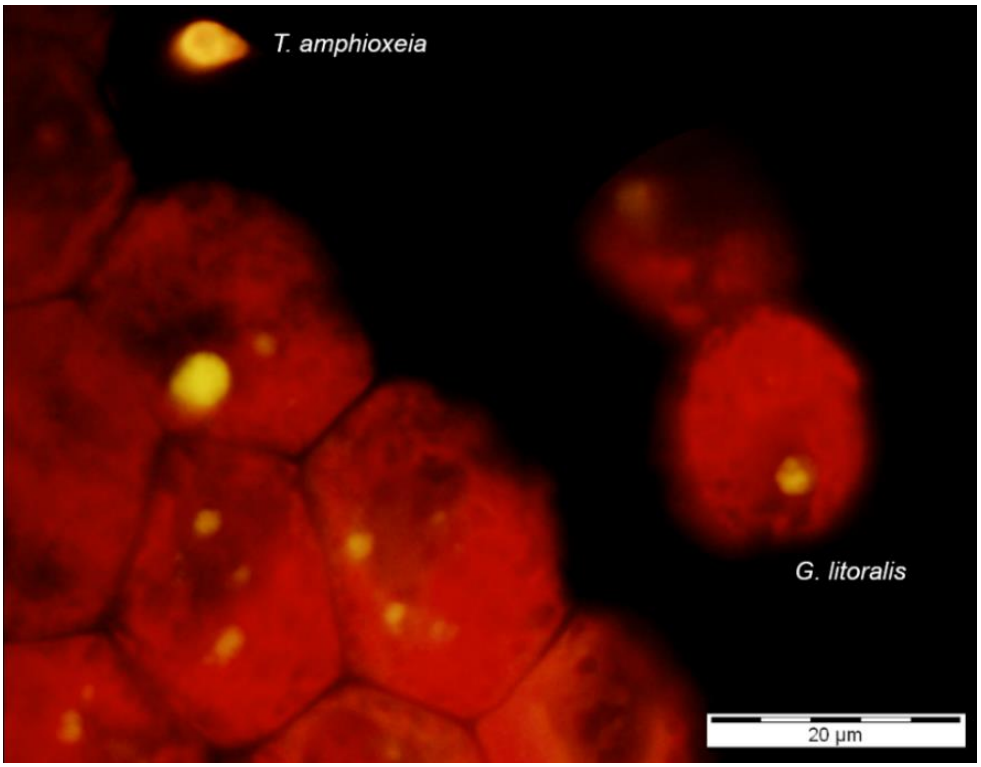

Figure 3-9 Detection of *T. amphioxeia* inside the previously unknown CM *G. litoralis* using epifluorescence microscopy under UV light excitation. *T. amphioxeia* contains phycoerythrin, i.e., seen as orange fluorescent inclusions as opposed to chlorophyll which glows in a bright red tone.

ii. Disadvantages of LFLA

a. Selectivity towards specific species

One of issues that affects experiments using LFLA as tracers for grazing was noticed on the first experiment and concerned the pSNCM *M. rubrum* thus justifying its exclusion from the **Figure 3-7**. This ciliate was, therefore, incubated with LFLA in two independent experiments, one containing the LFLA *I. galbana* as a sole prey and another using it as a tracer, i.e., provided in a mixture containing *T. amphioxeia* as well (**Figure 3-10a** and **3-10b** respectively).

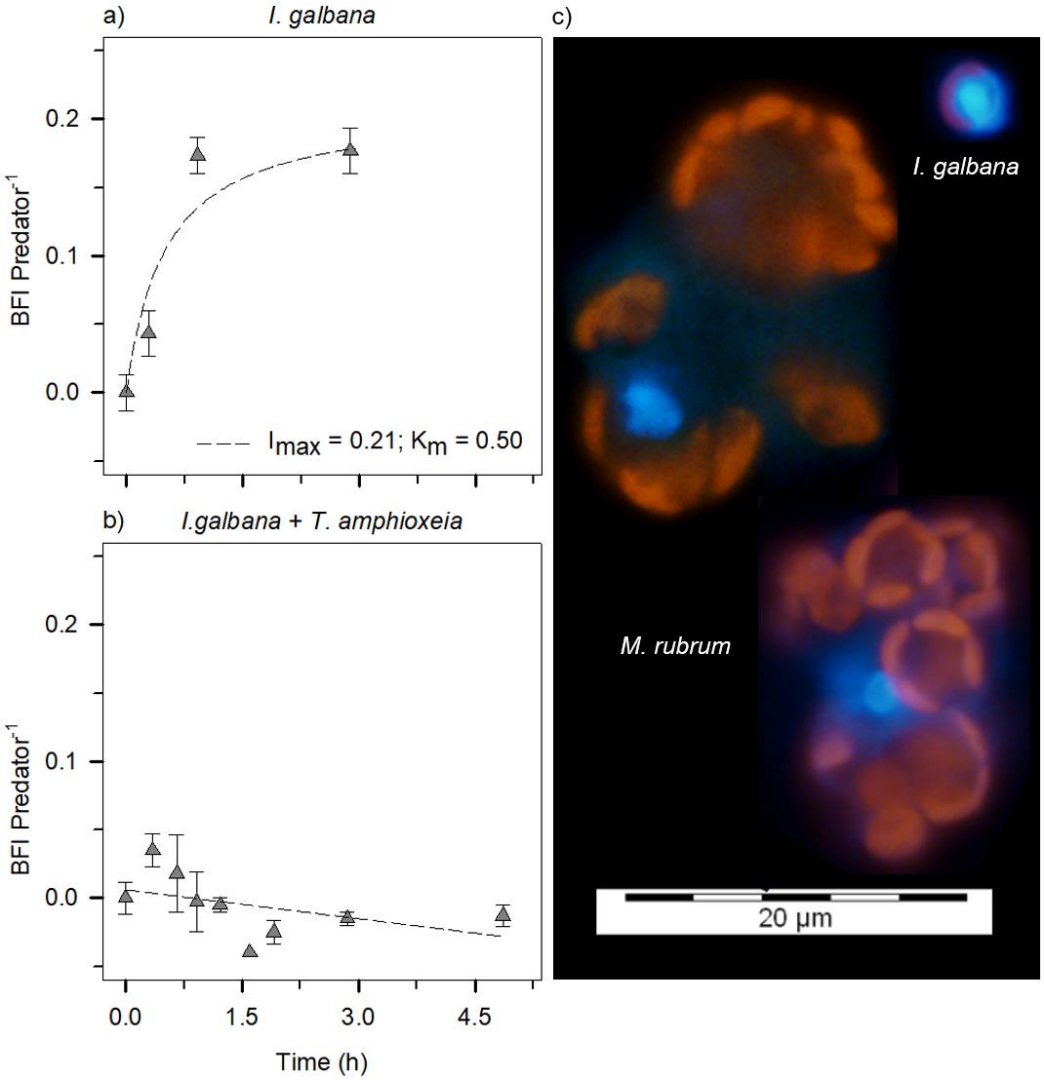

Figure 3-10 Incorporation of labelled *I. galbana* by *M. rubrum* over time: a) *I. galbana* was the only prey offered; b) the LFLA *I. galbana* was offered as a tracer particle, i.e., *T. amphioxeia* was also present in the mixture of prey and c) epifluorescence pictures from the experiment without *T. amphioxeia* obtained under UV light excitation where BFI can be seen inside *M. rubrum*.

There is an aspect that is immediately noticeable by comparing the **Figure 3-10a** and **3-10b**: when *I. galbana* was offered without an alternative prey (**Figure 3-10a,c**), *M. rubrum*

ingests it and the incorporation of BFI per predator followed the typical satiation pattern described above. On the other hand, if *T. amphioxeia* was provided in the mixture of prey (being *I. galbana* used only as a tracer, i.e., using the regular protocol for LFLA), the incorporation of BFI per predator is negligible.

b. Size and concentration-dependent selectivity

The first experiment highlighted a second issue with the LFLA technique, which can be seen in **Figure 3-11**. It concerns the selection for or against the tracer particle.

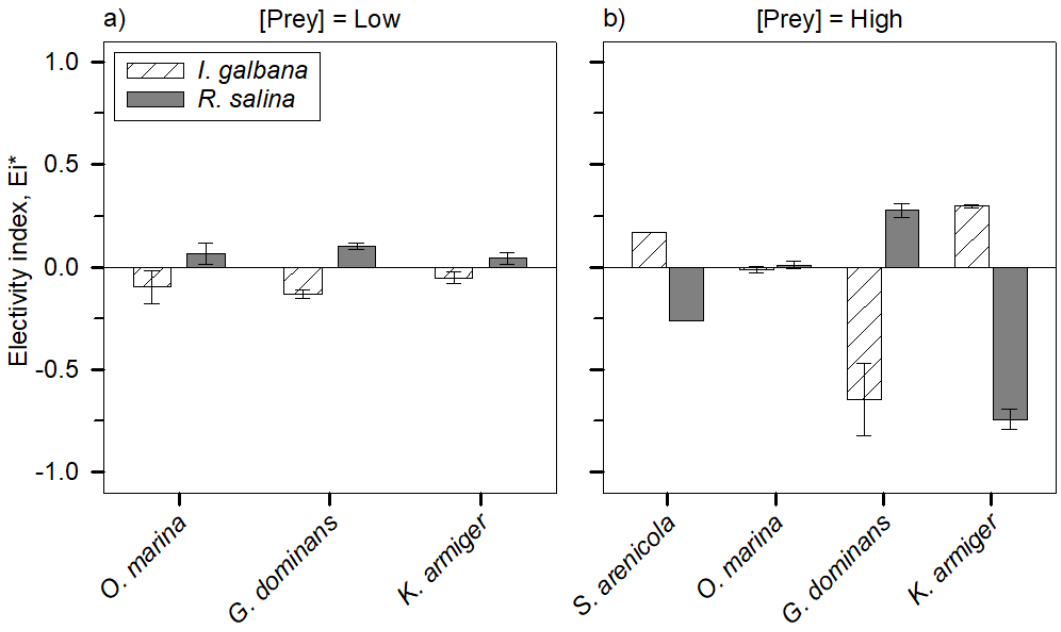

Figure 3-11 Electivity indexes calculated for *I. galbana* and *R. salina* for *S. arenicola*, *O. marina*, *G. dominans*, and *K. armiger* under a) non-saturating food conditions and b) saturating food conditions. This index varies between -1 and 1. Negative values imply a negative selection and vice-versa.

With non-saturating prey conditions (**Figure 3-11a**), the electivity indexes for all three dinoflagellates were close to zero (although positive values for *R. salina* in all cases), which suggests a close-to negligible prey preference in these conditions. Yet, this pattern was not retained when the total concentration of prey reached saturating levels (**Figure 3-11b**). While *O. marina* did not show any prey preference, *G. dominans* increased the electivity index for *R. salina* at the saturating prey concentration, which resulted in a selectivity against *I. galbana*. Also, *K. armiger* shifted from a non-selective predator at low prey concentrations to a highly selective one at saturating conditions, favouring *I. galbana* as prey over *R. salina*. This preference pattern was also shared by the ciliate *S. arenicola*.

c. *Tube, pallium, and toxic mucus trap feeding*

An interesting outcome of the comparison between the experiment with *K. veneficum* and *K. armiger* (**Figure 3-8c,d**) were the higher ingestion rates exhibited by the former. This result made us question whether or not the feeding mechanism could impact the conclusions drawn from an experiment with LFLA. Accordingly, we prepared a qualitative experiment with known tube-feeding dinoflagellates (**Figure 3-12**).

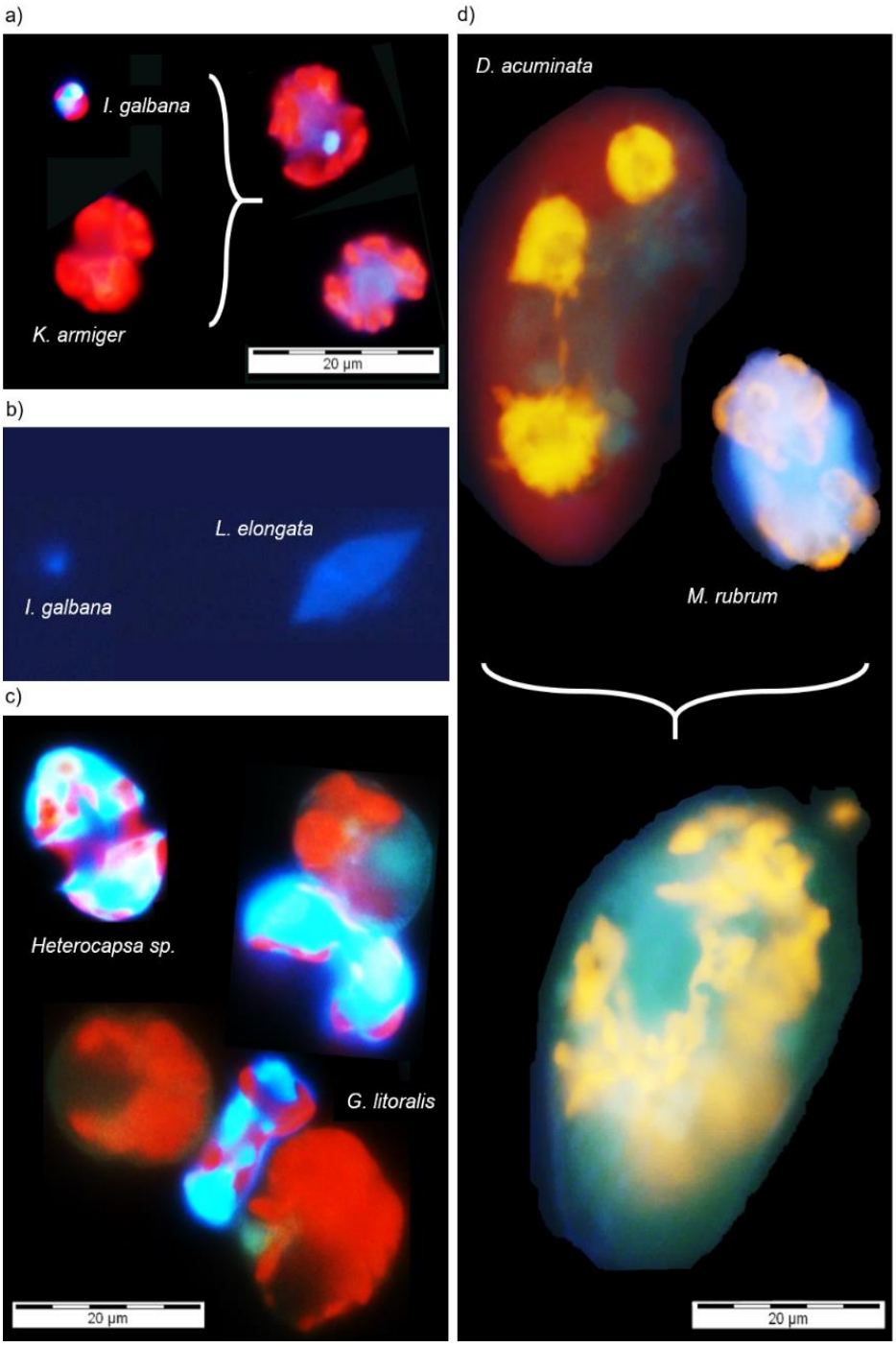

Figure 3-12 Examples of tube-feeding dinoflagellates before and after LFLA addition as seen under UV light in epifluorescence: a) *K. armiger*, where two situations can be found depending on the elapsed time after ingestion b) *L. elongata*, where the BFI cannot be distinguished from the predator c) *G. litoralis*, where the prey is clearly deformed due to the suction of its intracellular content but the predator is either unstained or completely blue, and d) *D. acuminata* where only completely blue cells were found after feeding on labelled prey. The red colour in this figure is due to the autofluorescence of Chl a, orange implies the presence of phycoerythrin, and blue is due to the presence of the fluorochrome CMAC.

The major issue demonstrated by this experiment is the complete cytoplasm staining noticeable irrespective of the chosen predator (i.e., an uncountable amount of prey inside), despite being particularly evident in *D. acuminata* (**Figure 3-12d**). The least affected predator was *K. armiger* (**Figure 3-12a**), whose cytoplasm staining was heavily dependent on the elapsed time after the beginning of the incubation. The experiment with *G. litoralis* (**Figure 3-12c**) demonstrated the same issues as those mentioned above; however, as the offered prey was similarly-sized to the predator, it was common to find half-eaten prey in the filter and/or more than one predator feeding on a single prey, further impairing the estimation of grazing. At last, the experiment with *L. elongata* (**Figure 3-12b**) demonstrated that using LFLA to quantify grazing in peduncle feeding protozooplankton is even worse than in mixoplankton, since the incorporation of LFLA by the former is further masked by the lack of distinguishing pigments themselves.

The analysis of this experiment suggests that dinoflagellates feeding with mechanisms other than direct-engulfment (such as those shown in **Figure 3-13**) may be systematically underestimated by the technique. From the live-pictures, we can presume that that these predators would probably appear either completely stained or completely unstained (**Figure 3-13a** and **3-13b,** respectively) if incubated with labelled prey (prey selectivity issues ignored).

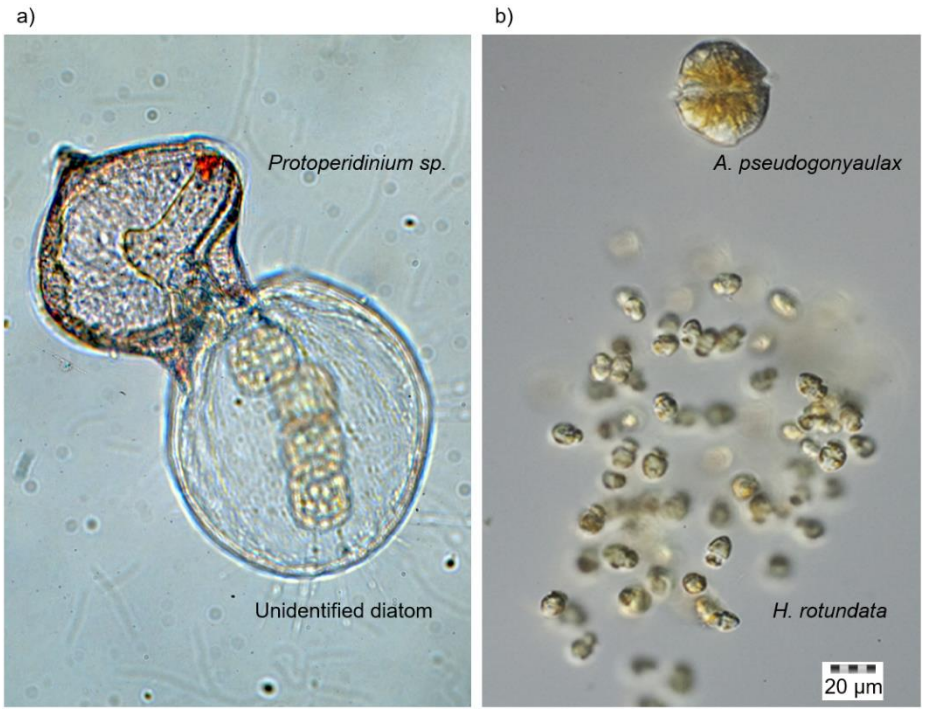

Figure 3-13 Live-pictures of a) the protozooplankton *Protoperidinium sp.* feeding on an unidentified diatom chain through a pallium; b) the mixoplankton *Alexandrium pseudogonyaulax* dragging multiple *Heterocapsa rotundata* which are immobilized inside a toxic mucus trap and eventually ingested. The first photo was taken by Albert Calbet (but see also Gaines & Tailor 1984 for the original description of pallium feeding) and the second by Hannah E. Blossom.

3.4.3 Discussion

The LFLA technique (as proposed by Li *et al.* 1996) offered unique possibilities that distinguished it from other techniques which were developed almost concurrently for the estimation of protist herbivory (e.g., the dilution technique - Landry & Hassett 1992). In particular, it enabled the direct visualisation of organisms, a characteristic which could provide a species/community-specific analysis (Caron 2001). In the particular case of mixoplankton, where knowing who is there is arguably not as important as knowing what are they doing and at what rate (Flynn *et al.* 2019), being able to observe phagocytosis is paramount. Additionally, the LFLA technique did not suffer from a major issue that hindered its predecessor (FLA - Rublee & Gallegos 1989), which was the discrimination against inert or dead particles (e.g., Sherr *et al.* 1987, Nygaard *et al.* 1988, Epstein & Rossel 1995, Jürgens & DeMott 1995) while remaining non-toxic throughout the incubation, as opposed to hydroethidine, the first-ever "vital stain" (Putt 1991). Nevertheless, the technique was not free from issues, as pointed out by its developers.

For instance, Li *et al.* (1996) stated that their stain, the green CMFDA, faded quickly in the light, which would be a major issue if attempting to conduct incubations over large periods of time. Martínez *et al.* (2014) confirmed that the blue stain CMAC (our stain), was better on this specific issue, in particular when following their optimised staining protocols. Indeed, we experienced no issues regarding stain bleaching or fading, both during the actual experiments (light intensities between 35 and 55 µmol photons m^{-2} s^{-1}) but also during the processing of the samples under the epifluorescence microscope. Nevertheless, the fact that predators typically reach the plateau phase within 45 minutes irrespective of prey concentration, trophic mode, and taxonomic group (see **Figures 3-7** and **3-10a**) seems to put this problem on a secondary level. That is, of course, if prey incorporation experiments are conducted instead of prey disappearance ones (see the discussion on FLB by Caron 2001).

The fact that this technique is useful mostly on short-term experiments is both an advantage and a disadvantage. As confirmed by our first experiment, there are a number of protist predators which incorporate LFLA without major issues and under different experimental conditions (**Figures 3-7** and **Figures 3-8**). Nevertheless, even when the incorporation of prey followed the typical satiation pattern, and maximum ingestion rates and half-saturation constants could be estimated, we encountered selectivity issues, both

for and against the tracer algae (**Figures 3-11**). One of the assumptions that is crucial for the estimation of grazing rates is that the tracer is incorporated at similar rates as the remaining prey. In fact, these issues are far from negligible as they shake the very foundations of the technique and, above everything else, are species-specific and unpredictable without experimentation. This is an issue that, as far as we know, has not been described in the past, as most efforts focused on the selection of prey based on the presence of the fluorochrome. For example, Kamiyama (2000) confirmed experimentally that stained and unstained algae were ingested at similar rates by *Schmidingerella taraikaensis* (previously known as *Favella taraikaensis*). Likewise, Martínez *et al.* (2014) demonstrated that *O. marina* grazed on labelled *I. galbana* and *T. chuii* as it did on unlabelled prey. However, in the same study, *G. dominans* seemed to have a slight preference for LFLA over unlabelled prey. In our own experiments, *G. dominans* was the species displaying the largest differences on both Imax and Km between saturating and non-saturating food concentrations. Additionally, this dinoflagellate exhibited a distinct selectivity for labelled *I. galbana* which was dependent on the concentration of prey. Despite not having been strongly emphasized in the past (but see Jürgens & DeMott 1995 and Dolan & Šimek 1999), this change in selectivity could partially explain the enormous differences seen between the afore mentioned parameters. We are unable to confirm whether this result is a direct consequence of size or fluorochrome selectivity (as per Martínez *et al.* 2014), however, we can undeniably state that the measured ingestion rate using the LFLA methodology did not represent the total ingestion of prey by this predator.

Similarly, the results obtained with *Karlodinium* spp. suggest that there could be problems in the extrapolation of community grazing rates for these species. For instance, we know that one *K. armiger* ingests ca. 10 *R. salina* per day at saturating food conditions (Berge *et al.*, 2008b), a value which is ca. 8.9 times higher than the one obtained for *K. veneficum* on the same prey (listed as K21 - Calbet *et al.* 2011a). Yet, the results from the LFLA experiment yielded an ingestion rate of 0.34 BFI *K. veneficum* h^{-1} and 0.38 BFI *K. armiger* h^{-1} (only 1.1 times higher), besides estimating a higher Imax for the former. Additionally, *K. armiger* exhibited a strong preference for *I. galbana* which, if due to a preference for smaller sized prey (Ferreira *et al.* in prep.), could further enhance the differences obtained with both *Karlodinium* spp. since *K. veneficum* is smaller and size preferences are typically correlated with one's own size (e.g., Hansen *et al.* 1994).

Aside from size selectivity, the experiments with the pSNCM *M. rubrum* confirmed that species selectivity is a problem that cannot be circumvented. When its preferential prey was absent (see for example Yih *et al.* 2004 and Smith & Hansen 2007) the number of BFI per *M. rubrum* followed the typical satiation pattern (**Figures 3-10a**). However, when *T. amphioxeia* was present, BFI were mostly absent. In the laboratory, it is possible to control both the grazer and the prey but in the field one cannot chose which species will be present. As the functional group name suggests, *M. rubrum* is a specialised predator and retains chloroplasts mostly from a specific clade of cryptophytes which comprise *T. amphioxeia* among others (e.g. Myung *et al.* 2011, Hansen *et al.* 2012). Still, *M. rubrum* can ingest some other flagellates as well (Park *et al.* 2007, *Hansen et al.* 2012, Ferreira & Calbet 2020, this study), and is mildly able to keep chloroplasts from *Rhodomonas* spp for short periods of time (Myung *et al.* 2011). Accordingly, our results with *I. galbana* are not surprising. Yet, in the field, the presence of *M. rubrum* is typically correlated with the presence of cryptophytes (e.g., Johnson *et al.* 2018), which means that it is extremely unlikely that a field experiment will be able to capture the feeding process of this ciliate using a tracer particle that is not its own preferred prey. This conclusion is likely valid for all the specialised protist predators that exist on Earth.

We have also confirmed the usefulness of the technique on the quantification of diel ingestion and digestion rates on an NCM species. We strongly believe that this is a close-to universal utility of the technique, as pigments/fluorescent tracers have been used numerous times to estimate digestion rates (e.g., Dolan & Šimek 1998, Li *et al.* 2001, Nishibe *et al.* 2002, Setälä *et al.* 2005). Still, even close-to universal approaches have their exceptions and we clearly demonstrated one of them using tube-feeding protozoo- and mixoplanktonic dinoflagellates. Indeed, as confirmed with 4 independent predator-prey combinations from distinct trophic modes, predators that feed using a peduncle tend to become entirely stained themselves instead of displaying individualized (and countable) BFIs. In fact, the low grazing obtained with *K. armiger* may have been due to the fact that this dinoflagellate feeds using a peduncle (Berge *et al.* 2008a). Based on our results with tube feeders, it is likely that some *K. armiger* did contain LFLA but we were unable to see them because of the dispersal of the fluorochrome through the predator's cytoplasm. This issue appears to become more relevant with the passing of time, as some cells did contain easily distinguishable and countable BFIs (see **Figures 3-12a,c**). To further complicate the peduncle feeding matter, it should be mentioned that the

incorporation of ingested material through a peduncle may flow into a single (e.g., Calado & Moestrup 1997) or several (smaller) food vacuoles (e.g., Hansen 1991). Also, small cells may be taken whole through a peduncle in some cases (e.g., Calado & Moestrup 1997), which could also be the reason why some *K. armiger* had countable BFI and some had not (*I. galbana*'s ESD is ca. 4.5 µm).

Tube feeding is a common characteristic in both naked and thecate dinoflagellates (Hansen & Calado 1999), suggesting that this caveat of the technique may be a truly important factor to take into consideration when applying this technique in mixed assemblages in the field. One other long-known feeding mechanism in dinoflagellates is through the deployment of a pallium (**Figures 3-13a**), which liquefies the cytoplasmic contents of the prey extracellularly (Gaines & Taylor 1984, Jacobson & Anderson 1986). Accordingly, pallium feeders do not transport particles into the main cell body and thus lack food vacuoles (Archer *et al.* 1996, Hansen & Calado 1999). We did not experiment on pallium feeders and, as such, we can only simply hypothesize on these organisms. Still, it seems reasonable to assume from these past observations and from our own on peduncle feeders that these dinoflagellates would probably appear as a very intense and uniformly bright cell, due to even incorporation of the fluorochrome. On a similar albeit almost species-specific note, comes the feeding by toxic mucus traps. This feeding mechanism has only been reported, as far as we know, in the species *Alexandrium pseudogonyaulax* (**Figures 3-13b**, Blossom *et al.* 2012, 2017) and on a *Prorocentrum sp. A. pseudogonyaulax* consumes whole cells through the sulcus but is unable to capture individual, motile prey cells. Therefore, it deploys a mucus trap that immobilises (but does not kill on a short time scale) prey and, by swimming with it attached to its own body, oftentimes end up entrapping several prey inside. Accordingly, these predators may affect the availability of prey without exhibiting food vacuoles or, even if showing clear and distinguishable BFIs, provide unrealistic grazing rates.

3.5 Extracting mixoplanktonic grazing from dilution grazing experiments

3.5.1 Methods

We constructed several artificial food webs involving protozooplanktonic and mixoplanktonic predators to gain insights into the dynamics of dilution grazing experiments. Being a laboratory experiment, we were able to control variables and unknowns that cannot be controlled in field experiments. In particular, we included prey controls and ascertained single grazer rates at the experimental conditions. These additions enabled us to determine the species-specific contributions to the concentration of chlorophyll and grazing in the mixed dilution grazing experiment. We conducted our experiments with and without light and sampled the bottles at several time points to have a better representation of the grazer and prey dynamics during the incubation.

i. Cultures

We conducted the experiments with the protozooplanktonic dinoflagellate *G. dominans* (strain ICM-ZOO-GD001) and ciliate *S. arenicola* (strain ICM-ZOO-SA001), the CM dinoflagellate *K. armiger* (strain ICM-ZOO-KA001), and the ciliated pSNCM *M. rubrum* (strain DK-2009). As prey for all experiments, we used the cryptophyte *R. salina* (strain K-0294) and the diatom *C. weissflogii* (strain CCAP 1085/18). *R. salina* was offered as prey *ad libitum* for the maintenance and growth of the two dinoflagellates and *S. arenicola*, being replenished upon depletion by the predator. *M. rubrum* was grown and maintained with *T. amphioxeia* (strain K-1837) in a proportion of approximately 5 prey per predator (Smith & Hansen 2007). Both *R. salina* and *T. amphioxeia* were kept in f/2 medium (Guillard 1975) and irradiated at ca. 150 µmol photons m^{-2} s^{-1} provided by cool white fluorescent lights. *C. weissflogii* was kept under the same conditions with the addition of silicate to the medium. All predators were kept in autoclaved 0.1 µm-filtered seawater. Protozooplankton were maintained at ca. 35 µmol photons m^{-2} s^{-1} whereas mixoplankton were kept at ca. 65 µmol photons m^{-2} s^{-1}. The stock cultures were up-scaled and maintained using a discontinuous culture (pseudo-chemostat) approach, i.e., the cultures were diluted every 1-2 days with the respective medium (between 20 and 50 % of the total volume), to maintain them under exponential growth (and within target concentrations) at any moment. Additionally, to avoid an increase in the pH beyond the limits for exponential growth, all cultures were bubbled with 0.2 µm-filtered air (Berge *et al.* 2010). We used a very slow cadence of bubbles (flow rate not measured) to diminish

the chances of stressing the predators (Berge *et al.* 2010). The direct effect of the bubbling process on the growth of the protists was not determined however, if any, it was likely minor as we confirmed that all cultures were healthy and actively feeding before starting the experiments. All cultures were kept in a temperature-controlled room at 19 °C with a 10:14 L/D cycle at a salinity of 38.

ii. Dilution grazing experiments

The dilution grazing experiments were conducted with a paired mixture of predators at a time; i.e., *G. dominans* simultaneously with *K. armiger*, and *S. arenicola* concurrently with *M. rubrum*. Both experiments were conducted with a mixture of *R. salina* and *C. weissflogii* as prey, in an equivalent carbon (C) concentration. Carbon values for all species were obtained from the average volume and C:µm^3 ratio provided by Traboni *et al.* (2020). *M. rubrum* was allowed to deplete *T. amphioxeia* before starting the experiment.

Two dilution series of 60, 30, and 15 % were prepared from the 100 % treatment, in duplicated 1100 mL transparent polycarbonate bottles (Thermo Scientific Nalgene). All bottles contained 200 mL of f/2 + Si per litre of suspension to reach a final concentration equivalent to f/10 + Si. The actual level of dilution was determined from the initial concentration of prey in each dilution relative to the initial concentration of prey in the 100 %. One of the dilution series was incubated with a 10:14 L/D cycle at 100 µmol photons m^{-2} s^{-1} (hereafter termed L/D treatment). The second series was wrapped in aluminium foil and covered with an opaque box (i.e. incubated in complete darkness) during the whole period (hereafter termed D treatment). The times of sampling were the only sources of culture vessel mixing during the incubation.

Additionally, a second, third, and fourth set of duplicated 100 % bottles were prepared under the same nutrient and light conditions mentioned above. The second set contained the two prey and no predators (termed 100prey). These bottles were used as a control and accounted for the net growth rate (both in cell numbers and Chl *a*) of each prey in the absence of grazing. The third and the fourth set of 100 % bottles comprised the two prey and only one of the predators (in the dinoflagellate experiment, 100gyro and 100karlo, or 100strom and 100meso in the ciliate experiment). These bottles eased the interpretation of the more complex mixed experiment by providing the outcome of the presence of a single predator.

All treatments were prepared with a final volume of 1 L per bottle. In the dilution series, the bottles from every dilution level were sampled after 0, 2, 4, 8, and 24 h for both Chl *a* (150 mL) and cell counts (70 mL, 2 % acidic Lugol's solution final concentration). The control bottles were sampled after 0, 8, and 24 h (150 mL for Chl *a* and 50 mL for cell counts). Samples collected after 2 and 4 h were only used to calculate Chl *a* per cell concentrations and are, therefore, not going to be further discussed. The 8 h sample of both L/D and D bottles were collected immediately before the beginning of the night period. For the D treatment, this did not imply any change in the light conditions despite effectively representing a day sample.

The samples preserved with acidic Lugol's solution were stored in the dark at 4 °C for 1-6 months before being counted. After stabilising the samples to room temperature (21±3 °C), the bottles were rotated softly and used to fill 10 mL methacrylate sedimentation chambers. The Utermöhl (1958) method was employed to analyse the samples after 24 h on an inverted microscope (XSB-1A) using a 25× objective. A minimum of 200 individuals of each species were counted per replicate count, being each sample counted twice.

iii. Chlorophyll, growth, and grazing analysis

The total chlorophyll *a* (Chl *a*, µg L^{-1}) was determined by filtering 150 mL of water from every bottle as specified before. The samples were collected into dark bottles and filtered through Whatman GF/C glass fibre filters under dim light conditions immediately after collection. The filters were folded in half twice, wrapped in aluminium foil and then kept at -20 °C for ca. 5 months until the extraction of pigments with 6 mL of acetone 90 %. The extraction was conducted in the dark at 4 °C and lasted ca. 24 h, thus avoiding the need to grind the filters (Holm-Hansen & Riemann 1978). The samples were measured before and after the addition of 100 µL of HCl 10 % (final concentration in the extract ca. 0.05 M) on a Turner Designs Fluorometer (Yentch & Menzel 1963). The fluorometer was calibrated against a pure Chl *a* standard (2.13 mg Chl *a* L^{-1}) of cyanobacterial origin (DHI, Hørsholm, Denmark). Phaeopigments (µg L^{-1}) were determined by dividing the chlorophyll concentration by the acid factor ratio between fluorescence values before and after acidification.

We determined individual species contribution to the total Chl *a* mathematically for each time point in the control bottles. First, 100prey bottles were used to determine Chl *a*

content of *R. salina* and *C. weissflogii*. These concentrations of pigment were then integrated into the controls with one predator and in the dilution series bottles to determine the pigment concentrations within each predator cell. We estimated the intermediate time points (those not directly assessed from control bottles) using linear progression.

Growth, clearance, and grazing rates were calculated for every time point using Frost (1972) equations as modified by Heinbokel (1978). These calculations yielded two different grazing estimates, one for each predator (and, consequently an estimated grazing from their sum), and one for the pooled incubation with two grazers. A third estimate of grazing can be obtained by measuring the slope of the linear regression that correlates the fraction of undiluted water and the apparent growth rates based on the changes in the concentration of prey during the incubation (Landry & Hassett 1982). It is important to notice that the second and third grazing estimates yield non-specific average ingestion rates per predator. Therefore, under these circumstances, individual ingestion rates were estimated by the proportion of measured ingestion rates in the 100gyro, 100karlo, 100strom, and 100meso bottles.

The results of some incubations denoted the presence of saturated feeding responses. Accordingly, under these circumstances, prey growth rates (μ, Chl *a* Chl a^{-1} h^{-1}) were determined from the interception of linear regression with the 3 most diluted treatments. Grazing rates were then calculated using **Equation 3.4**

$$g = \mu - K \qquad \mathbf{3.4}$$

K (Chl *a* Chl a^{-1} h^{-1}) being the apparent growth rates obtained in the undiluted bottles (Gallegos 1989, Dolan *et al.* 2000). We followed the same procedure to determine cell-specific grazing rates with the difference that cell counts were used instead of Chl *a*. For the sake of clarity, we decided to show only the regressions whose slope was significantly ($p < 0.05$) different from zero. Nevertheless, we calculated μ and g for all experiments as recommended by Latasa (2014) and Landry (2014).

3.5.2 Results

i. Dilution grazing experiments

The majority of the dilution grazing incubations yielded non-significant grazing rates ($p > 0.05$) when based on Chl *a* (**Figure 3-14**). The only exceptions were the experiment with dinoflagellates (**Figure 3-14a,c**), but the slopes of the linear regressions were positive on both instances. It is thus impossible to determine the actual grazing mortality using the traditional dilution approach of tracking Chl *a*. Species-specific Chl *a* content can be found in **Table 3-5** for each sampling point.

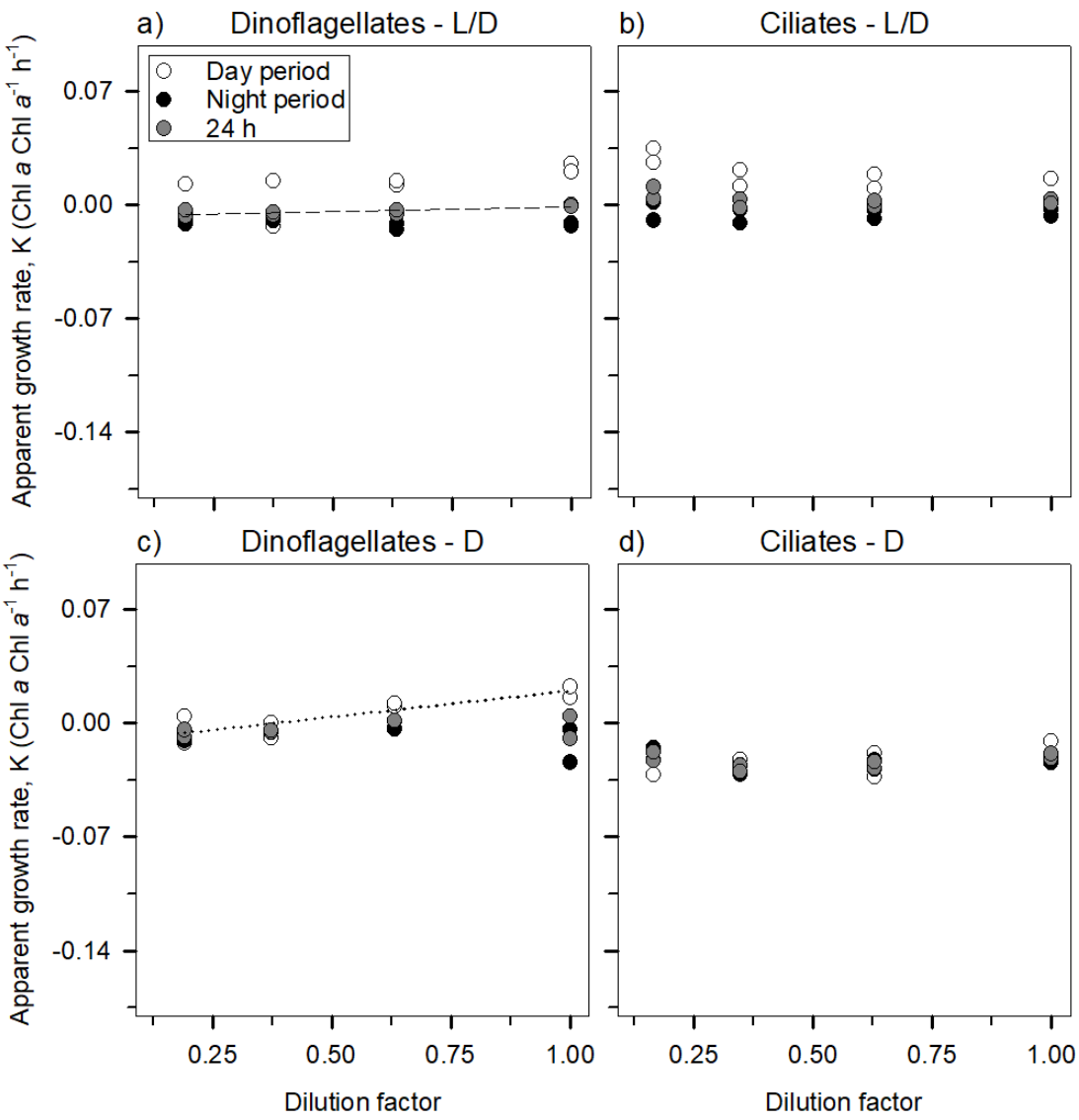

Figure 3-14 Chl *a*-based dilution grazing experiment results. The left panels (a and c) show experiments with dinoflagellates and the right panels (b and d) correspond to experiments with ciliates. The top section is relative to the L/D treatment whereas the bottom one relates to Dark (D) treatment. Plotted linear regressions imply a significant slope ($p < 0.05$). Dotted regression lines correspond to the day and dashed lines to the night.

Table 3-5 Chl *a* content (pg Chl *a* Cell^{-1}) of the target species at each sampling point as calculated from the control bottles. Columns highlighted in grey correspond to the Dark (D) treatment whereas the others correspond to the L/D treatment. The initial samples were the same for both treatments. The + indicates that the calculations yielded a negative value and, as an impossible solution, the value was forced to 0.

Species	Sampling points				
	Initial	Day	Day	Night	Night
R. salina	0.63	1.66±0.11	1.38±0.17	1.22±0.23	1.58±0.11
C. weissflogii	5.59	4.65±0.66	3.40±0.35	3.07±0.51	3.30±1.37
K. armiger	6.71	10.94±0.05	6.70±0.27	17.38±0.80	8.16±0.13
M. rubrum	19.98	21.97±1.14	12.50±2.82	19.97±2.09	15.22±0.74
G. dominans	19.88	15.23±3.90	6.69±0.52	2.74±0.78	1.84±4.58
S. arenicola	10.22	0.62±6.44	13.06±0.24	0.00^{+}	4.52±1.13

Cell-based dilution regressions for dinoflagellates showed very distinct patterns for the two prey (**Figure 3-15**). *R. salina* (**Figure 3-15a,b**) was always ingested irrespective of the period of the day and light conditions (although it had a higher grazing mortality during the day in the presence of light), but the diatom *C. weissflogii* was not (**Figure 3-15c,d**). In fact, the diatom seemed to benefit from the presence of predators, as suggested by the significantly positive slopes both in the L/D and D treatments (see the Methods section for the experimental conditions of each treatment). When the predator community was composed of ciliates instead of dinoflagellates (**Figure 3-16**), *R. salina* was subject to significant grazing mortalities (i.e., negative slope) only during the day in both L/D and D treatments, and in the integrated 24 h in the D treatment (**Figure 3-16a,b**).

All four species of predators showed a lack of response of growth rates to the dilution of the community (**Figure 3-15e,g,h** and **3-16e-h**), except for *K. armiger* in the D bottles (**Figure 3-15f**). It seems then that *K. armiger* was actively ingested by *G. dominans* in the D treatments as ascertained by the significant grazing mortality ($P < 0.05$). A summary of the species-specific growth and grazing rates can be found on **Table 3-6**.

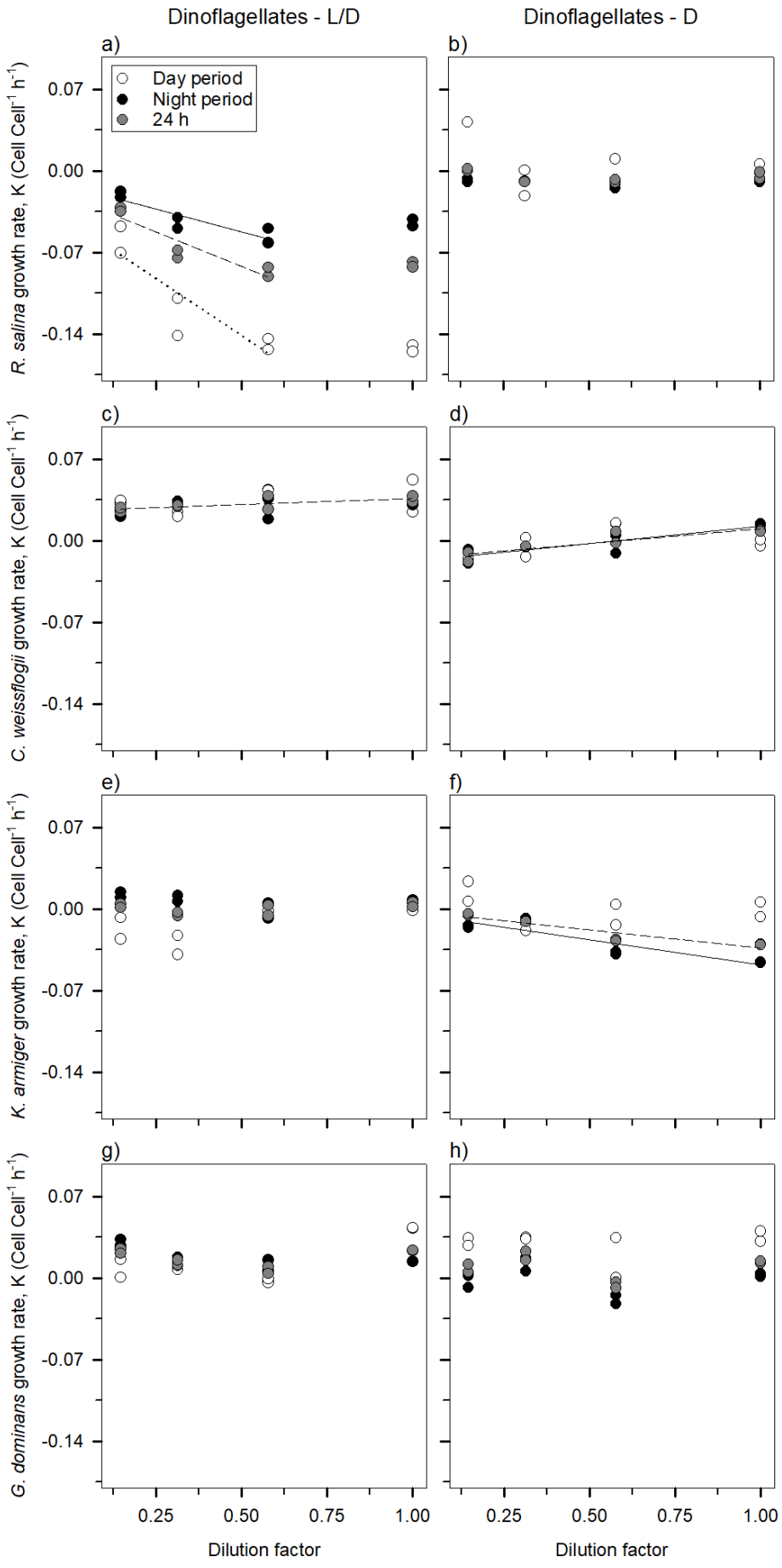

Figure 3-15 Cell-based dilution grazing experiment with dinoflagellates. The left panels (a, c, e, and g) depict the L/D bottles and the right ones (b, d, f, and h) correspond to the Dark (D) bottles. Only linear regressions with a slope significantly ($p < 0.05$) different from zero are plotted. Dotted regression lines, dashed regressions lines, and solid regression lines correspond to the day-time period, night-time period and the 24 h incubations respectively.

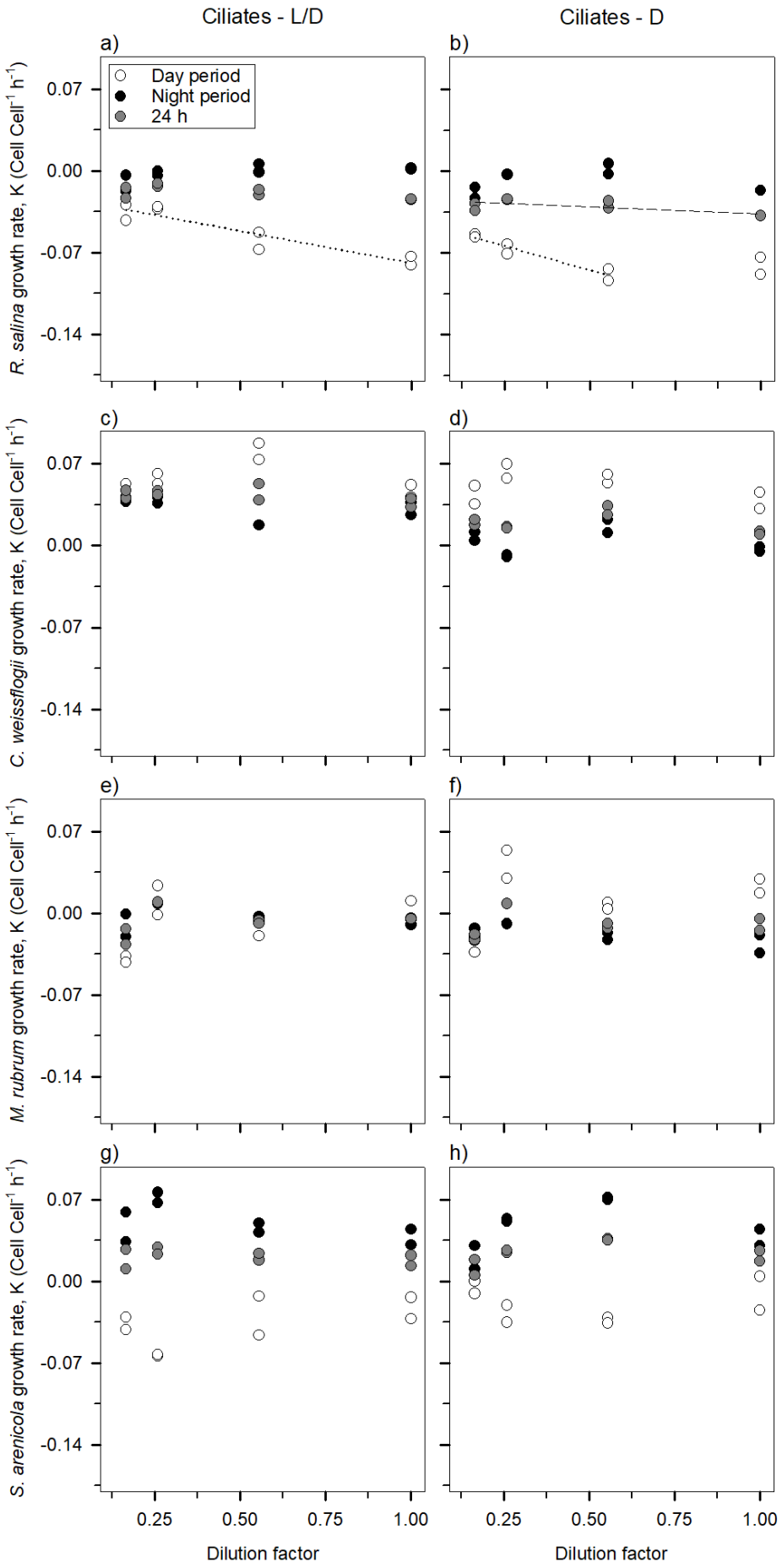

Figure 3-16 Cell-based dilution grazing experiment with ciliates. Legend as in **Figure 3-15**.

Exp	Rate, Species	Day	R^2	Day	R^2	Night	R^2	Night	R^2	24 h	R^2	24 h	R^2
Dinoflagellates	µ, Total Chl *a*	-0.0059	0.47	-0.0121	0.74**	-0.0081	0.31	-0.0032	0.13	-0.0071	0.60*	-0.0061	0.12
	g, Total Chl *a*	-0.0285		-0.0321		0.0049		0.0079		-0.0059		-0.0053	
	µ, *R. salina*	-0.0431	0.77*	0.0065	0.03	-0.0132	0.80*	-0.0102	0.06	-0.0229	0.85**	-0.0039	0.03
	g, *R. salina*	0.1091#		0.0102		0.0311#		-0.0025		0.0575#		0.0025	
	µ, *C. weissflogii*	0.0280	0.15	-0.0107	0.21	0.0249	0.19	-0.0172	0.76**	0.0259	0.50*	-0.0150	0.79**
	g, *C. weissflogii*	-0.0126		-0.0167		-0.0089		-0.0296		-0.0104		-0.0253	
	µ, *K. armiger*	-0.0278	0.48	0.0022	0.03	0.0110	0.23	-0.0049	0.81**	-0.0019	0.09	-0.0024	0.87**
	g, *K. armiger*	-0.0311		0.0073		0.0096		0.0431		-0.0039		0.0312	
	µ, *G. dominans*	-0.0043	0.49	0.0285	0.00	0.0249	0.33	-0.0004	0.01	0.0152	0.01	0.0093	0.00
	g, *G. dominans*	-0.0377		-0.0019		0.0147		0.0028		-0.0027		0.0012	
Ciliates	µ, Total Chl *a*	0.0277	0.36	-0.0281	0.13	-0.0056	0.00	-0.0233	0.00	0.0052	0.16	-0.0248	0.03
	g, Total Chl *a*	0.0171		-0.0087		0.0001		0.0010		0.0047		-0.0022	
	µ, *R. salina*	-0.0241	0.87**	-0.0432	0.92**	-0.0081	0.36	-0.0075	0.01	-0.0134	0.42	-0.0247	0.51*
	g, *R. salina*	0.0548		0.0382+		-0.0122		0.0033		0.0103		0.0120	
	µ, *C. weissflogii*	0.0585	0.00	0.0582	0.17	0.0417	0.24	0.0043	0.01	0.0474	0.27	0.0224	0.09
	g, *C. weissflogii*	0.0014		0.0152		0.0131		0.0025		0.0092		0.0068	
	µ, *M. rubrum*	-0.0225	0.17	-0.0028	0.11	0.0002	0.10	-0.0097	0.49	-0.0073	0.01	-0.0073	0.00
	g, *M. rubrum*	-0.0266		-0.0275		0.0089		0.0168		-0.0030		0.0020	
	µ, *S. arenicola*	-0.0540	0.33	-0.0204	0.00	0.0625	0.28	0.0404	0.03	0.0235	0.08	0.0200	0.07
	g, *S. arenicola*	-0.0322		-0.0024		0.0243		-0.0098		0.0053		-0.0075	

Table 3-6 Summary of growth (µ, h^{-1}) and grazing (g, h^{-1}) rates calculated from the slopes of dilution grazing experiments at the different periods of the day. The significance of the slope of the linear regressions is also listed. Columns highlighted in grey correspond to the Dark (D) treatment whereas the remaining correspond to the L/D ones. Values marked with an # showed saturation and g was then calculated according to Gallegos (1989) and Dolan *et al.* (2000). R^2 values marked with a * or ** are significant, i.e., $p < 0.05$ and $p < 0.01$ respectively.

ii. Incubation experiments

By having control bottles held under the same conditions as the dilution series, we were able to determine individual grazing rates for each predator species. Therefore, it was possible to: i) calculate the individual ingestion rate of each predator on both prey (**Table 3-7**), ii) combine the previous information to estimate what would be the merged ingestion rate per pair of predators, iii) calculate the actual ingestion rate for each pair of grazers by comparing data from the 100 % bottles and controls without grazers, and iv) calculate the ingestion rates based on the slopes of the dilution regressions.

Table 3-7 Carbon-specific ingestion rates (pg C pg C^{-1} h^{-1}) for each predator on both prey items as ascertained by the control bottles with a single predator. NS implies that the measured ingestion rate was not significantly different from 0. Columns highlighted in grey correspond to the Dark (D) treatment whereas the remaining are relative to L/D. Different letters within a given prey row imply statistically significant differences between treatments (One-Way ANOVA, Tukey HSD, $p < 0.05$).

Predator	Prey	Ingestion rates (pg C pg C^{-1} h^{-1})			
		Day	Day	Night	Night
G. dominans	*R. salina*	0.17 ± 0.02^{a}	0.02 ± 0.01^{b}	0.02 ± 0.00^{b}	NS
	C. weissflogii	-0.02 ± 0.01^{a}	0.00 ± 0.00^{a}	NS	-0.01 ± 0.00^{a}
K. armiger	*R. salina*	0.04 ± 0.00^{a}	0.03 ± 0.00^{a}	0.04 ± 0.00^{a}	NS
	C. weissflogii	-0.02 ± 0.01^{a}	NS	0.02 ± 0.00^{a}	-0.01 ± 0.00^{a}
S. arenicola	*R. salina*	0.16 ± 0.01^{a}	0.21 ± 0.00^{b}	0.06 ± 0.00^{c}	0.02 ± 0.00^{d}
	C. weissflogii	-0.04 ± 0.00^{a}	0.02 ± 0.01^{a}	0.02 ± 0.01^{a}	-0.04 ± 0.03^{a}
M. rubrum	*R. salina*	0.03 ± 0.02^{a}	NS	-0.02 ± 0.00^{b}	$0.01\pm0.01^{a,b}$
	C. weissflogii	-0.10 ± 0.01^{a}	-0.08 ± 0.06^{a}	NS	-0.07 ± 0.03^{a}

Most comparisons resulted in non-significant (i.e., not different from 0, two-tailed Student's t-test, $p > 0.05$) ingestion rates on *C. weissflogii*, with the exception of *S. arenicola* in some treatments, and *K. armiger* during the night-time in the L/D treatment (**Table 3-7**). In the L/D treatment, *G. dominans* clearly consumed more *R. salina* during the day than at night (Tukey HSD, $p < 0.05$), a pattern shared by all grazers except *K. armiger*, whose differences between day and night periods were negligible. *M. rubrum*

was the species with the largest day/night differences, as it was the only species displaying a significantly negative ingestion rate on *R. salina* during the night.

The D treatments affected the grazers in a different manner: *G. dominans* and *K. armiger* decreased their ingestion rates during the day (despite being significant only in the former) and displayed non-significant ingestion rates at night. Conversely, *S. arenicola* benefitted from the D treatment during the day (Tukey HSD, $p < 0.05$) despite having its ingestion rate decreased during the night (Tukey HSD, $p < 0.05$). Finally, ingestion rates by *M. rubrum* decreased to negligible levels during day-time in the D treatments (two-tailed Student's t-test, $p > 0.05$). The nightly ingestion rates of the D treatment were significantly positive whereas the same period in L/D yielded significantly negative ingestion rates (**Table 3-7**), however, this difference was not significant due to high variability of the data (Tukey HSD, $p > 0.05$). Protozooplankton displayed higher 24 h integrated ingestion rates on *R. salina* than did mixoplankton regardless of the light conditions. This difference was more evident in the presence of light but not negligible in its absence. In the L/D treatment, *G. dominans* exhibited carbon-specific ingestion rates ca. 1.5 times higher than *K. armiger*, and *S. arenicola* completely outcompeted *M. rubrum* with an ingestion rate ca. 21.4 times superior. In the D treatment, the differences were only ca. 1.3 and 6.7 times, respectively for dinoflagellates and ciliates.

The integrated 24 h period grazing for each predator tandem calculated as explained before is summarised in **Figure 3-17**. Since *C. weissflogii* was often not consumed in the experiments, we have shown only the data regarding *R. salina*. The estimated ingestion rates (obtained from the grazing impact of each individual grazer) were higher than those measured in the undiluted bottles against the respective controls. Additionally, ingestion rates calculated from the dilution slope (without controls) tend to be lower than those measured using the control bottles containing both grazers. However, the differences between methods used to ascertain ingestion rates were only significant in the L/D treatments.

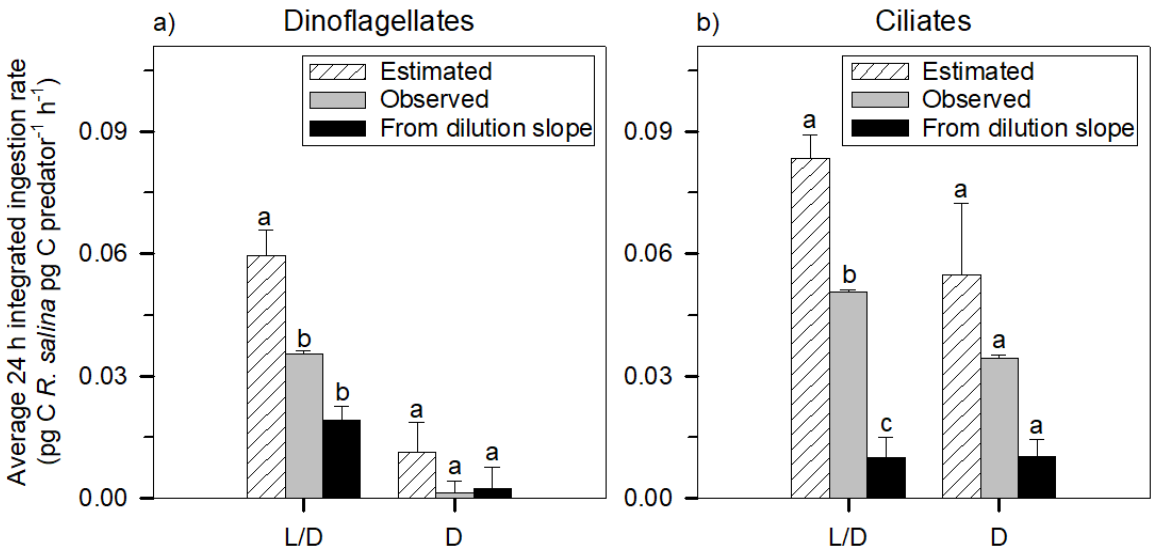

Figure 3-17 Comparison between estimated (▨), observed (□), and dilution-measured (■) ingestion rates (pg C *R. salina* pg C predator^{-1} h^{-1}) in the L/D and Dark (D) bottles over a 24 h period: a) experiment with dinoflagellates and b) experiment with ciliates. Notice that dilution-measured ingestion rates were calculated using g values listed in Table 2. See the Methods for a detailed explanation of the calculation of each value. Different letters within each group of bars (i.e., L/D evaluated independently from D bottles) imply statistically significant differences (One-Way ANOVA, Tukey HSD, $p < 0.05$).

To further understand the Chl *a* dynamics that shaped the outcome of the dilution experiments based on this proxy, we evaluated the contribution of each species to the total Chl *a* pool (**Figure 3-18** and **3-19**) both in the undiluted and most diluted treatments. Regarding the dinoflagellate experiment (**Figure 3-18**), both the diatom and *K. armiger* became more relevant to the total Chl *a* as time passed, in particular in the undiluted L/D treatment (**Figure 3-18a**) where they increased their contribution to the total Chl *a* by ca. 9.3 and 31.7 % respectively.

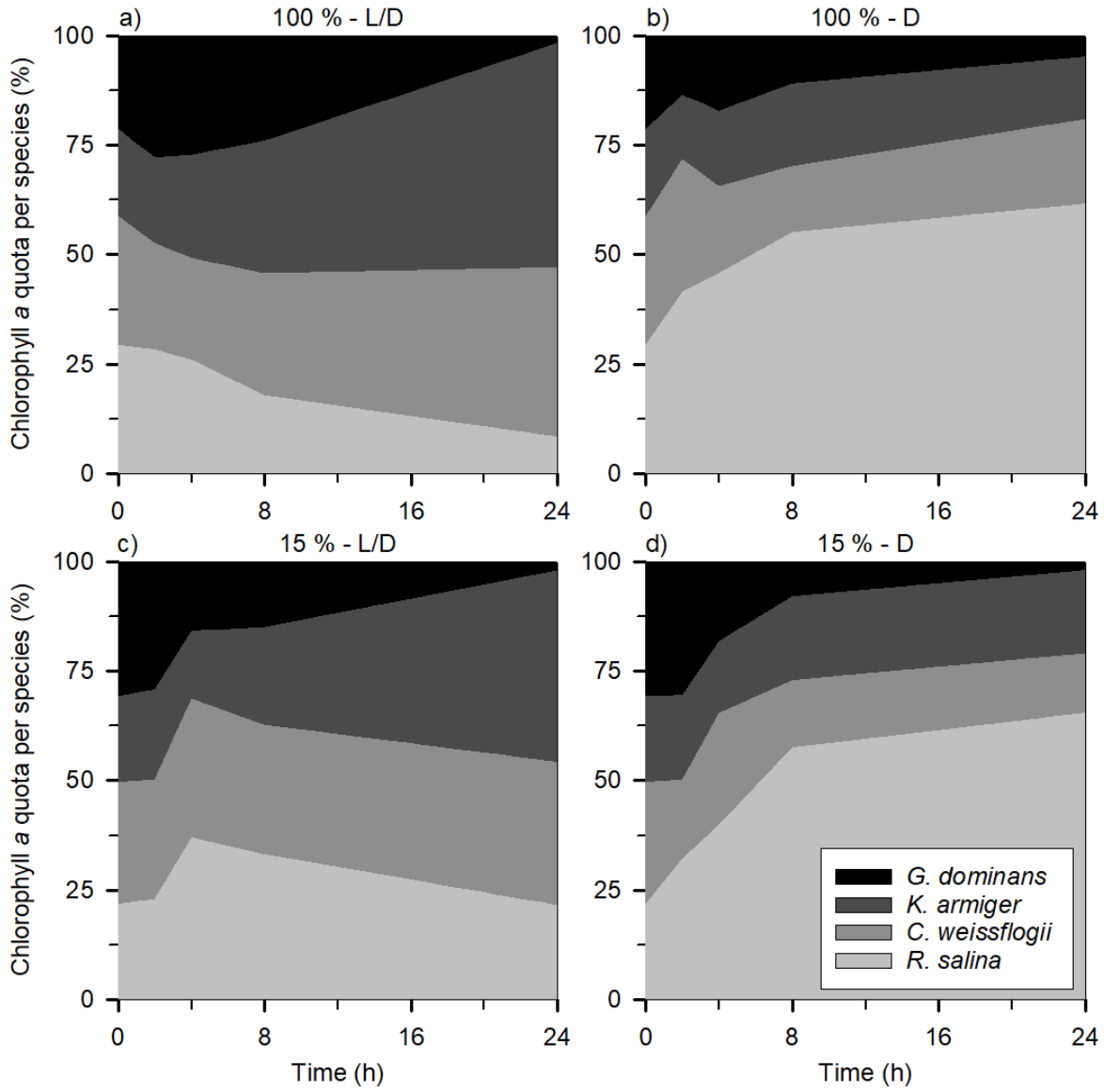

Figure 3-18 The proportion of the total Chl *a* (%) represented by each species (in different colours) in the dinoflagellate experiment throughout the incubation: a and c) L/D treatment with the undiluted and most dilute communities respectively; b and d) Dark (D) treatment with the undiluted and most dilute communities respectively.

The D treatment has a completely different pattern, with *R. salina* benefiting the most, in particular when the predator concentration was low (**Figure 3-18d**), becoming ca. 65.4 % of the total Chl *a* of the system at the end of the incubation (as compared to 21.8 % in the beginning). Irrespective of the light conditions, *G. dominans* displayed a particularly significant contribution to the total Chl *a* (up to 30.8 %) at the beginning of the incubation. The experiment with ciliates (**Figure 3-19**) followed a similar trend for the diatom and the protozooplankton (**Figure 3-19a**), albeit to a slightly larger extent in the former (an increase of ca. 10.9 %) and smaller in the latter (maximum contribution of ca. 12.7 %).

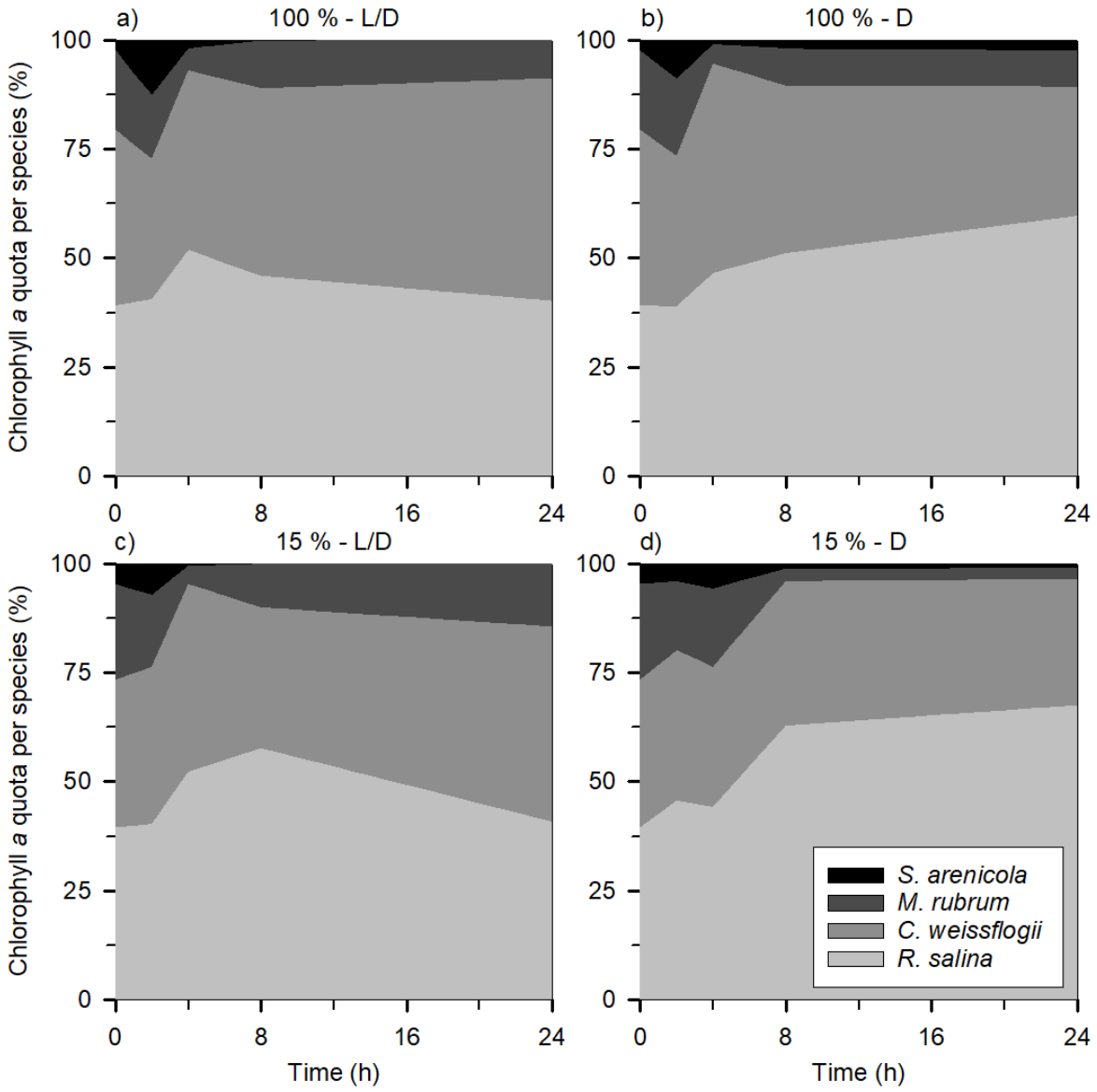

Figure 3-19 The proportion of the total Chl *a* (%) represented by each species (in different colours) in the ciliate experiment throughout the incubation. Legend as in **Figure 3-18**.

M. rubrum, in contrast with its dinoflagellate counterpart, decreased its contribution to the total Chl *a* by ca. 9.2 % (**Figure 3-19a**). Concerning the D treatment, *R. salina* was also the species that fared better with an increase of ca. 28.0 % in the diluted treatment (**Figure 3-19d**). In general, when the incubation contained only one predator species, the calculated individual Chl *a* content was, on average, ca. 8.5 % higher than when two predators were incubated together. Additionally, the magnitude of this effect differed between undiluted bottles, and the most diluted treatments (raw data not shown but incorporated in **Figures 3-18** and **3-19**).

3.5.3 Discussion

i. Consequences of using the wrong proxy for phytoplankton biomass and growth

Our results show that Chl *a* alone is not an adequate proxy for prey growth rates in dilution grazing experiments when mixoplankton are present (Paterson *et al.* 2008, Calbet *et al.* 2012). Chlorophyll is, in any case, a poor proxy for phototrophic plankton biomass (Kruskopf & Flynn 2006) because of inter-species variations, and also for the photoacclimation abilities of some species (for which very significant changes can occur within a few hours). The problem extends to the involvement of mixoplanktonic prey and grazers. Nevertheless, even very recent studies continue to rely on this parameter for quantifications of grazing despite acknowledging the dominance, both in biomass and abundance, of mixoplanktonic predators in their system (Morison *et al.* 2020). Moreover, the detailed analysis of the species-specific dynamics revealed that different prey species are consumed at very different rates. In our experiments, and contrarily to expectations (see Berge *et al.* 2008a and Nakamura *et al.* 1995), *C. weissflogii* was only actively ingested in the ciliate experiment and, according to the results from the control bottles (**Table 3-7**). Certainly, it is not the first time that a negative selection against diatoms has been seen; for example, Burkill *et al.* (1987) noticed that diatoms were less grazed than other phytoplankton species, as assessed by a dilution technique paired with High-Performance Liquid Chromatography for pigment analysis. Calbet *et al.* (2011b), in the Arctic, also found only occasional grazing over the local diatoms. In our study, diatoms were not only not consumed, but the presence of dinoflagellates appeared to contribute to their growth, this relationship being partly dependent on the concentration of the predator (see **Figures 3-15c,d**). This result could be a direct consequence of assimilation and use of compounds (e.g. Admiraal *et al.* 1984, Armbrust *et al.* 2004, Olofsson *et al.* 2019) released by microplankton such as ammonium (e.g. Caperon *et al.* 1979, Gao *et al.* 2018) and urea (e.g. Solomon *et al*. 2010), which were not supplied in the growth medium, but which would have supported prey growth. One *C. weissflogii* cell contains, on average, ca. 2.5 times more Chl *a* than one *R. salina* cell (initial value excluded, see **Table 3-5**). Taken together with the preference for *R. salina* it is not surprising that the proportion of total Chl *a* represented by the diatoms increased over time, in particular in the L/D treatment (**Figures 3-18a,c** and **Figures 3-19a,c**).

Another factor clearly highlighted by our experiments, but invariably ignored in a traditional dilution experiment, is that protozooplankton themselves contribute a significant portion of the total chlorophyll of the system (due to ingested Chl *a*), in particular at the beginning of the incubation (see **Figures 3-18** and **Figures 3-19**). Once again, this is not novel information, since Chl *a* and its degradation products have been found inside several protozooplankton species from different phylogenetic groups immediately after feeding (Kashiyama *et al.* 2012) and even after some days without food (Aristizábal 2009). An increase in intracellular Chl *a* concentrations immediately after feeding has also been found in mixoplankton (Johnson & Stoecker 2005, Berge & Hansen 2016), on which this increase is derived both from ingested prey as well as from new synthesis of their own Chl *a*. Additionally, several experiments with LFLA show that predators (irrespective of their trophic mode) seem to maximise the concentration of intracellular prey shortly after the initiation of the incubation (e.g. Rublee & Gallegos 1989, Setälä *et al.* 2005, see Section 3.4). Indeed, some authors have even been able to measure photosynthesis in protozooplankton, like the ciliates *Mesodinium pulex* (Tarangkoon & Hansen 2011) and *Strombidinopsis sp.* (Schoener & McManus 2017).

ii. When the whole is lower than the sum of the parts

In the previous section, we highlighted the need for a proxy other than Chl *a* to estimate phytoplankton biomass in dilution grazing experiments. This can be fairly easily solved by the quantification of the prey community abundance (e.g. Lawrence & Menden-Deuer 2012) by microscopy or by the use of signature pigments for each major phytoplankton group. The latter method, however, is not as thorough as the former, since rare are the cases where one pigment is exclusively associated with a single group of organisms (e.g. Jeffrey & Vesk 1997, Landry *et al.* 2000, Garcés *et al.* 2006). In any case, any pigment-based proxy is subject to the same problems, as identified by Kruskopf & Flynn (2006). Irrespective of the quantification method, it has been made evident that the different algae are consumed at different rates (e.g. pigments - Burkill *et al.* 1987, Paterson *et al.* 2008, Grattepanche *et al.* 2011; microscopy - Stelfox-Widdicombe *et al.* 2004, Calbet *et al.* 2011b, Arias *et al.* 2020b).

Prey selection in protistan grazers is a common feature (e.g. Flynn *et al.* 1996, Peltomaa & Johnson 2017, Johnson *et al.* 2018, Maselli *et al.* 2020). Given the diversity of grazers in natural communities and the array of preferred prey that each particular species

possesses, it is logical to think that dilution experiments will capture the net community response properly. Likewise, grazers interact with each other through allelopathy, competition, and intraguild predation among other factors. An example of intraguild predation could be the observed on *K. armiger* by *G. dominans* (see **Figure 3-15f** and **Table 3-6**), which caused an average loss of ca. 18.72 pg of *K. armiger* carbon per *G. dominans* per hour in the D treatment. Interestingly, in the same treatment, a slight negative effect of *K. armiger* on its predator *G. dominans* can also be deduced (i.e., positive g, **Table 3-6**), resulting in an average loss of ca. 0.33 pg *G. dominans* carbon per *K. armiger* per hour. This could be a consequence of allelopathy since *K. armiger* is a known producer of karmitoxin (Rasmussen *et al.* 2017), whose presence can have negative effects even on metazoan grazers (Berge *et al.* 2012). Regarding ciliates, none of the species used is a known producer of allelopathic compounds, which suggests that the average loss of ca. 1.25 pg *M. rubrum* carbon per hour in the D treatment was due to to *S. arenicola* predation. Altogether, it seems clear from our data that intraguild predation cannot be ignored when analysing dilution experiments. Furthermore, our results clearly show that single functional responses cannot be used to extrapolate community grazing impacts, as evidenced by the differences in estimated and measured ingestion rates based on the disappearance of prey in combined grazers experiments (**Figures 3-17**). Nevertheless, this is a common procedure (e.g. Kim & Jeong 2004, Yih *et al.* 2004, Lee *et al.* 2014). Often in modelling approaches, individual predator's functional responses have been used to extrapolate prey selectivity and community grazing responses (Ryabov *et al.* 2015); in reality complex prey selectivity functions are required to satisfactorily describe prey selectivity and inter-prey allelopathic interactions (Mitra & Flynn 2006).

It is however also evident that the measured ingestion rates in combined grazers experiments were not the same as those calculated from the slope of the dilution grazing experiment. This raises the question why was that the case? It is well known that phytoplankton cultures, when extremely diluted, show a lag phase of different duration (Fogg 1957, Aliyu *et al.* 2021) which has been attributed to the net leakage of metabolites (Flynn & Berry 1999). Assuming that the duration of the lag phase will be dependent on the level of dilution, it seems reasonable to deduce that after ca. 24 h the instantaneous growth rates (μ) in the most diluted treatments will be lower than that of the undiluted treatments. This has consequences, not only for the estimated prey growth rates, but also

for the whole assessment of the grazing rate, due to the flattening of the regression line (i.e., the decrease in the computed growth rate). This artefact may be more evident in cultures acclimated to very particular conditions (as the laboratory cultures used in this study) than in nature.

iii. When the lights go off

Another important finding of our research is the importance of light on the correct expression of the feeding activity by both mixoplankton and protozooplankton. We noticed that irrespective of the light conditions, all species exhibited a diurnal feeding rhythm (*R. salina* panels in **Figures 3-15** and **3-16**), which is in accordance to earlier observations (e.g. Strom 2001, Ng *et al.* 2017, Arias *et al.* 2020a, 2021). The presence of light typically increased the ingestion rates. Additionally, the ingestion rates differed during the night period between L/D and D treatments, which implies that receiving light during the day is also vital in modulating the night behaviour of protoozoo- and mixoplankton. In particular, mixoplankton grazing is usually affected by light conditions, typically increasing (e.g. Jakobsen *et al.* 2000, Li *et al.* 2000, Berge *et al.* 2008a, Kim *et al.* 2008), but also sometimes decreasing (Myung *et al.* 2006, McKie-Krisberg *et al.* 2015) in the presence of light. Different irradiance levels can also affect the magnitude of ingestion rates both in protozoo- and mixoplankton (Moeller *et al.* 2019 and references therein).

Therefore, we hoped for a rather consistent pattern among our protists that would help us discriminate mixoplankton in dilution grazing experiments. As a matter of fact, based on the results from Arias *et al.* (2020a), we expected that in the dinoflagellate experiment, the D treatment would have inhibited only the grazing of *K. armiger*, enabling a simple discrimination between trophic modes. The reality did not meet the expectations since the day and night-time carbon-specific ingestion rates (as assessed using the control bottles, **Table 3-7**) of *K. armiger* were respectively higher and equal than those of *G. dominans*. Conversely, in the ciliate experiment, protozooplankton were the major grazers in our incubations regardless of the day period and light conditions. This response was not as straightforward as one would expect it to be because *M. rubrum* has been recently suggested to be a species-complex containing at least 7 different species (Drumm *et al.* 2021 and references therein), which hinders any possible conjecture on their grazing impact. Indeed, the uneven responses found between and within trophic modes precluded such optimistic hypothetical procedure.

The D treatment in the present paper illustrated the importance of mimicking natural light conditions, a factor also addressed in the original description of technique by Landry & Hassett (1982). It is crucial for the whole interpretation of the dilution technique that incubations should be conducted in similar light (and temperature) conditions as the natural ones to allow for continued growth of the phototrophic prey. However, here we want to stress another aspect of the incubations: should they start during the day or the night? Considering our (and previous) results on diel feeding rhythms, and on the contribution of each species to the total Chl *a* pool, it is clear that different results will be obtained if the incubations are started during the day or the night. Besides, whether day or night, organisms are also likely to be in a very different physiological state (either growing or decreasing). Therefore, we recommend that dilution experiments conducted in the field should always be started at the same period of the day to enable comparisons (see also Anderson *et al.* (2017) for similar conclusions on bacterivory exerted by small flagellates). Ideally, incubations would be started at different times of the day in order to capture the intricacies of the community dynamics on a diel cycle. Nevertheless, should the segmented analysis be impossible, we argue that the right time to begin the incubations would be during the night, as this is the time where ingestion rates by protozooplankton are typically lower (e.g. Strom 2001, Ng *et al.* 2017, Arias *et al.* 2020a, 2021, this study) and would, consequently, reduce their quota of Chl *a* in the system.

3.6 Conclusions

Despite the inability of acting as a deterrent of protozooplanktonic grazing (noticed by the stronger effect on mixoplanktonic predation), rotenone can still be used as a good algal crop protector, especially if the predator is a sensitive organism like a ciliate (Section 3.3) or a rotifer (Van Ginkel *et al.* 2015, 2016). Nevertheless, future measures should always assess the effect of rotenone on the specific organism that is plaguing the algal culture, as differences in the sensitivity towards the compound are expected, as highlighted in the Section 3.3. Similarly, the sensitivity of the algal culture itself should also be acknowledged, as phytoplankton species are not all immune to this compound as expected. Factors such as the growth phase may be exploited to minimise the nefarious effects of the presence of rotenone in non-target organisms.

Regarding the second approach, the LFLA technique (as described in the Section 3.4) appears to be only directly applicable to organisms that feed by direct engulfment of prey. Indeed, all other feeding mechanisms (present both in protozoo- and mixoplanktonic dinoflagellates) result in biased or even unmeasurable ingestion rates. A way to avoid the size selectivity issue demonstrated by our results could be to use two distinct sizes of prey (Martínez *et al.* 2014). Ideally, both prey would be simultaneously labelled with fluorochromes whose emission spectrum would coincide but differing in the emitted fluorescent colour (Shields & Smith 2008, Nelson *et al.* 2009). For example, *I. galbana* could be labelled with CMFDA (green fluorescence, viable labelling - e.g., Li *et al.* 1996) and *T. chuii* could be simultaneously labelled with CMAC (blue fluorescence, viable labelling - e.g., Martínez *et al.* 2014). Still, even if a sample is dually-labelled there may be a selection for or against the labelled prey due to the presence of the fluorochrome. On these cases, an alternative could be to incorporate the fluorescent tracer on the genome of the tracer algae (for example, by fusing a green fluorescent protein, GFP, to a housekeeping gene). This is an advantage even over vital stains (Epstein & Rossel 1995) and is getting attention from the scientific community since the GFP vector is very bright and easily detectable, besides from being photostable (Bochdansky *et al.* 2015). Nevertheless, despite highly promising, this approach is only available for bacteria at the time of writing (e.g., Ishii *et al.* 2002, Fu *et al.* 2003, Bochdansky *et al.* 2015). At last, we have provided clear evidence that there is one issue that is likely never going to be accounted for using this technique. As seen in the *Teleaulax-Isochrysis-Mesodinium* incubation (and, on a qualitative extent, also on the *Mesodinium-Dinophysis* interaction),

this predator exhibits a species-specific selectivity, which hindered the quantification of ingested tracer prey.

To end on a positive note, let us now consider the Section 3.5. We are aware that our study does not represent natural biodiversity because our experiments were conducted in the laboratory with a few species. Nevertheless, we attempted to use common species of wide distribution for each major group of protists to provide a better institutionalisation of our conclusions. Indeed, our incubations contained cryptophytes and diatoms as prey, and both mixoplanktonic and pure protozooplanktonic predators, namely a dinoflagellate and a ciliate for each trophic mode. With these laboratory experiments, we have presented evidence calling for a cessation of the use of chlorophyll in dilution grazing experiments (Paterson *et al.* 2008, Calbet *et al.* 2012), and we have highlighted the need to observe the organismal composition of both initial and final communities to better understand the dynamics during the dilution grazing experiments (Lawrence & Menden-Deuer 2012). This approach will not incorporate mixoplanktonic activity into the dilution technique *per se* however, if combined with LFLA (see Calbet *et al.* 2012 and Martinéz *et al.* 2014), a semi-quantitative approach to disentangle the contribution of mixoplankton to community grazing could be achieved (although not perfect). An alternative (and perhaps more elegant) solution could be the integration of the experimental technique with *in silico* modelling. The modelling approaches of the dilution technique have already been used, for example, to disentangle niche competition (Beckett & Weitz 2017) and to explore nonlinear grazer responses (Sandhu *et al.* 2019). We believe that our experimental design and knowledge of the previously indicated data could be of use for the configuration of a dilution grazing model, which could then be validated in the field (and, optimistically, coupled to the ubiquitous application of the dilution technique across the globe). We cannot guarantee that having a properly constructed model that mimics the dilution technique will be the solution to the mixoplankton paradigm. However, it may provide a step towards that goal as it could finally shed much-needed light on the mixo- and protozooplanktonic contributions to the grazing pressure of a given system. To quote from the commentary of Flynn *et al.* (2019), it could provide the answer to the question of whether mixoplankton are *de facto* “another of the Emperor’s New Suit of Clothes” or, “on the other hand (…) collectively worthy of more detailed inclusion in models”.

3.7 References

Admiraal W, Laane RWPM, Peletier H (1984) Participation of diatoms in the amino acid cycle of coastal waters; uptake and excretion in cultures. *Mar. Ecol. Prog. Ser.,* 15, 303-306.

Aliyu A, Lee JGM, Harvey AP (2021) Microalgae for biofuels via thermochemical conversion processes: A review of cultivation, harvesting and drying processes, and the associated opportunities for integrated production. *Bioresour. Technol. Rep.,* 14, 100676.

Almeda R, Hyatt C, Buskey EJ (2014) Toxicity of dispersant Corexit 9500A and crude oil to marine microzooplankton. *Ecotoxicol. Environ. Saf.,* 106, 76-85.

Anderson OR (1978) Light and electron microscopic observations of feeding behavior, nutrition, and reproduction in laboratory cultures of *Thalassicolla nucleata*. *Tissue Cell,* 10, 401-412.

Anderson OR, Swanberg NR, Bennett P (1983) Assimilation of symbiont-derived photosynthates in some solitary and colonial radiolaria. *Mar. Biol.,* 77, 265-269.

Anderson R, Jürgens K, Hansen PJ (2017) Mixotrophic phytoflagellate bacterivory field measurements strongly biased by standard approaches: a case study. *Front. Microbiol.,* 8, 1398.

Archer SD, Leakey RJ, Burkill PH, Sleigh MA (1996) Microbial dynamics in coastal waters of East Antarctica: herbivory by heterotrophic dinoflagellates. *Mar. Ecol. Prog. Ser.,* 139, 239-255.

Arias A, Saiz E, Calbet A (2020a) Towards an understanding of diel feeding rhythms in marine protists: consequences of light manipulation. *Microb. Ecol.,* 79, 64-72.

Arias A, Saiz E, Tiselius P, Calbet A (2020b) Trophic interactions and diel feeding rhythms of microzooplankton in a productive Swedish Fjord. *ICES J. Mar. Sci.,* 77, 2718-2728.

Arias A, Selander E, Saiz E, Calbet A (2021) Predator chemical cue effects on the diel feeding behaviour of marine protists. *Microb. Ecol.*

Aristizábal M (2009) *Potential respiration in Oxyrrhis marina and Rhodomonas salina.* Universidad de Las Palmas de Gran Canaria.

Armbrust EV, Berges JA, Bowler C, Green BR, Martinez D, Putnam NH, Zhou S, Allen AE, Apt KE, Bechner M (2004) The genome of the diatom *Thalassiosira pseudonana*: ecology, evolution, and metabolism. *Science,* 306, 79-86.

Beal DL, Anderson RV (1993) Response of zooplankton to rotenone in a small pond. *Bull. Environ. Contam. Toxicol.,* 51, 551-556.

Beckett SJ, Weitz JS (2017) Disentangling niche competition from grazing mortality in phytoplankton dilution experiments. *PloS One,* 12, e0177517.

Berge T, Daugbjerg N, Andersen BB, Hansen PJ (2010) Effect of lowered pH on marine phytoplankton growth rates. *Mar. Ecol. Prog. Ser.,* 416, 79-91.

Berge T, Hansen PJ (2016) Role of the chloroplasts in the predatory dinoflagellate *Karlodinium armiger*. *Mar. Ecol. Prog. Ser.,* 549, 41-54.

Berge T, Hansen PJ, Moestrup Ø (2008a) Feeding mechanism, prey specificity and growth in light and dark of the plastidic dinoflagellate *Karlodinium armiger*. *Aquat. Microb. Ecol.,* 50, 279-288.

Berge T, Hansen PJ, Moestrup Ø (2008b) Prey size spectrum and bioenergetics of the mixotrophic dinoflagellate *Karlodinium armiger*. *Aquat. Microb. Ecol.,* 50, 289-299.

Berge T, Poulsen LK, Moldrup M, Daugbjerg N, Hansen PJ (2012) Marine microalgae attack and feed on metazoans. *ISME J.,* 6, 1926-1936.

Blossom HE, Bædkel TD, Tillmann U, Hansen PJ (2017) A search for mixotrophy and mucus trap production in *Alexandrium* spp. and the dynamics of mucus trap formation in *Alexandrium pseudogonyaulax*. *Harmful algae,* 64, 51-62.

Blossom HE, Daugbjerg N, Hansen PJ (2012) Toxic mucus traps: A novel mechanism that mediates prey uptake in the mixotrophic dinoflagellate *Alexandrium pseudogonyaulax*. *Harmful Algae,* 17, 40-53.

Bochdansky AB, Clouse MA (2015) New tracer to estimate community predation rates of phagotrophic protists. *Mar. Ecol. Prog. Ser.,* 524, 55-69.

Broglio E, Saiz E, Calbet A, Trepat I, Alcaraz M (2004) Trophic impact and prey selection by crustacean zooplankton on the microbial communities of an oligotrophic coastal area (NW Mediterranean Sea). *Aquat. Microb. Ecol.,* 35, 65-78.

Burkill PH, Mantoura RFC, Llewellyn CA, Owens NJP (1987) Microzooplankton grazing and selectivity of phytoplankton in coastal waters. *Mar. Biol.,* 93, 581-590.

Calado AJ, Moestrup Ø (1997) Feeding in *Peridiniopsis berolinensis* (Dinophyceae): new observations on tube feeding by an omnivorous, heterotrophic dinoflagellate. *Phycologia,* 36, 47-59.

Calbet A, Bertos M, Fuentes-Grünewald C, Alacid E, Figueroa R, Renom B, Garcés E (2011a) Intraspecific variability in *Karlodinium veneficum*: Growth rates, mixotrophy, and lipid composition. *Harmful Algae,* 10, 654-667.

Calbet A, Isari S, Martínez RA, Saiz E, Garrido S, Peters J, Borrat RM, Alcaraz M (2013) Adaptations to feast and famine in different strains of the marine heterotrophic dinoflagellates *Gyrodinium dominans* and *Oxyrrhis marina*. *Mar. Ecol. Prog. Ser.,* 483, 67-84.

Calbet A, Martínez RA, Isari S, Zervoudaki S, Nejstgaard JC, Pitta P, Sazhin AF, Sousoni D, Gomes A, Berger SA (2012) Effects of light availability on mixotrophy and microzooplankton grazing in an oligotrophic plankton food web: evidences from a mesocosm study in Eastern Mediterranean waters. *J. Exp. Mar. Biol. Ecol.,* 424, 66-77.

Calbet A, Saiz E, Almeda R, Movilla JI, Alcaraz M (2011b) Low microzooplankton grazing rates in the Arctic Ocean during a *Phaeocystis pouchetii* bloom (Summer 2007): fact or artifact of the dilution technique? *J. Plankton Res.,* 33, 687-701.

Caperon J, Schell D, Hirota J, Laws E (1979) Ammonium excretion rates in Kaneohe Bay, Hawaii, measured by a 15N isotope dilution technique. *Mar. Biol.,* 54, 33-40.

Caron DA (2001) Protistan herbivory and bacterivory. In: JH Paul (ed) *Marine Microbiology.* Vol. 30. Academic Press, Florida, USA, pp. 289-315.

Dawson VK, Gingerich WH, Davis RA, Gilderhus PA (1991) Rotenone persistence in freshwater ponds: effects of temperature and sediment adsorption. *N. Am. J. Fish Manag.,* 11, 226-231.

Decelle J, Probert I, Bittner L, Desdevises Y, Colin S, De Vargas C, Galí M, Simó R, Not F (2012) An original mode of symbiosis in open ocean plankton. *Proc. Natl. Acad. Sci.,* 109, 18000-18005.

Dolan JR, Gallegos CL, Moigis A (2000) Dilution effects on microzooplankton in dilution grazing experiments. *Mar. Ecol. Prog. Ser.,* 200, 127-139.

Dolan JR, Šimek K (1998) Ingestion and digestion of an autotrophic picoplankter, *Synechococcus*, by a heterotrophic nanoflagellate, *Bodo saltans*. *Limnol. Oceanogr.,* 43, 1740-1746.

Dolan JR, Šimek K (1999) Diel periodicity in *Synechococcus* populations and grazing by heterotrophic nanoflagellates: analysis of food vacuole contents. *Limnol. Oceanogr.,* 44, 1565-1570.

Dortch Q, Roberts TL, Clayton Jr JR, Ahmed SI (1983) RNA/DNA ratios and DNA concentrations as indicators of growth rate and biomass in planktonic marine organisms. *Mar. Ecol. Prog. Ser.,* 13, 61-71.

Drumm K, Norlin A, Kim M, Altenburger A, Juel Hansen P (2021) Physiological responses of *Mesodinium major* to irradiance, prey concentration and prey starvation. *J. Eukaryot. Microbiol.,* n/a, e12854.

El-Sayed WMM, Van Ginkel SW, Igou T, Ibrahim HA, Abdul-Raouf UM, Chen Y (2018) Environmental influence on rotenone performance as an algal crop protective agent to prevent pond crashes for biofuel production. *Algal Res.,* 33, 277-283.

Enge AJ, Wukovits J, Wanek W, Watzka M, Witte UF, Hunter WR, Heinz P (2016) Carbon and nitrogen uptake of calcareous benthic foraminifera along a depth-related oxygen gradient in the OMZ of the Arabian Sea. *Front. Microbiol.,* 7, 71.

Epstein SS, Rossel J (1995) Methodology of *in situ* grazing experiments: evaluation of a new vital dye for preparation of fluorescently labeled bacteria. *Mar. Ecol. Prog. Ser.,* 128, 143-150.

Fenchel T, Finlay BJ (1983) Respiration rates in heterotrophic, free-living protozoa. *Microb. Ecol.,* 9, 99-122.

Fenchel T, Hansen PJ (2006) Motile behaviour of the bloom-forming ciliate *Mesodinium rubrum*. *Mar. Biol. Res.,* 2, 33-40.

Ferreira GD, Calbet A (2020) Caveats on the use of rotenone to estimate mixotrophic grazing in the oceans. *Sci. Rep.,* 10, 3899.

Ferrier-Pagès C, Leal MC (2019) Stable isotopes as tracers of trophic interactions in marine mutualistic symbioses. *Ecol. Evol.,* 9, 723-740.

Flynn KJ, Berry LS (1999) The loss of organic nitrogen during marine primary production may be significantly overestimated when using ^{15}N substrates. *Proc. R. Soc. B,* 266, 641-647.

Flynn KJ, Davidson K, Cunningham A (1996) Prey selection and rejection by a microflagellate; implications for the study and operation of microbial food webs. *J. Exp. Mar. Biol. Ecol.,* 196, 357-372.

Flynn KJ, Mitra A, Anestis K, Anschütz AA, Calbet A, Ferreira GD, Gypens N, Hansen PJ, John U, Martin JL, Mansour JS, Maselli M, Medić N, Norlin A, Not F, Pitta P, Romano F, Saiz E, Schneider LK, Stolte W, Traboni C (2019) Mixotrophic protists and a new paradigm for marine ecology: where does plankton research go now? *J. Plankton Res.,* 41, 375-391.

Fogg GE (1957) Relationships between metabolism and growth in plankton algae. *J. Gen. Microbiol.,* 16, 294-297.

Fok AK, Valin EL (1983) Effects of dimethylsulfoxide (DMSO) on the digestive-lysosomal system in *Paramecium caudatum*. *Eur. J. Cell Biol.,* 32, 45-51.

Fredrickson KA, Strom SL (2009) The algal osmolyte DMSP as a microzooplankton grazing deterrent in laboratory and field studies. *J. Plankton Res.,* 31, 135-152.

Frost BW (1972) Effects of size and concentration of food particles on the feeding behavior of the marine planktonic copepod *Calanus pacificus*. *Limnol. Oceanogr.,* 17, 805-815.

Fu Y, O'kelly C, Sieracki M, Distel DL (2003) Protistan grazing analysis by flow cytometry using prey labeled by in vivo expression of fluorescent proteins. *Appl. Environ. Microbiol.,* 69, 6848.

Gaines G, Taylor FJR (1984) Extracellular digestion in marine dinoflagellates. *J. Plankton Res.,* 6, 1057-1061.

Gallegos CL (1989) Microzooplankton grazing on phytoplankton in the Rhode River, Maryland: Nonlinear feeding kinetics. *Mar. Ecol. Prog. Ser.,* 57, 23-33.

Gao H, Hua C, Tong M (2018) Impact of *Dinophysis acuminata* feeding *Mesodinium rubrum* on nutrient dynamics and bacterial composition in a microcosm. *Toxins,* 10, 443.

Garcés E, Fernandez M, Penna A, Van Lenning K, Gutierrez A, Camp J, Zapata M (2006) Characterization of NW Mediterranean *Karlodinium* spp. (Dinophyceae) strains using morphological, molecular, chemical, and physiological methodologies. *J. Phycol.,* 42, 1096-1112.

Grattepanche JD, Vincent D, Breton E, Christaki U (2011) Microzooplankton herbivory during the diatom–*Phaeocystis* spring succession in the eastern English Channel. *J. Exp. Mar. Biol. Ecol.,* 404, 87-97.

Guillard RRL (1975) Culture of phytoplankton for feeding marine invertebrates. In: WL Smith and MH Chanley (eds) *Culture of marine invertebrate animals.* Plenum Press, New York, NY, pp. 29-60.

Hansen B, Bjornsen PK, Hansen PJ (1994) The size ratio between planktonic predators and their prey. *Limnol. Oceanogr.,* 39, 395-403.

Hansen PJ (1991) Quantitative importance and trophic role of heterotrophic dinoflagellates in a coastal pelagial food web. *Mar. Ecol. Prog. Ser.,* 73, 253-261.

Hansen PJ, Calado AJ (1999) Phagotrophic mechanisms and prey selection in free-living dinoflagellates *J. Eukaryot. Microbiol.,* 46, 382-389.

Hansen PJ, Moldrup M, Tarangkoon W, Garcia-Cuetos L, Moestrup Ø (2012) Direct evidence for symbiont sequestration in the marine red tide ciliate *Mesodinium rubrum*. *Aquat. Microb. Ecol.,* 66, 63-75.

Heinbokel JF (1978) Studies on the functional role of tintinnids in the Southern California Bight. I. Grazing and growth rates in laboratory cultures. *Mar. Biol.,* 47, 177-189.

Hinson D (2000) Rotenone characterization and toxicity in aquatic systems. *Principles of Environmental Toxicity,* University of Idaho, Moscow.

Holm-Hansen O, Riemann B (1978) Chlorophyll a determination: improvements in methodology. *Oikos,* 30, 438-447.

Ignatiades L (2012) Mixotrophic and heterotrophic dinoflagellates in eutrophic coastal waters of the Aegean Sea (eastern Mediterranean Sea). *Bot. Mar.,* 55, 39-48.

Ishii N, Takeda H, Doi M, Fuma S, Miyamoto K, Yanagisawa K, Kawabata ZI (2002) A new method using enhanced green fluorescent protein (EGFP) to determine grazing rate on live bacterial cells by protists. *Limnology,* 3, 47-50.

Jacobson DM, Anderson DM (1986) Thecate heterophic dinoflagellates: Feeding behavior and mechanisms. *J. Phycol.,* 22, 249-258.

Jakobsen HH, Hansen PJ, Larsen J (2000) Growth and grazing responses of two chloroplast-retaining dinoflagellates: effect of irradiance and prey species. *Mar. Ecol. Prog. Ser.,* 201, 121-128.

Jeffrey SW, Vesk M (1997) Introduction to marine phytoplankton and their pigment signatures. In: SW Jeffrey, RCF Mantoura and SW Wright (eds) *Phytoplankton pigments in oceanography: guidelines to modern methods.* UNESCO Publishers, Paris, pp. 37-82.

Jeong HJ, Yoo YD, Kim JS, Seong KA, Kang NS, Kim TH (2010) Growth, feeding and ecological roles of the mixotrophic and heterotrophic dinoflagellates in marine planktonic food webs. *Ocean Sci. J.,* 45, 65-91.

Johnson MD, Beaudoin DJ, Frada MJ, Brownlee EF, Stoecker DK (2018) High grazing rates on cryptophyte algae in Chesapeake Bay. *Front. Mar. Sci.,* 5.

Johnson MD, Rome M, Stoecker DK (2003) Microzooplankton grazing on *Prorocentrum minimum* and *Karlodinium micrum* in Chesapeake Bay. *Limnol. Oceanogr.,* 48, 238-248.

Johnson MD, Stoecker DK (2005) Role of feeding in growth and photophysiology of *Myrionecta rubra*. *Aquat. Microb. Ecol.,* 39, 303-312.

Jürgens K, Demott WR (1995) Behavioral flexibility in prey selection by bacterivorous nanoflagellates. *Limnol. Oceanogr.,* 40, 1503-1507.

Kamiyama T (2000) Application of a vital staining method to measure feeding rates of field ciliate assemblages on a harmful alga. *Mar. Ecol. Prog. Ser.,* 197, 299-303.

Kashiyama Y, Yokoyama A, Kinoshita Y, Shoji S, Miyashiya H, Shiratori T, Suga H, Ishikawa K, Ishikawa A, Inouye I, Ishida K-I, Fujinuma D, Aoki K, Kobayashi M, Nomoto S, Mizoguchi T, Tamiaki H (2012) Ubiquity and quantitative significance of detoxification catabolism of chlorophyll associated with protistan herbivory. *Proc. Natl. Acad. Sci.,* 109, 17328.

Kim JS, Jeong HJ (2004) Feeding by the heterotrophic dinoflagellates *Gyrodinium dominans* and *G. spirale* on the red-tide dinoflagellate *Prorocentrum minimum*. *Mar. Ecol. Prog. Ser.,* 280, 85-94.

Kim M, Drumm K, Daugbjerg N, Hansen PJ (2017) Dynamics of sequestered cryptophyte nuclei in *Mesodinium rubrum* during starvation and refeeding. *Front. Microbiol.,* 8.

Kim S, Kang YG, Kim HS, Yih W, Coats DW, Park MG (2008) Growth and grazing responses of the mixotrophic dinoflagellate *Dinophysis acuminata* as functions of light intensity and prey concentration. *Aquat. Microb. Ecol.,* 51, 301-310.

Kruskopf M, Flynn KJ (2006) Chlorophyll content and fluorescence responses cannot be used to gauge reliably phytoplankton biomass, nutrient status or growth rate. *New Phytol.,* 169, 525-536.

Landry MR (2014) On database biases and hypothesis testing with dilution experiments: Response to comment by Latasa. *Limnol. Oceanogr.,* 59, 1095-1096.

Landry MR, Constantinou J, Latasa M, Brown SL, Bidigare RR, Ondrusek ME (2000) Biological response to iron fertilization in the eastern equatorial Pacific (IronEx II). III. Dynamics of phytoplankton growth and microzooplankton grazing. *Mar. Ecol. Prog. Ser.,* 201, 57-72.

Landry MR, Hassett RPL (1982) Estimating the grazing impact of marine micro-zooplankton. *Mar. Biol.,* 67, 283-288.

Latasa M (2014) Comment: A potential bias in the databases of phytoplankton growth and microzooplankton grazing rates because of the improper formulation of the null hypothesis in dilution experiments. *Limnol. Oceanogr.,* 59, 1092-1094.

Lawrence C, Menden-Deuer S (2012) Drivers of protistan grazing pressure: seasonal signals of plankton community composition and environmental conditions. *Mar. Ecol. Prog. Ser.,* 459, 39-52.

Lee KH, Jeong HJ, Jang TY, Lim AS, Kang NS, Kim J-H, Kim KY, Park K-T, Lee K (2014) Feeding by the newly described mixotrophic dinoflagellate *Gymnodinium smaydae*: Feeding mechanism, prey species, and effect of prey concentration. *J. Exp. Mar. Biol. Ecol.,* 459, 114-125.

Leroy F, Riera P, Jeanthon C, Edmond F, Leroux C, Comtet T (2012) Importance of bacterivory and preferential selection toward diatoms in larvae of *Crepidula fornicata* (L.) assessed by a dual stable isotope (^{13}C, ^{15}N) labeling approach. *J. Sea Res.,* 70, 23-31.

Li A, Stoecker DK, Coats DW (2000) Mixotrophy in *Gyrodinium galatheanum* (Dinophyceae): grazing responses to light intensity and inorganic nutrients. *J. Phycol.,* 36, 33-45.

Li A, Stoecker DK, Coats DW (2001) Use of the 'food vacuole content'method to estimate grazing by the mixotrophic dinoflagellate *Gyrodinium galatheanum* on cryptophytes. *J. Plankton Res.,* 23, 303-318.

Li A, Stoecker DK, Coats DW, Adam EJ (1996) Ingestion of fluorescently labeled and phycoerythrin-containing prey by mixotrophic dinoflagellates. *Aquat. Microb. Ecol.,* 10, 139-147.

López-Sandoval DC, Rodríguez-Ramos T, Cermeño P, Sobrino C, Marañón E (2014) Photosynthesis and respiration in marine phytoplankton: relationship with cell size, taxonomic affiliation, and growth phase. *J. Exp. Mar. Biol. Ecol.,* 457, 151-159.

Mansour JS, Norlin A, Llopis Monferrer N, L'helguen S, Not F (2021) Carbon and nitrogen content to biovolume relationships for marine protist of the Rhizaria lineage (Radiolaria and Phaeodaria). *Limnol. Oceanogr.,* 66, 1703-1717.

Martínez RA, Isari S, Calbet A (2014) Use of live, fluorescently-labeled algae for measuring microzooplankton grazing in natural communities. *J. Exp. Mar. Biol. Ecol.,* 457, 59-70.

Maselli M, Altenburger A, Stoecker DK, Hansen PJ (2020) Ecophysiological traits of mixotrophic *Strombidium* spp. *J. Plankton Res.,* 42, 485-496.

Mckie-Krisberg ZM, Gast RJ, Sanders RW (2015) Physiological responses of three species of Antarctic mixotrophic phytoflagellates to changes in light and dissolved nutrients. *Microb. Ecol.,* 70, 21-29.

Menden-Deuer S, Lessard EJ (2000) Carbon to volume relationships for dinoflagellates, diatoms, and other protist plankton. *Limnol Oceanogr,* 45, 569-579.

Mitra A, Flynn KJ (2006) Accounting for variation in prey selectivity by zooplankton. *Ecol. Modell.,* 199, 82-92.

Moeller HV, Johnson MD, Falkowski PG (2011) Photoacclimation in the phototrophic marine ciliate *Mesodinium rubrum* (ciliophora). *J. Phycol.,* 47, 324-332.

Moeller HV, Laufkötter C, Sweeney EM, Johnson MD (2019) Light-dependent grazing can drive formation and deepening of deep chlorophyll maxima. *Nat. Commun.,* 10, 1978.

Morison F, Franzè G, Harvey E, Menden-Deuer S (2020) Light fluctuations are key in modulating plankton trophic dynamics and their impact on primary production. *Limnol. Oceanogr. Lett.,* 5, 346-353.

Myung G, Kim HS, Park JS, Park MG, Yih W (2011) Population growth and plastid type of *Myrionecta rubra* depend on the kinds of available cryptomonad prey. *Harmful Algae,* 10, 536-541.

Myung G, Yih W, Kim HS, Park JS, Cho BC (2006) Ingestion of bacterial cells by the marine photosynthetic ciliate *Myrionecta rubra*. *Aquat. Microb. Ecol.,* 44, 175-180.

Naess T (1991) Tolerance of marine calanoid resting eggs: effects of freezing, desiccation and rotenone exposure-a field and laboratory study. *Mar. Biol.,* 111, 455-459.

Nakamura Y, Suzuki S-Y, Hiromi J (1995) Growth and grazing of a naked heterotrophic dinoflagellate, *Gyrodinium dominans*. *Aquat. Microb. Ecol.,* 9, 157-164.

Nelson BN, Lemieux EJ, Drake L, Kulis D, Burns K, Anderson D, Welshmeyer N, Smith S, Scianni C, Wier T (2009) Phytoplankton enumeration and evaluation experiments. In: AD-RaD Center (ed). Woods Hole Oceanographic Institute, Moss Landing Marine Laboratory, Naval Research Laboratory, Fluid Imaging Technologies, Key West, FL. 33040, pp. 126.

Ng WHA, Liu H, Zhang S (2017) Diel variation of grazing of the dinoflagellate *Lepidodinium sp.* and ciliate *Euplotes sp.* on algal prey: the effect of prey cell properties. *J. Plankton Res.,* 39, 450-462.

Nielsen LT, Krock B, Hansen PJ (2012) Effects of light and food availability on toxin production, growth and photosynthesis in *Dinophysis acuminata*. *Mar. Ecol. Prog. Ser.,* 471, 37-50.

Nishibe Y, Kawabata ZI, Nakano S-I (2002) Grazing on *Microcystis aeruginosa* by the heterotrophic flagellate *Collodictyon triciliatum* in a hypertrophic pond. *Aquat. Microb. Ecol.,* 29, 173-179.

Nygaard K, Børsheim KY, Thingstad TF (1988) Grazing rates on bacteria by marine heterotrophic microflagellates compared to uptake rates of bacterial-sized monodisperse fluorescent latex beads. *Mar. Ecol. Prog. Ser.,* 44, 159-165.

Olofsson M, Robertson EK, Edler L, Arneborg L, Whitehouse MJ, Ploug H (2019) Nitrate and ammonium fluxes to diatoms and dinoflagellates at a single cell level in mixed field communities in the sea. *Sci. Rep.,* 9, 1424.

Palmer G, Horgan DJ, Tisdale H, Singer TP, Beinert H (1968) Studies on the respiratory chain-linked reduced nicotinamide adenine dinucleotide dehydrogenase XIV. Location of the sites of inhibition of rotenone, barbiturates, and piericidin by means of electron paramagnetic resonance spectroscopy. *J. Biol. Chem.,* 243, 844-847.

Park JS, Myung G, Kim HS, Cho BC, Yih W (2007) Growth responses of the marine photosynthetic ciliate *Myrionecta rubra* to different cryptomonad strains. *Aquat. Microb. Ecol.,* 48, 83-90.

Paterson HL, Knott B, Koslow AJ, Waite AM (2008) The grazing impact of microzooplankton off south west Western Australia: as measured by the dilution technique. *J. Plankton Res.,* 30, 379-392.

Peltomaa E, Johnson MD (2017) *Mesodinium rubrum* exhibits genus-level but not species-level cryptophyte prey selection. *Aquat. Microb. Ecol.,* 78, 147-159.

Probert I, Siano R, Poirier C, Decelle J, Biard T, Tuji A, Suzuki N, Not F (2014) *Brandtodinium* gen. nov. and *B. nutricula* comb. Nov. (Dinophyceae), a dinoflagellate commonly found in symbiosis with polycystine radiolarians. *J. Phycol.,* 50, 388-399.

Putt M (1991) Development and evaluation of tracer particles for use in microzooplankton herbivory studies. *Mar. Ecol. Prog. Ser.,* 77.

Rajini PS, Krishnakumari MK, Majumder SK (1989) Cytotoxicity of certain organic solvents and organophosphorus insecticides to the ciliated protozoan *Paramecium caudatum*. *Microbios,* 59, 157-63.

Rasmussen SA, Binzer SB, Hoeck C, Meier S, De Medeiros LS, Andersen NG, Place A, Nielsen KF, Hansen PJ, Larsen TO (2017) Karmitoxin: an amine-containing polyhydroxy-polyene toxin from the marine dinoflagellate *Karlodinium armiger*. *J. Nat. Prod.,* 80, 1287-1293.

Rublee PA, Gallegos CL (1989) Use of fluorescently labelled algae (FLA) to estimate microzooplankton grazing. *Mar. Ecol. Prog. Ser.,* 221-227.

Rusterholz PM, Hansen PJ, Daugbjerg N (2017) Evolutionary transition towards permanent chloroplasts?-Division of kleptochloroplasts in starved cells of two species of *Dinophysis* (Dinophyceae). *PloS One,* 12, e0177512.

Ryabov AB, Morozov A, Blasius B (2015) Imperfect prey selectivity of predators promotes biodiversity and irregularity in food webs. *Ecol. Lett.,* 18, 1262-1269.

Saiz E, Griffell K, Calbet A, Isari S (2014) Feeding rates and prey: predator size ratios of the nauplii and adult females of the marine cyclopoid copepod *Oithona davisae*. *Limnol. Oceanogr.,* 59, 2077-2088.

Sandhu SK, Morozov AY, Mitra A, Flynn K (2019) Exploring nonlinear functional responses of zooplankton grazers in dilution experiments via optimization techniques. *Limnol. Oceanogr.,* 64, 774-784.

Schindelin J, Arganda-Carreras I, Frise E, Kaynig V, Longair M, Pietzsch T, Preibisch S, Rueden C, Saalfeld S, Schmid B (2012) Fiji: an open-source platform for biological-image analysis. *Nat. Methods,* 9, 676.

Schmoker C, Russo F, Drillet G, Trottet A, Mahjoub M-S, Hsiao S-H, Larsen O, Tun K, Calbet A (2016) Effects of eutrophication on the planktonic food web dynamics of marine coastal ecosystems: the case study of two tropical inlets. *Mar. Environ. Res.,* 119, 176-188.

Schoener DM, Mcmanus GB (2017) Growth, grazing, and inorganic C and N uptake in a mixotrophic and a heterotrophic ciliate. *J. Plankton Res.,* 39, 379-391.

Seemann J, Sawall Y, Auel H, Richter C (2013) The use of lipids and fatty acids to measure the trophic plasticity of the coral *Stylophora subseriata*. *Lipids,* 48, 275-286.

Setälä O, Autio R, Kuosa H (2005) Predator–prey interactions between a planktonic ciliate *Strombidium sp.* (Ciliophora, Oligotrichida) and the dinoflagellate *Pfiesteria piscicida* (Dinamoebiales, Pyrrophyta). *Harmful Algae,* 4, 235-247.

Sherr BF, Sherr EB, Fallon RD (1987) Use of monodispersed, fluorescently labeled bacteria to estimate *in situ* protozoan bacterivory. *Appl. Environ. Microbiol.,* 53, 958-965.

Shields AR, Smith WO (2008) An examination of the role of colonial *Phaeocystis antarctica* in the microbial food web of the Ross Sea. *Polar Biol.,* 31, 1091-1099.

Shilo M, Aschner M (1953) Factors governing the toxicity of cultures containing the phytoflagellate *Prymnesium parvum* Carter. *J. Gen. Microbiol.,* 8, 333-343.

Smith M, Hansen PJ (2007) Interaction between *Mesodinium rubrum* and its prey: importance of prey concentration, irradiance and pH. *Mar. Ecol. Prog. Ser.,* 338, 61-70.

Solomon CM, Collier JL, Berg GM, Glibert PM (2010) Role of urea in microbial metabolism in aquatic systems: a biochemical and molecular review. *Aquat. Microb. Ecol.,* 59, 67-88.

Srivastava P, Panda D (2007) Rotenone inhibits mammalian cell proliferation by inhibiting microtubule assembly through tubulin binding. *FEBS J.,* 274, 4788-4801.

Stelfox-Widdicombe CE, Archer SD, Burkill PH, Stefels J (2004) Microzooplankton grazing in *Phaeocystis* and diatom-dominated waters in the southern North Sea in spring. *J. Sea Res.,* 51, 37-51.

Stoecker DK, Hansen PJ, Caron DA, Mitra A (2017) Mixotrophy in the marine plankton. *Annu. Rev. Mar. Sci.,* 9, 311-335.

Strom SL (2001) Light-aided digestion, grazing and growth in herbivorous protists. *Aquat. Microb. Ecol.,* 23, 253-261.

Tarangkoon W, Hansen PJ (2011) Prey selection, ingestion and growth responses of the common marine ciliate *Mesodinium pulex* in the light and in the dark. *Aquat. Microb. Ecol.,* 62, 25-38.

Terrado R, Pasulka AL, Lie AA, Orphan VJ, Heidelberg KB, Caron DA (2017) Autotrophic and heterotrophic acquisition of carbon and nitrogen by a mixotrophic chrysophyte established through stable isotope analysis. *ISME J.,* 11, 2022-2034.

Traboni C, Calbet A, Saiz E (2020) Effects of prey trophic mode on the gross-growth efficiency of marine copepods: the case of mixoplankton. *Sci. Rep.,* 10, 12259.

Unrein F, Gasol JM, Not F, Forn I, Massana R (2014) Mixotrophic haptophytes are key bacterial grazers in oligotrophic coastal waters. *ISME J.,* 8, 164.

Utermöhl H (1958) Zur vervollkommung der quantitativen phytoplankton methodik. *Mitt. Int.Verein. Theor. Angew. Limnol.,* 9, 1-38.

Van Ginkel SW, Bidwell M, Igou T, Gijon-Felix R, Salvi EJNR, De Oliveira SHR, Duarte LHK, Steiner D, Hu Z, Johnston R (2016) The prevention of saltwater algal pond contamination using the electron transport chain disruptor, rotenone. *Algal Res.,* 18, 209-212.

Van Ginkel SW, Igou T, Hu Z, Narode A, Cheruvu S, Doi S, Johnston R, Snell T, Chen Y (2015) Taking advantage of rotifer sensitivity to rotenone to prevent pond crashes for algal-biofuel production. *Algal Res.,* 10, 100-103.

Vanderploeg HA, Scavia D (1979) Two electivity indices for feeding with special reference to zooplankton grazing. *J. Fish. Res. Bd. Can.,* 36, 362-365.

Verity PG (1991) Feeding in planktonic protozoans: evidence for non-random acquisition of prey. *J. Protozool.,* 38, 69-76.

Yentsch CS, Menzel DW (1963) A method for the determination of phytoplankton chlorophyll and phaeophytin by fluorescence. *Deep-Sea Res.,* 10, 221-231.

Yih W, Kim HS, Jeong HJ, Myung G, Kim YG (2004) Ingestion of cryptophyte cells by the marine photosynthetic ciliate *Mesodinium rubrum*. *Aquat. Microb. Ecol.,* 36, 165-170.

Zar JH (2010) *Biostatistical Analysis. 5th Edition.* Vol., Pearson Prentice-Hall, Upper Saddle River, New Jersey, USA.

MixITiN Deliverable 3.8 Report

Section 4

Reporting Interpretative Toolkit To Enable The Use Of Genomic Data Aligned With Physiological Status For Representative Mixoplankton

Konstantinos Anestis, Alfred Wegener Institute Germany
Joost S Mansour, Université Pierre et Marie Curie France
Maira Maselli, Kobenhavns Universitet Denmark
Per Juel Hansen, Kobenhavns Universitet Denmark
Fabrice Not, Université Pierre et Marie Curie France
Uwe John, Alfred Wegener Institute Germany

Table of Contents

4.1. Introduction

Mixotrophy is the combination of autotrophy and heterotrophy and in particular phototrophy and phagotrophy expressed within a single organism (Flynn et al., 2019). The term mixoplankton describes planktonic protists that express, or have potential to express both, phototrophy and phagotrophy. The functional classification of mixoplankton is based on how the cell incorporates photosynthesis. For mixotrophic protists (i.e. mixoplankton), the classification and the hypothesised evolutionary path is illustrated in Figure 1 (Mansour and Anestis, 2021). Mitra et al. (2016) introduced the general grouping of either constitutive mixoplankton (CM) or non-constitutive mixoplankton (NCM). A CM has an inherent capability for both phototrophy and phagotrophy. Constitutive mixoplankton are found in most microeukaryotic lineages including green algae, euglenophytes, cryptophytes, chrysophytes, haptophytes, and dinoflagellates. NCM which are defined by the need to acquire their photosynthetic ability through external means and are found mostly among ciliates, dinoflagellates, Foraminifera, and Radiolaria. Phototrophic activity in NCM can be broadly achieved by three methods which further divide NCM into sub-groups: 1) those that steal chloroplasts (kleptoplasts) of (any) prey (generalist non-constitutive mixoplankton, GNCM); 2) those that steal chloroplasts from a specific type of prey (plastidic specialist non-constitutive mixoplankton pSNCM) and 3) those that harbour photosynthetically active endosymbionts (endosymbiotic specialist non-constitutive mixoplankton, eSNCM) (acquired phototrophy reviewed in Stoecker et al., 2009).

Approaches to study species functionality and responses to environmental parameters are predominantly done using cultures. This becomes more complex for mixoplankton and specifically NCM, as they are characterised by their interactions to other organisms. The presence of other eukaryotes is in many cases (and especially for NCM) is obligatory in order to sustain a culture, if at all possible. This is a main obstacle, which could result in issues or ambiguity in downstream bioinformatics work and generally limits current knowledge on NCM. To tackle this, novel cultivation-independent approaches like single-cell sampling and analyses can be an outcome to study NCM. Such approaches will help improve our knowledge about the genomic aspects of interactions of kleptoplastic/karyokleptic and endosymbiotic mixotrophs, and, when unknown, could hint at physiological potential (Burns et al., 2018; Jimenez et al., 2020).

A major challenge in studies examine mixotrophy at the cellular bases and understanding the regulative processes of metabolic needs and photosynthetic activities is linking physiological potential to rate processes. For this reason, there is an emerging need to combine both eco-physiological parameters and genomics data in order to study the contribution of both phagotrophy and phototrophy in cellular physiology. To achieve that, we have made an effort to create integrative datasets that include sampling for genomic analyses in single-cell and batch cultures, aligned with physiological parameters for the studied nutritional status. This document gives an overview of how this was achieved, as well as the generated datasets and sample parameters which are available for future studies.

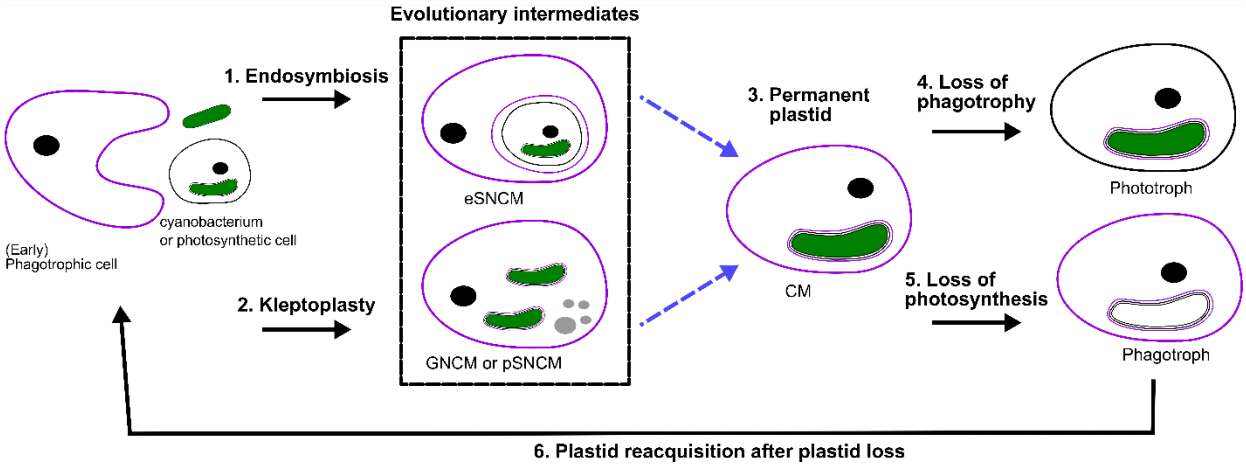

Figure 4-1. Perspective of protist plastid evolution and the role of mixotrophy. Conceptual illustration of plastid evolution depicting non-constitutive mixoplankton as hypothetical intermediate stages to permanent plastids. The cell nucleus is shown as a black circle, kleptokaryons as grey circles, and photosynthetic plastids in green. While complex permanent plastids gained by secondary or tertiary endosymbiosis are bound by three or four membranes, respectively as illustrated by the number of lines around the plastid. In secondary and higher plastid acquisition, the photosynthetic cell can be either a CM or phototroph with primary, secondary or higher-order plastid. Illustrated here is secondary plastid acquisition with the host membrane in purple. Blue dashed lines are the hypothetical route toward permanent plastid retention. (Reproduced from Mansour, J. S., and Anestis, K. (2021) under CC BY-4.0).

Transcriptomic studies of grazing are usually based on whole culture RNA extractions. As a result, information comes from a mix of cells that feed on prey. However, feeding is not a synchronized process and possibly only a small portion of the total cell population engages in phagotrophy at any instant. Performing single-cell isolations from cultures allows us to select only for cells that actively fed and thus contained a distinct food vacuole. Additionally, molecular markers are used for prey nuclei detection and improve the understanding of role and function of kleptoplasty in planktonic protists.

Before proceeding to the establishment of interpretative tools combining both physiological and genomic data, it is important to highlight the parameters important for studying processes of mixotrophy (here mixoplanktonic activities). The main question is how much the photosynthesis and ingestion contribute respectively to the energetic budget of the cells. Thus, the photosynthetic rates should be measured in conjunction with the ingestion rates. The 14C technique is an effective tool for measuring photosynthetic activity (Nielsen 1952; Rivkin and Seliger 1981) while ingestion rates are usually measured via prey disappearance during short incubations (Heinbokel 1978). Dissolved inorganic nutrients concentration in the media should be monitored during the incubation to estimate the cellular up-take and excretion rates. These measurements, together with the measurements of the elemental composition (C:N:P) of the organisms' biomass would allow a complete description of nutrients dynamics in the protists. These parameters have been measured on cultures of the CM P. parvum and the NCM S. basimorphum. Both bulk and single-cell samples have been taken for genomic analysis, allowing us to gain understanding of process in both population and single-cell level.

4.2. Approaches and methodology

4.2.1 Toxin biosynthesis in Prymnesium parvum (CM)

The CM Prymnesium parvum was used in order to study physiological processes such as toxin production as well as the dynamics of phagotrophy under different conditions (such as salinity and phosphorous availability). To provide new insights on toxin biosynthesis mechanisms, we compared the prymnesin (toxin) profile, the presence of polyketide synthase genes (PKSs), and the metabolic and cellular functions of nine P. parvum strains. We chose three strains for each of the prymnesin types, A, B and C. Transcripts encoding for PKS were used to assess the phylogeny of the KS domain and the relationship between prymnesin type and PKS genes. Furthermore, we measured the cellular toxin content of all nine strains, relating patterns between toxin types and cellular toxin contents with the presence of PKS genes. To understand the potential molecular and metabolic trade-offs of toxin production in P. parvum, we performed gene expression variance analysis to detect genes showing expression patterns that relate to the cellular toxin content (Figure 2). Detailed description of the methodology is provided in Anestis et al. (2021).

4.2.2 Eco-physiology of Prymnesium parvum (CM)

Cultures of the P. parvum (strain UIO-223) were grown under different salinity and phosphorus availability. The default medium used was K-medium. Low salinity was achieved by diluting filter-sterilised seawater (salinity 30) with MilliQ water to obtain a salinity of 5. All essential nutrients contained in K-medium were added, but in low phosphorus cultures, PO4- was added at a final concentration of 2.4 μM. The concentration of PO4- for the low phosphorus cultures was decided upon preliminary work and in accordance with pre-existing literature.

Mixotrophy in P. parvum was tested using Teleaulax acuta as prey. Incubations were set up using P. parvum cells at middle exponential phase for the non-limiting phosphorus condition and stationary phase for those in phosphorus deficiency. The initial cell concentration for the incubation was 30×103 cells mL-1 and the ratio between P. parvum and prey was 1:1. To estimate phagotrophy, the incubations were sampled at different time points and cells were fixed using Lugol. The samples were examined under light microscopy (Axio Vert.A1 Microscope equipped with a Colibri 7 light source Zeiss), and the number of P. parvum cells containing a food vacuole were estimated.

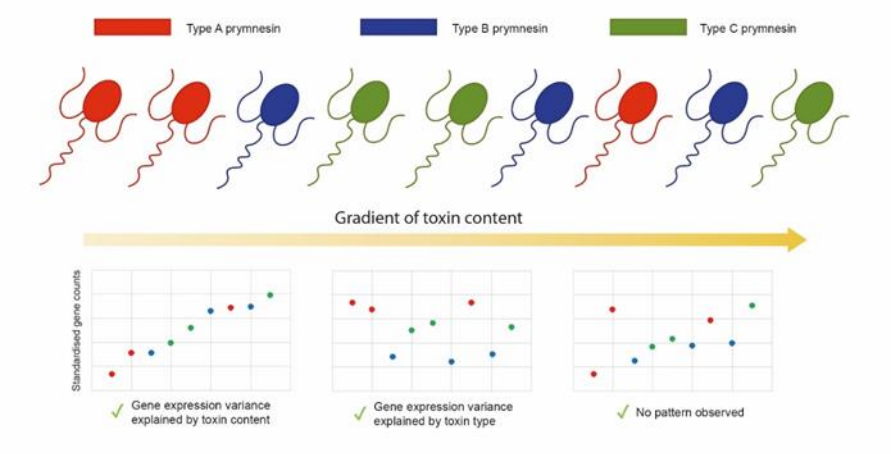

Figure 4-2. Conceptual illustration of the approach followed to analyse toxin content related gene variance. Strains of various toxin type (Type A, B and C) and toxin content were used. Gene expression variance could be explained by either toxin content amount, prymnesin type or neither of these parameters (residuals).

4.2.3 Mixotrophy in the kleptoplastidic and karyokleptic Strombidium cf basimorphum (NCM)

We used culture samples of the NCM ciliate Strombidium cf basimorphum (isolated and cultured as in Maselli et al. 2020) to study the dynamics of the kleptoplasts and the relative contribution of phagotrophy vs phototrophy. Strombidium cf basimorphum was cultured with saturating amount of prey (T0), allowed to deplete the prey (T1-T2) and then starved for several days (T3), after which the cultures were re-fed (T4-T5) (Figure 3). Physiological parameters (growth rate, ingestion rates, nutrients up-take and excretion rates, photosynthetic rates, chlorophyll content and CNP content) were measured and single cell samples were taken for transcriptomic analysis. Samples of the bulk cultures were taken at the different time points to investigate the potential retention of prey genetic material in the ciliates via qPCR and FISH (methods are described in Maselli et al., 2021).

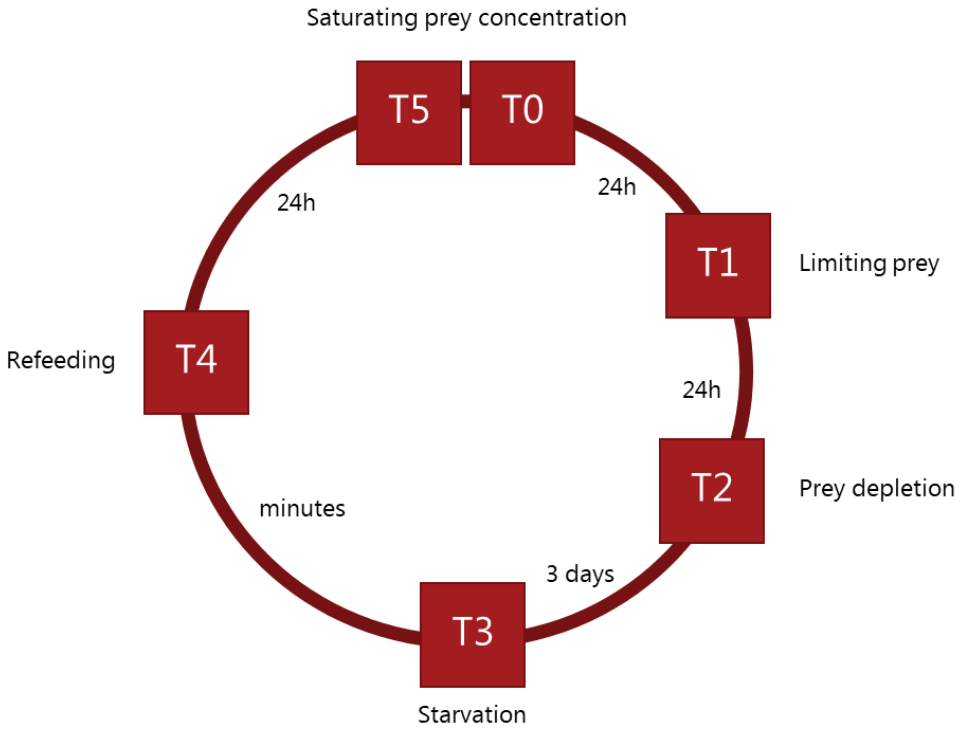

Figure 4-3. Sampling strategy over 5 sampling points (T0-T5) to study physiology and perform single cell transcriptomics and batch culture transcriptomics in cultures of the NCM S. basimorphum in different nutritional status.

To validate the presence of prey transcripts in the ciliate as an indicator of active nuclei, nucleomorph, and/or plastid genome, single-cell transcriptomics were performed. Eight single cells were isolated from the experimental cultures after 4 days of prey starvation. Each cell was individually picked with a drawn Pasteur pipette, washed three times by transferring it into clean filter-sterilised medium. Detailed protocols for the single-cell RNA isolation and library preparation are available at protocol.io (see Mansour et al., 2021b and Mansour et al., 2021a). Moreover, the full methodology we used is described in Maselli et al., 2021.

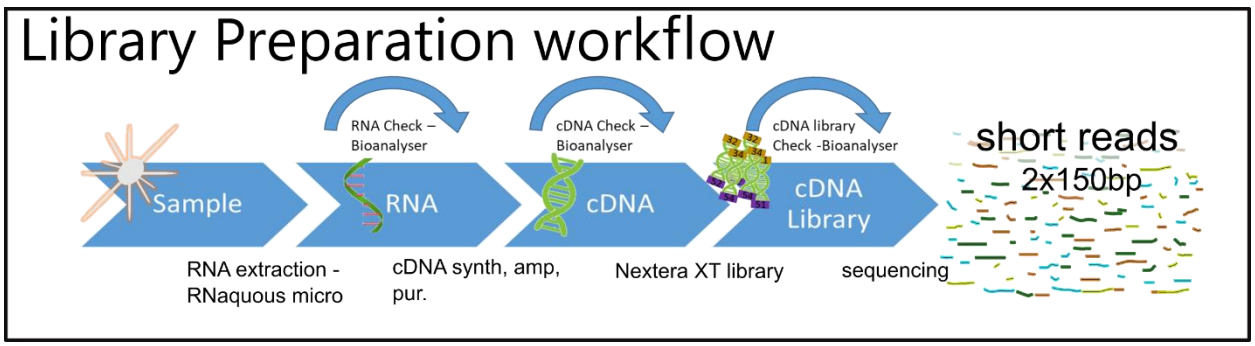

Figure 4-4. cDNA library preparation workflow from sample to transcriptome sequencing. All major steps are indicated including a quality check by Bioanalyzer.

4.2.4 Nutrient uptake capability of Acantharia (eSNCM)

For uncultivatable endosymbiotic mixoplankton (eSNCM) cultivation-independent single-cell approaches are especially important. In addition, the MixITiN proposal as well as various recent studies (Leles et al., 2017, 2019; Faure et al., 2019) have further highlighted the importance of establishing effective protocols for their sampling. Sampling using slow horizontal plankton net-tows are proven to be the best compromise between ease of sampling and keeping cell quality for subsequent physiological investigations (Graham et al., 1976; Mansour et al., 2021c). Detailed protocols for single-cell sampling have been reported in deliverable D3.8 and are publicly available at protocol.io (dx.doi.org/10.17504/protocols.io.bqvrmw56).

Acantharia were collected to investigate their carbon and nitrogen uptake capability and nutrient transfer dynamics between symbiont and host using molecular and chemical imaging techniques. Isolated single cells were transferred to experimental conditions and incubated in a controlled environment of 23 °C with light at 191-194 µmol photons m-2 s 1. Experimental treatments consisted of dark and light incubations of specimen in filter-sterilized seawater (FSW, 0.22-µm-pore-size) enriched with 13C and/or 15N (either nitrate or ammonium). The nutrient treatments are as follows: 1) 1 mM NaH13CO3; 2) 1 mM NaH13CO3 + 1 µM 15NO3; or 3) 1 mM NaH13CO3 + 0.4 µM 15NH4. Acantharia were incubated for five different durations (Figure 5), each time-point consisting of a separate incubation. For each treatment and time point 30 cells were incubated. At T4 the cells were transferred to fresh FSW, through an intermediate transfer step in FSW (by means of rinsing), to start the chase incubation period. Between 15 and 21 Acantharia were chemically fixed at each time point in 1% glutaraldehyde + 2% paraformaldehyde, for subsequent NanoSIMS analysis. Simultaneously, at each timepoint 7 Acantharia (in a max 5 µL volume of SW) were individually deposited in 100 µL lysis buffer (RNAqueous kit), immediately flash frozen in liquid nitrogen, and stored at -80 °C for transcriptomics analyses. Detailed protocols for the single-cell RNA isolation and library preparation are available at protocol.io (see Mansour et al., 2021a and Mansour et al., 2021b)

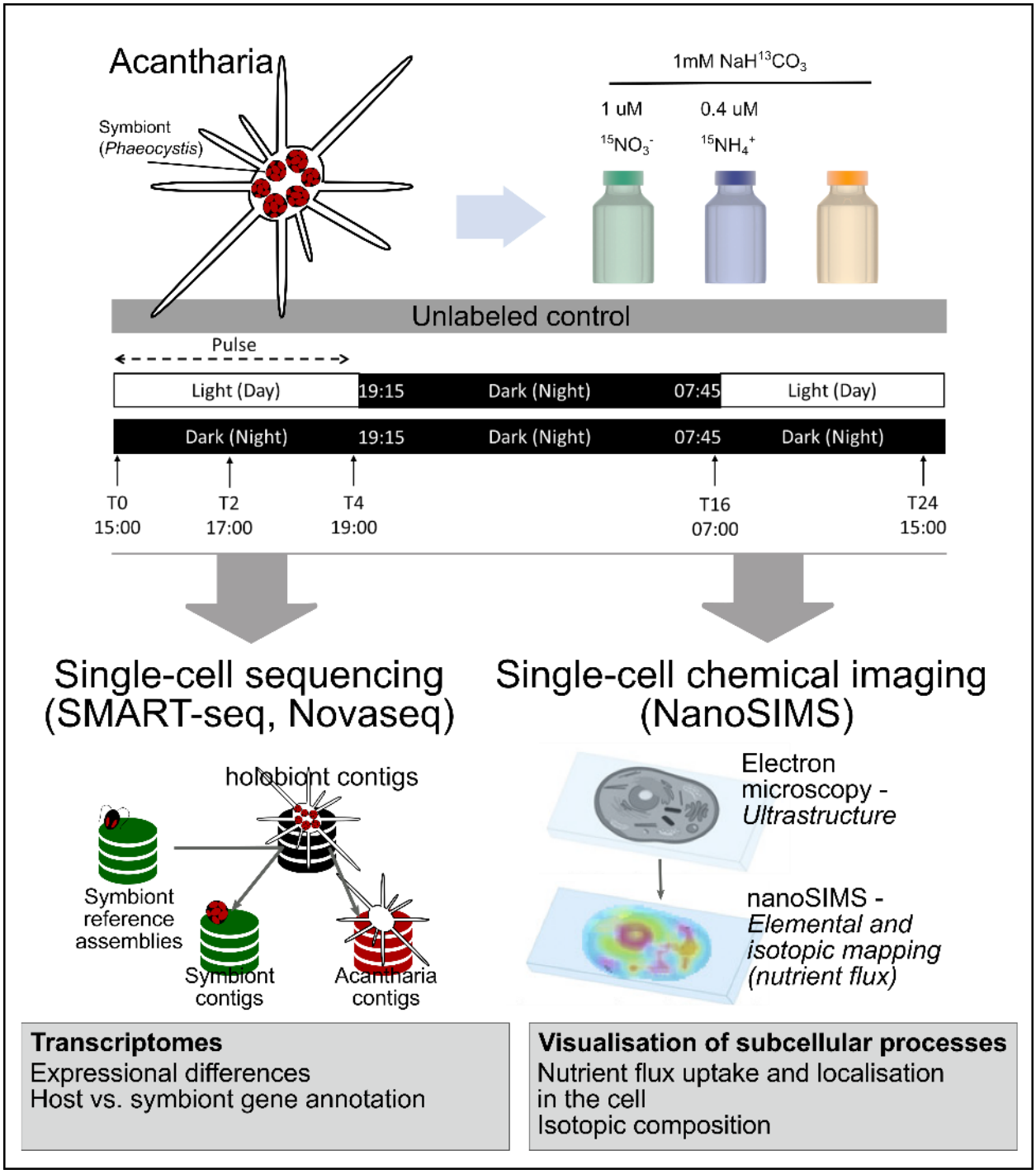

Figure 4-5. Experimental setup to investigate the effect of inorganic nutrients on Acantharia. Related gene expression can be linked to visualised (NanoSIMS) uptake of nutrients.

4.3. Linking genomic data to the experimental framework

4.3.1 Toxin production and molecular trade-offs in Prymnesium parvum

The role of polyketide synthases in the biosynthesis of marine secondary metabolites has been an emerging topic in marine molecular ecology. Dinoflagellates are the main protist group has been studied for the molecular basis of toxin biosynthesis, and has shed light on the diversity and presence of PKSs in this potentially toxic and phylogenetically diverse group (Monroe and Van Dolah, 2008; Kohli et al., 2016). Toxin production and uptake in P. parvum are strictly connected as toxins facilitate prey lysis and thus connected to its mixotrophic behaviour (Skovgaard and Hansen, 2003; Tillmann, 2003).

In P. parvum, the total number of PKS-related contigs across the nine strains varied from 37 to 109. The KS domain is highly conserved was used for phylogenetic purposes (John et al., 2008). The resulting phylogeny is in accordance with previous studies that involved KS domains from a wide range of protists (John et al., 2008; Kohli et al., 2016). The P. parvum ketoacyl synthase (KS) domains formed a well-supported haptophyte specific clade. Within this group, the P. parvum KS domains dominated in three clades. Two of those clades, A and C, were well supported with both of them having a bootstrap value of 100. Besides having P. parvum specific KS clades, no clear relation to the prymnesin type produced by the strains was found. This indicates the presence of phylogenetically similar core genes that are involved in the biosynthesis of prymnesins and are independent of the prymnesin type. Moreover, ‘unusual’ PKS domains were described and they highlight the high complexity of polyketide biosynthesis. These findings deserve more attention and need to be combined with biochemical approaches in order to gain deeper understanding of gene to product relationships. The first step has been achieved by providing a detail description of all PKS contigs found in P. parvum as well as the functional organization of PKS domains.

The gradient of toxin content across the nine strains was compared to gene expression data, providing a direct link between a physiological parameter and transcriptomic data. The production of prymnesins imply cellular and metabolic cost via the investment of carbon and energy resources. The toxin content was used to explain the expression variance of 6,335 genes. The pathways of further interest involved in metabolic pathways, as they are the ones more related to toxin biosynthesis. A general downregulation of the cell’s metabolism was observed, with 1,892 transcripts showing a negative correlation to toxin content and 631 transcripts showing a positive correlation (Figure 6).

The ability to produce prymnesin characterizes all P. parvum strains studied up to date (Binzer et al., 2019). However, in the natural environment, within populations the presence of strains of various toxicity has ecological implications and attributes different advantages on individual cells and the collective levels, the population (Tillmann and Hansen, 2009, John et al. 2015). Highly toxic strains are important for outcompeting other organisms and to avoid grazers (Donk and Ianora, 2011). This has been shown for toxigenic species (John et al., 2002; Tillmann and Hansen, 2009) and a mutual facilitation of toxic strains for non-toxic ones has been postulated (John et al., 2015).

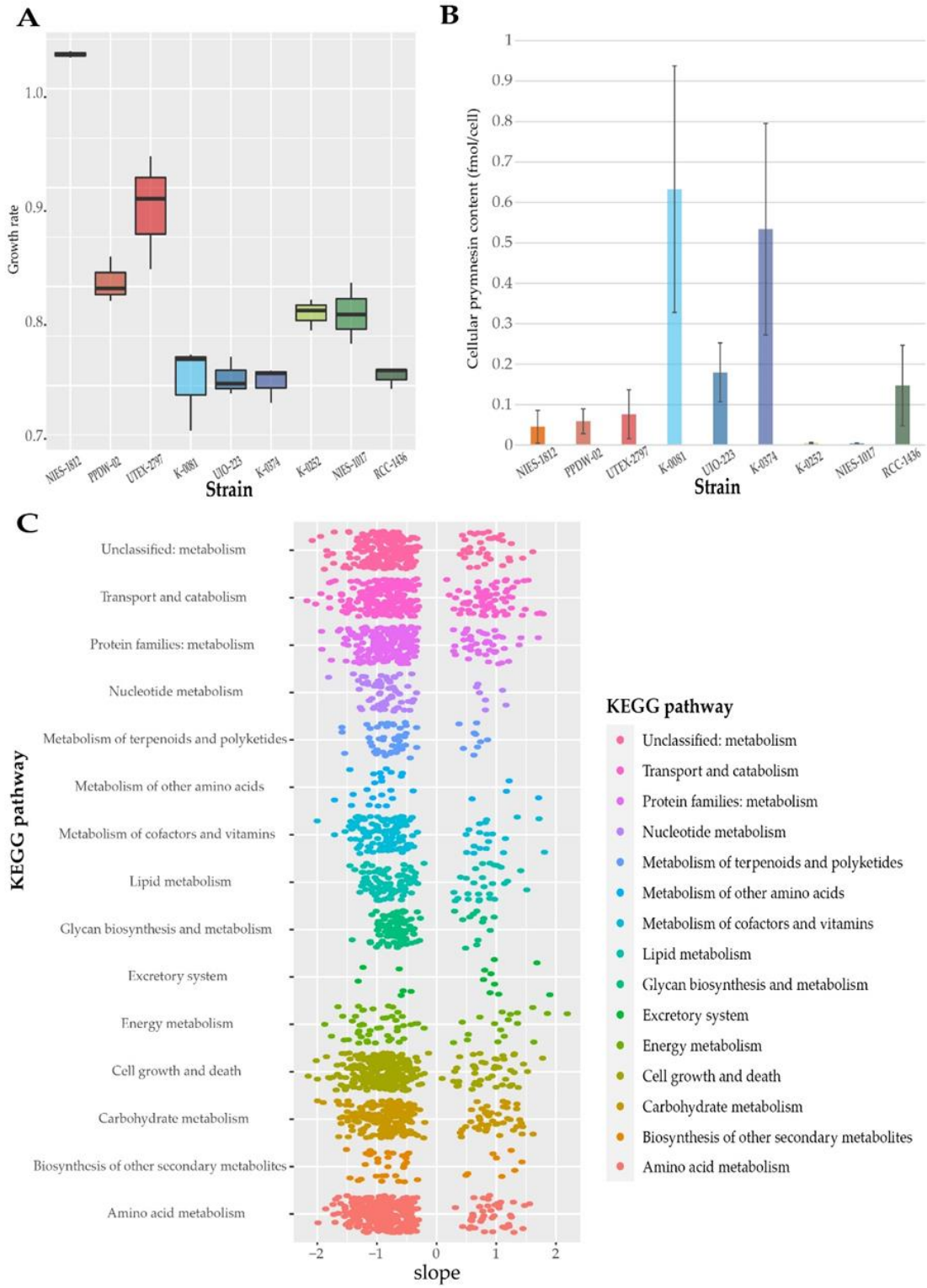

Figure 4-6. Growth rates (d-1) of the nine Prymnesium parvum strains (A) and their corresponding cellular toxin content expressed as fmol cell-1 (B). Chart of transcripts for which gene expression variance was explained by the cellular toxin content (C). The x axis indicates the slope of the correlation with <0 showing a negative correlation and >0 a positive correlation. (Figure from Anestis et al., 2021 under CC BY-NC-ND 4.0).

4.3.2 Eco-physiology of Prymnesium parvum

Studying phagotrophy in CM is challenging due to general low rates of phagotrophy. For example, in P. parvum cultures only a subset of cells feed on prey, which in some case can be 10-15% of the total cells. A P. parvum population is not homogeneous in regard to their response to the presence of prey, there can be cells that feed, cells that already contain a food vacuole (the digestion status can also be variable), and cells that do not show any response to the presence of prey. Applying batch culture approaches inevitably leads to an under representation of molecular pathways related to phagotrophy. To tackle this, it is important to incorporate novel methods that allow us to study transcriptomics of cells of a certain nutritional status, single-cell transcriptomics is a powerful tool towards this direction. We combined approaches that include both batch culture and single-cell transcriptomics (Figure 7). Library generation methodology of P. parvum single–cell total RNA is reported in Mansour et al., 2021a and Mansour et al., 2021b.

Transcriptomic data from single cells needs to be aligned with batch culture transcriptomes in order to compensate potential biased of single-cell transcriptomics over a general reference transcriptome representing the majority of expected genes of an organism. Such approaches have not been applied in protist research and can help answer many questions:

1. Can single-cell transcriptomics be insightful about molecular process in protists?

2. Is it able to compare single-cell and batch culture transcriptomes at level of molecular processes?

3. Are single-cell transcriptomics accurate enough and provide replicability of experiments and outcome?

4. What are the most efficient bioinformatics tools for analysing single-cell transcriptomic data?

Within MixITiN, we generated datasets that will combine traditional and novel transcriptomic approaches, with the objective to contribute to answering these technical and conceptual questions.

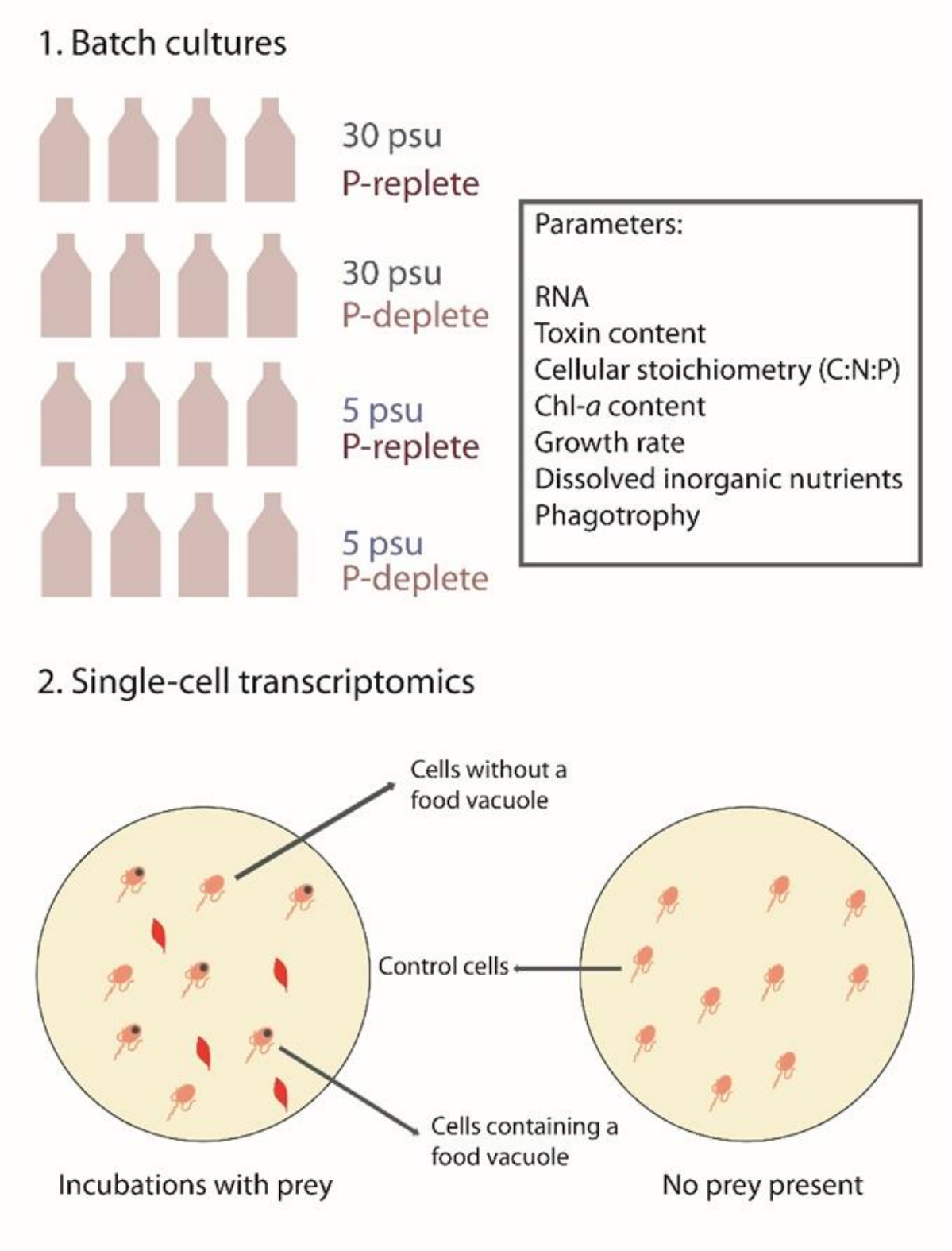

Figure 4-7. Conceptual illustration of the approach followed for studying the eco-physiology of Prymnesium parvum. The conditions that were tested included different salinity (5 and 30) and phosphorus (P) availability (replete and deplete). The cultures were sampled for various parameters and single cell transcriptomics were used for selected cells of a certain nutritional status.

4.3.3 Kleptoplastid dynamics in the mixotrophic Strombidium. cf. basimorphum

Unlike a permanent plastid, a stolen plastid or kleptoplast is transient. Retention time and functionality of the kleptoplasts are dynamic and can be from days to months. Both the ability of the host to control the upkeep of the plastid and the inherent stability of the original plastid can affect the retention time (Green et al., 2005). Genomic approaches aim to help to disentangle heterotrophic processes such as phagotrophy from osmotrophy and phototrophic-induced anabolic activities. This information will then support cellular and metabolic modelling by better elucidating the physiological mechanisms and quantifying their importance in different scenarios.

Application of 'omics approaches to the groups of NCM offers the potential to understand the evolutionary processes and establishment of permanent plastids. The increasing interest of the scientific community towards studying kleptoplastidic mixoplankton indicates the importance of such model organism in order to investigate the transition from heterotrophy to phototrophy with permanently established chloroplasts. General mechanistic understanding is needed to disentangle the dependency of the plastid from its own regulative processes and how the "host"/predator can control photosynthetic and other essential plastid processes for its own benefit. The presence of photosynthesis-related genes in kleptoplastidic mixoplankton could indicate a transition point towards heterotroph over mixo- to phototrophy, while the phylogenetic placement of those genes can provide crucial information about the selectivity and evolutionary trajectory of prey/plastid as well as the spectrum of preferred plastids by kleptoplastidic organisms (Hehenberger et al., 2019; Hongo et al., 2019).

This ciliate studied here (S. basimorphum) can maintain and keep chloroplasts functionality unaltered for several days when chloroplasts are not replaced via the ingestion of prey. However, cellular chlorophyll content decreases to about half in starved cells compared to well-fed cells. Despite that, S. basimorphum demonstrated to exploit chloroplasts for photosynthesis even more efficiently when starved of prey compared to when it is actively feeding (Figure 8).

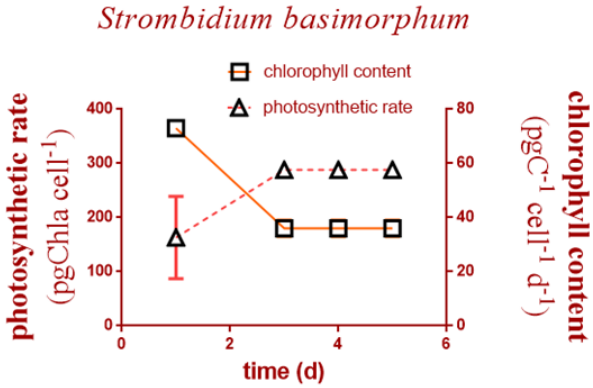

Figure 4-8. Strombidium cf. basimorphum chlorophyll content and photosynthetic rates when actively feeding (day 1) and after prey depletion and starvation (subsequent time points; day 3, 4 and 5).

Despite the fact that kleptoplasts seem to be better exploited when the ciliate does not ingest prey, S. cf basimorhpum is not able to survive as a pure autotroph in absence of prey and cultures decline in number as soon as prey get depleted (Figure 9).

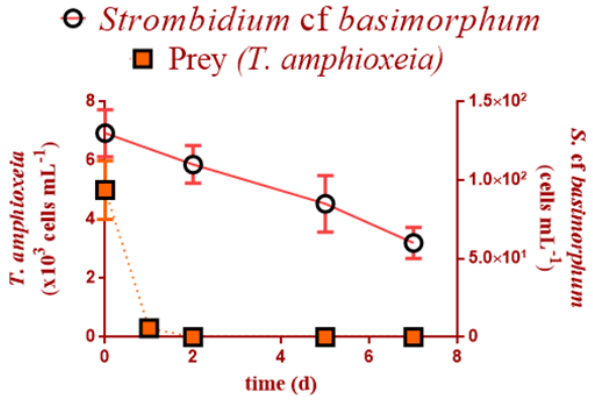

Figure 4-9. Growth performance of Strombidium cf. basimorphum (circles) and Teleaulax amphioxeia (squares) over a seven day feeding experiment. S. cf. basimorphum decline in cell number right after prey depletion (day 2).

Carbon acquired via photosynthesis is apparently not sufficient to sustain the energetic requirements of the ciliate which additionally looks to only rely on prey ingestion to obtain nutrients other than carbon. Indeed, no nitrogen or phosphorous uptake was observable in this species, as NO3- and PO4- concentration in the media didn´t change over time along the experiment (Figure 9).

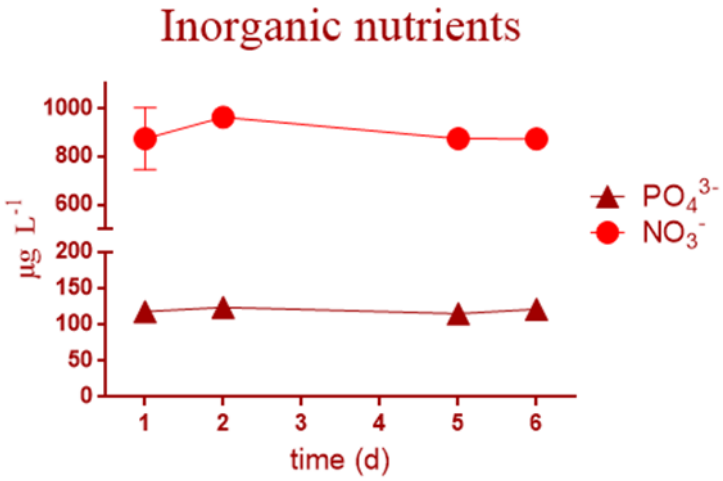

Figure 4-10. Inorganic nutrients concentration (µg L-1) during the experiment.

Laborious experimental work to understand physiological responses of a studied species towards different parameters are important prerequisites before proceeding to genomics-based studies. We used a wide range of molecular techniques to study kleptoplast and kleptokaryon retention in S. basimorphum.

Quantitative polymerase chain reaction assays can be used to detect the presence of prey genetic material in DNA extracted from mixoplanktonic grazers and provide a semi-

quantitative estimation of its concentration (Figure 11). If performed on cultures with a known feeding history would give indication about the potential retention of prey genetic material, which could be relevant in understanding the molecular mechanisms that stands behind the retention of functional chloroplasts in NCM organisms. Prey nuclear and nucleomorph 28S rDNA were detected in the DNA extracted from the ciliate using the qPCR assays. The relative concentration of these prey genes was lower in ciliates subjected to prey deprivation.

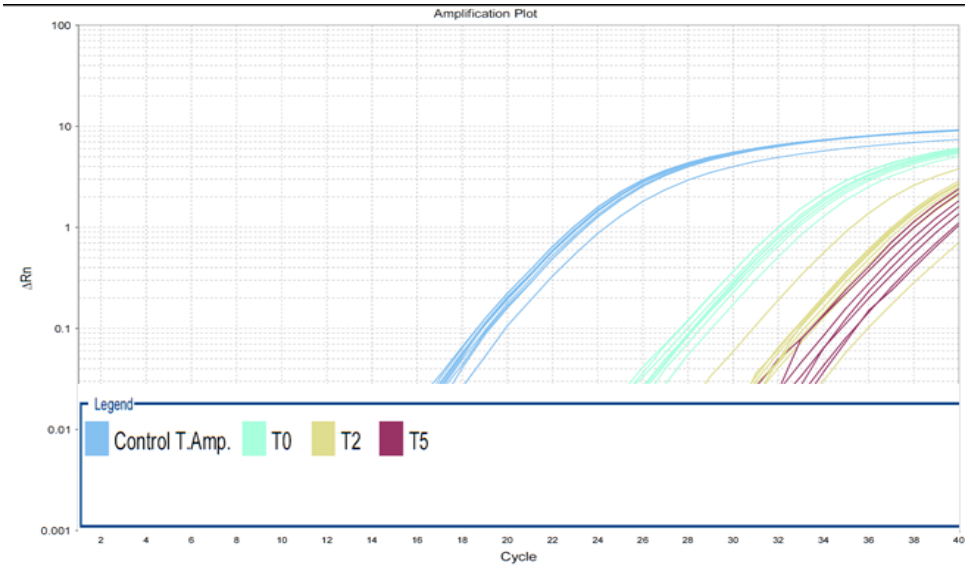

Figure 4-11. Amplification plots of the qPCR assays on the Teleaulax amphioxeia nuclear 28S D2 USE b) on DNA extracted from T. amphioxeia (control) and Strombidium cf. basimorphum at different time points over prey deprivation and starvation.

The fluorescent signals obtained upon hybridization of ciliates samples with a fluorescent in situ hybridisation (FISH) probe for prey rRNA seem comparable among individuals (single cells) sampled at different time points (Figure 12). Individual cells that contained the labelled genetic material as wells as individual cells that did not were found in all samples. The ribosomes observed via FISH could have been sequestered from the prey together with chloroplasts or actively transcribed from the prey nuclear gene. Fluorescent in situ hybridisation can be used for the same purpose as qPCR. However, different from qPCR, this technique does not allow the quantification of prey DNA in the sample. FISH is instead useful to discriminate for presence/absence of prey DNA within individual cells of the same population.

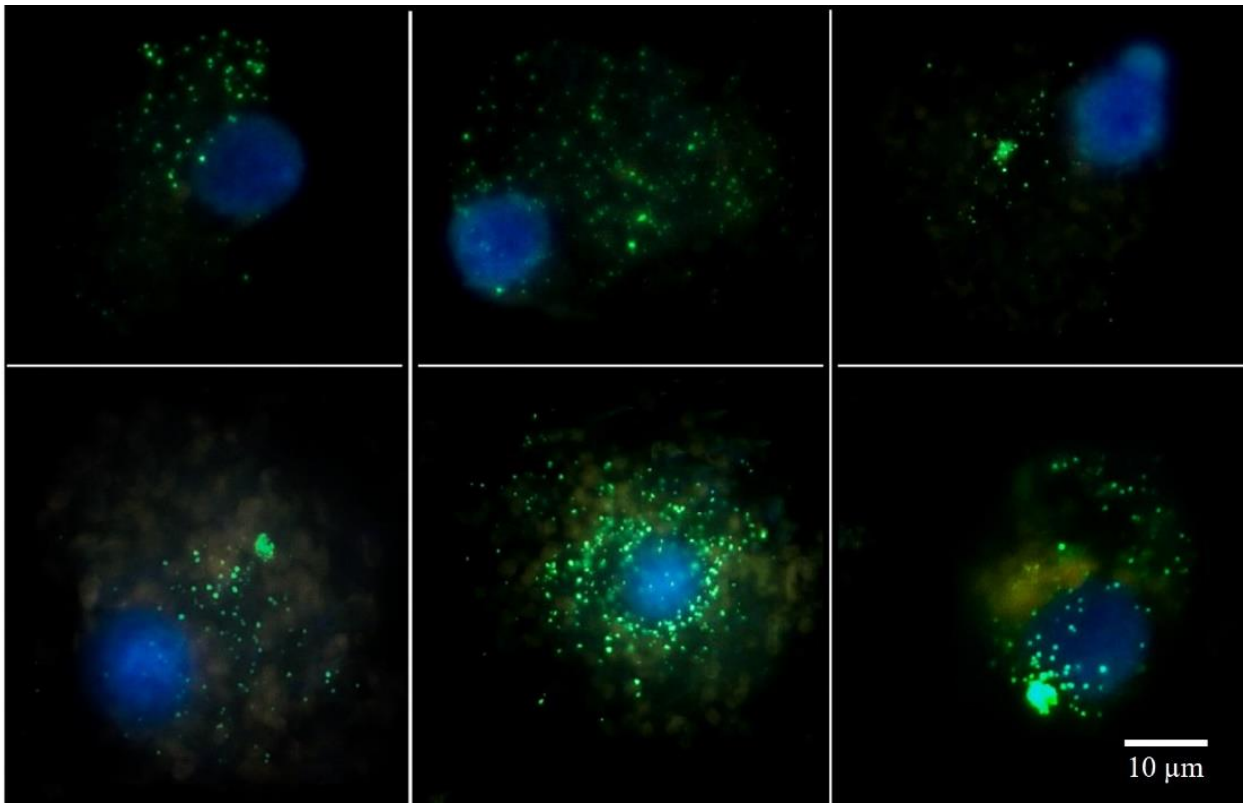

Figure 4-12. Micrographs of Strombidium cf. basimorphum (ciliate) cells in different nutritional status; fed of Teleaulax (prey) (top: well fed, bottom: prey starved) hybridized with a probe for prey rRNA. Blue: ciliates nuclei (DAPI stained), orange: kleptoplasts, green: prey rRNA probe (Alexa488).

Single-cell transcriptomics revealed the retention of Teleaulax genetic material by S. cf. basimorphum. A total of 282 transcripts of prey nuclear and chloroplast origin were present in starved cells. Among the 100 most expressed genes of prey origin there were transcripts encoded in the chloroplast genome (Figure 13). Chloroplast genes included photosystem I and II apoproteins, subunits and cytochromes. Moreover, we detected prey nuclear encoded genes involved in other metabolic processes such as amino acid biosynthesis and degradation. Genetic information pathways involved genes related to the transcription and translation of the prey nucleus within the host.

Figure 4-13. Heatmap representing the 100 most expressed transcripts of prey origin and their corresponding pathways according to Kyoto Encyclopedia of Genes and Genomes. The expression values are provided for each separate cell and are shown as transcripts per million (TPM) (Reproduced from rom Maselli et al., 2021 under CC BY 4.0).

Based on these observations, Strombidium cf basimorphum is evidently dependent on prey ingestion to sustain itself. However, the photosynthetic rates measured in the ciliate suggests potential for regulation of the photosynthetic activity of the sequestered chloroplasts in relation to the ciliate's nutritional status. Kleptoplastidic Strombidium spp. are thought to lack genes associated with chloroplasts functionality. Molecular methods are needed to investigate the potential role of genetic material of prey origin as well as the responses of the ciliate.

The retention of prey nuclei and the further analyses of their transcriptional activity within the ciliate will provide important information about the benefit of the ciliate by retaining the nuclei of the prey. The kleptoplastidic ciliate Mesodinium sp. does not only steal the plastid (kleptoplasts) from its cryptophyte prey but also the nucleus (kleptokaryon; Hansen et al., 2013, 2016). The kleptokaryon is transcriptionally active and could account for approximately half of the total transcriptome of the ciliate (Altenburger et al., 2020). The kleptokaryon, in this case, expresses genes for both maintaining the chloroplasts and synthesizing metabolites for which Mesodinium lacks the genetic toolkit (Lasek-Nesselquist et al., 2015; Kim et al., 2016). However, no photosynthesis-related genes were found to be transcribed by the genome of the ciliate (Altenburger et al., 2020).

Dinophysis (Dinoflagellata) are known to sequester plastids of cryptophyte origin, but not the nucleus (Park et al., 2014). Dinophysis harbour several nuclear transcripts which are involved in photosynthesis-related processes including plastid maintenance or pigment biosynthesis (Hongo et al., 2019).

S. cf. basimorphum, apart from retaining prey nuclei, it also has genes related to photosynthetic processes. We detected genes related to photosynthetic pathways. Two isoforms of PetH (ferredoxin--NADP+ reductase) were present in almost all cells (46 out of 47 cells) and showed high expression values. This gene is part of the photosynthetic electron transport system and its presence indicates that they facilitate the maintenance of the kleptoplasts. A gene involved in electron transport, PetF (ferredoxin), was also present alongside petC (cytochrome b6-f complex iron-sulfur subunit) which is part of the cytochrome b6/f complex. The photosystem II cytochrome b559 subunit alpha (psbE) and photosysytem II reaction center protein K (psbK) were also present in the ciliate transcriptome but both detected in only 2 cells, indicating low transcription level of these proteins. However, the rest of the genes involved in these pathways were not present in the transcriptome of the ciliate, which could be result of either absence from the ciliate genome or low transcription levels.

Multiple genes involved in porphyrin and chlorophyll metabolism are also present. These genes involve magnesium chelatase subunits. We found genes encoding for chelatase subunit D, G and H (chlD, chlD, chlG), which were present in multiple cells and with high expression values. Genes for other chelatase subunits were also found but their expression levels were very low. However, it confirmed their presence in the transcriptome of the ciliate.

All these findings are similar to the case of Dinophysis, which does not retain prey nuclei itself, but does inherently harbour photosynthesis related genes (Hongo et al., 2019). S. cf. basimorphum could thus similarly be considered an intermediate case, given its ability

to use the kleptokaryon of the prey and at the same time own photosynthetic genes which are connected to the functionality of the kleptoplasts.

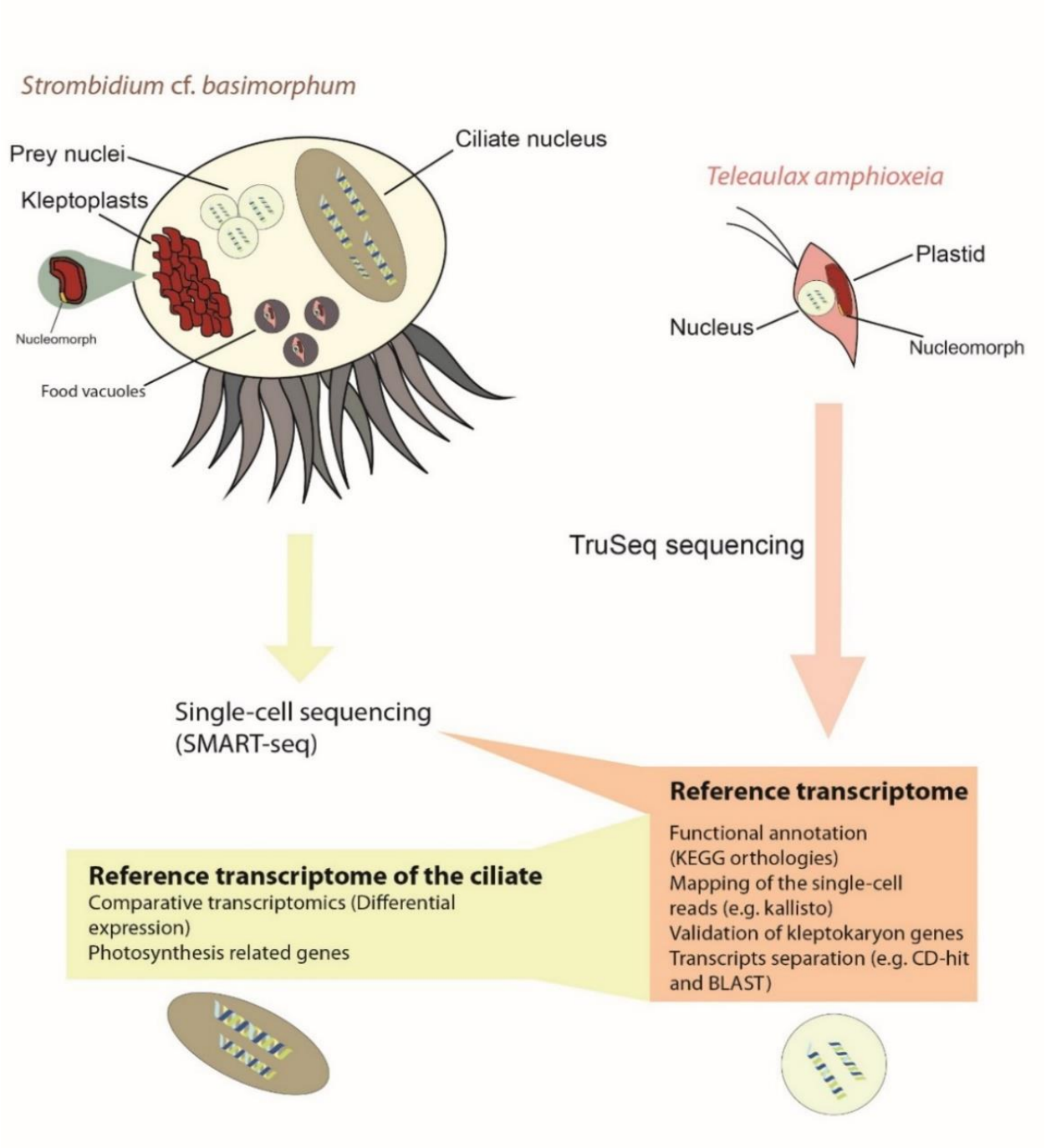

Figure 4-14. Conceptual illustration of the approach followed for elucidating molecular processes in Strombidium cf. basimorphum feeding on the cryptophyte Teleaulax amphioxeia.

4.3.4 Acantharian nutrient acquisition capabilities

A total of 2.1 billion 2x100bp paired-end reads were generated by Novaseq S1 flowcell sequencing. 19.4 to 116.2 million sequence reads per sample. Bioinformatic quality filtering with Trimmomatic removed only 0.003% read pairs, SortmeRNA filtered out 328 million reads (15%) leaving 1.8 billion prospected paired mRNA reads, 4.8 – 70.2 million read per sample. De novo assembly generated 2,108,782 transcripts totalling 2,649,628,289 bp, with a N50 of 2073 and an Ex90N50 of 3200. The GC content of the transcripts exhibited a bimodial distribution (Figure 15), low GC% transcripts are assumed to be transcripts from the Acantharia host, while the high GC% transcripts from the algal symbiont (Liu et al., 2019). The holobiont transcriptome assembly includes complete sequences for 96.9% of searched eukaryotic BUSCOs. More complete transcriptomes contain more full-length BUSCOs, which are well-conserved genes for the representative genomes of each BUSCO group. BUSCOs provide a method to quantitatively assess the quality of a transcriptome in terms of gene content.

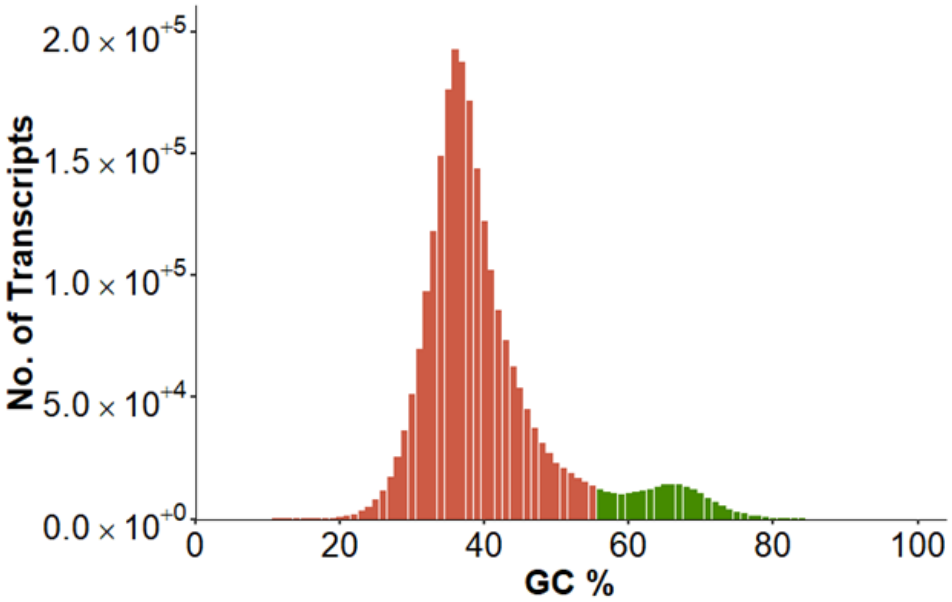

Figure 4-15. GC content of the Acantharia holobiont de-novo assembly, indicated in red and green, respectively, are presumed Acantharia and symbiont GC% ranges.

All the assembled sequences were searched against a custom database containing four of Phaeocytis transcriptomes (i.e. METDB_00327, METDB_00333, METDB_00329, and https://github.com/maggimars/PcordataSymbiosisDGE/blob/2b7836d2f6ebf9a5d80cbcce22988f161428e459/pc_euk_seqs.fasta) using MegaBLAST. All hits with bitscores > 90 were considered Phaeocytis transcripts. The hits were separated out of our assembly. Only using the Blast results to filter out the symbiont of the holobiont transcriptome results in a GC-content profile for the presumed host transcripts that still contains a small high-GC-content tail. For that reason, we additionally use a Gaussian Mixed Model (GMM) to filter out those contigs, i.e. contigs with 99% certainty of belonging to the high GC content model. The GC% of the transcripts assigned to either the symbiont or host is shown in

Figure 16. The split assembly had 91% and 89% complete eukaryotic BUSCOs for the contigs assigned to Phaeocystis and those assigned to Acantharia respectively.

Our combined experimental setup for transcriptomics and chemical imaging aimed to corroborate the capabilities in C and N uptake of Acantharia from both a molecular and physiological angle (Figure 5). With the chemical imaging approach, we aimed to follow nutrient transport and localization over time using stable isotopes and NanoSIMS. Thereby we aimed to visualize and quantify carbon uptake, incorporation, and photosynthate translocation between symbionts and host over time, and the effect of nitrogen (NO3- or NH4+) thereon. The transcriptomics approach is utilised to assess gene expressional difference under the same treatments and time series. Thereby investigating transcriptional difference, adaptability/plasticity of nutrient uptake when increased nutrients are present (eutrophication). As well as, N Metabolism adjustment and capabilities of symbiont and/or hosts). Separation of the holobiont transcriptome allows us additionally to detangle specific processes, such as those involved in carbon and nitrogen metabolism, that are due to host or symbiont transcriptional activity.

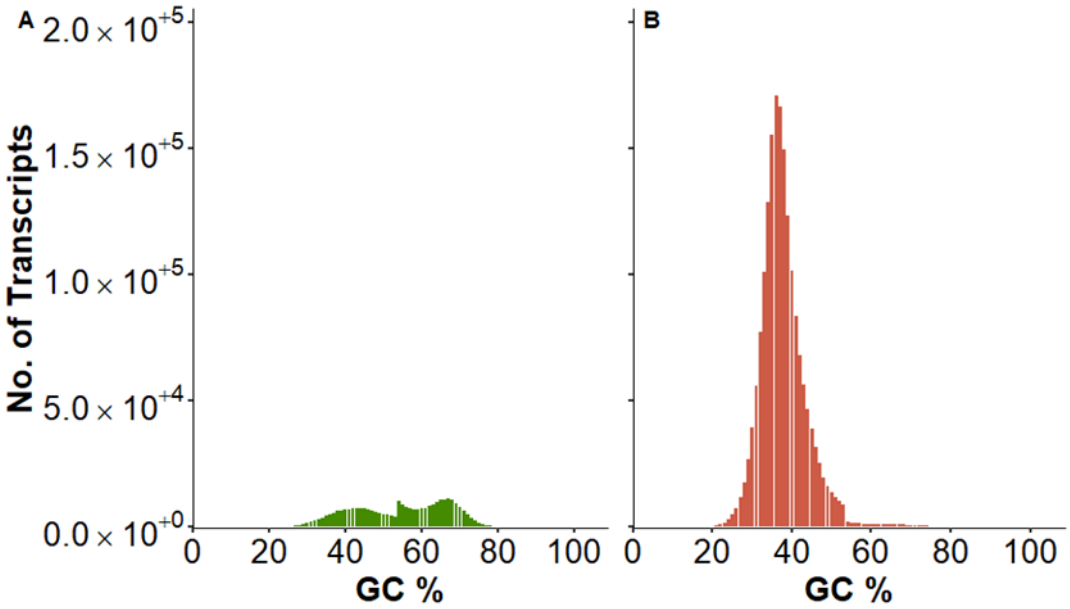

Figure 4-16. GC content of the de novo Assembly split into (A) Phaeocytis contigs, and (B) Non-Phaeocytis (i.e. presumed Acantharia contigs), by means of BLASTn and GMM results.

For example, a preliminary investigation of KEGG pathway annotations indicated that most transcripts associated with energy metabolism are linked to the symbiont partition of the transcriptome. Notably, the only nitrogen metabolism enzymes linked to the host are involved in ammonium metabolism, i.e. glutamate dehydrogenase and glutamine synthetase, whereas enzymes involved in nitrate metabolism are also found for the symbiont. The number of unique KEGG annotation for the symbiont transcriptome is, however, much more than for the host, 2214 versus 1511 KEGGs for symbiont and host respectively (Figure 17). Even though, the host transcriptome is considerably larger with 1,803,192 transcripts to 305,580 transcripts of the symbiont, a lower annotation rate was indeed expected the host transcriptome. Nonetheless, such indications of absence or

presence of enzymatic pathways allow us to hypothesis the role of the host in said pathway, and combine it with the interpretation of chemical imaging for better interpretation.

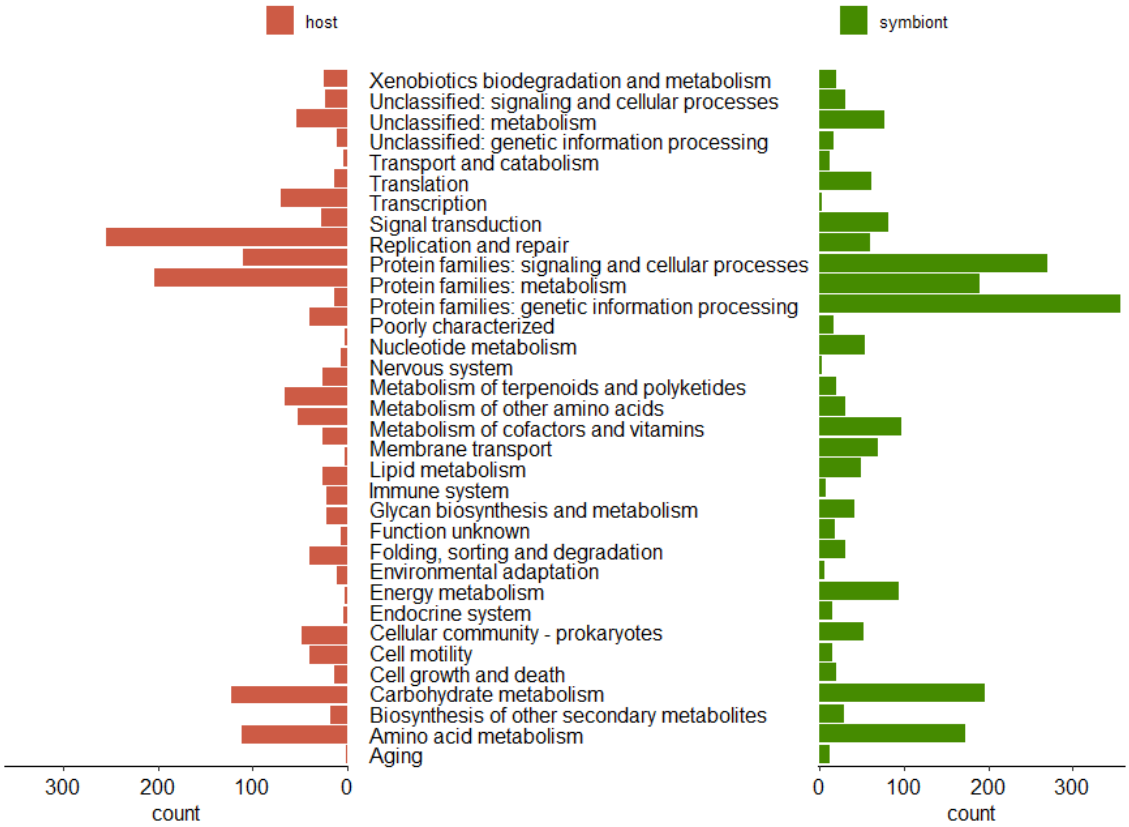

Figure 4-17. K- Number annotated transcript counts for symbiont and host transcripts and the relevant KEGG pathways.

4.4. References

Altenburger, A., Cai, H., Li, Q., Drumm, K., Kim, M., Zhu, Y., et al. (2020). Limits to the cellular control of sequestered cryptophyte prey in the marine ciliate Mesodinium rubrum. ISME J. 15, 1056–1072.

Anestis, K., Kohli, G.S., Wohlrab, S., Varga, E., Larsen, T.O., Hansen, P.J., John, U. (2021). Polyketide synthase genes and molecular trade-offs in the ichthyotoxic species Prymnesium parvum. Sci. Total Environ. 795.

Andrews, S. (2010). FastQC A quality control tool for high throughput sequence data. Babraham Bioinforma.

Binzer, S.B., Svenssen, D.K., Daugbjerg, N., Alves-de-Souza, C., Pinto, E., Hansen, P.J., et al.,2019. A-, B- and C-type prymnesins are clade specific compounds and chemotaxonomic markers in Prymnesium parvum. Harmful Algae 81, 10–1

Bolger, A. M., Lohse, M., and Usadel, B. (2014). Trimmomatic: A flexible trimmer for Illumina sequence data. Bioinformatics 30, 2114–2120.

Bryant, D. M., Johnson, K., DiTommaso, T., Tickle, T., Couger, M. B., Payzin-Dogru, D., et al. (2017). A tissue-mapped axolotl de novo transcriptome enables identification of limb regeneration factors. Cell Rep. 18, 762–776.

Burns, J. A., Pittis, A. A., and Kim, E. (2018). Gene-based predictive models of trophic modes suggest Asgard archaea are not phagocytotic. Nat. Ecol. Evol. 2, 697–704.

Donk, E. Van, Ianora, A., 2011. Induced defences in marine and freshwater phytoplankton:a review. Hydrobiologia 668, 3–19.

Ewels, P., Magnusson, M., Lundin, S., and Käller, M. (2016). MultiQC: Summarize analysis results for multiple tools and samples in a single report. Bioinformatics 32, 3047–3048.

Faure, E., Not, F., Benoiston, A.-S., Labadie, K., Bittner, L., and Ayata, S.-D. (2019). Mixotrophic protists display contrasted biogeographies in the global ocean. ISME J. 13, 1072–1083.

Flynn, K. J., Mitra, A., Anestis, K., Anschütz, A. A., Calbet, A., Ferreira, G. D., et al. (2019). Mixotrophic protists and a new paradigm for marine ecology: where does plankton research go now? J. Plankton Res.

Grabherr, M. G., Haas, B. J., Yassour, M., Levin, J. Z., Thompson, D. A., Amit, I., et al. (2011). Full-length transcriptome assembly from RNA-Seq data without a reference genome. Nat. Biotechnol. 29, 644–652.

Graham, L. B., Colburn, A. D., and Burke, J. C. (1976). A new, simple method for gently collecting planktonic protozoa. Limnol. Oceanogr. 21, 336–341.

Green, B. J., Fox, T. C., and Rumpho, M. E. (2005). Stability of isolated algal chloroplasts that participate in a unique mollusc/kleptoplast association. Symbiosis 40, 31–40.

Haas, B. J., Papanicolaou, A., Yassour, M., Grabherr, M., Blood, P. D., Bowden, J., et al. (2013). De novo transcript sequence reconstruction from RNA-seq using the Trinity platform for reference generation and analysis. Nat. Protoc. 8, 1494–1512.

Hansen, P. J., Nielsen, L. T., Johnson, M., Berge, T., and Flynn, K. J. (2013). Acquired phototrophy in Mesodinium and Dinophysis - a review of cellular organization, prey selectivity, nutrient uptake and bioenergetics. Harmful Algae 28, 126–139.

Hansen, P. J., Ojamäe, K., Berge, T., Trampe, E. C. L., Nielsen, L. T., Lips, I., et al. (2016). Photoregulation in a kleptochloroplastidic dinoflagellate, Dinophysis acuta. Front. Microbiol. 7:785.

Hehenberger, E., Gast, R. J., and Keeling, P. J. (2019). A kleptoplastidic dinoflagellate and the tipping point between transient and fully integrated plastid endosymbiosis. Proc. Natl. Acad. Sci. U. S. A. 116, 17934–17942.

Heinbokel, J. F., Diego, S. and Jolla, L. (1978) Studies on the functional role of tintinnids in the Southern California Bight. I. Grazing and growth rates in laboratory cultures. Mar. Biol., 189, 177–189.

Hongo, Y., Yabuki, A., Fujikura, K., and Nagai, S. (2019). Genes functioned in kleptoplastids of Dinophysis are derived from haptophytes rather than from cryptophytes. Sci. Rep. 9, 1–11.

Jimenez, V., Burns, J., Le Gall, F., Not, F., and Vaulot, D. (2020). No evidence of phago-mixotropy in Micromonas polaris, the dominant picophytoplankton species in the Arctic. J. Phycol. 57, 435-446.

John, U., Tillmann, U., Medlin, L.K., 2002. A comparative approach to study inhibition ofgrazing and lipid composition of a toxic and non-toxic clone of Chrysochromulina polylepis (Prymnesiophyceae). Harmful Algae 1, 45–57

John, U., Tillmann, U., Hülskötter, J., Alpermann, T.J., Wohlrab, S., Van de Waal, D.B., 2015.Intraspecific facilitation by allelochemical mediated grazing protection within a toxigenic dinoflagellate population. Proc. R. Soc. B Biol. Sci. 282

Katoh, K., Kuma, K. I., Toh, H., and Miyata, T. (2005). MAFFT version 5: Improvement in accuracy of multiple sequence alignment. Nucleic Acids Res. 33, 511–518.

Kim, G. H., Han, J. H., Kim, B., Han, J. W., Nam, S. W., Shin, W., et al. (2016). Cryptophyte gene regulation in the kleptoplastidic, karyokleptic ciliate Mesodinium rubrum. Harmful Algae 52, 23–33.

Kopylova, E., Noé, L., and Touzet, H. (2012). SortMeRNA: Fast and accurate filtering of ribosomal RNAs in metatranscriptomic data. Bioinformatics 28, 3211–3217.

Lasek-Nesselquist, E., Wisecaver, J. H., Hackett, J. D., and Johnson, M. D. (2015). Insights into transcriptional changes that accompany organelle sequestration from the stolen nucleus of Mesodinium rubrum. BMC Genomics16:805.

Leles, S. G., Mitra, A., Flynn, K. J., Stoecker, D. K., Hansen, P. J., Calbet, A., et al. (2017). Oceanic protists with different forms of acquired phototrophy display contrasting biogeographies and abundance. Proc. R. Soc. B Biol. Sci. 284, 20170664.

Leles, S. G., Mitra, A., Flynn, K. J., Tillmann, U., Stoecker, D., Jeong, H. J., et al. (2019). Sampling bias misrepresents the biogeographical significance of constitutive mixotrophs across global oceans. Glob. Ecol. Biogeogr. 28, 418–428.

Liu, Z., Hu, S. K., Campbell, V., Tatters, A. O., Heidelberg, K. B., and Caron, D. A. (2017). Single-cell transcriptomics of small microbial eukaryotes: Limitations and potential. ISME J. 11, 1282–1285.

Mansour, J., Anestis, K., Not, F., and John, U. (2021a). cDNA library preparation from total RNA extracts of Single-cell marine protists (e.g. Acantharia, Strombidium basimorphum, and Prymnesium parvum) for transcriptome sequencing V.2. protocols.io.

Mansour, J., Anestis, K., Not, F., and John, U. (2021b). Single-cell total RNA extraction from marine protists (e.g. Acantharia, Strombidium cf basimorphum, and Prymnesium parvum) V.2.

Mansour, J. S., Norlin, A., Llopis Monferrer, N., L'Helguen, S., and Not, F. (2021c). Carbon and nitrogen content to biovolume relationships for marine protist of the Rhizaria lineage (Radiolaria and Phaeodaria). Limnol. Oceanogr. 66, 1703–1717.

Mansour, J.S., and Anestis, K. (2021d). Eco-evolutionary perspectives on mixoplankton. Front. Mar. Sci.

Maselli, M., Anestis, K., Klemm, K., Hansen, P.J., John, U. (2021). Retention of prey genetic material by the kleptoplastidic ciliate Strombidium cf. basimorphum. Front. Microbiol.

Mitra, A., Flynn, K. J., Tillmann, U., Raven, J. A., Caron, D., Stoecker, D. K., et al. (2016). Defining planktonic protist functional groups on mechanisms for energy and nutrient acquisition: Incorporation of diverse mixotrophic strategies. Protist 167, 106–120.

Park, M. G., Kim, M., and Kim, S. (2014). The acquisition of plastids/phototrophy in heterotrophic dinoflagellates. Acta Protozool. 53, 39–50.

Rivkin, R. B. and Seliger, H. H. (1981) Liquid scintillation counting for 14C uptake of single algal cells isolated from natural samples. Limnol. Oceanogr., 26, 780–785.

Schoener, D. M., and McManus, G. B. (2012). Plastid retention, use, and replacement in a kleptoplastidic ciliate. Aquat. Microb. Ecol. 67, 177–187.

Song, Y., Milon, B., Ott, S., Zhao, X., Sadzewicz, L., Shetty, A., et al. (2018). A comparative analysis of library prep approaches for sequencing low input translatome samples. BMC Genomics 19, 1–16.

Stamatakis, A. (2014). RAxML version 8: a tool for phylogenetic analysis and post-analysis of large phylogenies. Bioinformatics 30, 1312–1313.

Steemann Nielsen, E. 1952. The use of radioactive carbon (C14) for measuring organic production in the sea. J. Conseil, Perm. Intern. Exploration Mer, 18: 117-140.

Stoecker, D. K., Silver, M. W., Michaels, A. E., and Davis, L. H. (1988). Obligate mixotrophy in Laboea strobila, a ciliate which retains chloroplasts. Mar. Biol. 99, 415–423.

Stoecker, D. K., Johnson, M. D., De Vargas, C., and Not, F. (2009). Acquired phototrophy in aquatic protists. Aquat. Microb. Ecol. 57, 279–310.

Tillmann, U., Hansen, P.J., 2009. Allelopathic effects of Alexandrium tamarense on otheralgae: evidence from mixed growth experiments. Aquat. Microb. Ecol. 57, 101–112.

MixITiN Deliverable 3.8 Report

Section 5

Novel Systems Dynamics Modelling Approaches For Investigating Marine Planktonic Mixotrophy

Aditee Mitra, Cardiff University UK
Kevin J Flynn, Plymouth Marine Laboratory UK
Anna-Adriana Anschütz, Cardiff University UK

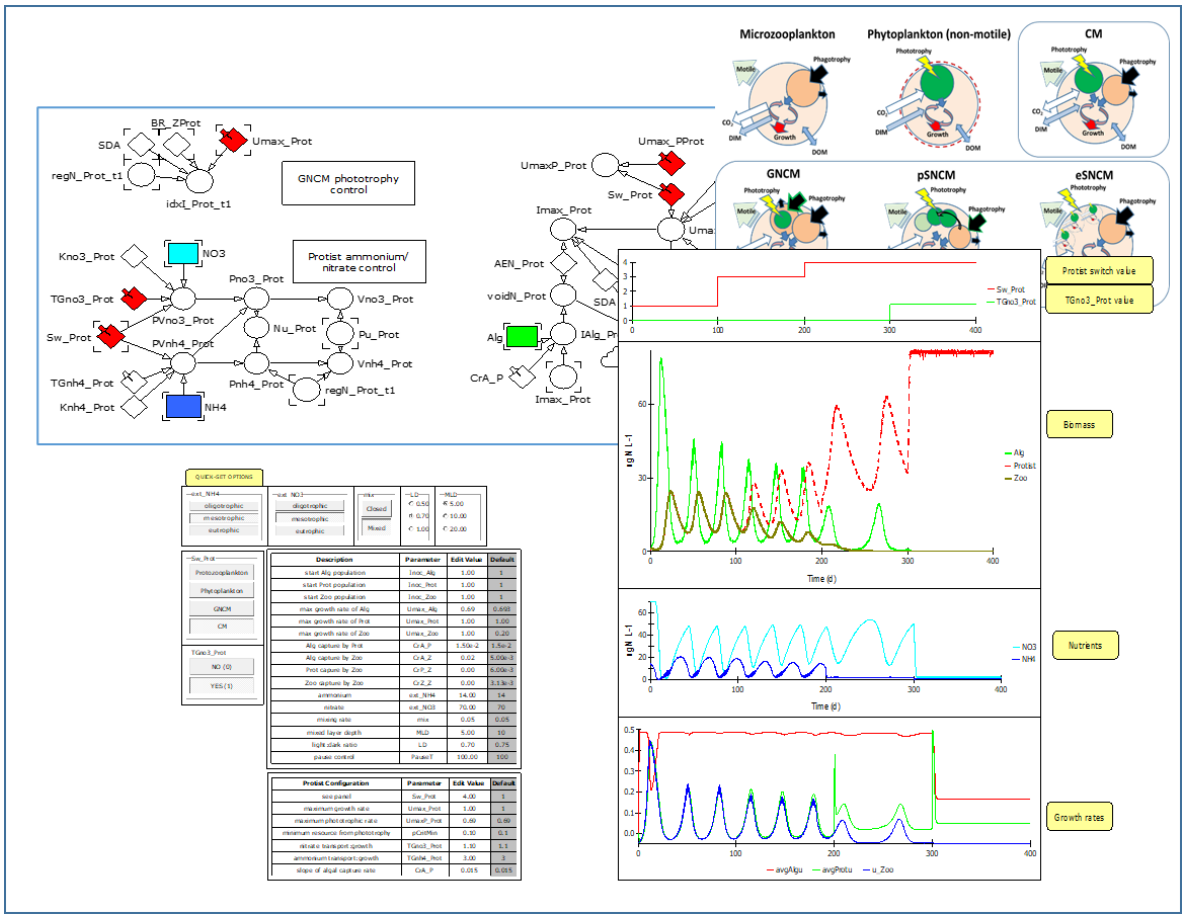

Table of Contents

5.1 Introduction

Marine planktonic mixotrophy, in the context of MixITiN, describes the coupling of phototrophy and phagotrophy within plankton protists. Since the project started, these organisms have been termed '**mixoplankton**' (Flynn *et al.* 2019), and we use this descriptor throughout this Section.

Mixoplankton are above all else dynamic organisms, modulating phototrophy, phagotrophy and osmotrophy against a background of changing resource abundances, not least of light as that varies by the minute. Simulation models provide a platform for exploring what we know and highlight what we do not know. Few biologists build or even use models, and the converse is also true – few modellers are experimental or field biologists. This section of Report D3.8 considers the potential of models in exploring mixoplankton science from eco-physiological as well as biological perspectives, and how MixITiN furthers that aspiration.

5.2 Managing expectations

Mixoplankton science encompasses the empirical fields of molecular biology, organismal biology and ecology, and the computational field of modelling. Modelling is a catch-all term for any mathematical simplification and ranges from simple linear regression fits through a cloud of data points, to the complexity of systems biology approaches. Even the most complex systems biology description is of trivial complexity compared to real biology. As a fundamental requirement for modelling is simplification, it is thus worth considering differences between the science fields and thence how they may interact.

5.2.1 Molecular biology

Molecular biology includes the 'omics and, also overlaps into what would traditionally have been termed biochemistry. The 'omics (genomics, transcriptomics, proteomics, metabolomics) all provide the potential for high resolution detail but with little if any quantification of value for simulation models. Thus, genomics tells us whether an organism has genes for particular traits, while transcriptomics tells us whether that gene is transcribed, for example into a protein (i.e., proteomics). Data from metabolomics gives information on particular metabolic pathways. However, none of these approaches provides information about concentrations of enzymes and rates of activity at the cellular level. In terms of modelling such presence/absence information can only provide support to the initial conceptual steps in model development. Even data provided by state-of-the-art molecular techniques such as NanoSIMs are of limited utility for modelling except in support for (usually steady-state) flux modelling of specific biochemical pathways at sub-cellular level.

Genomic approaches yield high resolution data on who is where, but with little quantification or any data for vital rate processes – the most important driving factors in biology and ecology (Santoferrara 2019). Models for simulating field scenarios, in contrast, needs not only information about presence/absence of organisms but also quantification to enable categorisation of species abundance into different functional types. A major challenge in mixoplankton research is that closely related species can

show very different physiologies, not only at the finer level of (de)repression regulation, but even at higher levels such as resource acquisition potential. Thus, *Karlodinium armiger* differs from *K. veneficum* in that the latter can use nitrate while the former cannot (Calbet *et al*. 2011, Rasmussen *et al*. 2017).

The interface between molecular biology and simulation modelling is thence largely qualitative, guiding conceptual design of models and for broad-level validation only.

5.2.2 Organismal biology

Laboratory-based physiological studies, if conducted appropriately with respect to experiment design and execution, have great potential to aid modelling, and conversely for modelling to aid hypothesis setting and experiment design. Data, of exactly the types required to support modelling, can be collected with respect to quantification of what modellers term state variables (e.g., nutrients, biomass, cell abundance), and of rate processes (here for mixoplankton, notably phototrophy and phagotrophy).

The reality is often very different; very few studies of physiology report the range of data required to properly support modelling. The most common problem is reliance on the individual (i.e., cells) as the core unit, while models usually require element mass abundances (e.g., carbon biomass). Values expressed as cell L^{-1} are of little value unless they can be reliably transformed into units such as gC L^{-1}. The problems for mixoplankton research are made all the greater by the necessity of conducting both ‘phytoplankton’ and ‘protozooplankton’ measurements simultaneously.

If experimental scientists and modellers work hand-in-hand, the potential for advancing mixoplankton science is much greater.

5.2.3 Ecology

The challenges in organismal biology linked to modelling are similar but exacerbated in field work because of an inability to constrain conditions, and also the inability to replicate experiments in time and space. Simply establishing biomass abundances is a challenge, especially in the calmer waters frequented by mixoplankton, where the organisms form patches. Such patches may or may not be adequately sampled and hence give a skewed impression of depth-integrated biological activity. Organisms then also need to be allocated into functional type descriptions, which often also separates them into different allometric groups. This is required not only for the mixoplankton, but for all the other plankton as befits the study needs in question.

5.2.4 Coupling to models

Ultimately the justification for and thence acceptance (or otherwise) of the mixoplankton paradigm will come from coupling field and ecosystem-level modelling. The construction of those mixoplankton models will have been developed at a conceptual level using information from molecular biology and physiology (a notable example in this regard has been the use of molecular biological data on the relationships between cryptophytes, *Mesodinium* and *Dinophysis*; Stoecker *et al*. 2017, and references there in) and validated against physiological data.

5.3 Types of 'novel' modelling tools

Novelty comes from developing new approaches and also from new applications of established approaches. The challenges at hand for mixoplankton research are similar to those for 'phytoplankton' or 'protozooplankton', though more complex in execution because of the merging of physiologies.

5.3.1 Mixoplankton models

MixITiN aimed to deliver a suite of mixoplankton models ranging from the simplest structure (single N-based model) to complex descriptions containing various feedback functionalities. In order to do this, we considered all the protist plankton functional types (**Fig.5.1;** Mitra *et al.* 2016, Flynn *et al.* 2019). In this section the history of this development is described with reference to **Figure 5.2** and **Table 5.1.**

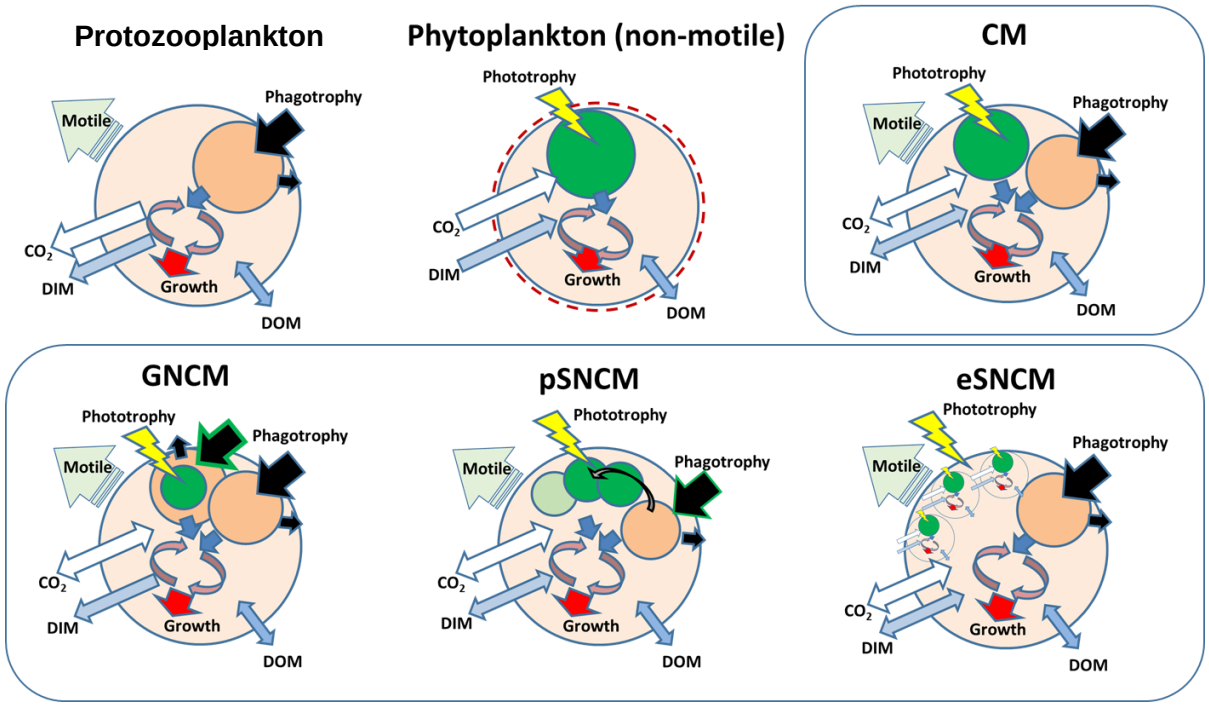

Figure 5.1 Schematics showing differences between protist plankton physiologies. Protozooplankton are osmo–phagotrophic using dissolved organic matter (DOM); they are incapable of phototrophy. Phytoplankton are photo-osmo mixotrophic; they are incapable of phagotrophy. The constitutive mixoplankton (CM) and non-constitutive mixoplankton (NCM) are all photo-, osmo- and phago-mixotrophic. The generalist NCM (i.e., GNCM) may acquire phototrophy from many types of phototrophic prey; pSNCM are plastidic specialists acquiring phototrophy from specific prey only. eSNCM are endosymbiotic NCM, acquiring phototrophy by harbouring specific phototrophic prey. See Mitra *et al*. (2016) and Flynn *et al*. (2019) for further information.

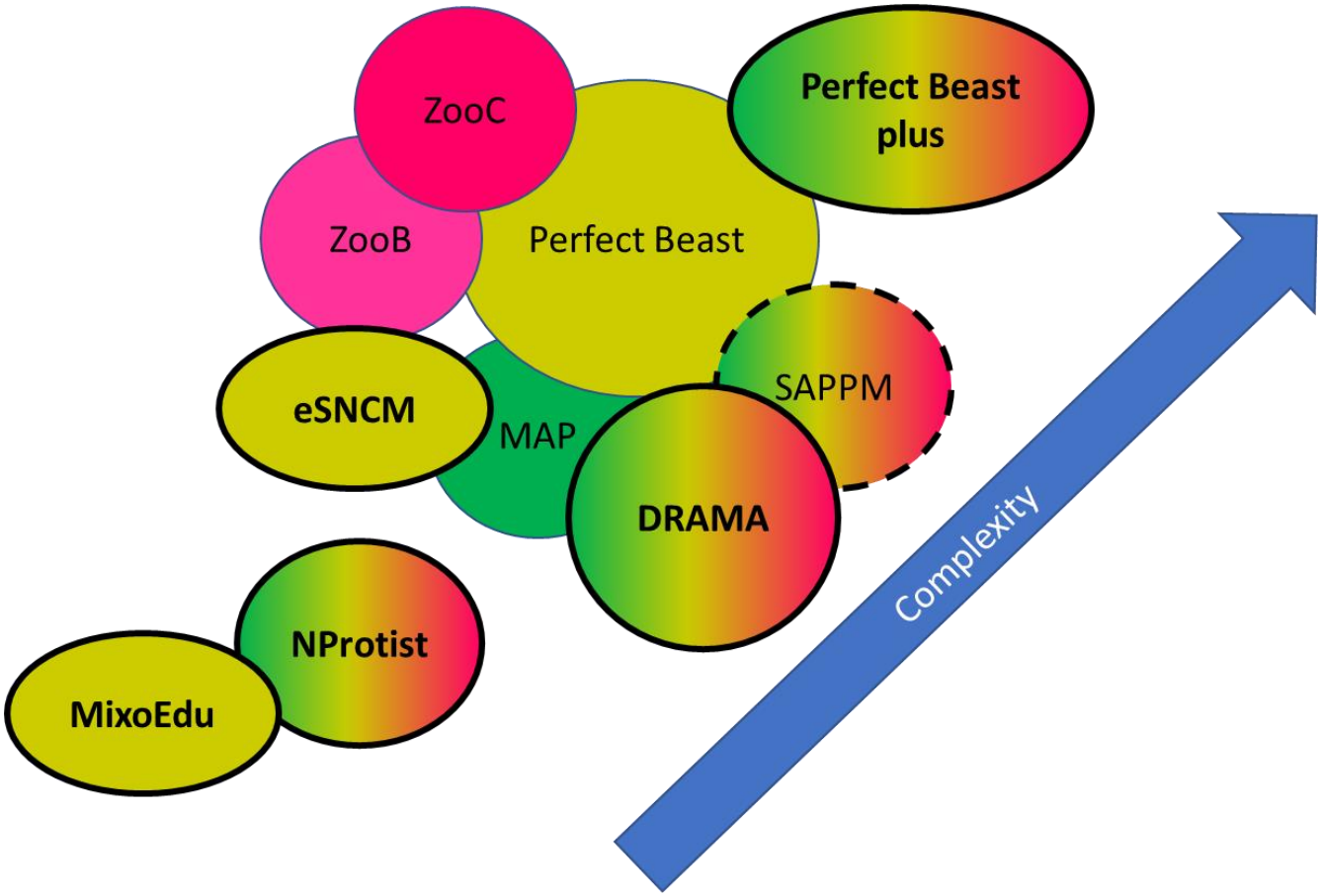

Figure 5.2 Genealogy of mixoplankton models. Those circled in thick black are outputs of MixITiN; SAPPM was an intermediate development, replaced by DRAMA. Green denotes phototrophy, red/pink denotes phagotrophy, khaki denotes mixoplanktonic model only (i.e., the model does not describe other protist plankton types). SAPPM and DRAMA also describe osmotrophy, as do some versions of MAP. See also **Table 5.1**.

Table 5.1 Summary of models describing plankton protists; see also **Figures 5.1 & 5.2**. **SV**, state variable (min, minimum); **RC**, response control for acclimation; **C**, carbon; **N**, nitrogen; **P**, phosphorus; **Si**, silica; **Fe**, iron; **Chl**, chlorophyll; **G**, gut; **H**, history function (e.g., day-averaged growth rate); **Rub**, RuBisCO; **pNA**, plastid nucleic acid; **sym**, symbiont; **mC** (in DRAMA) metabolite C; **Var Stoich**, variable stoichiometric; ○, Zooplankton models (ZooB & ZooC assume fixed C:N:P for the predator but handle variable C:N:P prey). Models stemming from MixITiN are indicated including the authorship under the model name.

Feature ↓	MAP *Flynn 2001*	ZooB *Mitra 2006*	ZooC *Mitra & Flynn 2007*	Perfect Beast *Flynn & Mitra 2009*	MixoEdu *Flynn & Mitra* ***MixITiN***	Nprotist *Anschütz & Flynn 2020* ***MixITiN***	SAPPM *Flynn 2021* ***MixITiN***	DRAMA *Flynn & Mitra* ***MixITiN***	Perfect Beast plus *Mitra & Flynn* ***MixITiN***	eSNCM *Mitra* ***MixITiN***
Phytoplankton	●					●	●	●	●	
Diatom	●						●	●	●	
Protozooplankton		●	●			●	●	●	●	
CM				●	●	●	●	●	●	
GNCM				●		●	●	●	●	
pSNCM				●		●	●	●	●	
eSNCM										●
SV# (min)	6 (4)	1	2	9	1	2 (1)	7 (6)	7 (6)	9 (8)	4
SV type	C, N, P, Si, Chl, Fe	C	C, GC	C, N, P, Chl, GC, GN, GP, GChl, H	N	N, H	C, N, P, Si, Chl, 2*H	C, mC, N, P, Si, Chl, Rub, pNA	C, N, P, Chl, GC, GN, GP, GChl, pNA	host C,N sym C,N
Var Stoich	●	○	○	●			●	●	●	●
Phototrophy	●			●	●	●	●	●	●	●
Phagotrophy		●	●	●	●	●	●	●	●	●
Osmotrophy	●						●	●		
Nutrient RC	●						●	●		
Photo RC	●			●			●	●	●	
Grazing RC			●	●				●	●	●
History function				●		●	●			

The following descriptions are given in chronological order across the width of **Table 5.1**; see also **Figure 5.2.**

MAP The MAP series of models (Flynn 2001, 2003) describe ***M**odel(s) of **A**lgal **P**hysiology*, for phytoplankton including diatoms. In the base form the model is multi-nutrient including carbon (C), nitrogen (N), phosphorus (P), chlorophyll (Chl), with silica (Si) for diatoms. Iron (Fe) could also be included. The model delivers variable cell size as well. The model deploys a unified normalised quota construction, including a response-curve control of nutrient transport and assimilation.

ZooB This multi-nutrient (C,N,P) stoichiometric zooplankton description provides scope to control grazing selectively with reference to prey quality and quantity, and also modulate assimilation efficiency accordingly (Mitra 2006).

ZooC This multi-nutrient (C,N,P) variable stoichiometric model also includes an explicit description of the zooplankton gut, and thus enables an explicit feedback control of satiation upon grazing and gut (or food vacuole) clearance rates (Mitra & Flynn 2007).

Perfect Beast This was the first ever comprehensive, variable stoichiometric description of mixoplankton where phototrophy and phagotrophy were integrated synergistically to describe what are now termed constitutive and generalist non-constitutive mixoplankton (Flynn & Mitra 2009). Lacking, however, is a capacity to portray the physiology of plastidic specialist non-constitutive mixoplankton (pSNCM). It combined facets of MAP, ZooB and ZooC, and thus has explicit descriptions of the contents of the food vacuoles. It was built at a time when the assembly of knowledge of mixoplankton physiology was at an early stage; the model construct was consistent with the conceptual models of Jones (1997) and Stoecker (1998). Perfect Beast uses a history function, related to day-average growth rate, to modulate photo- with phago- trophy.

MixoEdu This is a single nutrient (N-based) model describing four protist plankton functional types – phytoplankton, constitutive mixoplankton (CM), generalist non-constitutive mixoplankton (GNCM) and protozooplankton; this was specifically developed within MixITiN for educational purposes (Flynn & Mitra 2021).

NProtist Developed from MixoEdu, this MixITiN product is also a single nutrient (N-based) model but it can be configured as any one of 5 protist functional types – phytoplankton, protozooplankton, CM, GNCM and pSNCM (Anschütz & Flynn 2020). It uses a history function to modulate acquired phototrophy of pSNCM.

SAPPM This was developed to be an intermediate-level complexity mixoplankton model for MixITiN. In contrast with Perfect Beast, SAPPM (***S**witchable **A**cclimative **P**rotist **P**lankton **M**odel*) does not have an explicit food vacuole (‘gut’). It explicitly describes CM, GNCM and pSNCM functional types, and also describes mixotrophy via osmotrophy. The model uses a novel mechanism to modulate resource acquisition, developed from an approach used in MAP. The model has two history functions, deriving day-average growth rate and C-fixation rate. The SAPPM model is published as an annex to Flynn (2021), attributed to MixITiN, deployed in that instance for a Decision Support Tool for commercial exploitation of microalgae.

DRAMA This is an intermediate-level complexity mixoplankton model, developed within MixITiN, to replace SAPPM. DRAMA (***D****ynamic* ***R****esource* ***A****ssimilation with* ***M****odulated* ***A****cquisition*) retains the resource acquisition control of SAPPM but has no history functions. DRAMA has state variables describing both RuBisCO (replacing the C-fixation history function of SAPPM), and the plastid nucleic acid content. The growth rate history function is not needed as DRAMA uses a C-C-quota construction. DRAMA describes all protist plankton types except endosymbiotic specialist non-constitutive mixoplankton (eSNCM). The model is, at the time of writing this report, in Beta-test mode.

Perfect Beast plus (PB+) This is a complex model structure developed within MixITiN from Perfect Beast. An intermediate development had been used in works published by Leles *et al*. (2018, 2021) which enabled the original Perfect Beast to describe phytoplankton and diatoms. PB+ developed from that to include encounter and allometric based feeding (Flynn and Mitra 2016), and an ability to track the history of acquired plastids for GNCM and pSNCM. PB+ thus provides explicit descriptions of all protist functional types (phytoplankton, CM, GNCM, pSNCM, protozooplankton) except eSNCM. Within MixITiN, PB+ has been implemented in food-webs to study the interactions of the *Teleaulax-Mesodinium-Dinophysis* complex (Anschütz, Flynn & Mitra*,* in preparation) and also the impact of grazers (copepods) on mixoplankton dynamics (Traboni, Mitra , Flynn & Saiz *,* in preparation).

eSNCM This model, an output from MixITiN, is explicitly constructed to describe the activity of eSNCM groups; it is the first model to do so. It combines a dual currency (C,N) variable stoichiometric protozooplankton host model with a dual currency (C,N) variable stoichiometric phytoplankton symbiont model to describe the interactions between host and symbiont under different conditions of light and prey abundance. The model structure is in beta-testing stage at the time of writing.

5.3.2 Deployment options

The models described above present various deployment options as ‘novel approaches’. Those approaches are:

i) **Educational**: a major challenge in coupling empirical and computational aspects of mixoplankton research is breaking the cross-science-language barrier. While many, if not all, biologists and ecologists understand something of the empirical sciences (from molecular tools, physiology, to sampling at sea), few understand much about simulation modelling. While the converse is undoubtedly true (modellers understand little about the details of biology and ecology), the subject of mixoplankton science is ‘owned’ by biologists and ecologists. So, one could argue that a taster in modelling mixoplankton would be a useful tool to those scientists. Further, it would also be a useful training tool for the next generation of students and ECRs, helping them to gain a better understanding of how plankton food webs in the oceans function.

ii) **Simulating physiological processes**: these consider the intracellular events that define mixoplankton types, and their success in nature. While models will always be much simpler than reality, models of a certain conceptual basis can

be usefully deployed, not least to draw attention to which factors are of most consequence in explaining competitive success.

5.4 Novel mixoplankton models in education

There are very few models of mixoplankton in the literature. Those that are there are either very simple (directed at mixotrophy in general rather than at mixoplankton *per se*), or, are extremely complex. However, models are widely used in aquatic sciences, for example in climate change studies, fisheries management etc. Therefore, it is important that the next generation (from school pupils to university students) are provided and insight into model development and deployment. With this in mind, we developed ***MixoEdu*** for educational purposes. This is a relatively simple single nutrient (nitrogen-based) model that simulates constitutive and non-constitutive mixoplankton growth dynamics. The model is described in a booklet (Flynn & Mitra 2021; http://doi.org/10.5281/zenodo.5040445), and is available open access as is the accompanying model to run for using free-to-end-user software.

The ***MixoEdu*** booklet describes the conceptual and then mathematical basis for a N-based model of protist plankton types (protozooplankton, phytoplankton, CM and NCM mixoplankton), that allows the user to experiment with different organism configurations. The form of the model can be judged from **Figures 5.3** and **5.4**.

Working through the booklet, the reader can better appreciate what goes into constructing a simulation model, not only with respect to the equations, but equally, and perhaps more importantly, the need to have data available of a certain type. In this instance, with a N-based model, to compare the model with reality all biomass data would need to be expressed with units of mgN m^{-3}.

The form of the MixoEdu description in Flynn & Mitra (2021) builds on the free self-teaching book on modelling ecosystem dynamics of Flynn (2018). The booklet provides two options for the users – (i) to follow the step-by-step instructions and build the model from scratch, or, (ii) to download a fully working Powersim Cockpit version (free download) and use this to run *in silico* ecological experiments. This model has been deployed within MixITiN to train the project's early stage researchers (ESRs) and also, used by the ESRs themselves in outreach activities (delivered to range of different audiences, families, school pupils etc.).

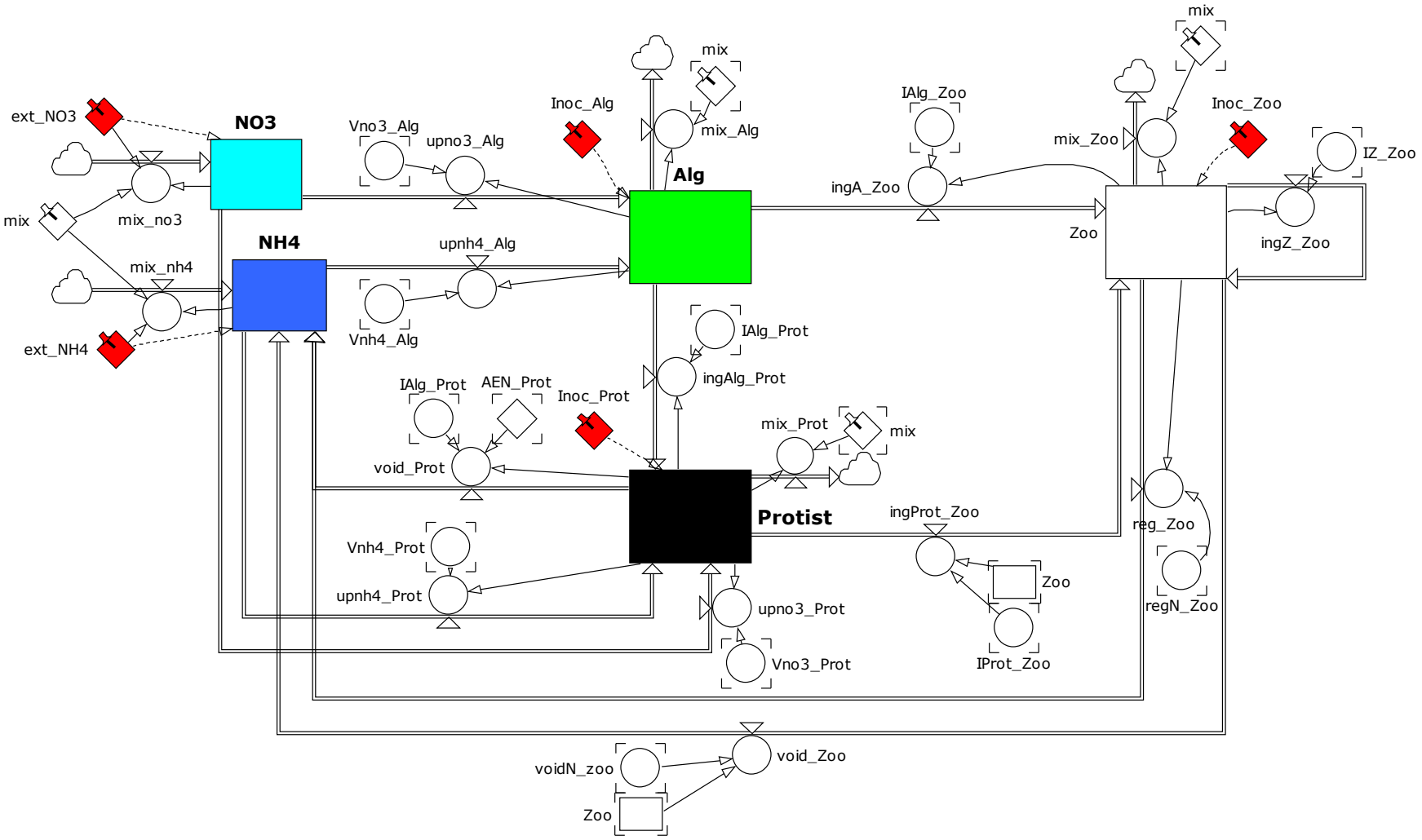

Figure 5.3 Forrester diagram of the main ***MixoEdu*** model structure showing the state variables for ammonium (NH4), nitrate (NO3), and for the organisms "Alg", "Zoo", and "Protist". The "Protist" model can itself be configured to be any one of four functional types - protozooplankton, phytoplankton, GNCM or CM. Taken from Flynn & Mitra (2021); see also Table 5.1.

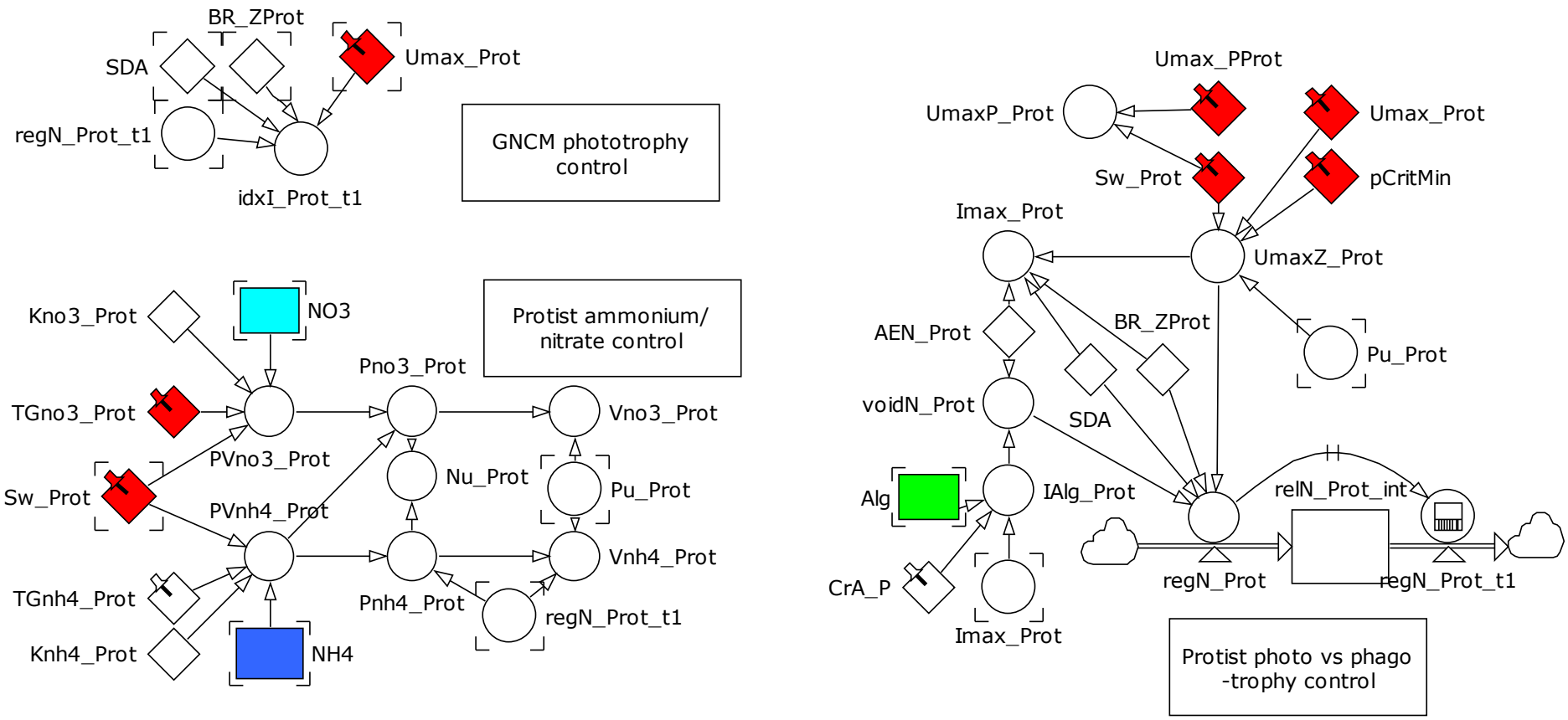

Fig.5.4 Forrester diagram for the protist submodel within the ***MixoEdu*** simulator. Taken from Flynn & Mitra (2021).

.

5.5 Models to align with physiological and molecular biological studies

To explicitly simulate mixoplanktonic processes that a molecular biologist, biochemist or physiologist/ecologist could identify with, requires models with a certain form of conceptual underpinning. Most plankton models deploy extremely simple summative descriptions of physiology; that is part of their allure, also making them computationally inexpensive. However, such an approach severely limits the flexibility needed to consider different mixoplankton types, and also limits the realism of their outputs (noting from above, that our knowledge of reality is itself limited by the absence of good data to support modelling of mixoplankton).

A common feature of the models of Flynn and Mitra (**Table 5.1**) is the deployment of sigmoidal feed-back/feed-forward functions that operate in a fashion akin to allosteric (de)repression processes. Although from a biological perspective, these functions may appear overly simplistic, merging as they do many 10's of real processes, mathematically they look overly complicated to many modellers. They are, however, mathematically robust, ecologically realistic and require only simple parameterisation.

As an example, **Figure 5.5** shows a Forrester modelling diagram for the simulation of ammonium-nitrate interactions in phytoplankton (Flynn *et al*. 1997). This simulates changes in transport potential for the two N-sources, of the synthesis, degradation and activity of the enzymes of nitrate and nitrite reductase, and the activity of GS-GOGAT to make amino acids. While one can identify links to biochemistry ('omics), the model remains far too simple to warrant anything other than conceptual phenomenological validation. It must be said, though, that some level of such validation is essential; too many models lack a firm link to reality beyond 'rules' such as allometric linkages established from big-data analyses and assumed biophysical interactions. This creates conflicts between what models purporting to describe mixoplankton simulate versus what real organisms actually do.

Complex models, with physiological detail that we may wish to evolve or otherwise modify, are already costly in computational terms (see **SV#** row in **Table 5.1**; a multi-nutrient phytoplankton model may contain 6 state variables). To add evolution costs an additional state variable per modelled trait to be evolved (Flynn & Skibinski 2020). Each of those modelled traits are actually meta-traits, described by many 10's of genes, and in ecosystem models they represent meta-traits expressed by a whole functional group of organisms that are likely only distantly related genetically. Making links between 'omics and modelling can immediately be judged as being conflicted.

For application to mixoplankton, the already challenging situation is complicated further by the synergy of photo-phago-osmo-trophy. **Figure 5.6** gives an indication of the linkages as considered in the Perfect Beast model of Flynn & Mitra (2009), while **Figure 5.7** shows differences between protist functional types with respect to physiological capabilities.

Of the models developed in MixITiN, the two that are most suited for linkage to explicit considerations of molecular biology and physiology are Perfect Beast plus (PB+) and DRAMA (see also **Table 5.1**).

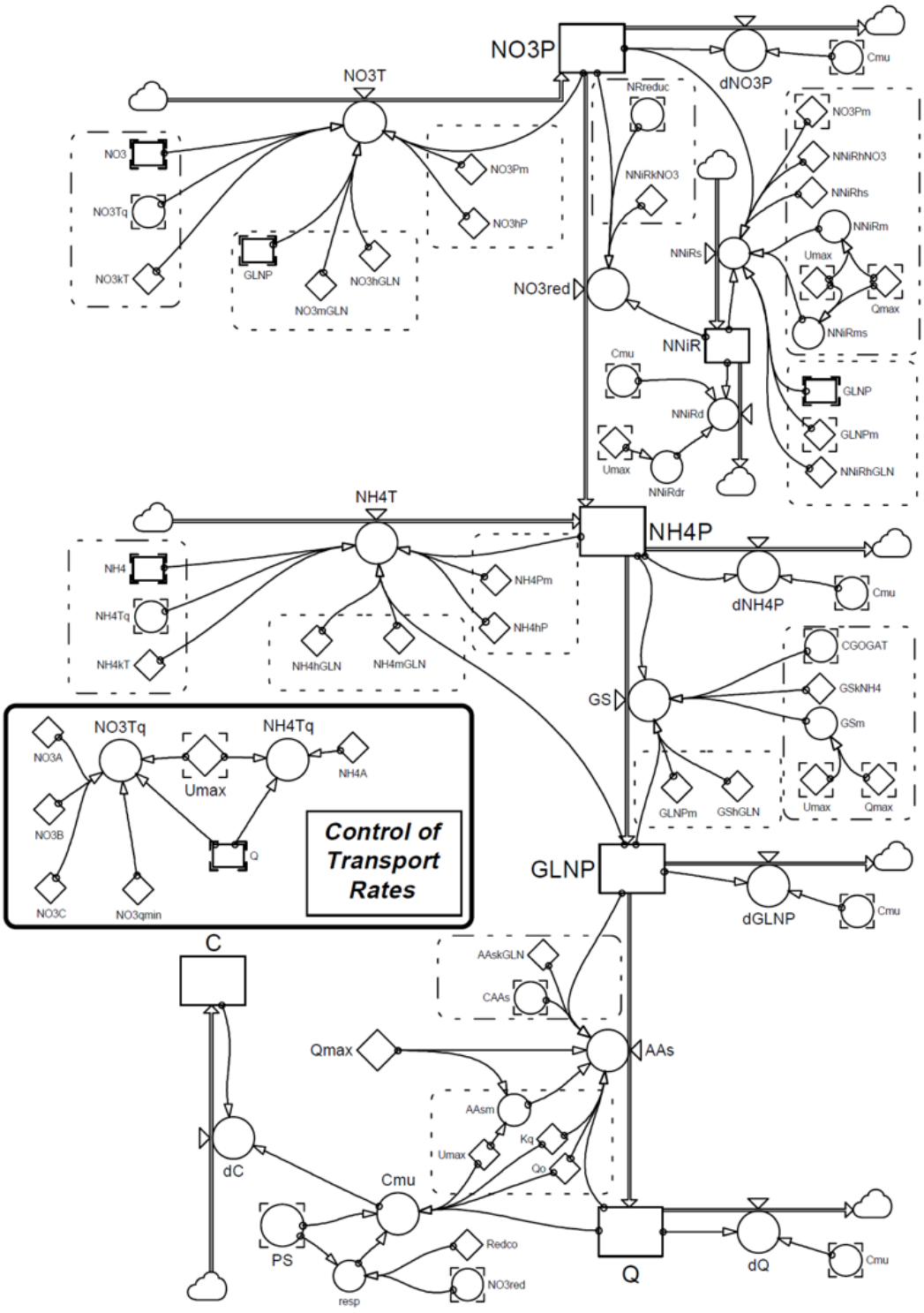

Figure 5.5 Forrester diagram of ammonium-nitrate interactions in phytoplankton controlling nutrient uptake and organism growth. From Flynn *et al*. (1997).

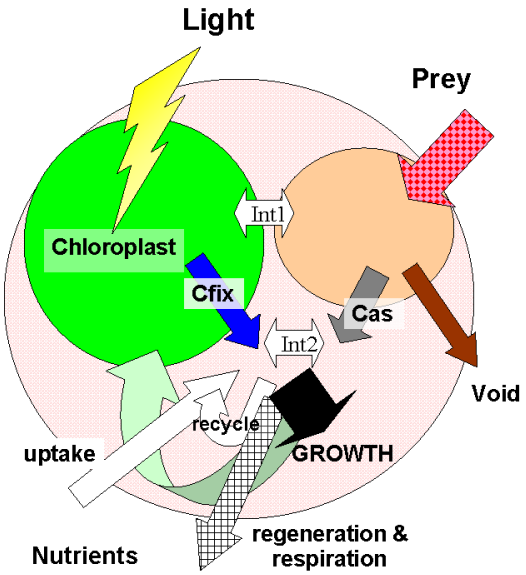

Figure 5.6 Interactions modelled in the Perfect Beast model of Flynn & Mitra (2009). The latest iteration, Perfect Beast plus (PB+), includes additional functionality (**Table 5.1**).

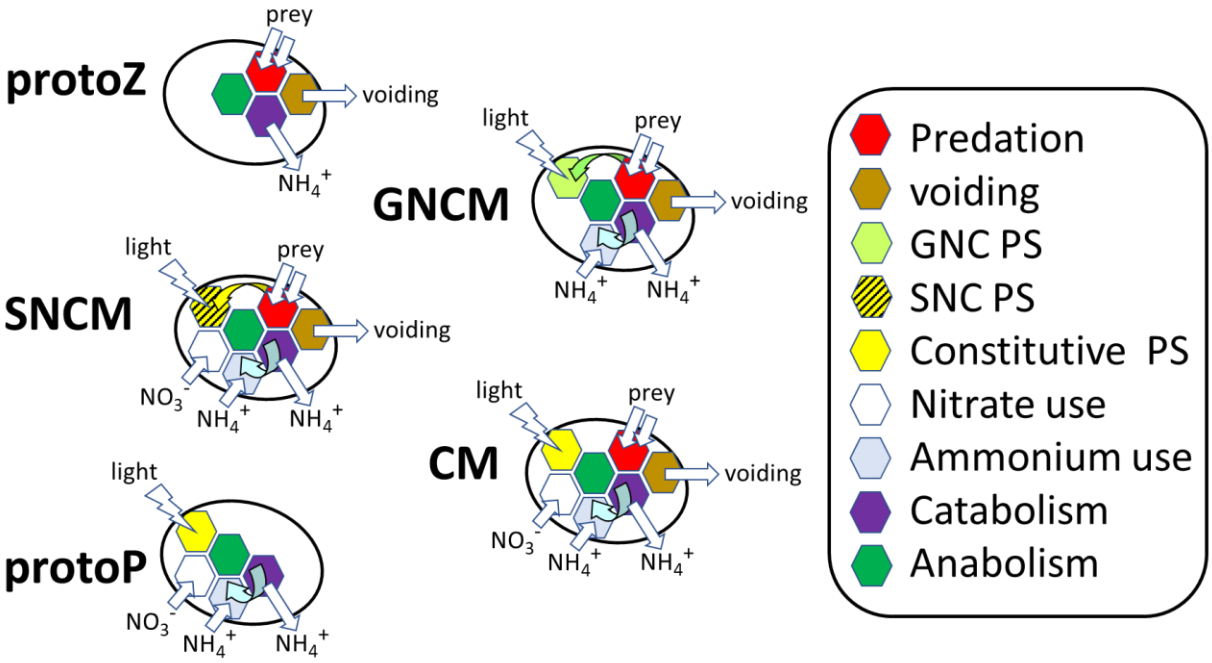

Figure 5.7 Schematic representations of the 5 protist functional type configurations. They contain the submodels for various physiological functions as indicated. protoZ – protozooplankton, GNCM – generalist non-constitutive mixoplankton; SNCM – specialist non-constitutive mixoplankton; CM - constitutive mixoplankton; protP – protist phytoplankton. From Anschütz & Flynn (2020).

5.5.1 Perfect Beast plus (PB+)

The original Perfect Beast structure is described in Flynn & Mitra (2009). It is the only mixoplankton model to have been tuned against laboratory data (Lin *et al*. 2018) and also against field data (Leles *et al*. 2021).

As shown in **Table 5.1** and **Figure 5.6**, PB+ has the capacity to describe many of the salient features of mixoplankton physiology. PB+ is particularly well suited for simulations of short-duration experimental work where the explicit description of feeding vacuoles can be important. It is thus well placed to explore interactions between photosynthesis and prey handling. It does, however, not have an explicit description of phototrophic capacity in the way that DRAMA does.

5.5.2 DRAMA

DRAMA is a newly developed model structure which, like PB+, has a lineage from earlier mechanistic models (**Figure 5.2**, **Table 5.1**). Unlike PB+, DRAMA describes explicitly the presence of RuBisCO and also (for NCMs) the status of the DNA transferred with prey kleptoplastids. A schematic of the model is given in **Figure 5.8**, its Forrester diagram in **Figure 5.9**, and with salient details given for different protist plankton configurations in **Table 5.2**. Example model output is shown in **Figures 5.10 – 5.15**. The range of physiological descriptions, and the ways that they can be modulated, and the whole conceptual framework gives more flexibility than is present in other constructs.

DRAMA provides a common platform to describe all protist plankton other than the eSNCM group. That specialist mixoplankton group may be described by combining a protozooplankton ‘host’ with a phytoplankton or CM ‘symbiont’.

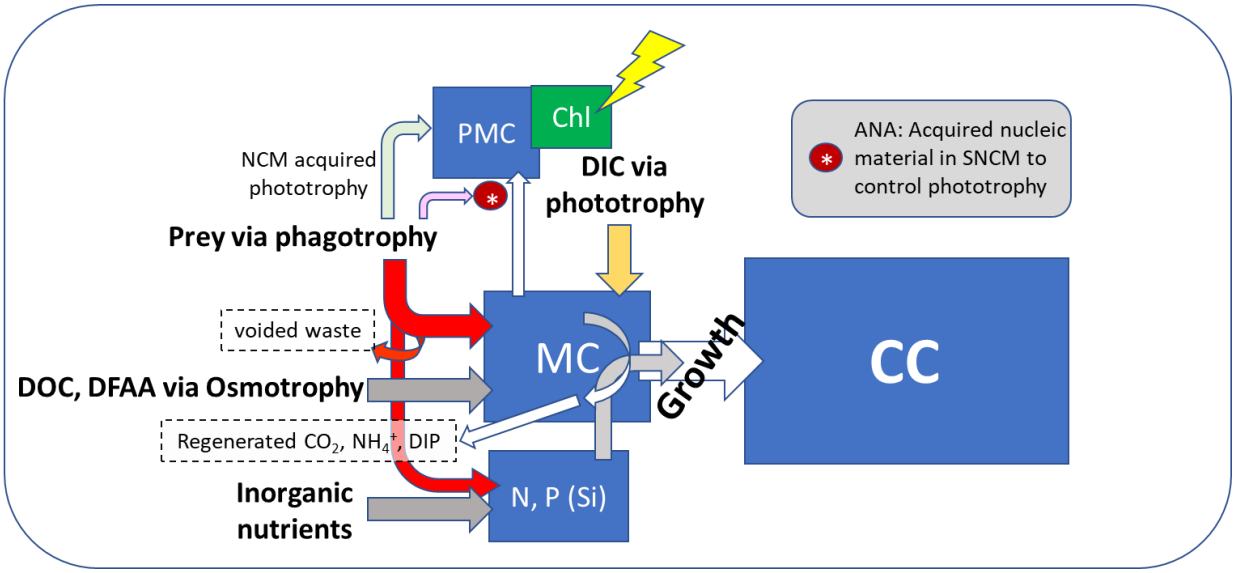

Figure 5.8 Schematic of the DRAMA concept as configured for a protist plankton model. Carbon enters a metabolic pool (MC) via osmotrophy, phagotrophy and/or phototrophy. Constitutive (CM) have full control over the synthesis of the photosynthetic machinery (PMC) and Chl. Non-constitutive mixoplankton (NCM) acquire phototrophy from their prey; GNCM only acquire PMC and Chl, while SNCM also acquire some level of control over phototrophy by acquisition of nucleic material (ANA) from their special prey. Acquired phototrophy decays over time, very rapidly in GNCM, slowly in SNCM. The size of MC feeds back to control resource acquisition and also, for CM and SNCM, to control synthesis of PMC and Chl. The size of MC then controls growth of the core biomass (CC), affected also by N and P (and for diatoms, Si) acquisition. Materials are voided as particulates as a by-product of phagotrophy, and regenerated as inorganics from respiratory processes. Not shown is the leakage of excess production of Dissolved Organic C and Dissolved Free Amino Acids.

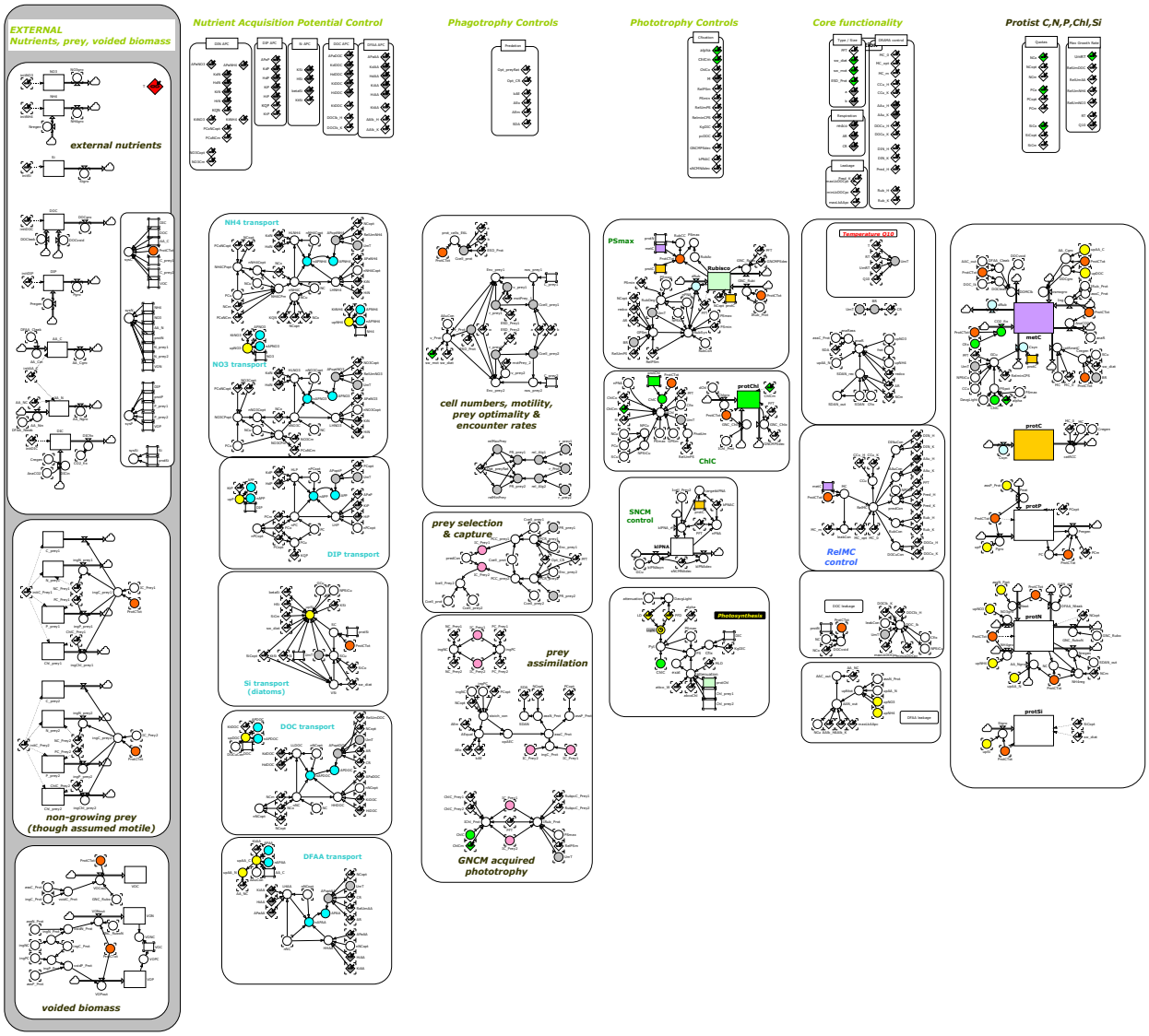

Figure 5.9 Overview of the Forrester diagram of the DRAMA model, giving an indication of the size and complexity of the model.

Table 5.2 Protist plankton functional type characteristics in DRAMA. protoZ, protozooplankton; phyto, phytoplankton. See also Table 5.1. N no; Y yes.

Category	Feature	protoZ	GNCM	SNCM	CM	phyto	phyto, diatom
General	size (µm)	3-1000	40-100	40-100	3-200	3-200	3-200
	motility	Y	Y	Y	Y	N/Y	N
	motility linked to satiation	Y	Y	Y	Y		
Osmotrophy	osmotrophy enabled	Y	Y	Y	Y	Y	Y
	can use DOC	Y	Y	Y	Y	Y	Y
	can use DFAA	Y	Y	Y	Y	Y	Y
Predation	predation enabled	Y	Y	Y	Y	N	N
	abundance dependant	Y	Y	Y	Y		
	selective by allometry & quality	Y	Y	Y	Y		
	variable AE with quality	Y	Y	Y	Y		
	variable AE with quantity	Y	Y	Y	Y		
	NH_4^+, DIP, DIC, regeneration depends on prey quality	Y	Y	Y	Y		
	SDA-N recovery with C fixation	N	Y	Y	Y		
	feeding linked to light	N	N but enhanced	N but enhanced	N but enhanced		
Phototrophy	phototrophy enabled	N	Y, indirectly	Y, indirectly	Y	Y	Y
	constitutive				Y	Y	Y
	non-constitutive		Y, frequent generalist acquisition	Y, infrequent specialist acquisition			
	essential phototrophy		Y	Y	Y	Y/N	Y/N
	PE-curve kinetics		Y	Y	Y	Y	Y
	photoacclimation		N; depends on acquired plastids	Y; depends on acquired DNA	Y	Y	Y
Use of dissolved nutrients	nutrients use enabled	partial	partial	partial/full	partial/full	full	full
	NH_4^+ use	N	N/Y	Y	Y	Y	Y
	DFAA supresses NH_4^+ use	NA	Y	Y	Y	Y	Y
	NO_3^- use	N	N	Y	Y (some N)	Y (some N)	Y
	NH_4^+ supresses NO_3^- use			Y	Y	Y	Y
	DIP	Y	Y	Y	Y	Y	Y
	Si	N	N	N	N	N	Y; critically dependant

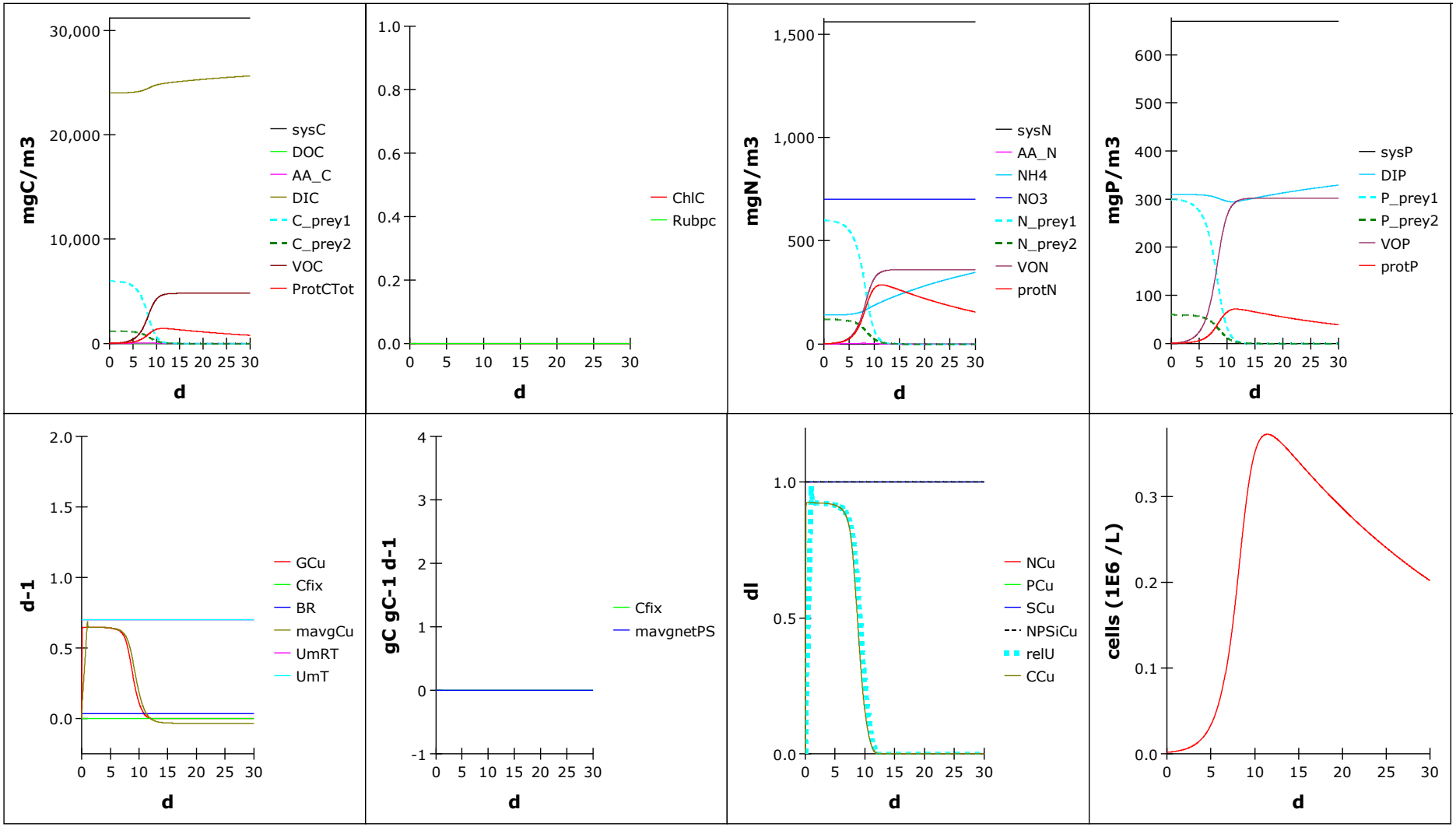

Figure 5.10 Example output when DRAMA is configured as a protozooplankton. There is no photosynthesis and hence no ChlC or RuBisCO. The two prey types are consumed, with the accumulation of voided waste and regenerated nutrients. On exhaustion of the prey, the protozooplankton respires itself to death.

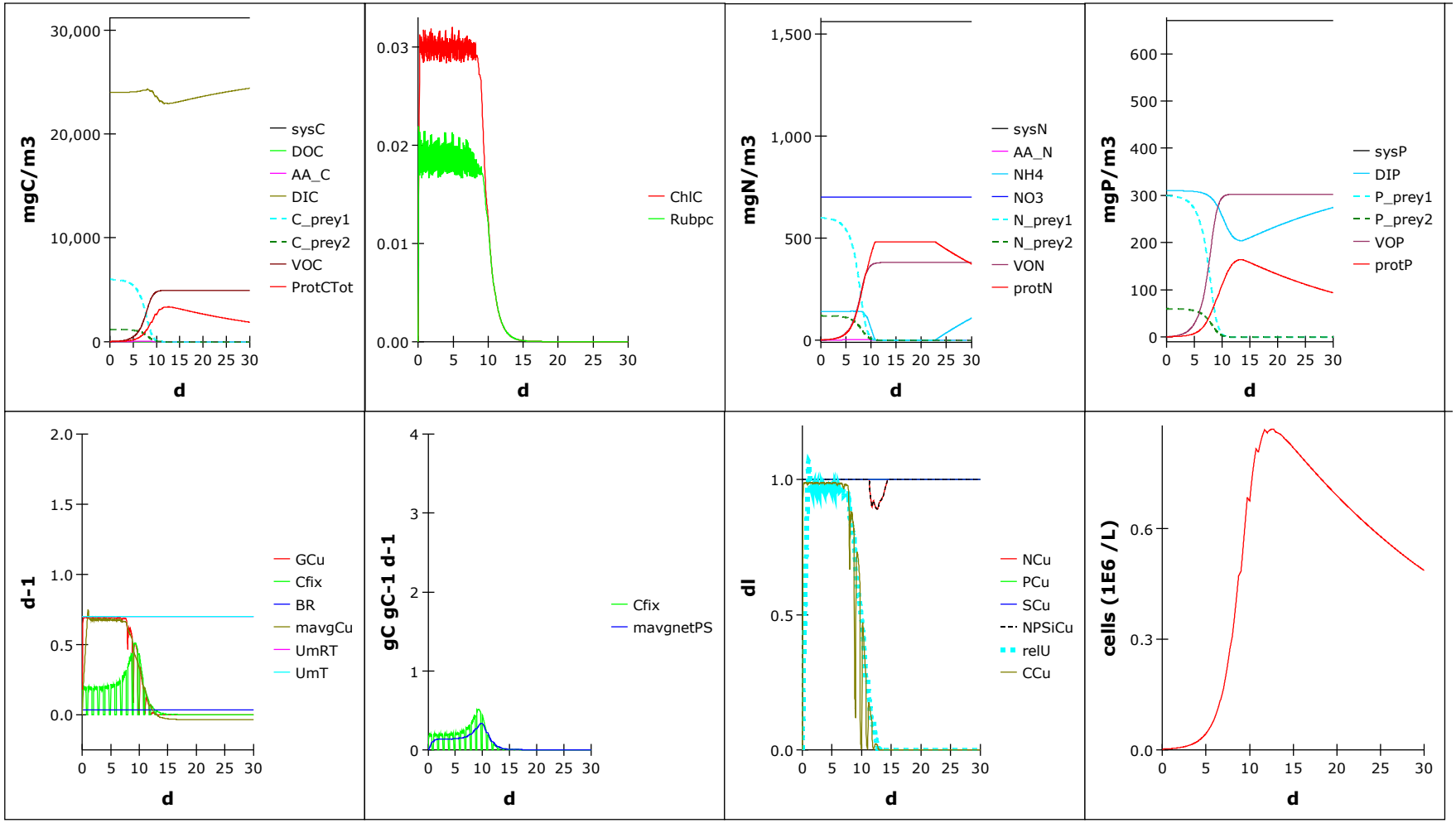

Figure 5.11 Example output when DRAMA is configured as a GNCM. The ability to photosynthesize is acquired through consumption of prey. Nitrate cannot be used, though (in this instance) there is uptake of external ammonium. Note that photosynthesis becomes more important (Cfix is higher) at the end of the prey consumption; this is because more light becomes available with the decrease of shading at lower prey abundance. Ultimately, on exhaustion of prey, the GNCM respires itself to death.

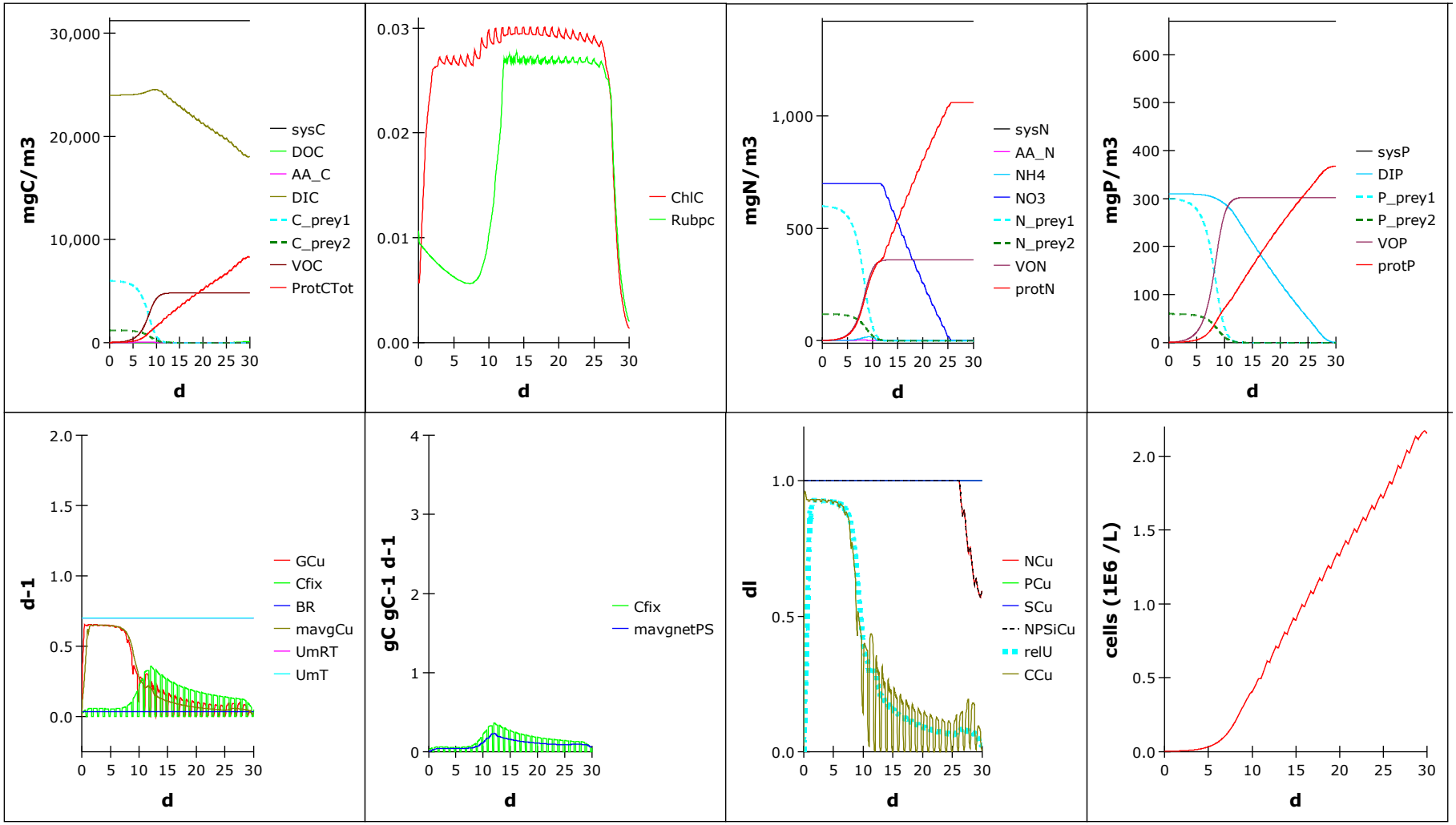

Figure 5.12 Example output for an SNCM. These acquire the ability to photosynthesize from a specific prey (here, prey2). Note that in contrast to the GNCM, the SNCM continue to photosynthesize after the prey have been consumed, though at the end of the simulation this ability is degrading rapidly. Growth of the SNCM is linear due to increasing self-shading.

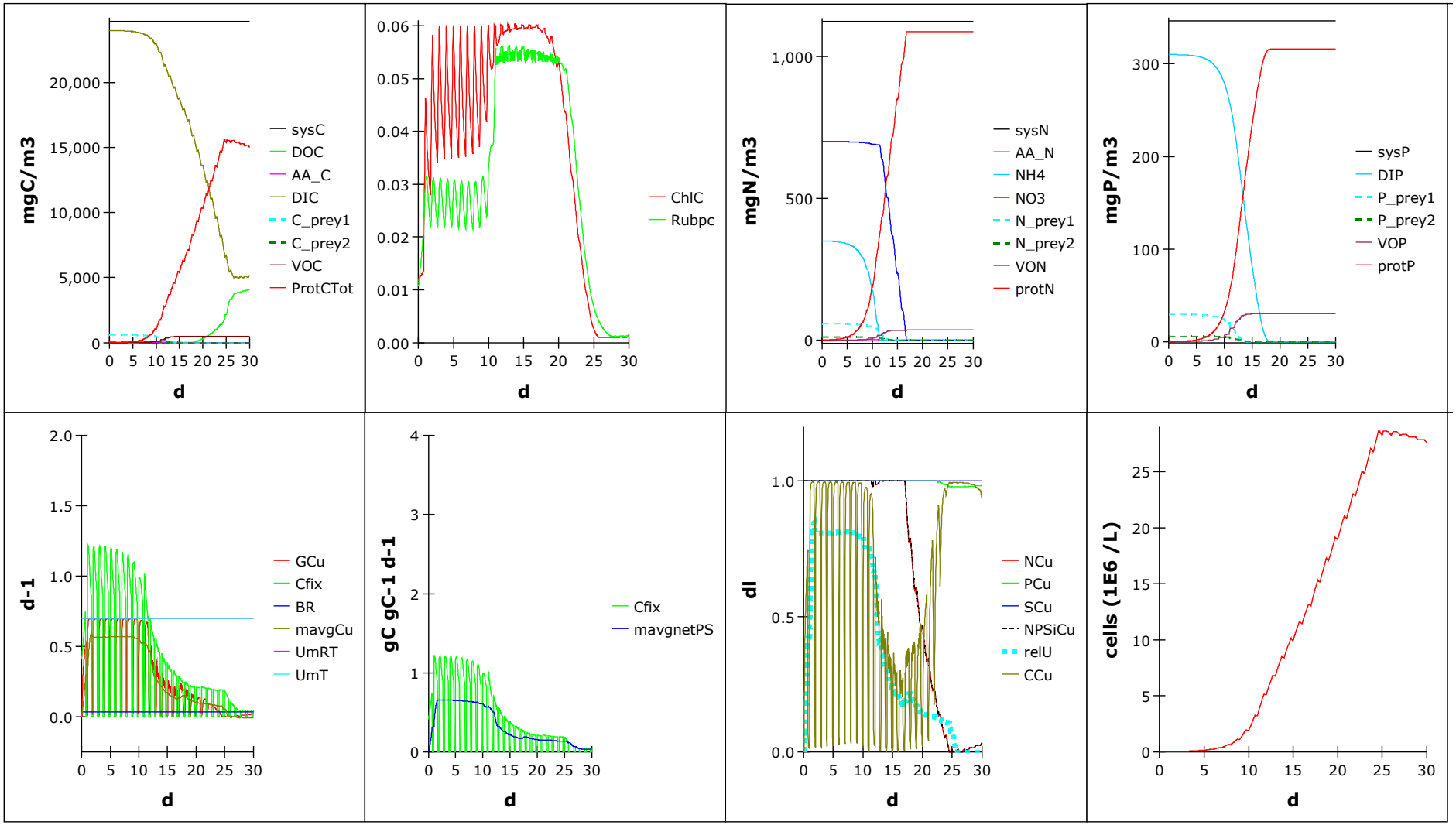

Figure 5.13 Example output for a CM. These have their own photosynthetic capabilities. They grow like phytoplankton but also consume prey. Here the prey are of low abundance. With increasing self-shading and the use of nitrate rather than ammonium after d10, ChlC and RuBisCO increase, falling on exhaustion of the DIN.

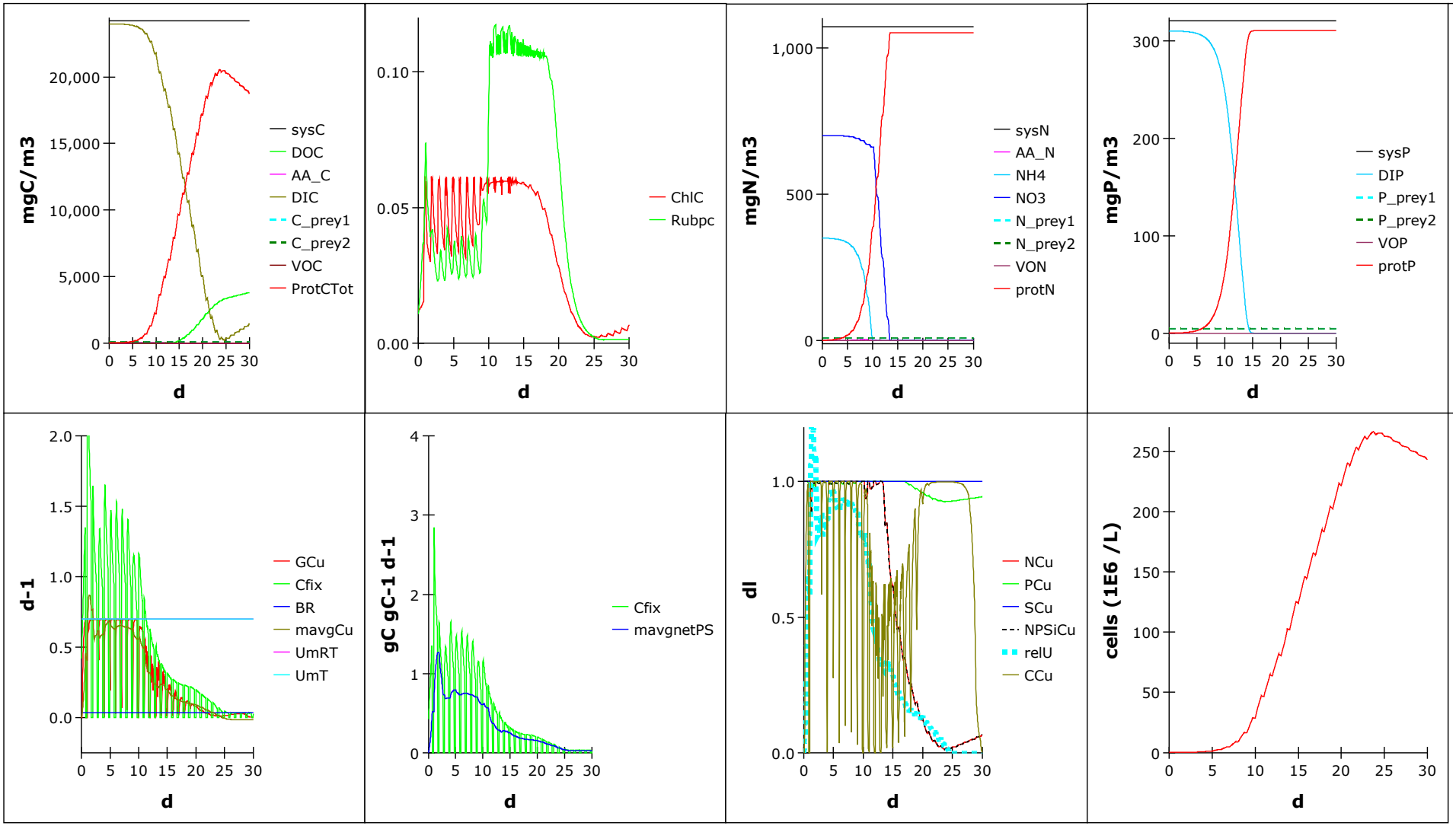

Figure 5.14 Example output when DRAMA is configured as a (non-diatom) phytoplankton. Rather like the CM, but with no prey to consume.

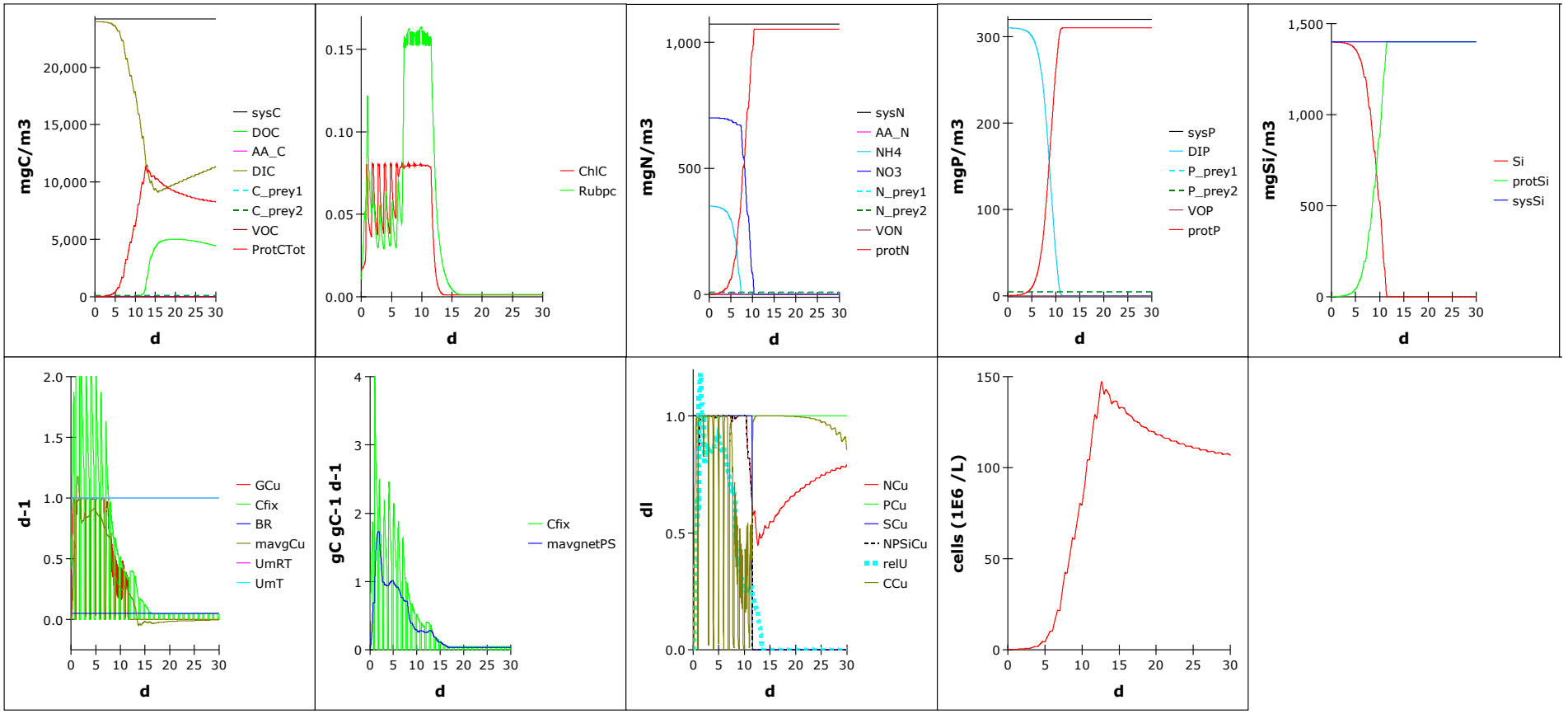

Figure 5.15 Example output when DRAMA is configured as a diatom. Rather like the phytoplankton but with higher growth rate potential and the consumption of (and ultimately limitation by) silicate availability.

5.6 Future directions

The most important step required moving forwards, for those who aspire to merge molecular biology through to mechanistic modelling of plankton under the mixoplankton paradigm, is the need to better understand the potentials and also the limitations of these disparate sciences. Biologists and ecologists often make reference in publications and grant applications to the value that simulation models have for predicting the consequences of climate change as justifications, and of the value of molecular biology in supporting such modelling. However, even after two decades (Caron *et al*. 1999, Santoferrara *et al.* 2020), qualitative molecular data which could aid modelling efforts remain elusive (**Figure 5.16**).

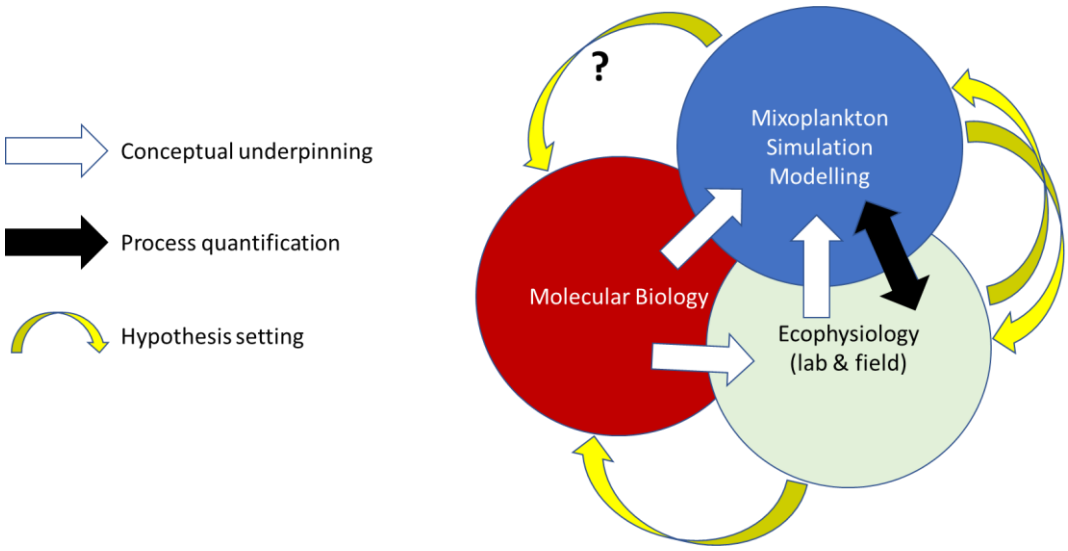

Figure 5.16 Cooperation between different scientific approaches in support of mixoplankton research, showing potential linkages. While ecophysiological studies are relatively easily linked to modelling, linkages from the semi-quantitative science of molecular biology to the other, strongly quantitative, sciences is primarily via conceptual underpinning

Some suggestions for guiding discussions between the sciences of 'omics and modelling follow.

5.6.1 Considering the explicit representation of 'omics data in simulation models

- Is this needed? What would it achieve?
- What would it achieve that is not already achieved through other routes? Not least because of the nature of research funding likely means that molecular biology would be funded at the expense of physiological studies, and vice versa.

- Is there an unrealistic expectation to exploit 'omics in modelling? If there is, who is driving such an expectation, and why?
- If there is indeed a need to merge 'omics with simulation modelling, when and where is it required? (Which model traits vs which 'omics signatures?)
- How can the semi-quantitative 'omics signatures be related to the quantitative responses required in dynamic models?
- How can the extreme detail in 'omics data be compressed to gross simplifications in models (physiologically and with respect to organism functional type)?

5.6.2 Starting from either end …

Another approach, as illustrated in **Figure 5.17**, is to attempt to align the widely varying approaches of 'omics, ecophysiology and modelling, acknowledging the significant caveats with respect to quantification and specific details. There are various ways of linking or otherwise transforming information or data types, as indicated in **Table 5.3**.

Table 5.3 Example of features identifiable using 'omics approaches, and possible surrogates with high quantification possibilities, together with an indication of alignment with features of models. Quotas of N:C, P:C, Chl:C and (*de facto*) Gln:Glu have been exploited in the MAP models (Flynn 2001), and, excluding Gln:Glu, in Perfect Beast and DRAMA (See **Figure 5.2**, **Table 5.1**). **GRH**, growth rate hypothesis.

'omics feature	Surrogates of 'omics with greater quantitative data	Modelled features (examples)
DNA (genomics)	-	State variable, conceptual basis, potential trait functionality as the values of constants
mRNA, tRNA (transcriptomics)	DNA:RNA	N:P (GRH), trait expression
Proteomics, enzymes	Quotas of DNA:RNA, N:P, N:C, P:C, Chl:C	Potential rates, acclimation, feedback (de)repression
Metabolomics	Gln:Glu	Product of rates, synthesis and recycling, feedback (de)repression

.

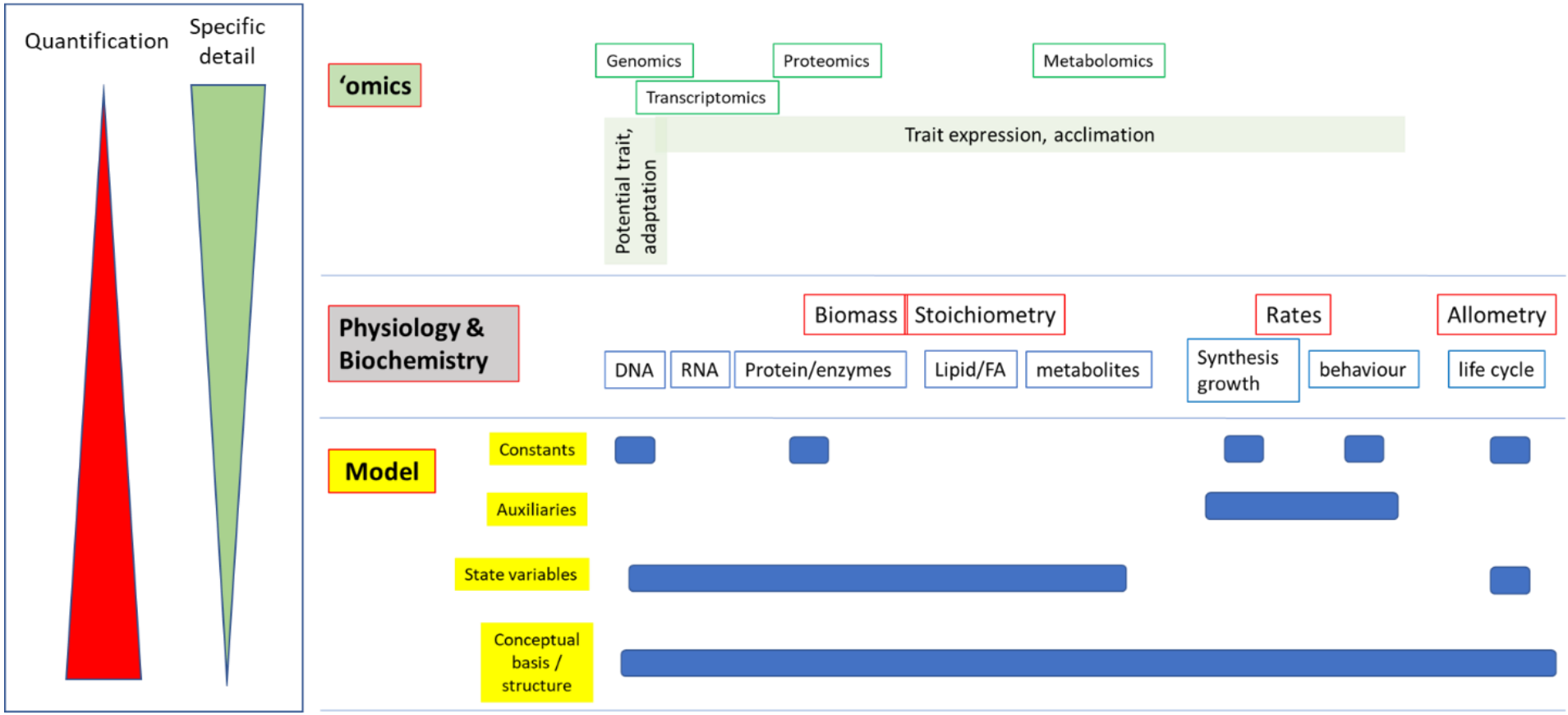

Figure 5.17 Interplay between molecular biology 'omics, physiology and biochemistry (the latter including some aspects of molecular biology), and simulation modelling. Alignment with aspects in each science area is in the vertical plane, with the level of quantification and specific detail between the techniques shown top to bottom.

5.7 Conclusions

Within MixITiN we have developed a range of models to support novel applications in mixoplankton research. Specifically, we have developed 2 simple models (including one specifically for education), 2 models of intermediate complexity, and 1 complex model. These provide us with a range of platforms for exploring different facets of mixoplankton science, to test hypotheses, and to generate new hypotheses.

The linkage between ecophysiological plankton science and simulation modelling is well founded over many decades (back to Monod and Droop, in the 1940's and 1960's respectively). That linkage remains just as valuable, as essential, today. Indeed, these are the linkages that have driven the mixoplankton paradigm (see references in Mitra *et al*. 2016; Flynn *et al*. 2019). Data from experimental work conducted in MixITiN will further developments, supporting the testing of new models.

The linkage between modelling and molecular biology remains far less clear. Other than in direct support of conceptual developments, it seems far more likely that any linkage will come indirectly, via the support of ecophysiological studies by molecular approaches. We thus await the fulfilment of the promise of molecular biology (Caron *et al*. 1999) for marine science, and specifically for modelling to provide quantitative information across functional groups of organisms.

5.8 References

Anschütz A-A, Flynn KJ (2020) Niche separation between different functional types of mixoplankton: results from NPZ-style N-based model simulations. *Marine Biology* 167; 3 doi:10.1007/s00227-019-3612-3.

Calbet A, Bertos M, Fuentes-Grünewald C, Alacid E, Figueroa R, Renom B, Garce E (2011) Intraspecific variability in *Karlodinium veneficum*: Growth rates, mixotrophy, and lipid composition. *Harmful Algae* 10; 654–667.

Caron DA, Gast RJ, Lim EL, Dennett MR (1999) Protistan community structure: molecular approaches for answering ecological questions. In: *Molecular Ecology of Aquatic Communities* Springer, Dordrecht. pp. 215-227.

Flynn KJ (2001) A mechanistic model for describing dynamic multi-nutrient, light, temperature interactions in phytoplankton. *Journal of Plankton Research* 23; 977-997. doi: 10.1093/plankt/23.9.977.

Flynn KJ (2003) Modelling multi-nutrient interactions in phytoplankton; balancing simplicity and realism. *Progress in Oceanography* 56; 249 – 279.

Flynn KJ (2018) *Dynamic Ecology - an introduction to the art of simulating trophic dynamics*. Swansea University, Swansea, UK. ISBN: 978-0-9567462-9-0.

Flynn KJ (2021) *Enhancing Microalgal Production - constructing decision support tools using system dynamics modelling*. Zenodo. http://doi.org/10.5281/zenodo.5036605

Flynn KJ, Mitra A (2009) Building the “perfect beast”: modelling mixotrophic plankton. *Journal of Plankton Research* 31; 965-992 DOI: 10.1093/plankt/fbp044.

Flynn KJ, Mitra A (2016) Why plankton modelers should reconsider using rectangular hyperbolic (Michaelis-Menten, Monod) descriptions of predator-prey interactions. *Frontiers in Marine Science* 3; 165.

Flynn KJ, Skibinski DOF (2020) Exploring evolution of maximum growth rates in plankton. *Journal of Plankton Research* 42; 497–513doi:10.1093/plankt/fbaa038.

Flynn KJ, Mitra A (2021). *A Simple N-based Mixoplankton Model*. Zenodo. http://doi.org/10.5281/zenodo.5040445

Flynn KJ, Fasham MJR, Hipkin CR (1997) Modelling the interaction between ammonium and nitrate uptake in marine phytoplankton. *Philosophical Transactions of the Royal Society* 352; 1625-1645.

Flynn KJ, Mitra A, Anestis K, Anschütz AA, Calbet A, Ferreira GD, Gypens N, Hansen PJ, John U, Martin JL, Mansour J, Maselli M, Medić N, Norlin A, Not F, Pitta P, Romano F, Saiz E, Schneider L, Stolte W, Traboni C (2019) Mixotrophic protists and a new paradigm for marine ecology: where does plankton research go now? *Journal of Plankton Research* 41; 375–391.

Leles SG, Luca Polimene L, Bruggeman J, Blackford J, Ciavatta S, Mitra A, Flynn KJ (2018) Modelling mixotrophic functional diversity and implications for ecosystem function. *Journal of Plankton Research* 40; 627-642. doi:10.1093/plankt/fby044

Leles SG, Bruggeman J, Polimene L, Blackford J, Flynn KJ, Mitra A (2021) Differences in physiology explain succession of mixoplankton functional types and affect carbon fluxes in temperate seas. *Progress in Oceanography* 190; 102481

Lin C-H, Flynn KJ, Mitra A, Glibert PM (2018) Simulating effects of variable stoichiometry and temperature on mixotrophy in the harmful dinoflagellate *Karlodinium veneficum*. *Frontiers in Marine Science* 5; 320. doi: 10.3389/fmars.2018.00320

Mitra A (2006) A multi-nutrient model for the description of stoichiometric modulation of predation (SMP) in micro- and mesozooplankton. *Journal of Plankton Research* 28; 597–611.

Mitra A, Flynn KJ (2007) Importance of interactions between food quality, quantity, and gut transit time on consumer feeding, growth, and trophic dynamics. *American Naturalist* 169; 632-646.

Mitra A, Flynn KJ, Tillmann U, Raven JA, Caron D, Stoecker DK, Not F, Hansen PJ, Hallegraeff G, Sanders R, Wilken S (2016) Defining planktonic protist functional groups on mechanisms for energy and nutrient acquisition: incorporation of diverse mixotrophic strategies. *Protist* 167; 106-120.

Rasmussen SA, Binzer SB, Hoeck C, Meier S, de Medeiros LS, Andersen NG, Place A, Nielsen KF, Hansen PJ, Larse TO (2017) Karmitoxin: An Amine-Containing Polyhydroxy-Polyene Toxin from the Marine Dinoflagellate *Karlodinium armiger*. *Journal of Natural Products*. 80; 1287–1293

Santoferrara LF (2019) Current practice in plankton metabarcoding: optimization and error management. Journal of Plankton Research 41; 571–582

Santoferrara L, Burki F, Filker S, Logares R, Dunthorn M, McManus GB (2020) Perspectives from ten years of protist studies by high-throughput metabarcoding. *Journal of Eukaryotic Microbiology* 67; 612-22.

Stoecker DK, Hansen PJ, Caron DA, Mitra A (2017) Mixotrophy in the marine plankton. *Annual Review of Marine Science* 9; 311-35.